UNIVERSITY OF WALES, CARDIFF

Star formation history and evolution of the nearest gas-rich dwarf galaxies

by

Marco Grossi

A THESIS SUBMITTED TO THE
UNIVERSITY OF WALES, CARDIFF
FOR THE DEGREE OF

Doctor of Philosophy

Cardiff, UK
Sep 2004

ProQuest LLC
789 East Eisenhower Parkway
P.O. Box 1346
Ann Arbor, MI 48106-1346

Abstract

Neutral hydrogen surveys in the last decade have revealed a new class of galaxies where the gas component can be dominant compared to the stellar one ($M_{HI}/L_B \gtrsim 1$). These objects may be either young (< 1 Gyr) or in a way "retarded", having evolved at a very slow rate without efficiently converting their large amount of gas into stars within a Hubble time.

Here we analyse three such galaxies in the Centaurus A group at a distance of about 4.5 Mpc (discovered with the HIPASS survey), which have no analogues in the Local Group (Banks et al. 1999). From their optical morphology they appear to be dwarf spheroidals and low surface brightness, yet they are gas-rich ($M_{HI}/L_B > 1$) with gas-mass-to-stellar light ratios larger than typical dwarf irregular galaxies. These systems should be favoured hosts for starburst, yet a faint star formation region has been detected in only one object. Are these galaxies truly young? Or rather, what inhibits the conversion of gas into stars slowing down their evolution? Is there a connection with the environment they are evolving in?

In the attempt to answer some of the above questions we have analysed data in HI , Hα, V and I bands (taken with the Hubble Space Telescope) and the optical spectrum of the HII region of one dwarf (HIPASS J1337-39). In particular we have constructed I, $(V - I)$ Colour Magnitude Diagrams (CMDs) and we have compared the data-sets with theoretical models, using isochrones of various metallicities (Bertelli et al. 1994) and simulated CMDs (Harris & Zaritsky 2001).

All three galaxies have well determined Red Giant Branches (RGBs) which put them in the Centaurus A group at distances between 4.5 and 5 Mpc. The well populated RGBs suggest that these systems cannot be younger than 2 Gyr. The evidence of asymptotic giant branch (AGB) stars in two out of three galaxies suggest that they contain populations with ages of up to 10 Gyr. Older Horizontal Branch (HB) and RR Lyrae stars would be two magnitudes fainter than the photometric limit reached with the HST at this distance, therefore we cannot infer the presence of an old (> 10 Gyr) stellar population. The age-metallicity degeneracy has been broken in one case (HIPASS J1337-39) where we measured a low metal abundance (Z $\sim$ 1/30 solar) from the analysis of the HII region. The remaining two galaxies do also show properties which are at least consistent with similarly low metallicities.

From the comparison of the observed and model CMD's we infer that all three galaxies are gas-rich because their Star Formation Rates have been very low during their long lives ($\lesssim 10^{-3}\ M_\odot\ \mathrm{yr}^{-1}$). We argue that in such systems, star formation (SF) may have been sporadic and local, although one object (HIPASS J1321-31) has a peculiar red plume in its CMD suggesting that most of its stars were formed in a "miniburst" 300 - 500 Myr ago.

Neither their low HI surface densities, nor their low metal content favour high star formation rates or starbursts, although we can not exclude connections with the local environment. Two out of three galaxies seem to be located in the outskirts of the group, being at about or less than 1 Mpc from the more massive galaxies of the group.

The low metal abundances may be the consequence of the ejection of enriched material via supernovae-driven winds during the SF episodes, but it is likely they were not violent enough to blow away the majority of gas (Mac Low & Ferrara 1999, Ferrara & Tolstoy 2000).

The question of why there are no similar dwarf galaxies in the Local Group remains open and the study of similar objects in the nearby groups is necessary to widen the sample of galaxies with such properties.

In the Appendix A we present the first part of a still ongoing project with the aim of studying the stellar population of "retarded" galaxies at the other end of the mass scale - spirals with $M_{HI} > 10_{10}\ M_\odot$ and $M_{HI}/L_B \gtrsim 1$. The optical, near IR and 21cm observations are briefly presented and discussed.

Contents

Chapter 1

Introduction

The big question in star formation is not how to form stars,
but how to prevent stars from forming.
Mordecai-Mark Mac Low

1.1 What drives or slows down the evolution of a galaxy: a history of star formation

Star formation (SF) is the conversion of gas from a low to a high density state until self-gravity becomes dominant and drives the transition from condensed clouds of atomic gas to the first protostars via the formation of molecular gas. A galaxy's chemical and photometric evolution is thus strictly related to the rate at which its gas content is consumed and transformed into stars.

Along the Hubble sequence SF appears to be very efficient, and a clear trend holds between gas content and morphological type with gas-poor early-type galaxies at one end of the sequence and gas-rich late-type Sd spirals at the other. However the process does not seem to work in the same way in all systems as

suggested by finding galaxies where star formation is highly suppressed such as in Low Surface Brightness (LSB) galaxies. A theory able to successfully predict the rate of star formation in galaxies is still lacking. Nevertheless there are three main conditions which are essential for the process to occur (Elmegreen 2002).

- First, the formation of diffuse HI clouds which allows the interstellar gas density to increase up to $\sim$ 100 cm^{-3} and reach a moderately low temperature of about 100 K. The higher gas and dust column density start blocking diffuse starlight and cause a further decrease in temperature. The gas then reaches a higher density state ($\sim 10^3$ cm^{-3}) to maintain pressure equilibrium and the opacity to the UV background increases.

- These conditions favour the transition from atomic to molecular hydrogen on dust grains - the second step necessary for the process to continue. Dust plays a key role both as a shield from the stellar ultraviolet (UV) emission and as the catalyst of H_2 formation. These molecules accelerate the cooling of the gas, via line emission of their rotational transition and they block even more of the external radiation so that other molecules such as CO can form and survive. The cooling is much more efficient when the gas is molecular because rotational transitions have lower energy levels than the common electronic ones in atoms. The gas reaches even lower temperatures until cold ($\sim$ 10 K), opaque, molecular cores form.

- Finally, gravitational attraction begins to dominate pressure, the core contracts and then finally collapses into a star+disc system. The lumps of gas with masses comparable to a solar mass form single and binary systems, while cluster of stars originate in clouds with much larger masses.

Massive star formation brings to an end the SF process by ionising and progressively disrupting the cloud. At the same time massive stars push and sweep up the dissipated material and supernova shocks re-accumulate and compress unstable gas. The condensation of new HI clouds in other regions of a galaxy eventually will trigger new star formation. The cycle can start again.

If any of these steps is inefficient or lacking, the star formation chain is broken. If the ambient pressure is low and there are moderately high radiation fields the formation of a cool HI phase is prevented, which is the first step in the transition from the average ISM to the dense molecular clouds. This is what generally happens in the outer discs of galaxies where the gas is warm and star formation is inhibited there, although spiral arms sometimes may act as a pressure source and make enough cool gas to start the process even in

such an environment. Faint HII regions in fact can be found at the extreme periphery of some spiral galaxies (Le Lilièvre & Roy 2000; Ferguson, Gallagher. & Wise 1998; Cuillandre et al. 2001).

A low metal abundance or dust content implies a lower efficiency in shielding the gas from the UV stellar emission and it reduces the formation rate of molecular gas. The temperature will not drop below several hundred degrees Kelvin unless a large pressure fluctuation somehow arises.

The understanding of the mechanism of star formation is yet incomplete. However, by studying systems and regions where SF has stopped or is highly suppressed, we can learn a lot about the process itself.

In this thesis I will analyse the properties of four gas-rich dwarf galaxies ($M_{HI} \sim 10^7\ M_\odot$) recently discovered at 21-cm in the Centaurus A group (Banks et al. 1999) with the HI Parkes All-Sky Survey (HIPASS) (Meyer et al. 2004, Zwaan e al. 2004). The high gas-mass to stellar ratio ($M_{HI}/L_B > 1$) and the low optical surface brightnesses make these objects a unique sample with no similar counterparts in the Local Group.

What makes these systems interesting and puzzling compared to 'typical' galaxies is that, given their large gas reservoirs, they should, in principle, be favoured hosts for starbursts and should by now have consumed most of their gaseous fuel. Nevertheless they seem to lead very 'quiet' existences and assuming that they are as old as the Hubble time their SFRs appear to be surprisingly low ($\lesssim 10^{-3} M_\odot yr^{-1} kpc^{-2}$). Which factors might have slowed down the evolution of these systems and inhibited the conversion of gas into stars? Is there a connection with the environment they are evolving in? Have they experienced a recent infall of gas which has in a way "rejuvenated" them? Or rather, are these galaxies truly young?

I will discuss these issues by sampling both the young and old stellar population and the gas properties.

Colour magnitude diagrams (CMDs) have been used to study the stellar population and the star formation history of the galaxies in the Centaurus A group. This approach has been successfully applied to the Local Group (LG) galaxies and can be performed only for very nearby objects (within approximately 10 Mpc) by using the Hubble Space Telescope (HST). Comparison of model and observed CMDs enable one to obtain an idea of the evolution of a galaxy. Nevertheless deriving an accurate SFH for galaxies outside the LG is complicated: our CMDs are not deep enough to resolve the stars corresponding to the early stages of galaxy evolution. Secondly, it is hard to disentangle the combined effects of age and metallicity to interpret the CMDs if independent measures of the metallicity are not available. Thus, such an analysis is challenging, yet it is still worthwhile because this is one of the nearest samples of galaxies where one can investigate the

star formation history in a puzzling environment of low stellar density and high gas content.

In the Appendix A, I present the optical, near IR, and high resolution 21-cm observations of seven HI massive galaxies ($M_{HI} \gtrsim 10^{10}\ M_{\odot}$) which, although identified by previous optical surveys, have been selected from a subset of HIPASS, the southern cap catalogue (SCC) (Kilborn et al. 2002). They have been chosen because of their large gas fractions, suggesting that star formation has been highly inefficient. In fact, the M_{HI}/L_B ratio among giant galaxies is generally found to be less than 0.5, while our sample with $M_{HI}/L_B > 1$, shows that most of the baryonic mass in these systems is surprisingly still stored as unprocessed gas. This sample is morphologically more varied and consists of spirals with and without bars and ring structures, and extended low surface brightness discs. Yet in a few cases the optical counterparts have high central surface brightnesses. Blind HI surveys such as HIPASS are finding a new class of galaxies which are both massive and gas-rich (M_{HI}/L_B up to around 5) (Disney 2002). A detailed study of their stellar population is still lacking and the aim of the last part of this thesis is to combine HI and optical data to begin to build a picture of the SFH of these systems.

This introductory chapter will be used to present the main topics which may affect the star formation of a galaxy and to describe the main properties of gas-rich systems.

- In section 1.2 I present an overview on how star formation varies along the Hubble sequence from early-type and gas-poor to irregular and gas-rich galaxies.

- Section 1.3 and 1.4 are dedicated to the discussion of the known mechanisms able to affect star formation in galaxies. First I describe the role of gas, both in atomic and molecular form as the fundamental ingredient for star formation. Secondly the effects of bars, galaxy-galaxy interactions and mergers are presented. Lastly, I discuss the mechanisms which drive the evolution of a galaxy in a high-density environment, which are able to remove its gas content and alter its morphology, progressively reducing the SF activity.

- Section 1.5 and 1.6 give examples of two classes of objects that are experiencing very different levels of current star formation activity: starburst galaxies on the one hand with very high present star formation rates; LSB and low mass systems, on the other, where SF proceeds and seems to have proceeded at a very low rate. In particular, I review the properties of LSB galaxies obtained by the most recent studies and I discuss the dwarf population in the Local Group (LG) whose relative closeness allows us to thoroughly investigate their star formation history.

- The following sections are used to introduce the reader to the main properties of the gas-rich galaxies I am interested in. After a brief introduction (§1.7), I discuss the importance of "blind" 21-cm surveys to find such a population of galaxies (§1.8), then their general properties (§1.9) and spatial distribution (§1.10). To conclude, in section 1.11 I summarise the main issues brought up in this introductory discussion, and in particular the current picture and main issues of the SF process resulting from the study of the Local Group members. §1.12 gives a general outline of the structure of the thesis.

1.2 Star formation along the Hubble Sequence

Galaxies along the Hubble sequence show a wide range in young stellar content and star formation activity. Moving from late to early-type galaxies the ratio of current to past star formation rate decreases. This variation is partly the basis of Hubble classification itself and the understanding of this trend is fundamental to disentangling how galaxies evolve during their existence.

The most used tracer of star formation is Hα emission. The UV radiation from massive stars ionises the diffuse gas left over from the original cloud. The ionised hydrogen, HII , in such a region is continuously recombining, but not necessarily straight into the ground state. The different recombination lines are grouped into series, each one corresponding to a particular lower level. In the Balmer series electrons end up in the level n = 2, the emission lines fall in the optical domain and the so-called Hα line at λ = 6563 Å(from n = 3 to n = 2) is the strongest. For a given stellar initial mass function (IMF) it is possible to derive the average emission per star of UV radiation, so from the Hα luminosity one can infer how many massive stars have formed in the last few Myr (Kennicutt, Tamblyn, & Congdon 1994).

The *UV continuum* and the *far infrared* (FIR) emission have also been used as indicators of the young stellar content of galaxies. The 1250 - 2500 Åwindow is particularly useful to minimize the contribution from older stellar population, although these wavelengths cannot be observed from the ground due to the opacity of the Earth's atmosphere. Dust in galaxies absorbs UV and optical photons and re-emits in the FIR (10 - 300 μm). The absorption is most efficient in the UV regime, thus the FIR emission is strictly correlated to the emission of young stars and a good indicator of the SFR (Lonsdale & Helou 1987; Sauvage & Thuan 1992).

The SFRs in galaxies expressed in solar masses per year varies over a wide range along the Hubble sequence: from almost zero in gas-poor elliptical and lenticular (S0) galaxies to about 20 $M_{\odot}$ yr^{-1}in gas-rich

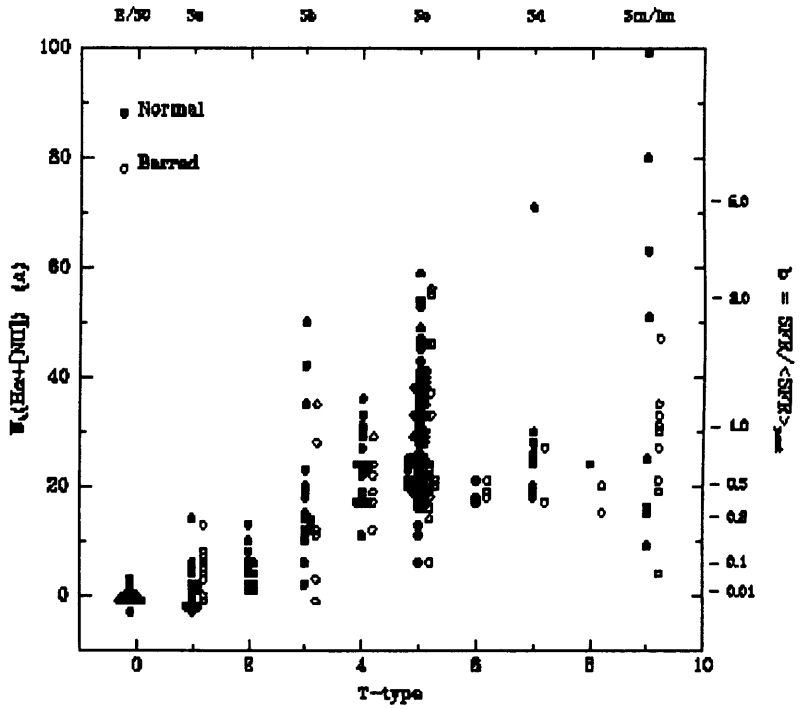

Figure 1.1: Distribution of $H\alpha+[NII]$ equivalent widths for different morphological type galaxies. The right axis shows the corresponding values of the stellar birthrate parameter b, which is the ratio of the present to past SFR (from Kennicut 1998a).

spirals. Optically selected starburst galaxies can have rates around 100 $M_\odot$ yr^{-1}, which go up to 1000 $M_\odot$ yr^{-1}in the most luminous IR starburst galaxies (see §1.4). "Normal" galaxies like the Milky Way or M31 are characterized by intermediate levels of SF (around 1 $M_\odot$ yr^{-1}). Their gas consumption rates are too low to exhaust the gas supply in less than a Hubble time and this leads to the co-existence of different stellar populations with a range of different ages and colours.

However, to compare different galaxies one needs to introduce a normalized SFR, either to a measure of the past star formation rate - expressed by the red continuum emission - or to some measure of the size of the galaxy. Therefore in Fig. 1.1 (Kennicutt 1998a) is shown the dependence of the SFR on the morphological type for a sample of 227 nearby bright galaxies ($B_T < 13$) (Kennicut & Kent 1983, Romanishin 1990), where the SFR is expressed as the Hα + N [II] equivalent width. This parameter is in fact defined as the luminosity

	E, S0	S0a, Sa	Sab, Sb	Sbc, Sc	Scd, Sd	Sm, Im
M_{HI}/L_B	0.04	0.12	0.21	0.29	0.36	0.66

Table 1.1: Variation in gas content according to the galaxy morphological type (from Roberts & Haynes 1994).

of a certain emission line normalized to the adjacent continuum flux, thus it represents the SFR per unit red luminosity. The normalized SFRs show a clear dependence on the morphological type and they vary over a range of almost two orders of magnitude in the SFR per unit luminosity (see Fig. 1.1). Similar results have been obtained by using the UV continuum and optical colours (Larson & Tinsley 1978, Donas et al. 1987, Deharveng et al. 1994).

There is a striking evidence of a dispersion in SFRs within each Hubble type (Fig. 1.1). According to Kennicut (1998a) there are several factors which could explain this, such as variations in gas content, possible galaxy-galaxy interactions increasing the SFR, or more simply intrinsic fluctuations in the SFR within individual objects.

Early-type disc galaxies (S0-S0a) show in general very low star formation activity, according to deep Hα observations (Caldwell et al. 1994), where only three out of eight objects observed do have HII regions and the galaxies have very low SFR ($< 0.01\ M_\odot\ \mathrm{yr}^{-1}$). However a sub-class of so-called 'HI -rich' S0 galaxies with HI masses up to $M_{HI} = 10^9 M_\odot$ (and a median $M_{HI}/L_B = 0.13$) do reveal a higher fraction of disc and/or circum-nuclear star-forming regions. There is also evidence of a correlation between low M_{HI}/L_B , which is usually used as an indicator of the gas-richness of a galaxy, and the absence of disc HII regions (Pogge & Eskridge 1993).

The trend continues in **spiral galaxies**. Bulge-dominated early-type spirals, Sa, have redder colours compared to the disc-dominated Sc galaxies, indicating an increasingly younger population from Sa, to Sd (Larson & Tinsley 1974). This is also related to a variation in the gas content from late to early-type spirals. The hydrogen mass to luminosity ratio, M_{HI}/L_B , is found to decrease moving from late-type Sc to gas deficient Sa (Roberts & Haynes 1994) (Table 1.1).

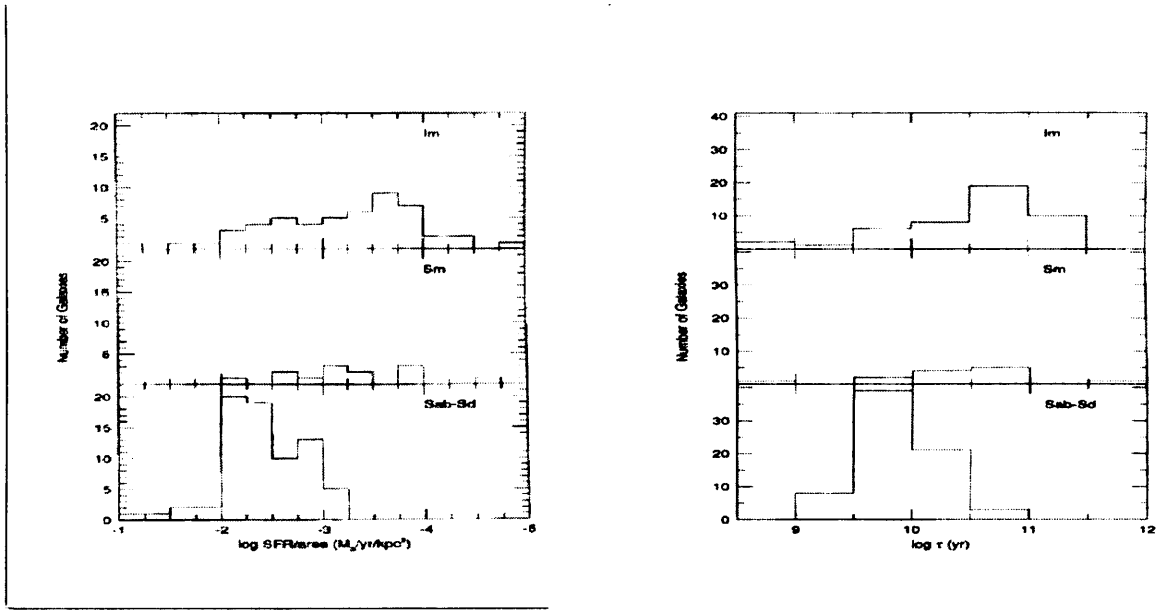

Figure 1.2: **Left:** The SFR per unit area (within D_{25}) of a sample of Irregular galaxies (Hunter 1997), compared with spiral galaxies from Kennicutt (1983). **Right:** Time scale from the same sample of galaxies to exhaust their total gas content (HI + He + H_2) at their current SFRs (from Hunter 1998).

Irregular galaxies represent an extension of the Hubble sequence of spirals right after Sm galaxies, systems where the spiral structure can just barely be identified. The definition of an Im galaxy is based on the lack of an evident organized structure, but irregular galaxies are also distinguished from spirals for being bluer, less luminous and massive, more gas-rich, less dusty and with low metallicities. In addition, irregular galaxies tend to be relatively isolated.

Their star formation properties may be extremely varied. In a survey of 60 nearby (D < 27 Mpc) irregular galaxies, Hunter (1997) found that these systems may span a range of four magnitudes in star formation rate per unit area (Fig. 1.2), where the rates have been normalised to the area of the galaxy within D_{25} , the radius at a B surface brightness of 25 magnitudes arcsec^{-2}. In some objects SFRs are comparable to those of the spirals, others are experiencing a wide-scale starburst that involves most of the optical galaxy such as NGC 1569 (Gallagher, Hunter, & Tutukov 1984) or IC 10 (Massey & Armandroff 1995). On the other hand, the majority of irregular galaxies in the sample have SFRs per unit area lower than spirals.

Most irregulars show a long time depletion scale for their gas content. In Fig. 1.2 is shown the time scale needed to convert their gas content into stars at their current star formation rate. It appears that they are able to continue to form stars for several Hubble times.

At the high end of the star formation activity belong a class of irregulars defined as blue compact dwarfs (BCD) galaxies. These objects, while being generally isolated, seem to experience central starbursts without an obvious external cause. Therefore the reason for their intense star formation activity is not completely clear. The properties of these galaxies will be further discussed in section §1.9 and 1.10.

1.3 Triggering and inhibiting star formation in galaxies

1.3.1 The relation between gas and star formation: the Jeans and Toomre criteria

Stars are formed from the gravitational contraction of gas clouds. In a simplified approach, gravitational instabilities in an homogeneous medium are the result of the competition between self-gravity and the internal pressure of the medium. A first quantitative description to describe the collapse of a self gravitating gas cloud was given by Jeans. Given a linear perturbation in an homogeneous and isotropic medium with density ρ, the Jeans criterion defines the critical length scale of the perturbation beyond which gravity wins on the internal pressure and the collapse is triggered. The Jeans length is given by

$$\lambda_J = \left(\frac{\pi c_s^2}{G\rho}\right)^{1/2} \tag{1.1}$$

where c_s is the sound speed of the medium, ρ its density, G the gravitational constant.

The Jeans instability is believed to be the fundamental mechanism that has given rise to galaxies and stars. Nevertheless this is a very rough treatment where other factors such as the rotation of the galaxy and the magnetic fields are left out.

The gravitational instabilities in gaseous rotating thin discs are the result of an interplay between pressure, the centrifugal force and self-gravity. Toomre (1964) for the first time worked out the solution for such instabilities and showed that rotation adds another stabilizing term to balance gravity which becomes more important on large scales. The so-called Toomre-Quirk criterion (Quirk 1972) defines the balance

between the centrifugal and the gravitational forces. If the former exceeds the latter, then there are no instabilities. This is the threshold condition usually written as

$$Q = \Sigma_c/\Sigma_g > 1.$$

Here Σ_g is the gas surface density, and Σ_c is the critical gas surface density threshold given by

$$\Sigma_c = \frac{\alpha c \kappa}{3.36G} \tag{1.2}$$

where c is the velocity dispersion which ranges between 6 - 9 $\mathrm{km\,s^{-1}}$, α is a dimensionless geometrical parameter with a value of 0.7 for spiral galaxies (Kennicutt 1989), and κ the so-called epicyclic frequency:

$$k^2 = \frac{2V}{R}\left(\frac{dV}{dR} + \frac{V}{R}\right) \tag{1.3}$$

where Ω is the angular velocity at radius R, leading to $\kappa^2 = 2\Omega^2$ in the case of a flat rotation curve. The Toomre-Quirk criterion basically implies that if $Q > 1$ the gas is too stable to form clouds and star formation is inhibited, while $Q < 1$ ($\Sigma_g > \Sigma_c$) corresponds to gravitational instability.

How might this affect the SFR of a galaxy? Is there observational evidence of the expected tight correlation between the gas properties and the large-scale SFR of a galaxy? Schmidt (1959) was the first to quantify this relationship and introduced a simple parametrization where the SFR depended only on the local gas density, Σ_{gas} averaged on the optical disc, via a simple power law:

$$\Sigma_{SFR} = A\Sigma_{gas}^n \tag{1.4}$$

where n falls in the range 1 - 2.

Kennicutt (1998b) verified the Schmidt law in a sample of normal disc and starburst galaxies, spanning a dynamic range of approximately 10^5 in local gas surface densities and 10^6 in SFR per unit area. He confirmed the power law dependence within the optical size of a galaxy and found a best-fit index $n = 1.4$ (Fig. 1.3).

On scales larger than the optical disc, at low gas densities, the Schmidt law is substituted by a sharp

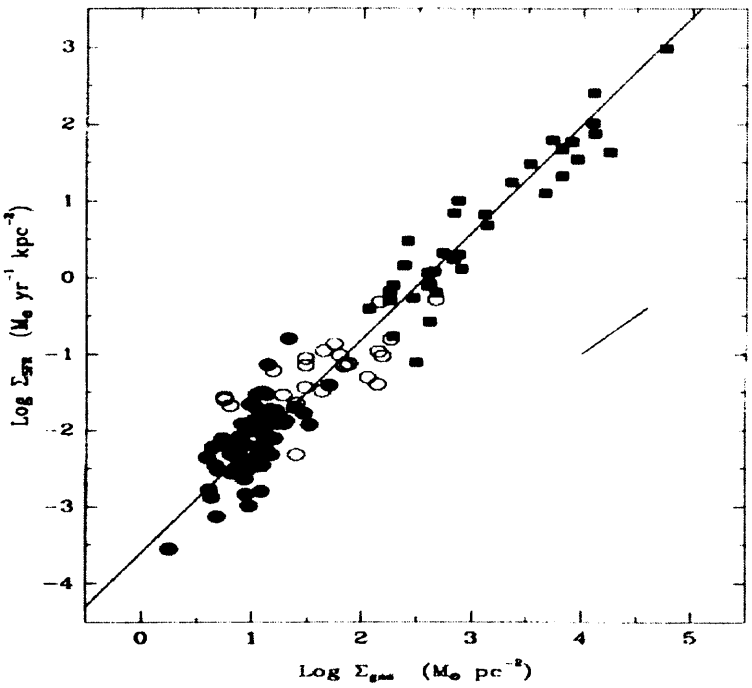

Figure 1.3: Star formation law for the normal disc (*filled circles*) and starburst galaxies (*squares*) taken from Kennicutt (1998b). The open circles refer to the centre of the normal disc galaxies. The line represents a least-squares fit with index $n = 1.40$.

decline of the SFR. The detection of HI in discs of spiral galaxies well beyond their optical extension gave the first evidence of a gas density threshold for star formation to occur (Kennicutt 1989).

Kennicutt (1989) tested the Toomre criterion on Sc spiral galaxies. By studying a sample of 15 late-type spirals he plotted the ratio of the observed gas density Σ_g to the model critical gas density Σ_c as a function of radius and found that massive star formation was occurring in regions of the disc where $Q < 0.67$. In addition Q does not vary much as a function of radius within the regions of the disc were SF is ongoing.

Moreover these systems deviate from the assumption of thin discs and the gas distribution may appear rather clumpy and irregular in overall shape.

The correlation between star formation and gas density holds for normal spiral and starburst galaxies. There are though some exceptions to the law: O'Neil, Bothun and Schombert (2000) found low surface

brightness galaxies with $\Sigma_g > \Sigma_c$ without ongoing star formation. The inner parts of M 33 and NGC 2403 (Martin & Kennicut 2001) or NGC 4736 and 5457 (Wong & Blitz 2002) have gas densities below the threshold yet star formation is still occurring.

At pressures higher than this threshold, collisional cooling balances stellar heating and a cool atomic phase of gas can exist in equilibrium (Wolfire et al. 1995).

The validity of the HI column density threshold as a trigger of star formation has been checked for other systems such as LSB galaxies (van der Hulst et al. 1993), gas-rich dwarf galaxies (van Zee et al. 1997a) blue compact dwarfs (BCD) (Taylor et al. 1994) and Irregulars (Hunter, Elmegreen, & Baker 1997, Hunter 1998).

LSB galaxies (van der Hulst et al. 1993), gas-rich dwarfs (van Zee 1997a) and Irregulars (Hunter 1998) are generally found to have global gas densities lower than the Toomre instability threshold given by the thin rotating disc model (Q = 1), and even lower than the threshold observed for star formation in spiral galaxies, where Q= 0.67. This implies that the gas disc is *globally* stable against gravitational collapse, and the star formation process is inefficient in those types of galaxies. *Locally* the gas density threshold can be reached and the stability broken as it is stressed by a good correlation between the peaks in the gas density and the regions of active star formation (van der Hulst 1993, van Zee et al. 1997a, Taylor et al. 1997). However, it is unlikely that any large region will increase its density enough to exceed the threshold, thus SF will occur at a very low rate across the disc and in a stochastic way (van Zee 2001a). Stellar winds or possible weak interactions may enhance the gas density in small regions and trigger the gravitational instability of the clouds.

A similar result came from the analysis of the averaged gas densities in Sextans A (Hunter & Plummer 1996), where Σ_g/Σ_c is roughly a factor of two lower than in Sc galaxies.

Skillman et al. (1987) found that star formation in dwarf irregulars occurs at a column density of 5×10^{20} cm^{-2} where the threshold depends inversely on the metallicity. Elmegreen (2002) suggested that this column density corresponds to the minimum pressure necessary for the existence of a cool diffuse atomic phase.

Blue compact dwarf (BCD) and HII galaxies instead show higher HI column densities (peaks above 10^{21} cm^{-2} , Taylor et al. 1994, van Zee et al. 1998, Pustilnik et al. 2003) which agree with the threshold predicted by the instability theorem, again highlighting the critical role of gas density in the SF process.

1.3.2 The interplay between molecular gas, dust and metallicity

Molecular hydrogen plays a central role in the conventional picture of star formation in galaxies. Once the gas is molecular and at densities above $n \approx 100$ cm^{-3} , the cooling rate in gas clouds is so high that rapid collapse follows and stars start forming. Little is known about the distribution of diffuse H_2 in the interstellar medium (ISM) in our and other galaxies, its formation, destruction or how it is recycled after the disruption of molecular clouds. According to Allen (2001) all of the HI in the galaxy has been in the form of H_2 many times during a galaxy lifetime since it can be produced and destroyed in a very short time-scale.

The basic requirement for the atomic to molecular transition is the presence of dust. In pure HI gas a collision of two atoms can form an H_2 molecule, but the reaction rate is considerably enhanced if the encounter of two H atoms occurs on the surface of dust grains (Hollenbach & Salpeter 1970, 1971). The efficiency of this process depends on several factors: the collision rate between H atoms and dust grains, the probability for atoms to stay on the grain surface, and the mobility and lifetime of hydrogen on the grains. For instance, if the temperature is above $\sim$ 100 K, hydrogen atoms start evaporating from the grain surface, preventing the formation of H_2 .

There are two main factors which regulate the transition from atomic to molecular hydrogen in the interstellar medium.

a) the ultraviolet (UV) interstellar radiation field that dissociates H_2 molecules recreating two HI atoms.

b) The metal and consequently the dust content of a galaxy. Dust plays a key role both in shielding molecules from the ambient UV radiation field and as a formation site for H_2 molecules. Lower metallicity implies fewer dust grains to drive the transition from HI to H_2 .

In low metallicity environments and in the primordial universe H_2 may form via the so-called H^- process (Lequex & Viallefond 1980; Jenkins & Peimbert 1997) which does not involve the presence of dust. It consists of the formation of a negative ion first, $H + e \rightarrow H^- + \gamma$, followed by the faster reaction $H^- + H \rightarrow H_2 + e$.

There is still a lack of information about how the UV background, or the metallicity affect the abundance of molecular gas and consequently the star formation process. This is mainly due to the lack of direct H_2 measurements, which makes it extremely difficult to test a relation between the H_2 surface density and the star formation rate in a disc. The bulk of molecular hydrogen in a galaxy is around 10 - 20 K, with its first rotational level, accessible only through a quadrupolar transition ($\Delta J = 2$), occurring at a characteristic

temperature T= 512 K ($\lambda = 28\mu$m). This limits the detection of H_2 in emission to hot regions only, which are not representative of the general conditions of the interstellar medium. Measures of H_2 have so far been inferred by CO submillimetric observations, under the assumption that they are tightly correlated (Young & Scoville 1982; Sanders, Solomon, & Scoville 1984,). Carbon monoxide is the most abundant molecule after H_2 and its dipole moment is small, therefore it is easily excited, with the transition line from the rotational level J = 1 $\rightarrow$ 0 at λ = 2.6 mm. The conversion from the observed CO line intensity to the total H_2 column density is done via the so-called X-factor. This factor has been calibrated by studies on molecular clouds of the Milky Way by Solomon et al. (1987) at $X = N(H_2)/I_{CO} = 2.8 \times 10^{20}$ cm^{-2}/(K km s^{-1}). Although the same value has been applied to galaxies along the Hubble sequence in previous studies (Young & Knezek 1989), there is evidence that X varies with the metallicity of a galaxy (Maloney & Black 1988, Wilson 1995) and that it may not be possible to set a universal X factor. Lower metal abundances imply less Carbon and Oxygen in the gas, therefore the amount of molecular gas traced by CO may underestimate the presence of H_2 if a constant conversion factor is assumed. Rubio et al. (1993) show that in clouds of the SMC, where the metallicity is about 17 times smaller than in the solar neighbourhood, X is between 4 and 20 times higher than the Galactic values. Such high values found in the SMC are due to a higher rate of photodissociation of CO because of the strong UV radiation field and the lower dust content which reduces the shielding of molecules from the radiative fields. Therefore SMC structures, having a lower content of carbon monoxide, are less luminous in CO compared to galactic structures of the same size, which would result in a different value of X.

From observations of 5 galaxies in the Local Group (M 31, M 33, IC 10, NGC 6822, SMC) Wilson (1995) finds that X depends inversely on metallicity. de Blok & van der Hulst (1998) from the non detection of CO in 5 LSB galaxies with an average metallicity of 12 + log (O/H) $\sim$ 8.4 (roughly 1/3 solar) argue that the conversion factor X is likely to be $\sim$ 4 times higher than the galactic value.

The picture of molecular gas distribution in galaxies derived from CO is drastically different from the atomic one (Fig. 1.4): the HI distribution typically extends beyond the optical disc, while the CO extent is typically one-half the optical radius (Young 1989). Young stars and molecular gas show similar distributions (Young & Knezek 1989).

From CO observations of a sample of 142 galaxies and galaxy pairs Knezek & Young (1989), assuming a constant conversion factor $X = 2.8 \times 10^{20}$ cm^{-2}/(K km s^{-1}), inferred a morphological type dependence of the global molecular to atomic gas ratio. Early-type disk galaxies have higher molecular fractions than

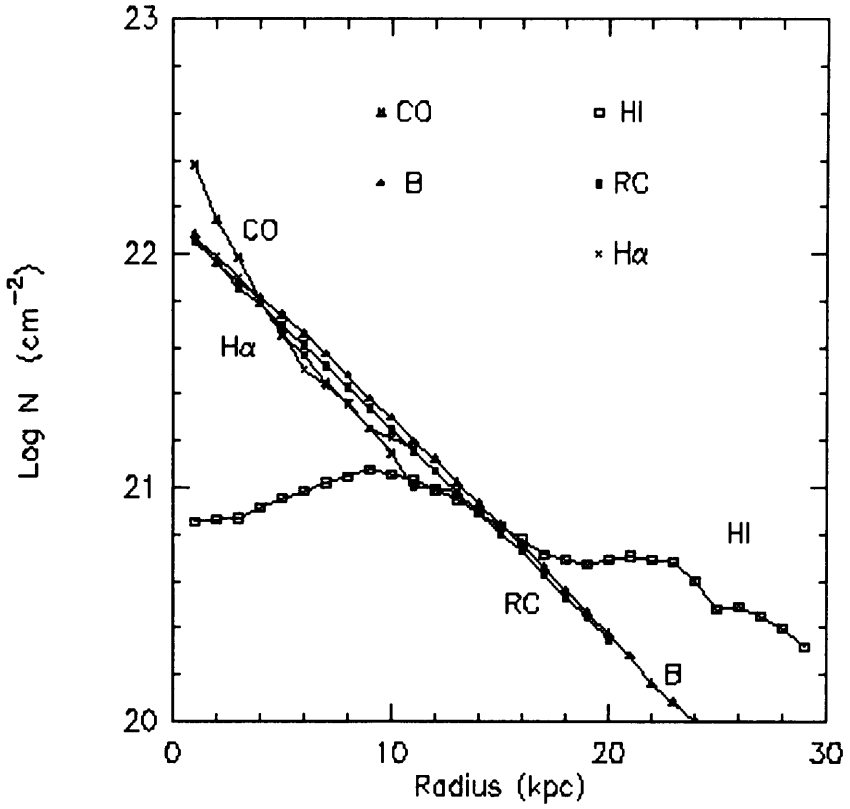

Figure 1.4: Radial distribution of molecular gas, atomic gas, blue, radio-continuum and $H\alpha$ surface densities in a typical spiral galaxy, NGC 6946 (from Combes 1999).

late type, with the mean ratio M(H_2)/M(HI) ranging between 4, in S0 - Sa galaxies and 0.2 in Sd - Sm types. This could be explained by the fact that early-type galaxies have higher metallicities and lower UV interstellar emissivities compared to late-type spirals.

In low surface brightness (LSB) objects (see section §1.5.1), characterized by low star formation efficiency and low metallicity, CO is generally very rare (de Blok & van der Hulst 1998). Recent studies have claimed the detection of molecular gas in a giant LSB, PO6-1 (O'Neil, Hofner, & Schinnerer 2000) and in three low mass LSB spirals (Matthews & Gao 2001).

Taking into account that the galactic conversion factor, X, may give a wrong estimate of the H_2 content of low metallicity systems, the upper limits on the molecular content of LSB galaxies are still lower than

those found in the "normal" high surface brightness (HSB) objects (de Blok & van der Hulst 1998). A plausible conclusion would be that there are no large amounts of H_2 in LSB galaxies, and the low star formation rates are the consequences of a reduced molecular component. On the other hand, systems with very active star formation but low average metallicity, such as the blue compact dwarf (BCD) galaxies, do not show so far traces of CO (Combes 1986; Young et al. 1986; Israel, Tacconi, & Baas 1995; Gondhalekar et al. 1998) giving an idea of the difficulty of studying the correlation between SFR and H_2 content .

A way of directly detecting H_2 is in absorption through far-ultraviolet (FUV) spectroscopy in the Lyman and Werner bands (912 Å$< \lambda <$ 1130 Å) toward a UV bright background source. Previous FUV satellites such as ORFEUS (de Boer et al. 1998, Richter et al. 1998) could only observe stars as far as in the Magellanic Clouds. The launch of the Far Ultraviolet Spectroscopic Explorer (FUSE) (Moos et al. 2000) in 1999 has allowed observations of molecular hydrogen in absorption outside the Milky Way. So far only a small number of extragalactic sources have been investigated with FUSE, such as several lines of sights in the Magellanic Clouds (Tumlinson et al. 2002), HII regions in M33, and a few BCDs - I Zw 18 (Vidal-Majar et al. 2000), Mrk 59 (Thuan, Lecavalier des Etangs, & Izotov 2002), Mrk 36 (Lebouteille et al. 2004). H_2 lines have been only detected so far in the Magellanic clouds and in M 33, and the picture obtained from these observations is far from being clear and complete: more objects need to be analysed in order to understand the interplay between molecular hydrogen and metallicity in HII regions, especially in low metallicity environments.

The overall abundance of molecular hydrogen in the Magellanic clouds is lower than the Milky Way, a result that is consistent with the lower metallicity and higher diffuse UV background of the two satellites. In addition, a correlation is found between higher values of the extinction parameter - E($B-V$), an indicator of the dust content - and higher molecular abundances, although it does not appear to hold at low values of E($B-V$) (Tumlinson et al. 2002).

The main result of FUSE observations of BCDs is the non detection of molecular hydrogen up to its sensitivity limit of N(H_2) $\sim 10^{15}$ cm^{-2} . This is consistent with the lack of a CO component. The remarkable absence of diffuse H_2 can be explained by the low abundance of dust grains and the high ultraviolet flux arising from the starforming regions of BCD galaxies. A prediction of the expected H_2 column density in I Zw 18 (Vidal-Majar et al. 2000), the most-metal deficient starburst galaxy known to date, suggests that it may be lower than the FUSE observed upper limit by more than two orders of magnitude.

1.3.3 Bars and spiral arm structures

Stellar bars can, according to numerical simulations, strongly perturb the gas flows in discs and trigger nuclear star formation, but the correlation between the presence of bars and the total disc star formation activity is not a clear-cut one.

Numerical models (Friedli & Benz 1993) have indicated that the intensity of the gas fuelling phenomenon strongly depends on the bar-axis ratio (b/a) also called the "strength" parameter. The stronger the bar, the faster is the accumulation of gas in the center. In less than a Gyr, strong bars ($b/a < 0.6$) have nearly pushed all the gas initially inside the bar region into the center, while weak bars have only accreted a small fraction of it. The formation of a spontaneous or induced (due to a merger) strong bar in a gas-rich Sc-like disc typically triggers a starburst of intermediate power and duration.

However this correlation is rather controversial according to the observations. Some authors claim that SF is enhanced in barred galaxies (Hawarden et al. 1986, Dressel 1988, Huang 1996) while other suggest that barred galaxies have SF levels similar or lower than those in normal spirals (Pompea & Rieke 1990, Isobe & Feigelson 1992).

A general interpretation seems to be that bars increase the SF activity in the center but that they do not appear to significantly affect the total disc star formation rate. Comparing the Hα emission of normal and barred spiral galaxies, Kennicutt (1998a) did not find evidence of a correlation between bars and the star formation rates of the disc (see Fig. 1.1). A similar conclusion was derived from FIR emission of a large sample of normal spirals (139) and barred Sa-Sc galaxies (260) by Tomita et al. (1996), confirming the results of Hα observations.

Martinet & Friedli (1997) claim that the relation between bars and SFR may be more complicated and introduce a possible connection between SF activity and the structural properties of bars. In a sample of 32 late-type barred galaxies, comparing SFRs from Hα and far Infrared (FIR) emissions, they found a correlation between SFR and both the strength (the axis ratio b/a) and length of the bar. The late-type galaxies with higher SFRs have both strong ($b/a < 0.6$) and long bars. Not all strong and long bars are actively forming stars, which indicates that after a first strong starburst due to the formation of a young bar, the galaxy falls back in a more quiescent state. Weak bars do not display any significant increase in the SF activity. However the authors underline that their sample is too small to derive definite and more detailed conclusions.

1.4 The role of the environment

1.4.1 Galaxy-galaxy interactions

Star formation is a local process in galaxies, but different external factors can affect and vary the overall star formation rate.

Several studies have been concentrated on the observational properties of mergers and close encounters between galaxies. There is a general correlation between an increased star formation activity and interactions, which is particularly evident between strong nuclear starbursts and mergers of galaxies.

Tidal interactions and mergers can modify the overall gas distribution by the formation of bars (Barnes & Hernquist 1996). Bars drive radial flows of the gas, which gets compressed in the center, possibly leading to bursts of star formation. A close encounter or an accretion event may perturb the orbits of molecular clouds and cause their collision, with the ultimate effect of an increase in SF.

Observations of interacting systems at different wavelengths show strong non thermal radiocontinuum (Hummel et al. 1987) and far-infrared emissions (Sanders & Mirabel 1986, Heckman 1999), or unusually large scatters in optical colours (Larson & Tinsley 1978) that can be explained by adding starbursts to an underlying normal stellar population.

Kennicutt et al. (1987) analysed the Hα and far infrared emission of a set of 50 galaxies in pairs and 32 strongly interacting systems, and compared them with a field sample. Both Hα and FIR emission are enhanced in this sample of galaxies. However the increase in SFRs varies largely. The majority of paired galaxies is characterised by relatively short bursts (about 10^7 yr) with modest enhancements in the SFR, about 2 - 3 times the prior rate . The most luminous star forming systems belong to the interacting sample, are associated almost exclusively with strong tidal interaction and imply bursts 5 - 30 times stronger than their previous activity. Rates larger than 20 $M_\odot$ yr^{-1}are rarely observed in isolated galaxies (Kennicut 1998a).

The large range in SFRs observed (Kennicutt 1987) and the evidence that many galaxy pairs have modest or very low star formation activity suggest that factors other than gravity can play a key role in this mechanism, such as the morphological structure, the mass distribution of the pair, and the orbital parameters (Kennicut 1987).

Finally, Barton et al. (2000) in a sample of 502 galaxies in close pairs (less than 50 h^{-1} kpc) and small groups find an anti-correlation between the intensity of the starburst and the spatial and velocity separation of the galaxies. When the separation on the sky between the systems is larger, the corresponding starburst is less intense and appear to be older. Therefore they infer that bursts are initiated only in close passages between galaxies and the intensity of the burst decreases with time as the pair separation increases.

1.4.2 Interactions in clusters: "harassment" and ram pressure stripping

There are two main processes in clusters which might drive the evolution of galaxies and can severely modify the star formation rate, the gas content and the morphology:

- **tidal encounters** with several members of a cluster, also known as "harassment", to indicate frequent high velocity interactions in a high density environment (Moore et al. 1996, 1998);

- **ram pressure stripping** due to the interactions of the hot intra-cluster medium (ICM) with the inter-stellar medium (ISM) of a galaxy.

Both mechanisms act simultaneously in a cluster and their relative effects on the evolution of its members are not always easy to disentangle (Combes 2004). Although their long-term effect is the removal of gas from galaxies determining a gradual decline in SF, both mechanisms can induce, at least temporarily, star formation.

Tidal interactions remove gas from galaxies that come closer than a galaxy diameter (Toomre & Toomre 1972). The likelihood that a galaxy will suffer a tidal collision depends on parameters like the relative orientation of spin and orbital angular momentum, but to a first order approximation it is proportional to $1/a^2v$, where a is the separation between galaxies and v their relative velocity. Thus, at a given distance, a tidal encounter in a loose group is more harmful than in a cluster because the tidal pull will last longer. On the other hand, tidal encounters are more likely to occur in clusters, favoured by the higher number density and relative velocities of galaxies.

Harassment was introduced by Moore et al. (1996, 1998) to explain the observations of a larger fraction of blue galaxies in clusters at z $\sim$ 0.4 (Butcher & Oemler 1978, 1984). At this redshift, 90% of objects with

luminosity $L < L_*{}^1/5$ in clusters are bulgeless, blue, Sd disc systems, while 90% of galaxies within nearby clusters are now dwarf ellipticals (dEs) or S0 galaxies. This indicates that much more SF was occurring in the recent past in such environments. The additional evidence that such blue galaxies appear disturbed in their morphologies (Dressler et al. 1994) and have multiple starbursts suggests that tidal interactions may have been very efficient in profoundly and rapidly modifying the galaxy morphologies.

According to Moore et al. (1998), harassment implies that close encounters ($\lesssim$ 50 kpc) with galaxies as luminous as L_*, cause gravitational shocks that can severely damage the fragile discs of Sc-Sd galaxies. After a bursting transient phase, tidal interactions can completely alter the morphology of these galaxies from spirals to "spheroidals". Due to the cumulative effect of the perturbations the transformation can occur over a period of a few Gyr. The remnants produced in the simulations have properties that match the spheroidal systems in present day clusters.

Galaxies travelling at high velocities through clusters with a dense ICM may also be subjected to the removal of their gas content via the interaction with the hot medium. **Ram pressure stripping** is more effective in clusters with a high velocity dispersion and higher ICM density. A galaxy moving with a velocity v_G through a hot diffused gas undergoes a ram pressure $p_{ram} = \rho_{ICM} v_G^2$, where ρ_{ICM} is the density of the medium. Neutral hydrogen is removed from the galaxy if the ram pressure of the ISM is greater than the gravitational force per unit area provided by the galaxy's disc. The condition for this mechanism to effectively remove the atomic gas content of a galactic disc is given by (Gunn & Gott 1972)

$$\rho_{ICM} v_G^2 \geq 2\pi G \Sigma_* \Sigma_{gas} \tag{1.5}$$

where ρ_{ICM} is the intracluster gas density, Σ_* and Σ_{gas} are respectively the stellar and gas surface densities. The relation can more easily be expressed as

$$\rho_{ICM} v_G^2 \geq \frac{\Sigma_{gas} v_{rot}^2}{R} \tag{1.6}$$

with $\Sigma_* = (2\pi G)^{-1} v_{rot}^2 R^{-1}$ (Binney & Tremaine 1987), and having used the fact that the gravitational mass of the galaxy, M_*, is given by $R v_{rot}^2/G$, with v_{rot} the rotational velocity of the galaxy. For a constant gas density $\Sigma_{gas} = 10^{21}$ cm^{-2}, $v_{rot} = 150$ km s^{-1}, and a radius $R = 15$ kpc, the minimum pressure to affect

[1] L_* is the characteristic knee in the galaxy luminosity function, and in the B band it corresponds to $L_B^* = (1.2 \pm 0.1) h^{-2} \times 10^{10} L_\odot$

the gaseous distribution is $p_{ram}^{min} \sim 500$ cm^{-3} (km s^{-1})^2.

For instance, according to Vollmer et al. (2001), a galaxy in the Virgo cluster with a disc rotational velocity $v_{rot} \sim 150$ km s^{-1}, which is on a circular orbit within the cluster, has to be at an estimated distance of 250 kpc from the centre to be significantly affected by ram pressure.

Abadi et al. (1999) show that HI gas is effectively stripped in the core of rich clusters for discs oriented perpendicularly to the wind. Galaxies can lose up to 80% of their gas, with the final disc being restricted to 4 kpc radius in a time-scale of 10^7 yr. The process is much less efficient in the outer parts of the cluster or for inclined discs with respect to the wind. According to simulations by Kundic, Hernquist & Gunn (1992), only the outer parts of gas discs will be stripped in this case.

This latter conclusion finds some support in observations, especially in the case of the Virgo cluster. Haynes & Giovannelli (1986) found a significant HI deficiency for a subpopulation of Virgo spirals in an HI survey within 5° ($\sim$ 1.4 Mpc at an assumed distance of $\approx$ 16 Mpc; Jerjen, Binggeli, & Barazza 2004) of the Virgo center. The colours of the HI deficient galaxies were found to be redder than normal, indicating that SF had stopped at some stage ("quenching"). The gas deficiency has been taken as evidence of ram pressure stripping.

However gas-stripped galaxies are not completely 'inert' and SF activity can be found in their inner discs. An R band and Hα imaging study of 63 spiral galaxies in the Virgo cluster has been recently undertaken (Kenney & Koopmann 1998; Kenney, Koopman & Young 2001) and compared to a sample of isolated galaxies. Star formation is normal or enhanced in the centre of Virgo galaxies (compared to the isolated sample) and strongly depleted in the outer part of the discs, which makes the overall star formation rate appear reduced. Thus taking into account only the overall SFR, can lead to a misleading classification criteria, these galaxies being wrongly classified in the past as early-type or S0 galaxies.

Kenney & Young (1989) surveyed the molecular gas masses and distribution of Virgo cluster bright spirals via the CO emission and found that their molecular content is not greatly deficient or particularly unusual, compared to the lack of HI in the outer discs. Thus molecular gas seems to be unaffected by the stripping.

To summarise, tidal interactions and ram pressure stripping both contribute to the evolution of clusters by reducing the gas content of galaxies, and inhibiting SF. Gas stripping by tidal interactions appears to be dominant at the initial stages of cluster evolution (Combes 2004). Interactions with the Intra Cluster

medium (the ram pressure stripping) is more efficient at more recent epochs, after the virialisation, when galaxies have acquired the high velocity required for the interactions to be strong enough to strip the gas. This mechanism is thought to be responsible for the gas-stripping from galaxy discs infalling today into a cluster in nearly radial orbits.

1.5 Where SF is currently very efficient: starburst galaxies

Starburst galaxies are systems going through a phase of enhanced SF activity, where the present SFR is much higher than the average. The large number of these galaxies at high redshift suggests that this was a dominant phase of early galaxies' evolution. The term 'starburst' was introduced by Weedman et al. (1981) when studying the bright and blue nucleus of NGC 7144.

Starburst galaxies can be divided into two types: the UV bright and the UV faint ones. The former have very blue colours and spectral energy distributions dominated by OB stars. Dust extinction occurs, but only in localized patchy regions. The latter are dominated by dust and thus their UV emission is absorbed and re-emitted at far infrared wavelength. These so-called (Ultra) Luminous Infrared Galaxies - (U)LIRG - have infrared luminosities $L_{FIR} > 10^{12}\ L_{\odot}$ and their emission in the range 5 - 500 μm is higher than all other wavelengths combined. Even though starburst galaxies had been identified from ground-based studies, it was only with the Infrared Astronomical Satellite (IRAS) that the ubiquity of these systems was revealed.

Currently 25% of star formation in the nearby universe is occurring in these galaxies (Gallego et al. 1995), while the fraction of star formation in starbursts at high redshift is much greater (Lilly et al. 1996).

Massive star formation is generally concentrated in the nuclei of the galaxies, in particular in the strongest ones (ULIRG). However there are some exceptions and star formation appears to be triggered in regions far from the nuclei, in spiral arms and sometimes in tidal tails (see Combes 2001). The high star formation rates in these systems would quickly lead to the consumption of their gas fuel in less than a Hubble time, thus these events must be correspondingly short-lived.

Strong interactions and mergers of molecular gas-rich spirals are primary mechanisms to induce starbursts (Sanders & Mirabel 1996), particularly at high redshift and for the most luminous ones (see also §1.3.4). Nearly all ULIRGs show morphological evidence of mergers and represent a significant fraction of known distant starburst galaxies (Sanders & Mirabel 1996; Conselice 2002).

Internal physical processes may trigger a starburst in isolated galaxies, such as bar instabilities (Shlosman, Begelman, & Frank 1990), stochastic star formation in spiral density waves[2] (Elmegreen 2002), or kinematics effects from supernovae or stellar winds (Heckman, Armus, & Miley 1990) . However the evidence of these mechanisms being the source of the starburst at high redshift is lacking: galaxies have less organised structures and more irregular morphologies at high z (van den Bergh et al. 2001) and the frequency of bars in galaxies decreases as a function of redshift (Abraham et al. 1999). It seems plausible that different mechanisms may be more efficient at low and high redshift, as if the way of triggering star formation had evolved through time (Conselice 2002). Mergers between galaxies and interactions seem to be the dominant processes at high redshift.

At low redshift the situation is more controversial. According to Telles & Terlevich (1995) many nearby starbursts appear to be isolated. Pustilnik et al. (2002) in an HI survey of blue compact galaxies conclude also that interactions are not the only trigger of SF bursts in starburst galaxies, but their results contradict those of Telles & Terlevich. They find for the majority of the objects surveyed a connection between massive star formation and evidence for interactions with the local environment, such as low mass faint companions or disturbed morphologies. However, in their survey also, a number of galaxies do not seem to show sign of interactions.

1.6 Where SF is inhibited

1.6.1 Low surface brightness galaxies

Freeman (1970) pointed out for the first time that disc galaxies in the Hubble sequence seems to show a very narrow range of surface brightness (SB) in the blue band. In a sample of 36 spirals and S0 galaxies Freeman found that the central SB was centered around the value $\mu_0 = 21.65 \pm 0.35$ B mag arcsec^{-2}. This value is roughly one magnitude brighter than the SB of the darkest night sky. The narrow range of SB has since been interpreted as evidence of a selection effect, implying that our observation of the sky is biased towards the detection of *high surface brightness galaxies*, i.e. brighter than the sky background (Disney 1976; Disney & Phillips 1983). Disc galaxies with SB significantly higher than the Freeman value do not seem to exist.

[2]According to the Lin-Shu hypothesis (1964) the arms are density waves that propagate at global constant speed different from the speed of gas and stars: in this scenario a small perturbation can quickly grow by gravitational instability triggering SF into neighbouring regions

Corteau (1996) for instance, finds that there is a rather well-defined cut-off at a central SB in R of $\sim$ 20.08 mag arcsec^{-2}.

Nevertheless, deep surveys of the sky have revealed the presence of a large population of galaxies with different properties from the "normal" Hubble sequence galaxies and SB dimmer than the Freeman value. Such *low surface brightness* (LSB) galaxies have by definition, central surface brightness, μ_0 fainter than 22.7 mag arcsec^{-2}in the B band.

It was originally thought that galaxies with low SBs were either early or late-type dwarfs (van den Bergh 1959, Nilson 1973), but low surface brightness does not necessarily mean low luminosity or low mass. Previous surveys (Sprayberry et al. 1993, Sprayberry et al. 1995, Impey & Bothun 1997) have shown that these systems are neither exclusively dwarfs, nor the faded counterpart of HSB spirals (de Blok et al. 1995), but rather that they can have a wide range of morphologies and colours (Davies, Phillips, & Disney 1990), scale lengths comparable to the Milky Way and can even reach very high luminosities ($L_B \sim 10^{10}\ L_\odot$) and HI masses ($M_{HI} \gtrsim 10^{10}\ M_\odot$) (Schombert et al. 1992, Impey et al. 1996, Matthews et al. 2001, Knezek 1999, Kilborn et al. 2002). Thus LSB galaxies (LSBGs) span as large a range of masses and sizes and morphological types as HSB galaxies do.

Studies on LSB systems have shown that:

- LSBGs are on average much more gas-rich, in terms of gas-mass-to-stellar light ratio, than brighter galaxies and have extended gaseous discs with low surface densities (van der Hulst et al. 1993, de Blok, McGaugh, & van der Hulst 1996). However numerous gas-poor LSBGs such as early-type dwarf spheroidals are also found in optical surveys. Usually a measure of the richness in gas of a galaxy is described in terms of its gas-mass to blue stellar luminosity ratio, M_{HI}/L_B . I have shown in section §1.2 how this parameter changes along the Hubble sequence. For LSBGs the gas-mass-to-stellar light ratios can reach up to $M_{HI}/L_B \approx 50$ (O'Neil, Bothun, & Schombert 2000).

- the very blue colours of LSBGs and their low average metallicities (around 0.2 - 0.5 solar) initially suggested that these are unevolved, low density systems with a young mean stellar age (McGaugh & Bothun 1994, de Blok et al. 1995). This scenario does not seem to fit the range of properties observed in such galaxies. A survey by O'Neil et al. (1997, 1997a) in the Cancer and Pegasus clusters revealed a significant population of red LSBGs with colour indexes similar to E0, S0 galaxies ($0.8 < B - V < 1.2$, $0.4 < U - B < 0.8$ and $1.0 < V - I < 1.7$). Combined near IR and optical observations in the

last few years have provided a powerful probe to analyse the underlying stellar population of LSBGs disentangling the effects of age and metallicity which can bias pure optical observations. Bell et al. (2000) found that red and blue LSBGs have had very different star formation histories and represent two independent path of evolution of LSB discs: a low, roughly constant SFR for the blue sample, while the red one is more consistent with a "faded HSB disk" scenario, with a period of more intense SF in the past and roughly solar metallicities. From a much larger sample of LSBGs observed in J and Ks bands, Galaz et al. (2002) concluded that a red, old population of LSBGs does exist, exhibiting clear bulges and showing higher SBs in the near IR than in the optical. Morphologically the sample spans the full range of spiral Hubble types, from Sa to Im, and in several cases they appear to be late-type in the optical but with prominent bulges in the IR.

- The lack of strong dust features in optical images (McGaugh & Bothun 1994, de Blok, van der Hulst & Bothun 1995) and generally low Balmer decrements in HII regions (McGaugh 1994) seem to indicate that LSBGs are dust poor systems.

The reasons behind the low evolution rate of LSBs and why they seem to be "frozen" in an apparently stable state are still controversial. The average low gas density throughout the discs has been usually considered as the most likely explanation for their low star formation rates (van der Hulst 1993). If the star formation rate is low, the enrichment in metal of the galaxy is prevented. Metals play a key role in cooling the interstellar medium, and this results in a warm one-phase ISM where gas collapse and subsequent formation of giant molecular clouds is inhibited (de Blok et al. 1999).

A wider description of the issues related to star formation in gas-rich LSBGs will be discussed in the following chapters, through a detailed analysis of the star formation history of three gas-rich dwarf galaxies in the Centaurus A group and their HI properties.

1.6.2 Star formation in low mass systems: dwarf galaxies in the Local Group

The relative closeness of Local Group (LG) dwarfs makes it possible to resolve their stellar populations and trace in detail their star formation histories. These nearby galaxies include different morphological types with stellar populations covering a wide range of ages and metallicities. All the dwarfs in the LG seem to have experienced very different and complicated star formation histories.

The gas-poor dwarf Spheroidal (dSph) galaxies are low mass and luminosity ($-9 < M_V < -14$), poorly

evolved systems usually found within 300 kpc from the two most massive members of the group. They have in general no young stars, yet their stellar population is dominated by old (> 10 Gyr) and intermediate-age stars (between 1 and 10 Gyr) indicating that star formation (SF) continued for many Gyr after their formation. Dwarf spheroidal galaxies must have had in their past higher amounts of gas in order to form their stellar populations. Apart from Sculptor (Carignan et al. 1999), there appears to be no gas within the tidal radius of LG dSphs down to a column density limit of a few times 10^{17} cm^{-2} (Young 1999, 2000). How they lost their gas reservoirs is still an enigma. Dwarf spheroidal galaxies must have had in their past higher amount of HI in order to form their stellar populations. The absence of neutral gas may indicate that the SF process has been very efficient in the evolution of these systems. One of the possible explanations is that the starburst phase rapidly consumes or blows out the interstellar medium (Dekel & Silk 1986). However, the spatial distribution of dSphs close to giant spirals implies that environmental factors may be responsible for the removal of the ISM in these galaxies. Tidal and/or ram pressure stripping are the most popular mechanisms suggested and discussed in the literature.

Nevertheless this scenario can not explain why some dSphs have formed stars in the last 1 or 2 Gyr. Fornax for instance, contains the youngest population of stars (100 - 200 Myr) detected so far in a dSph galaxy (Grebel & Stetson 1999), which are located in a loose association spread over a wide area of the galaxy. A possible solution has been suggested by Maschenko, Carignan, & Bouchard (2004): the far ultraviolet emission from nearby massive spirals such as the Milky Way or Andromeda can be strong enough to ionise the neutral gas content of a dwarf, making it undetectable at 21-cm. If the galaxy is massive enough, the ionised gas is still gravitationally bound. When the dwarf is orbiting around a giant spiral, if it happens to be in such a location that the spiral's UV flux is shadowed by its more massive HI disk, the ionised gas can recombine and, potentially, reform stars for a short period of time.

dSphs galaxies in the Local Group show varied star formation histories. Carina is, with Fornax, the only dSph showing an episodic SFH: its stellar population spans a range of 2 - 14 Gyr but it seems to have experienced a surprisingly long quiescent period from 8 to 12 Gyr (Smecker-Hane et al. 1996). Leo I dSph shows a complex SF history: the majority of its stellar population formed between 1 and 7 Gyr ago, then its star formation rate dropped approximately 1 Gyr ago and stopped around 300 Myr (Gallart et al. 1999). From its CMD it is not clear if it contains an old population of stars (> 10 Gyr old), thus it has been claimed that it is dominated by an intermediate/age, metal poor stellar population (Gallart et al. 1999) That is not the case of the Leo II dSph where the ages of the dominant stellar population can be set between 7 - 14 Gyr

(Mighell & Rich 1996). Among the Milky Way's companions, only Sagittarius and Fornax, the two largest and brightest dwarf spheroidals, are known to contain globular cluster systems (Grebel 1997).

Dwarf spheroidals are generally dominated by either old (> 10 Gyr) or intermediate-age (1 - 10 Gyr) populations (Grebel 2002). In the first case, the galaxies seem to have experienced a rapidly decreasing SFR, to explain the absence of a significant intermediate-age population. Systems dominated by less than 10 Gyr old populations appear to have had a continuous SF in their past that increased soon after the birth of the first generation of stars and stopped after the intermediate-age stars were formed. In these objects SF extended over a period of 7 Gyr or more.

The reason for this different behaviour is still not fully understood. However it is found that the fraction of intermediate-age stars in dSphs increases with the distance from the Galaxy, a trend that could be explained by the decreasing efficiency of gas removal mechanisms like ram pressure and tidal stripping with the galactocentric distance (van den Bergh 1994, Grebel 2002).

Lastly, other galaxies like the very faint Draco and Ursa Minor systems ($M_V \sim -9$) or Sculptor seem to have undergone only a single burst of star formation, although rather extended in time. Their colour magnitude diagrams (CMDs), in fact, resemble those of the globular clusters in the halo of the Milky Way (Carraro 2002).

Dwarf Irregulars (dIrr) show a larger range in both mass and luminosity compared to dSphs, a less clustered distribution and a large variety of SFRs and surface brightnesses. They have ongoing star formation and $M_{HI}/L_B \lesssim 1$. Thus their stellar populations are in general characterised by young stars mostly concentrated in the center (where the gas density is higher), and an underlying more diffuse population of intermediate-to-old population. Unlike dSphs, dIrrs can be found not only in clusters and groups but also in the field.

LG dIrrs appear to have experienced a continuous star formation activity with a constant or varying star formation rate over the Hubble time and gradual chemical enrichment. Their past histories do not seem to be marked with large bursts (Dohm-Palmer et al. 1998) such as those of blue compact dwarf galaxies (with SFRs ranging from 10^{-2} to 1 $M_\odot$ yr^{-1}kpc^{-2}; Tosi et al. 1999). In Sextans A for example, which is among the most active LG dwarfs, the average star formation rate in the last 50 Myr (5×10^{-3} $M_\odot$ yr^{-1}kpc^{-2}) has increased by only a factor of three compared to its recent star formation activity between the age of 100 and 600 Myr.

	Sextans A	Leo A	GR 8	Peg DIG
M_{HI}/L_B	1.4	1.3	0.76	0.47
SFR (10^{-3} $M_\odot$ yr^{-1} kpc^{-2})	2.5	1.5	0.6	0.8

Table 1.2: The M_{HI}/L_B ratios of 4 dIrr galaxies of the LG and the related average SFR over the last 600 Myr. A higher M_{HI}/L_B seems to be related to a larger SFR as it appears in Sextans A and Leo A (from Dohm-Palmer 1998).

Among the dIrrs in the LG the average SFR/area increases with larger M_{HI}/L_B ratios as is observed comparing Sextans A, LeoA, GR 8, and Peg DIG in Tab. 1.6.2 (Dohm-Palmer et al. 1998).

Dwarf galaxies represent a useful laboratory to study star formation and the relation between environment and evolution. Having a simpler structure than spirals, without density waves, bars, shear, or jets global star formation should be, in theory, more straightforward to understand, even if in reality this is not the case. Secondly, small systems are more vulnerable to those effects which can either suppress or enhance star formation, such as feedback, gas loss driven by supernovae shocks, gas-stripping by the interaction with the hot intracluster medium or by the interactions with other systems, and the accretion of new material which can reinvigorate SF for a brief time. dSphs can tell how star formation drops out once the gas has been lost or consumed, while studying dIrrs can give hints on how star formation occurs in low mass galaxies.

1.7 Gas-rich galaxies: young or old systems?

The neutral hydrogen content of a galaxy is a key parameter in determining its own evolutionary status. In the previous sections we have seen how the gas content of galaxies in the Hubble sequence changes according to the morphological type. "Normal" galaxies have M_{HI}/L_B values which in general don't exceed 0.5 (Roberts & Haynes 1994). Nevertheless neutral hydrogen surveys in the last decade have shown the presence of a class of gas-rich objects characterized by large M_{HI}/L_B ratios as high as a few tens (Kilborn et al. 2001, O'Neil, Bothun & Schombert 2000).

High values of the M_{HI}/L_B ratio indicate that a large fraction of the galactic gas reservoir has not been converted into stars yet. One possible explanation is that HI surveys are finding a large local population of *young* galaxies. Alternatively these systems would have been forming stars at a very low rate throughout their evolution. Studying the stellar population of these systems is a key to understanding why they have large amounts of neutral hydrogen compared to their luminosities and eventually to discriminate between the different evolutionary paths. Failure to detect an old population of stars would support the first scenario.

1.8 How to find gas-rich galaxies: 21-cm blind surveys

The obvious way to look for HI rich galaxies is by tracing the emission at 21-cm wavelength of their primordial gaseous content.

Until a few years ago 21-cm observations had been performed on objects that had first been identified in the optical or in the infrared domain, therefore HI studies were affected and limited by optical selection effects. It is well known that optical catalogues are biased against the detection of low surface brightness galaxies and dwarfs (Disney 1976, 1999; Impey & Bothun 1997). Therefore, to obtain a wider understanding of galaxy populations, "blind" HI surveys scanning large areas of the sky represent an extremely important alternative, with the additional advantage of providing redshifts for the HI detections.

There have been a few blind HI surveys in the recent past, although technological limitations have prevented the possibility of mapping large areas of the sky. Before the advent of the multibeam receivers the Arecibo Dual Beam Survey (ADBS) (Rosenberg & Schneider 2000) and the deeper Arecibo HI Strip Survey (AHISS) (Zwaan et al. 1997, Zwaan, Briggs, & Sprayberry 2001) were the largest 21-cm surveys. The ADBS covered an area of 430 deg^2 detecting 265 galaxies, of which 81 were uncatalogued, while AHISS found 66 galaxies half of which were new detections.

The multibeam receivers at the 64 m Parkes telescope in Australia and later on the 76 m Lovell telescope in the UK have made it possible, for the first time, to extend blind 21-cm surveys to large area of the sky reaching reasonable sensitivities and observing comparatively large volumes.

1.8.1 The HI Parkes All-Sky Survey (HIPASS)

The HI Parkes All-Sky Survey (HIPASS) (Meyer et al. 2004, Zwaan et al. 2004) is the largest blind survey to date, covering the whole sky south of $\delta = +25°$ in the velocity range $-1200\ \mathrm{km\,s^{-1}} < cz < 12700\ \mathrm{km\,s^{-1}}$. A multibeam receiver with thirteen feeds has been installed at the focus of the Parkes radio telescope in Australia since January 1997. Therefore the system is at least 13 times faster than previous single-dish surveys. The full-width half-maximum (FWHM) angular resolution of the Gaussian beam of the telescope is 14'.8 at 21 cm. Each receiver is sensitive to a bandwidth of 64 Mhz which is divided into 1024 channels and allows to sample a wide velocity range of $\sim 14000\ \mathrm{km\,s^{-1}}$, with a velocity resolution of $18\ \mathrm{km\,s^{-1}}$.

As underlined before, the primary aim of the multibeam project was to obtain a large area survey of the extragalactic population of galaxies free of optical selection effects by investigating the distribution of neutral hydrogen in the nearby universe. It consisted of three major parts:

- a survey for HI emission over the entire southern sky south of declination +25°, with an effective integration time per pointing of 450 s;
- a factor of two deeper survey of a part of the "Zone of Avoidance" (ZOA) region (l = 213° to 33° , $|b| < 5°$) with the same velocity range
- a deep survey of a 4° × 8° region in the Centaurus cluster area with a total integration time higher by a factor of twenty: HIDEEP (Minchin et al. 2003).

The complete HIPASS catalogue has now been released and is available to the astronomical community (Meyer et al. 2004), including 4315 sources identified by their HI content.

However subsets of the HIPASS database had been already analysed and published. Among which, the south celestial cap region (SCC) at declinations $\delta < -62°$, covering an area of $\sim 2400\ \mathrm{deg^2}$ has been the first catalogue presented. 536 galaxies have been found including 114 newly discovered objects, a small number of HI massive galaxies with $M_{HI} > 10^{10}\ M_{\odot}$ (about one order of magnitude larger than the HI mass of our galaxy), and a small population of low-velocity HI clouds without a corresponding visible counterpart. The average M_{HI}/L_B ratios of the sample is greater than 1 and increases with the morphological type, from 1.8 for early-type to 3.2 for late-type galaxies. The HIPASS Bright Galaxy Catalogue (BCG) consisting of the 1000 galaxies with the highest peak flux densities has been also recently released (Koribalski et al. 2004). The BCG has been used to measure the HI Mass Function (HIMF) (Zwann et al. 2003), which is the

neutral hydrogen equivalent of the optical Luminosity Function (LF) and can be fitted as well by a Schechter function. Determining the faint-end slope of the HIMF is crucial to understanding galaxy formation models. The HIMF measures the baryonic component of galaxies which has not yet processed into stars. Determining the HIMF from a non optically selected sample prevents from missing low luminosity HI rich galaxies from cataloguing.

Different results have been obtained for the faint-end slope α of the HIMF. Zwaan et al. (1997) found $\alpha = -1.2$, while Rosenberg & Schneider (2002) claimed α to be -1.53. The result found by Zwaan et al. (2003) from the BCG set $\alpha = -1.30$ and the slope is found to be morphological type dependent. In particular, according to Zwaan and collaborators, Sbc-Sc galaxies are the main contributors to the total HI mass density, while LSB galaxies contribute only to the 15% of the total HI mass density. Minchin et al. (2004) claim that this can only be a lower limit because Zwaan assumed that LSBG's are just as easily detected as HSBGs.

1.8.2 HIJASS: a blind HI survey in the northern hemisphere

The HI Jodrell All-Sky Survey (HIJASS) (Lang et al. 2003) is the analogue of HIPASS in the northern hemisphere. When completed, it will provide a 21-cm map of the sky at a declination $\delta > 22°$. A multibeam receiver with 4 elements (compared to the 13 at the Parkes telescope) has been mounted on the Lovell telescope at Jodrell Bank Observatory (UK). The technical characteristics of the two surveys are very similar: a 64 Mhz bandpass with 1024 channels is used, the velocity resolution is 18 $\mathrm{km\,s^{-1}}$, and the spatial positional accuracy corresponds to $\sim 2.5'$. Local interference corrupts the range of useful frequencies to investigate, restricting the velocity range to between -1000 and 4500 $\mathrm{km\,s^{-1}}$, and between 7500 $\mathrm{km\,s^{-1}}$and 10000 $\mathrm{km\,s^{-1}}$. The survey has covered so far about 2000 $\mathrm{deg^2}$, of which 1115 $\mathrm{deg^2}$, including the whole strip with $70^o < \delta < 78^o$ and part of another strip at $62^o < \delta < 70^o$, has been published. Among the 222 published detections, 170 correspond to previously catalogued galaxy, 23 are associated with an optical counterpart for which previous measurements of the redshift are not available, and 29 objects are previously uncatalogued.

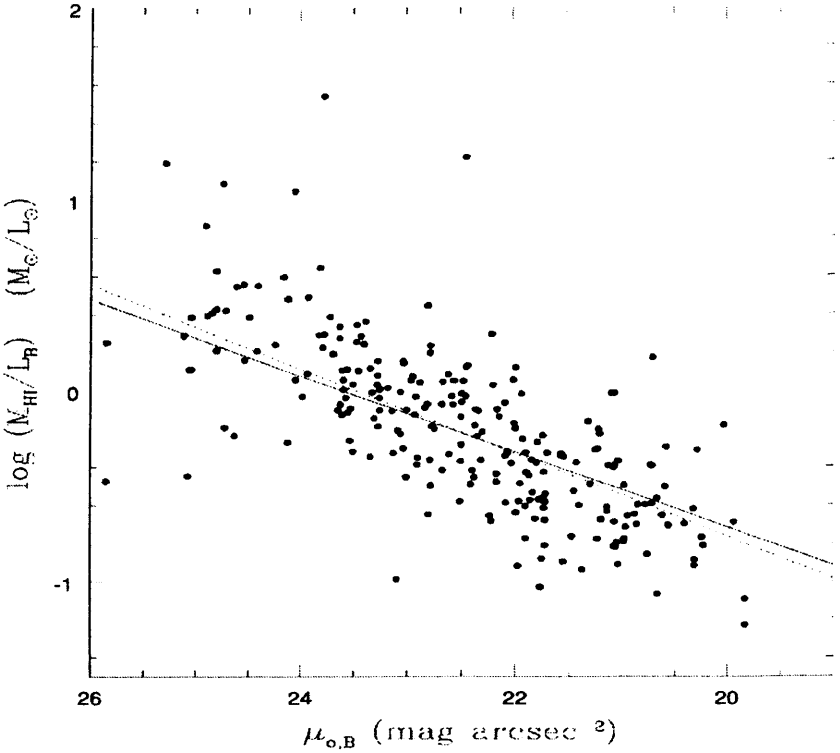

Figure 1.5: The correlation between M_{HI}/L_B and surface brightness for a sample of galaxies taken from the APM survey. The dotted line corresponds to a slope of 0.22. (from Burkholder, Impey, & Sprayberry 2001).

1.9 Properties of gas-rich galaxies

The properties of gas-rich galaxies partially overlap with those of LSB and dwarf Irregulars described in the previous sections. The general picture coming out from studies of gas-rich galaxies is that they cover a large range in masses, morphology, and optical luminosity.

There is strong evidence for a relation between M_{HI}/L_B and central surface brightness (μ_0) in galaxies (McGaugh & de Blok, 1997; Burkholder, Impey, & Sprayberry 2001): M_{HI}/L_B ratios increase for lower surface brightness (SB) disc galaxies (see Fig. 1.5). This has been interpreted as an evolutionary effect (McGaugh & de Blok 1997). M_{HI}/L_B is well correlated with the gas fraction of a galaxy as it can be shown by

$$f_g = \frac{M_g}{M_g + M_\star} = \left(1 + \frac{\Gamma_\star L}{\eta M_{HI}}\right)^{-1} \tag{1.7}$$

where M_g is the total gas mass, $M_\star$ is the mass in stars, $\Gamma_\star$ is the stellar-mass-to-light ratio, and $M_g = \eta M_{HI}$, where η is a correction factor that takes into account the contribution of helium and molecular phases to the total gas mass. Therefore, such a correlation between μ_0 and M_{HI}/L_B implies that the central SB of a galaxy is a good indicator of the amount of gas that is converted into stars and of the evolutionary state of a galaxy. The high M_{HI}/L_B may indicate that these galaxies formed recently. However, recent studies are finding increasing evidence for a substantial old population of stars which supports the hypothesis that these objects are not young. Some of these studies are briefly presented and discussed in the rest of this section.

Among the population of LSB galaxies discovered by O'Neil et al. (1997) a subset of red ($B - V \gtrsim 1$) and extremely gas-rich galaxies ($M_{HI}/L_B > 9$) have been found in a follow-up with the Arecibo telescope (O'Neil, Bothun, & Schombert 2000). Surprisingly these galaxies can have amongst the largest gas-mass-to-stellar luminosity ratios ever observed. The red colours of these systems indicate that they have been capable of forming and evolving at least one generation of stars to reach such colours. It is unclear why the SF process stopped when they still contain a large fraction of gas. Since the optical counterparts are characterized by small scale-lengths, around or less than 2 kpc for the highest M_{HI}/L_B ratios, one possible explanation may be that the small optical cores are the visible counterpart of a more extended HI distribution whose average gas density is too low to trigger star formation. Thus the bulk of the gas content is in the form of a very diffuse and low column density ISM. However, if their optical and HI size coincide, their average gas density is above 10^{21} cm^{-2} and these objects are inexplicably not forming stars (O'Neil et al. 2000).

A sample of LSB gas-rich dwarf galaxies (mean $M_{HI}/L_B = 5$) extracted from the Second Palomar Sky Survey has been investigated both in the optical (V,I) and in their HI content (Schombert et al. 2001). A young mean age due to either constant or increasing star formation rate with e-folding timescales between 7 and 11 Gyr is, according to the authors, the most likely scenario to explain the optical colours observed. Comparison with star formation models in fact indicates that the dominant stellar populations is less than 5 Gyr old, although, according to the authors, this does not exclude the existence of an old (t > 10 Gyr) population of stars. The SF rates of around 0.01 $M_\odot$ yr^{-1}and the consequent long time scale to consume the gas content at such rates, may explain why gas-rich LSB dwarfs typically have much higher gas fractions than disc galaxies.

van Zee (1997b) studied a sample of 28 isolated gas-rich galaxies detected in a survey of isolated galaxies with no known neighbour closer than 20′ (at least 140 kpc) with the Arecibo telescope (van Zee, Haynes, & Giovannelli 1995). The galaxies showed an inhibited star formation process, with rates between 0.0015 and 0.35 $M_{\odot}$ yr^{-1}, and very long gas depletion time scales (about 10^{11} yr). For those galaxies with the highest M_{HI}/L_B ratios, 15 in total, broad band colours ($UBVR$) have been obtained to constrain the evolutionary history (van Zee et al. 1997c). The dominant stellar population as it appears from combined $UBVR$ photometry is at least 2 - 4 Gyr old. Another gas-rich dIrr galaxy, UGCA 20, with $M_{HI}/L_B = 2.8$ (about three times higher than typical dIrrs) and low metallicity (oxygen abundance $\sim 1/17$ of solar), shows an old stellar population, and star formation occurring at a constant but suppressed rate for the last 4 Gyr (van Zee et al. 1996).

However gas-rich dwarf galaxies can be found also with high star formation rates. Blue compact dwarfs are gas-rich objects undergoing an intense burst of star formation. They are metal poor, with luminosities ranging between -12 $\lesssim M_B \lesssim -17$ and extremely blue colours. The observed HI mass-to-light ratios are in the range $0.1 \leq M_{HI}/L_B \leq 2.0$ in solar units, which makes BCDs as gas-rich as spirals or dIrrs but less than LSB dwarfs. Taking into account the significant brightening during the burst, BCG progenitors may well have had larger M_{HI}/L_B ratios, comparable to those of gas-rich dwarf galaxies found in other samples (van Zee 1997a,b,c). The detection of an underlying older stellar populations in BCDs, in addition to the young and bright blue stars, confirms that, rather than forming now their first generation of stars, BCDs have experienced star formation in episodic short bursts separated by long quiescent periods (Papaderos 1996, Kunth 2000 and references therein). BCDs can be included in the general dIrr classification, but starbursting episodes in low mass galaxies seem to be rare rather than being a necessary phase in their evolution (van Zee et al. 2001). Studies of dwarf irregular galaxies have shown that their SFHs are essentially characterised by a low but continuous level of activity (van Zee 2001a). Therefore, the class of dIrrs include a wide range of properties from the low to high surface brightness regime, where galaxies can have varied star formation rates and gas content.

1.10 Distribution of gas-rich galaxies

Recent large HI surveys are providing a picture of the largescale distribution of gas-rich galaxies. The HI detected galaxies tend to follow the large-scale structure traced by galaxies sampled in optical surveys.

Nevertheless they are found in regions of low galactic densities, where the chances of gas losses due to interactions with other galaxies and/or stripping are lower. For instance, HI rich galaxies are not preferentially detected in the core region of galaxy clusters, rather they tend to be found in the infall regions beyond the core, as a survey in Fornax has recently shown (Waugh et al. 2002).

HIPASS and HIJASS have found previously uncatalogued gas-rich galaxies, but these systems do not fill the voids either, and they follow the general distribution of the optically catalogued galaxies (Kilborn et al. 2002).

In the search for Malin type objects, i.e. extremely gas-rich galaxies which appear similar to LSB dwarf ellipticals in the optical, Davies et al. (2000) built a sample of 26 galaxies with high M_{HI}/L_B by cross-correlating HIPASS data with an optical LSB galaxy sample of Morshidi-Esslinger et al. (1999) and studied their spatial distribution. While the complete optical sample of galaxies is concentrated in the centres of the groups and clusters in the survey area (such as Fornax, Dorado, Sculptor), the gas-rich galaxies tend to be found in the outskirts of the group/clusters in the regions of low galactic density. However, HI rich galaxies have radial velocities which are similar to those expected for the bright galaxies. For example the majority of the HI galaxies of the sample is found around 1500 $\mathrm{km\,s^{-1}}$, and the groups/clusters inspected have all redshift below 2000 $\mathrm{km\,s^{-1}}$. Again, this result suggests that even if gas-rich systems occupy low galactic density regions, their distribution is still associated with the large scale structure traced by the brighter galaxies.

1.11 Summary: what do we know about star formation

Star formation regulates the transformation and the "recycling" of matter in galaxies and it determines the main properties of a system such as total luminosity, colour and metallicity. Our knowledge of the process is primarily based on the observations of the Milky Way and the galaxies of the Local Group where more detailed information can be collected.

Molecular clouds are the formation sites of stars and clusters, and their detection is performed using tracer molecules such as carbon monoxide (CO). The typical mass of the giant molecular clouds in the Local Group ranges from 10^5 to 10^6 $M_\odot$, with radii $R \sim 50-100$ pc. Local starbursts in such environments offer a unique opportunity to gain a close insight into the efficiency, the evolution and the stellar population of the SF events. The giant galactic HII region NGC 3603, at a galactocentric distance of $\sim$ 8 kpc, and 30 Doradus

in the Large Magellanic Cloud, the most luminous starburst in the Local Group, are the closest regions to study very high star formation rates. The presence of multiple stellar generations with ages from 25 Myr (red supergiants) to 1 - 2 Myr (main sequence O stars) seems to indicate that SF in these environments occurs as a "continuous" and still ongoing process rather than being a single event (Brandner 2002). The SF activity in 30 Doradus seems to be currently slowing down, in agreement with the typical dispersion timescale (20 - 30 Myr) for molecular clouds (Brandner 2002). The original central starburst appears to be replaced now by a peripheral SF activity due to the creation of a supershell (or arc) after the explosion of several supernovae which compresses the ISM inducing further activity at the border of the region.

The Milky Way satellites where stars can be resolved not only with the HST, but also with ground-based telescopes, provide ideal targets to investigate and compare global evolutionary histories and chemical evolution.

The best example is the Large Magellanic Cloud (LMC), which, at a distance of 50 kpc, is the nearest satellite with a significant mass (around 10^{10} $M_{\odot}$). Thus, stars with masses as low as 0.6 $M_{\odot}$, down to the oldest main sequence turn off (MSTO) and beyond, can be detected with the HST. Finding such stars is extremely important because they have not evolved significantly during the history of the galaxy, thus they provide information on the early stages of the evolution of the galaxy. Its SFH though appears to be complicated. The LMC bar and disc experienced a similar SFH at older ages (between 7.5 and 15 Gyr) (Smecker-Hane et al. 2002). At younger epochs instead, the bar is dominated by two distinct enhancements in the SFR from 4 to 6 Gyr and between 1 and 2 Gyr ago, while the disc experiences a rather constant SFR. The increase in the SF activity around 6 Gyr appears to correspond to a period of close interaction between the LMC, the Small Magellanic Cloud (SMC) and the Milky Way.

The case of the dSph Sagittarius, located behind the galactic bulge at a distance of 25 kpc, provides a more dramatic example of a very close system which is being disrupted by the gravitational potential of the Milky Way. The current understanding of the SFH of Sagittarius suggests three principal episodes at 11, 5 and between 0.5 and 3 Gyr creating populations with increasing metal abundances ([Fe/H][3] = -1.3, -0.7 and -0.4 respectively) and its disruption is thought to have been going on for at least several Gyr (Majewski et al. 2002).

Therefore very nearby satellites enable us to study the effects of the environment, in particular of the gravitational interactions, on the SFHs of galaxies.

[3]The metallicity of stellar populations is often expressed as the mean iron abundance where [Fe/H]= $\log(Z/Z_{\odot})$

The other satellites of the Milky Way are essentially gas-poor dwarf spheroidal galaxies (excluding the Small Magellanic Cloud) where SF has now stopped, which show a wide range of evolutionary histories. Gas-rich dIrrs, usually found at larger distance from the Milky Way with ongoing star formation activities provide a sample to study how this mechanism is currently taking place in nearby low-mass systems.

There are a number of issues and common properties worth summarising that will be analysed and discussed in the following sections:

1. All galaxies studied so far in the LG appear to have a population of old stars that in many cases represent the dominant stellar population. This is valid for both dSphs and the dIrrs with deep enough photometry to detect such faint stars. Therefore, LG galaxies share a common past of ancient SF and there seems to be no apparent evidence of a delayed start in the star formation activity in the LG so far: there are no recently formed galaxies in our neighbourhood. But has the SF process started at the same time everywhere in the nearby Universe? Are there "young" objects which have formed in the last few Gyrs or so outside the Local Groups, in the closest clusters of galaxies?

2. Star formation rates in nearby galaxies occur in the following modes (Grebel 2002)

   - Continuous over the Hubble type (either constant or varying) causing gradual chemical enrichment as in massive dIrrs.
   - Continuous decreasing SFR, eventually leading to an interruption of the SF activity, as in most dSphs, dEs and low-mass dIrrs.
   - Episodic SF events with periods of quiescence lasting a few or several Gyr as has occurred in the puzzling evolution of the dSph Carina.

   What are the mechanisms that drive such differences in the evolution of galaxies? What is the connection between different SFHs and the varied gas contents? How does metallicity affect the formation of molecular gas and consequently the star formation rate of a galaxy, especially in low mass systems?

3. Dwarf galaxies in the LG are essentially divided into two classes: those with gas and those without. dIrrs have an abundant supply of gas and yet they have not converted it into stars in an efficient manner and their recent SF does not seem to be characterized by large bursts of SF (Skillman 2001). dSphs instead seem to have consumed or lost all their gas content. This scenario though shows some exceptions, such as the presence of a young population of stars in the Fornax dSph. Galaxies such

as LGS 3, Phoenix or Aquarius (DDO 254) may hold the key to finding answers to some of these issues, since they contain some gas but are not currently forming stars. Therefore, does the evidence of galaxies with intermediate properties between dSphs and dIrrs suggests an evolutionary link between dSphs and dIrrs? Is there a connection with the environment that may explain such a morphological evolution?

Substantial issues remain to be addressed. One way to try to find some answers is to study other groups and compare properties of different environments with those of the LG. This is extremely important to widen our knowledge of the star formation process, and to look for objects with different properties that may help in the understanding of the evolution of galaxies. It is from this basis that we start this work on a sample of gas-rich dwarf galaxies in the Centaurus A group that I will present in the following sections.

1.12 Map of the thesis

In **Chapter 2** I present the sample of three gas-rich dwarfs in the Centaurus A group for which we have obtained HST/WFPC2 images and 21-cm high resolution maps and the main targets and difficulties of our analysis. I briefly introduce the structure and members of the group, the results of the previous surveys, the HST/WFPC2 and 21-cm observations, and finally the data reduction.

In **Chapter 3** I present the tools that will be used to analyse and discuss this data set: colour magnitude diagrams as an age indicator, the radial gradients in the stellar population, the use of synthetic CMD to simulate the star formation history of a galaxy, and the search for HII regions to derive independent constraints on the metallicity of these systems.

In **Chapter 4, 5, 6** I discuss the properties of the three dwarfs, each chapter being dedicated to a single object: HIPASS J1337-39, HIDEEP J1337-33, HIPASS J1321-31 respectively. I describe the stellar population resulting from their CMD, the way young and old stars, if present, are distributed throughout the galaxy, the gaseous properties and their link to the star formation activity, and finally the model star formation history obtained with the StarFISH code (Harris, & Zaritsky 2001). Other studies of gas-rich dwarf galaxies are presented and used as a comparison.

Chapter 7 contains a discussion and summary of the main issues and results for this data set.

In the **Appendix A** I discuss a small sample of HI massive galaxies ($M_{HI} > 10^{10}\ M_{\odot}$) selected

from HIPASS. This is part of an ongoing project and we present the data set and the preliminary results. Optical (B, V, I), near infrared observations (J, only for a few of them) and 21-cm high resolution maps are described here. Previous works on HI massive galaxies are reviewed and compared.

Chapter 2

Gas-rich dwarfs in Centarus A: the data

2.1 Overview

An HI study of the Centaurus A group was carried out in 1997 as the pilot survey for HIPASS (Banks et al. 1999). The group was chosen because of its proximity (3.5 - 4.5 Mpc), because a very careful survey had been completed in the optical which could serve as a comparison (Côté et al. 1997), and to give an idea of the promise of multibeam 21-cm surveys. The HI survey found new gas-rich members: among them five previously uncatalogued very LSB galaxies with HI masses around 10^7 $M_\odot$, and $M_{HI}/L_B > 1$. An additional dwarf with similar properties was found in the same region in another 21-cm blind survey, HIDEEP (Minchin et al. 2003), which covered a smaller region ($4° \times 8°$) in the Centaurus cluster area, being about $\sqrt{20}$ times deeper than HIPASS in column density sensitivity. Given their 'extreme' characteristics - i.e. very gas-rich, low surface brightness and low luminosity - which do not seem to have analogues in the Local Group, four among such detections were chosen to be followed up with the Wide Field Planetary Camera 2 (WFPC2) on board of the HST and with the Australian Telescope Compact Array (ATCA). Thus far, objects with such a high gas mass fractions have not been found in our "neighbourhood". Secondly the relative closeness of the Centaurus A group would allow, in principle, the derivation of the star formation histories of these dwarfs directly from their resolved stellar populations, though it would be a very challenging

undertaking given their distances. These galaxies are puzzling because, in principle, they represent an ideal SF environment, given their large gas fractions and their presence in a such a fairly populated group such as Centaurus A, that would provide the opportunity for tidally induced SF events. Yet their M_{HI}/L_B 's indicate that SF has been suppressed during their evolution.

Our purpose was to study the SFH of such objects to try to understand why they are able to retain a large amount of gas without converting it into stars. As a first step we need to identify their different stellar populations providing information on the age of the galaxy. Secondly, tracing the spatial clumping of the stars may help distinguishing between different types of SFH: for example, little clumping of young blue stars and a diffuse distribution of more evolved red ones may be interpreted as the consequence of a continuous but low star formation activity. This scenario would also imply low stellar metallicity because a small fraction of the gas has been processed into stars. Therefore it is important to set constrains on the abundances of these objects from metallicity indicators such as the colour of the red giant branch or by investigating the spectra of HII regions, if any. Finally the analysis of the HI distribution and the comparison between column density maps and the stellar spatial clumping is an essential tool to investigate the relation between gas density and star formation rates and to understand why they are able to retain a large amount of gas without converting it into stars.

Nevertheless, several difficulties affect such an analysis: only the brightest feature of the CMD (i.e. those at $M_I \lesssim -2$) would be resolved with the HST, and we would not unambiguously constrain the old (> 10 Gyr) star formation history, since indicators such as RR Lyrae stars (see Chapter 3) are too faint to be detectable. Secondly, due to the age-metallicity degeneracy, constraining the age of the stars, in particular of those in the red giant branch, without an independent measure of the metallicity, would be extremely difficult. As previously mentioned, HII regions might be used to set an upper limit on the metallicity of a galaxy, although the presence of star forming regions in such low surface brightness galaxies could not be guaranteed. These issues will be thoroughly discussed in the following chapters.

After discussing the general properties of the Centaurus A group in sections §2.2, I will present our data set: the 21-cm high resolution maps taken with ATCA (§2.3) and the WFPC2 followups (§2.4).

2.2 The Centaurus A group

Centaurus A is one of the nearest groups of galaxies outside the Local Group and covers about 1000 square degrees of sky (12^h < RA < 15^h , 30° < δ < 54°) down and through the Galactic plane. It is a heterogeneous assembly of early to late-type galaxies, characterised by the largest dispersion of morphological types observed among the 55 nearest groups (de Vaucoulers 1979). Almost all of its main members show peculiar properties. Its brightest and most massive galaxy, NGC 5128 (Cen A), is classified as a S0 peculiar, is the nearest early-type giant and a very active radio galaxy with huge double radio lobes extending about 9° from north to south. It is the strongest continuum radio source in the sky and also shows extended ($\sim 7° \times 1°.5$) X-ray jets associated with the radio lobes (Arp 1994). Its rather chaotic morphology is believed to be the consequence of a recent merger with a spiral galaxy (Dufour et al. 1979, Graham 1979). According to de Vaucouleurs (1979) early-type systems are very unusual in loose groups. The second main member is the spiral SBc(s) NGC 5236 (M 83). It is undergoing a strong burst of star formation probably due to gas accretion from NGC 5253 (Telesco and Harper 1980; van de Bergh 1980), an irregular galaxy which has experienced in its recent past a vigorous burst of star and cluster formation, now restricted to the nuclear region (van den Bergh 1980). The amorphous morphology of NGC 5253 and the anomalous supernovae rate (two in less than a century), confirm that it has recently emerged from an epoch of unusual activity, probably related to a close encounter with M 83 less than 1 Gyr ago (Thim et al. 2003). The third largest galaxy, NGC 5102, is an S0 galaxy with a significant amount of neutral hydrogen ($M_{HI} = 3 \times 10^8\ M_\odot$, $M_{HI}/L_B = 0.13$, Gallagher et al. 1975) which bears evidence of recent star formation activity and appears to be in a post-starburst phase (Pritchet 1979, Deharveng et al. 1997). Lastly, the 'S-shape' barred spiral NGC 4945, is a starburst galaxy hosting a Seyfert nucleus. It is one of the brightest extragalactic sources at 100 keV (Done, Madejski, & Smith 1996) and one of the closest examples where an AGN and a starburst coexist.

The group members appear to be experiencing intense SF activity that has been interpreted in previous studies as the effect of the accretion of gas-rich dwarf objects (Graham 1979; van Gorkom et al. 1990).

The distance of the group was originally set by de Vaucouleurs at d = 4.0 Mpc (1975). Soria et al. (1996) place NGC 5128 at 3.6 ± 0.2 Mpc - $(m - M)_0 = 27.8 \pm 0.2$ by determining the tip of the Red Giant Branch (TRGB) with WFPC2 observations, while, also from the TRGB, Harris et al. (1998) obtained a distance modulus of $(m - M)_0 = 27.89 \pm 0.15$ corresponding to 3.9 ± 0.2 Mpc. Karachentsev et al. (2002) assumed a distance of d = 3.6 Mpc for the galaxy based on Soria et al. (1996) result.

M 83 appears to be farther than Cen A: Thim et al. (2003), from the observation of Cepheids, derive a distance $d = 4.5 \pm 0.3$ Mpc - $(m - M)_0 = 28.25 \pm 0.15$. From Cepheid luminosities and Type Ia supernova 1972E, NGC 5253 appears to be at $d = 4.0 \pm 0.3$ Mpc (Saha et al. 1995, Thim et al. 2003). Given its angular separation of only 2° (150 kpc) from M 83, it is likely that NGC 5253 is a close neighbour of the bright spiral galaxy.

The spatial separation between M 83 and NGC 5128 amounts to almost 1 Mpc, and for this reason Karachentsev et al. (2002) suggested that Centaurus A is divided into two subgroups. This hypothesis will be discussed in the following section.

2.2.1 Previous surveys of the CenA group

de Vaucouleurs (1975) originally recognized 5 galaxies clustered around NGC 5128 and designated the group as "G4", since it was the fourth closest group of galaxies in his catalogue.

A more recent optical survey in the region was carried out by Côté et al. (1997). They surveyed an area of approximately 900 square degrees and found 20 dwarf galaxies in the group (mainly gas-rich dwarf irregulars) of which 2 were newly identified. Subsequent HI and Hα follow-ups were used to confirm the membership of potential candidates. From this first survey the main members appeared to be aligned in a long chain, with the HI detected dwarfs (dIrr) having a wider spatial and velocity distribution. Four gas-rich neighbours were found around M 83 in this survey, but none near NGC 5128, presumably because its strong X-ray emission makes Cen A a very hard environment for the "survival" of gas-rich satellites.

As I have mentioned in the Overview of this chapter, a multi-beam HI survey was carried out of the Centaurus A group region in 1997 (Banks et al. 1999). This "blind" 21-cm survey investigated the HI content of a nearby group independently of previous optical observations for the first time. In fact, most of the studies of HI in groups up to that time had been performed on members originally selected from their optical properties as in van Driel et al. (1997) and Hutcheimer & Skillman (1998) in the M 81 group or Hutcheimer, Karachentsev & Karachentseva (1998) in the IC342/Maffei, NGC 6946 and NGC672/IC1727 groups. Maia & Willmer (1998) investigated the HI content of "loose" groups, again starting from pointed optical observations. The HIPASS survey of Centaurus A covered a region of 600 square degrees at a mean velocity of $v_{helio} \sim 500$ km/sec and added 10 new group members, among which five were known galaxies with wrong or no redshift measurements, and five were previously un-catalogued gas-rich dwarf galaxies with

HI masses around 10^7 $M_\odot$ (close to the threshold sensitivity of the survey at a distance of 3.5 Mpc), and $M_{HI}/L_B > 1$. The newly identified galaxies showed varied optical morphologies. The already catalogued galaxies had high central surface brightnesses, thus they were likely to be mistaken as background galaxies. The uncatalogued instead were faint, LSB objects with small angular size and could be found in such a blind survey only because they are anomalously rich in gas. Another eighteen sources were found, which were identified with previously known group members. The HI detections were used to determine the low mass slope of the HI mass function, as $\alpha = 1.30 \pm 0.15$. Another dwarf, with lower HI mass (5×10^6 $M_\odot$) was found in the same region by the deeper 21-cm blind survey, HIDEEP (Minchin et al. 2003). All of the new six detections appear to have optical counterparts, although very faint ($M \sim 11$) and LSB (central surface brightness, $\mu_0^B \gtrsim 24$ mag arcsec^{-2}).

A similar survey aimed at finding exclusively dwarf elliptical candidates has been pursued by Jerjen and collaborators (2000a). The survey covered the same area as Côté et al. (1997) and added 13 new dSph members to the group. They calculated the distance of five dSphs (Jerjen, Freeman, & Binggeli 2000b) by the method of Surface Brightness Fluctuations and inferred the membership of another 8 dwarfs to the group on the basis of morphological and photometrical similarities (Sersic parameters). The survey led also to the addition of two more dIrr galaxies (ESO381-018 and AM1318-444).

As part of the Hubble Space Telescope snapshot (SNAP) program the distances of seventeen galaxies in the group were obtained by Karachentsev et al. (2002) from the magnitude of the tip of the red giant branch. The majority of the targets were taken from the results of an all-sky search for nearby dwarf galaxy candidates, based on the POSS II and ESO/SERC plates and were mainly dwarf spheroidal, low surface brightness galaxies. The survey added seven more members to the group.

The projected distribution of the 62 members of the group is plotted in Fig. 2.1 together with the three dimensional map of those members whose distance is known.

2.2.2 Comparison with the Local Group

The brightest members of the group are distributed along a "loose chain", as originally described by de Vaucouleurs (1975), elongated in the north south direction (see upper panel of Fig. 2.1). The dwarf spheroidal galaxies seem to follow the main structure defined by the bright galaxies, while the HI detected dIrr galaxies are more irregularly distributed and can also be found in regions of low density far from the

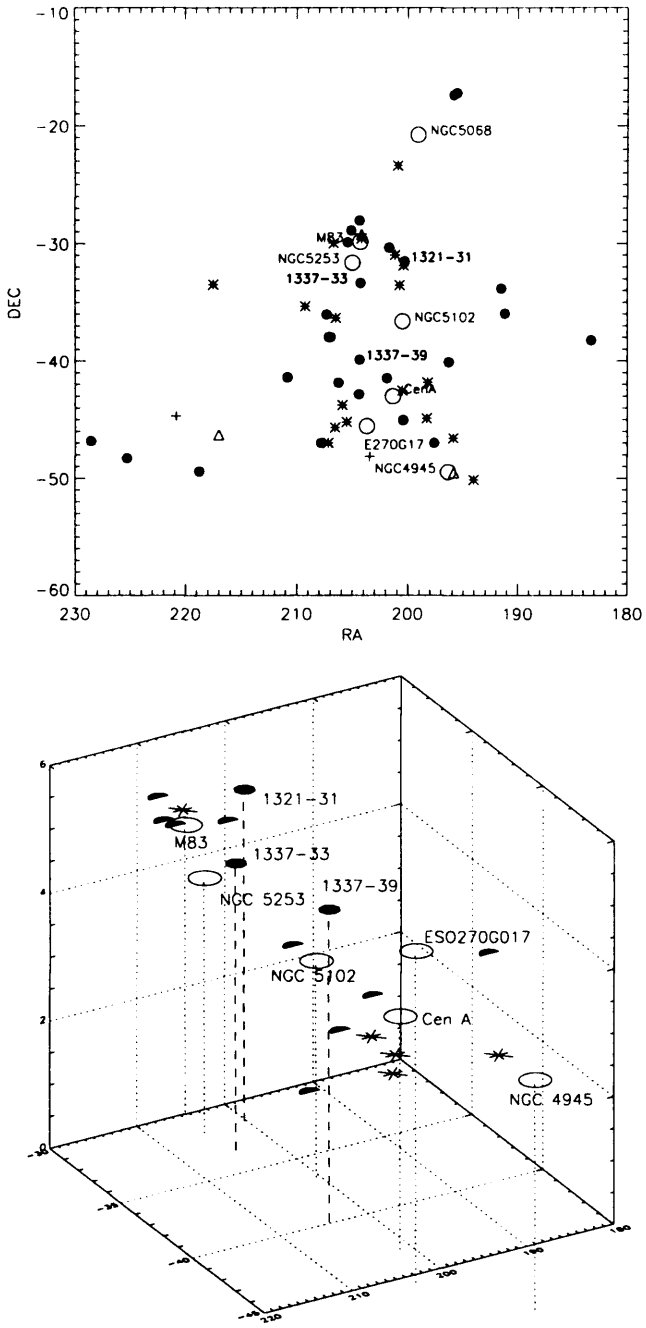

Figure 2.1: The Centaurus A group: **up)** sky-projected distribution of its members. The brightest galaxies are identified by the *big circles* and their ID, the dIrrs are the black *filled circles* where the three HIPASS/HIDEEP dwarfs studied in this thesis are indicated by their HIPASS catalogue numbers. *Asterisks* indicate the population of dSphs. The *crosses* correspond to the galaxies with Hα but no HI detection in the Côté survey and the *triangles* to those with HI but no Hα detection in the same survey. **down)** The three dimensional map of the group for the members whose distance is known: the *big circles* correspond to the main members, the *asterisks* to the dSphs, the *filled half moons* represent the dIrr population. The *filled circles* corresponds to the three HIPASS/HIDEEP dwarfs.

largest members, as is also observed in the Local Group.

The inner structure of the Centaurus A group remains uncertain: according to Karachentsev (1996, 2002) the two massive galaxies, NGC 5128 (CenA) and NGC 5236 (M 83) are the centres of two separate subgroups. However, Van den Bergh (2000), Tully (1987) and de Vaucouleurs (1975) instead consider that all the brightest members form a single group.

Assuming that the centre of Centaurus A is NGC 5128 - at a distance of 3.9 Mpc - van den Bergh (2000a) estimated the total mass of the group using the HI velocities of its members from Banks et al (1999). He found a total mass of $M_{tot} = 1.8 \times 10^{13}\ M_{\odot}$ with an half mass radius $R_h = 640$ kpc and a radial velocity dispersion $\sigma_r = 114 \pm 21\ \mathrm{km\,s^{-1}}$. This would make it about seven times as massive as the Local Group and almost two times more extended ($R_h \sim 350$ kpc). Its mass-to-light ratio, $M/L_B = 155 - 200$ in solar units, would be comparable to that of less populated clusters (Girardi et al. 2000) but significantly larger than the Local Group ($M/L_V = 44 \pm 12(M/L)_{\odot}$; Corteau & van den Bergh 1999).

According to Karachentsev et al. (2002) however, the two spatially separated subgroups are centred at $d_{CenA} = 3.66 \pm 0.07$ Mpc and $d_{M83} = 4.57 \pm 0.05$ Mpc and the M 83 group is moving away from Cen A at a relative radial velocity of 55 $\mathrm{km\,s^{-1}}$. Their estimated orbital masses are respectively $2.1 \times 10^{12}\ M_{\odot}$ and $M = 0.8 \times 10^{12}\ M_{\odot}$ and their mass-to-light ratios are comparable to that of the LG.

Whether the two groups are separated or not partly depends on the assumed distance of NGC 5128, which is found to range in the literature between 3.6 and 4.0 Mpc. However, determining the distances of the M 83 and NGC 5128 neighbours can help discriminating between the two scenarios. Karachentsev and collaborators find a clear distinction between objects with average distance around 3.6 Mpc and those with average distance is 4.5 Mpc: a result that strengthens the two subgroups interpretation.

If it is a single group, Centaurus A is the richest environment within the Local Volume, with a variety of members spanning different morphological types, especially early-type galaxies. Sculptor, for instance, is a very low density group, lacking both early-type members and bright Milky-Way-like spiral galaxies. The M 81 group has about 28 members of which 23 are dwarf candidate members. It is a very compact group, where the core galaxies - the large spiral M 81, the peculiar galaxies M 82 and NGC 3077, and the small spiral galaxy NGC 2976 are strongly interacting as it is indicated by the big HI structure which surrounds them (van Driel et al. 1997; Boyce et al. 2001).

One last thing that should be underlined in the comparison of the Centaurus A and the LG is the

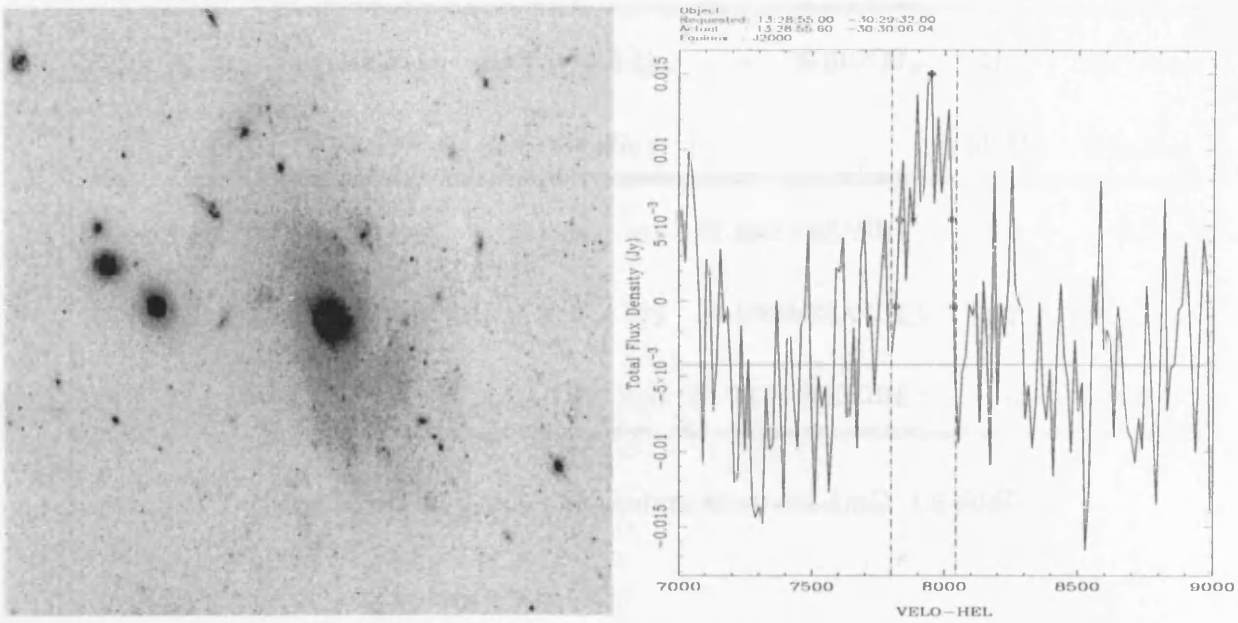

Figure 2.2: HIPASS J1328-31. **Left:** WFPC2 image taken with the filter F814W. **Right:** 21-cm spectrum taken from the HIDEEP survey.

difference in HI content. The average number of gas-rich objects in Centaurus A is higher than the LG, in particular one can find objects with $M_{HI}/L_B > 1$, where the gas component is dominant, that are missing from our group. Even early-type objects such as NGC 5102 and 5128 are fairly gas-rich. This may be due to the loose nature of the group. The gas removal mechanisms taking place in higher density environments may be less efficient in loose groups and this may explain why the majority of Cen A dwarf members have been detected at 21-cm and have HI masses greater than 10^7 $M_\odot$.

2.3 ATCA HI observations

Among the six gas-rich new dwarf candidates four were chosen to be followed-up with the Australian Compact Array and WFPC2. Given the wide range of SFHs, to ensure to obtain a reasonably wide view of possible evolutionary scenarios for gas-rich galaxy it was important to select a number of objects large enough to span any potential diversity. The remaining two dwarf galaxies (HIPASS 1348-37, 1351-47) have both high M_{HI}/L_B ratios, respectively 2.7 and 3.9, but they were not included in the list because they were already

SOURCE	$(\int Sdv)_{HIPASS}$	$(\int Sdv)_{ATCA}$
	Jy km s^{-1}	Jy km s^{-1}
HIPASS J1337-39	6.8	6.0
HIPASS J1321-31	5.9	5.8
HIDEEP J1337-33	1.1	1.0

Table 2.1: CenA dwarfs integrated flux values from HIPASS and ATCA

observed with WFPC2 as part of the SNAP survey.

As regards the ATCA observations, the four galaxies were followedup in the 750-D configuration in May 2001, then in the higher resolution configuration at 1.5 km in October, November 2001 and February 2002. The total integration time on each source for each array configuration was fixed at 12 hours. We used a bandwidth of 4 Mhz divided into 1024 channels, giving a velocity resolution of 0.8 km/sec. The source PKS 1934-638 was used as a flux calibrator, while PKS 1320-446 was chosen as the phase calibrator.

The first ATCA run (750 m array) gave low resolution HI images, necessary in a first section of the work to check if the HIPASS detections were real, determine the accurate position of the object and have a first estimate of the neutral hydrogen column density and distribution.

Originally the targets of the observations were four, but one of the sources, HIPASS J1328-30, turned out to be a more distant uncatalogued LSB galaxy which overlaps a local high velocity cloud with a velocity $v_{helio} \sim 200$ km s^{-1}. The WFPC2 image of this objects is displayed in Fig. 2.2. The galaxy shows a compact fairly bright core, with an extended LSB disc with spiral arms. The corresponding dereddened total magnitude is $m_{I,tot} = 11.65 \pm 0.03$ mag. To infer the distance of this galaxy we have looked for Hα emission, and have obtained an optical velocity of $v_{opt} \sim 8100$ km s^{-1}(Freeman, *private communication*). The galaxy is in the area of the HIDEEP survey, and its 21-cm HIDEEP spectrum is shown in Fig. 2.2, confirming the optical velocity result. The HI mass is $M_{HI} = 7.7 \times 10^9 M_\odot$, with $\Delta v_{20} \simeq 220$ km s^{-1}.

The data processing was performed with the ATNF reduction software MIRIAD. The data-sets corre-

SOURCE	RA	DEC	v_{helio}	r	m_B	M_B	M_{HI}	M_{HI}/L_B
	J2000	J2000	($\mathrm{km\,s^{-1}}$)	(")			$10^7 M_\odot$	$(M_\odot/L_\odot$
HIPASS J1337-39	13:37:26	-39:52:15	491	30	16.5	-11.9	3.9	3.1
HIPASS J1321-31	13:21:06	-31:32:25	572	40	17.1	-11.5	3.7	5.1
HIDEEP J1337-33	13:37:01	-33:21:47	590	20	17.5	-10.7	0.5	1.4

Table 2.2: Observed properties of the three Centaurus A dwarfs

sponding to the two runs at different array configurations (750m and 1.5 km) were first calibrated, continuum subtracted and then combined with the task INVERT. Given the different intensity of the HI lines of the three dwarfs, different reductions strategies have been adopted. I have used the uniform weighting option when reducing the data of HIPASS J1337-39, which gives slightly better resolution at the expense of surface brightness sensitivity. For HIPASS J1321-31 and HIDEEP J13373320 I have added the option ROBUST = 0.5 (in the task INVERT) while combining the data-sets. This was done because the two dwarfs have a lower signal-to-noise ratio than HIPASS J1337-39. This choice resulted in a lower noise level (and thus better surface brightness sensitivity) at the expense of losing angular resolution with an increase of the beam shape. The average noise in the HIPASS J1337-39 cube (with no Hanning smoothing) was 5 mJy per channel, with a synthesised beam $\sim 31''\times 24''$. The noise in the other two cubes is 3 mJy per channel with beam-sizes $\sim$ $57''\times 29''$(HIPASS J1321-31) and $\sim 59''\times 32''$(HIDEEP J1337-33).

In order to check if a component of the flux was missing in the interferometric detections, we compared ATCA (750m configuration) and single dish fluxes obtained by the HIPASS survey with the Parkes telescope (see Table 2.1). As an example, both spectra of HIDEEP J1337-33 are shown in Fig. 2.3. Variations are in the order of the 10%, and they are consistent with the errors in HIPASS fluxes, showing that the interferometric data are not missing a considerable amount of the flux.

The main optical and HI properties of the three HIPASS dwarfs are shown in Table 2.2. The HI mass has been calculated using (Roberts 1969)

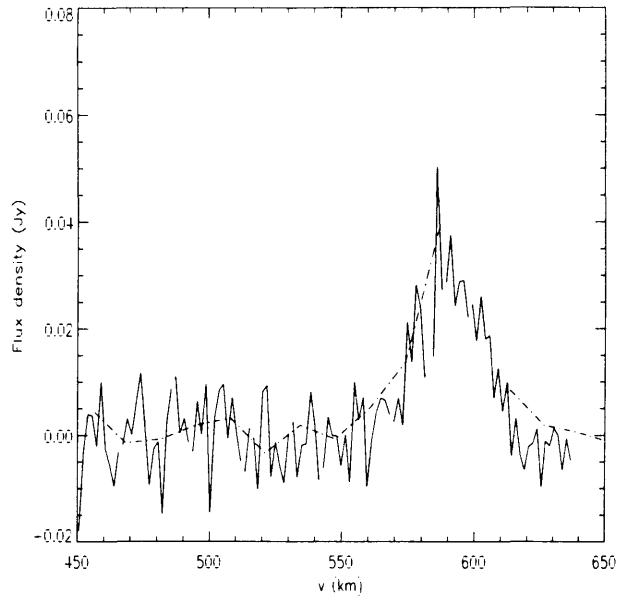

Figure 2.3: HIDEEP J1337-33: comparison between ATCA (solid line) and HIPASS (dash-dot line) HI spectrum. There is no evidence of a large component of the flux missed in the interferometric detection.

$$\frac{M_{HI}}{M_{\odot}} = 2.35 \times 10^5 d^2_{Mpc} \int S(v)dv \tag{2.1}$$

where the distances have been obtained from our HST observations of the tip of the RGB (see following chapters) and $\int S(v)dv$ is the integrated flux in units of Jy km s^{-1}. The column density has been derived using

$$N_{HI} = 1.81 \times 10^{18} \int T(K)dv \ cm^{-2} \tag{2.2}$$

where

$$T(K) = \frac{1.36S\lambda^2}{\theta_\alpha \theta_\beta}$$

and θ_α, θ_β are the major and minor axes of the beam expressed in arcseconds, λ the wavelength of the observations in cm and S the flux in units of mJy beam^{-1}.

2.4 WFPC2 optical observations

The three targets were followed up with WFPC2 in June 2001 in the filters F555W and F814W as part of cycle X. The two bandpasses were chosen because they can be easily transformed to the Johnson/Cousin V and I system which is the standard for observing both old and young stellar populations. To get the largest spatial coverage possible the galaxies were centred in the chip WF3 of the camera, with a spatial sampling of $0''.1$ per pixel and a field of view of $80'' \times 80''$. Four orbits were assigned to each target for a total of 5000 s with filter F555W and 5200 with F814W.

2.4.1 Photometric Reduction

The frames were debiased, zero-corrected, dark-subtracted and flat-fielded by the STScI pipeline process before being made available. They were then combined with the task CRREJ in IRAF to remove contamination by cosmic rays on the frames. The photometry was done using the IRAF version of the package DAOPHOT and ALLFRAME (Stetson 1987). A parallel analysis of the data (Pritzl et al. 2003) has been performed by our collaborators at the National Optical Astronomy Observatory (NOAO) using the stand-alone version of DAOPHOT. A preliminary selection of stars with $S/N > 3$ was performed with the automatic star-finding algorithm DAOFIND and their magnitudes obtained with the task PHOT using an aperture radius of 2.0 pixels. An empirical point-spread function has been built with the task PSF by selecting several isolated and bright stars in each frame containing the galaxies. The instrumental magnitudes were measured with the ALLSTAR algorithm (Stetson 1994) by fitting the pointspread function to the brightness profile of any given object.

When measuring the photometry of stars in a crowded field some mistakes and wrong detections are inevitable. Defective pixels, cosmic rays, background objects, and stellar blends can "pollute" the output of the measured photometry performed by ALLSTAR. However the routine produces indices that give an indication of the reliability of the fit and provide a tool to flag and reject dubious detections.

These indices are:

- χ is the square root of the standard χ^2 goodness-of-fit index and represents a dimensionless measure of the agreement between the measured brightness profile and the model PSF for any given stellar detection. In principle $\chi \approx 1$, but significantly larger values may indicate non-stellar objects or profiles

corrupted by image defects (Stetson, Bruntt, & Grundhal 2003). At increasingly faint magnitudes χ tends to converge around 1 because the background noise dominates over any intrinsic abnormalities in the objects' brightness profile. For the brightest stars χ tends to assume values much greater than 1.

- The residuals of the fitting, σ, that are representative of the errors on the derived instrumental magnitudes.

- Lastly, sharp is a first order estimate of the intrinsic angular radius of a resolved source: if the PSF has a characteristic radius s_{PSF} and the measured image profile has a radius s_{obs}, $sharp^2 = |s^2_{obs} - s^2_{PSF}|^2$. *Sharp* values should be tightly clustered around zero for bright stars, while the deviation from zero increases for fainter stars. When *sharp* is positive but too large, it can be taken as an indication of a resolved non-stellar object. If $s_{obs} < s_{PSF}$, sharp assumes a negative value, and when it is too small, it is probably related to an image blemish or a cosmic ray.

I have chosen to include only detections with $-0.5 < sharp < 0.5$ and $\chi < 2$. In order not to reject bright stars with $\chi > 1$ that appear to belong to the dwarfs, the $\chi < 2$ criterion has been applied only to stars where the errors on the instrumental magnitudes were larger than 0.1. Therefore stars with good photometry, i.e. low errors, and large values of χ are not rejected. This choice should provide a representative sample of detections for each dwarf, excluding both objects smaller than the size of a star, such as cosmic rays or image defects, and extended objects like galaxies, HII regions, stellar blends and any remaining blemishes. As an example, I have shown in Fig. 2.5 the plots of V and I magnitudes (for HIPASS J1337-39) versus their relative photometric errors calculated by ALLSTAR, before and after having applied the rejection criteria.

The transformation from the F555W and F814W magnitudes to the Johnson-Cousin system was performed using the iterative procedure described in Holtzmann et al.(1995a) and the colour terms given in their Table 7.

Using bright and isolated stars in each frame containing the galaxies I have determined the aperture corrections from the 2 pixels to the 5 pixels aperture considered in Holtzmann et al.(1995a). Further corrections for the exposure time and the gain factors were applied. In particular, I have used the following relation between ALLSTAR magnitudes v and i and the standard magnitudes V and I

$$V = v + 2.5log\, t_{exp} - Z_V - 0.052 \times (V - I) - 0.027 \times (V - I)^2$$

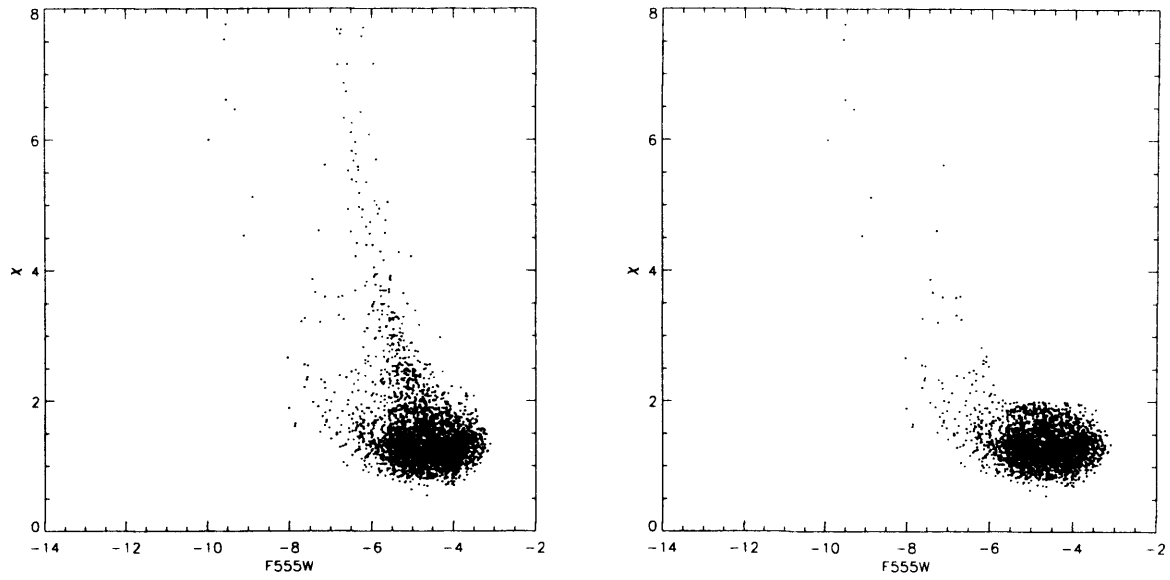

Figure 2.4: HIPASS J1337-39: plot of the goodness-of-fit index χ vs. the instrumental magnitudes F555W before applying the rejection criteria (*left*) and after (*right*).

$$I = i + 2.5log\ t_{exp} - Z_I - 0.062 \times (V - I) - 0.025 \times (V - I)^2$$

where $Z_V = 22.02$ and $Z_I = 21.17$ are the sum of the zero point, minus the gain factor (0.75 mag for WF3 and the $7e^-$ gain), and the aperture correction term.

The WFPC2 CCDs have a parallel charge transfer efficiency (CTE) problem which causes the loss of part of the signal when the charge is transferred down the chip during the readout. Thus, objects at the top of the chip (at y = 800) appear fainter than objects with the same magnitude placed at the bottom of the chip (at y = 0). The effect depends on the temperature of the CCDs. Initially the temperature was set at 76 °C and the effect could be as high as a 10% - 15% loss of the light within an aperture of 0.5″(Holtzmann et al. 1995a). After having cooled down the CCD operating temperature to 88 °C in 1994, the maximum amplitude of the effect is now estimated at $\sim$ 4% (Holtzmann et al. 1995b). To take this effect into account, CTE corrections have been applied, using the equations derived by Dolphin (2000a).

Lastly, the stars on the vignetted regions of the CCD with pixel coordinates X < 75 and Y < 75 were

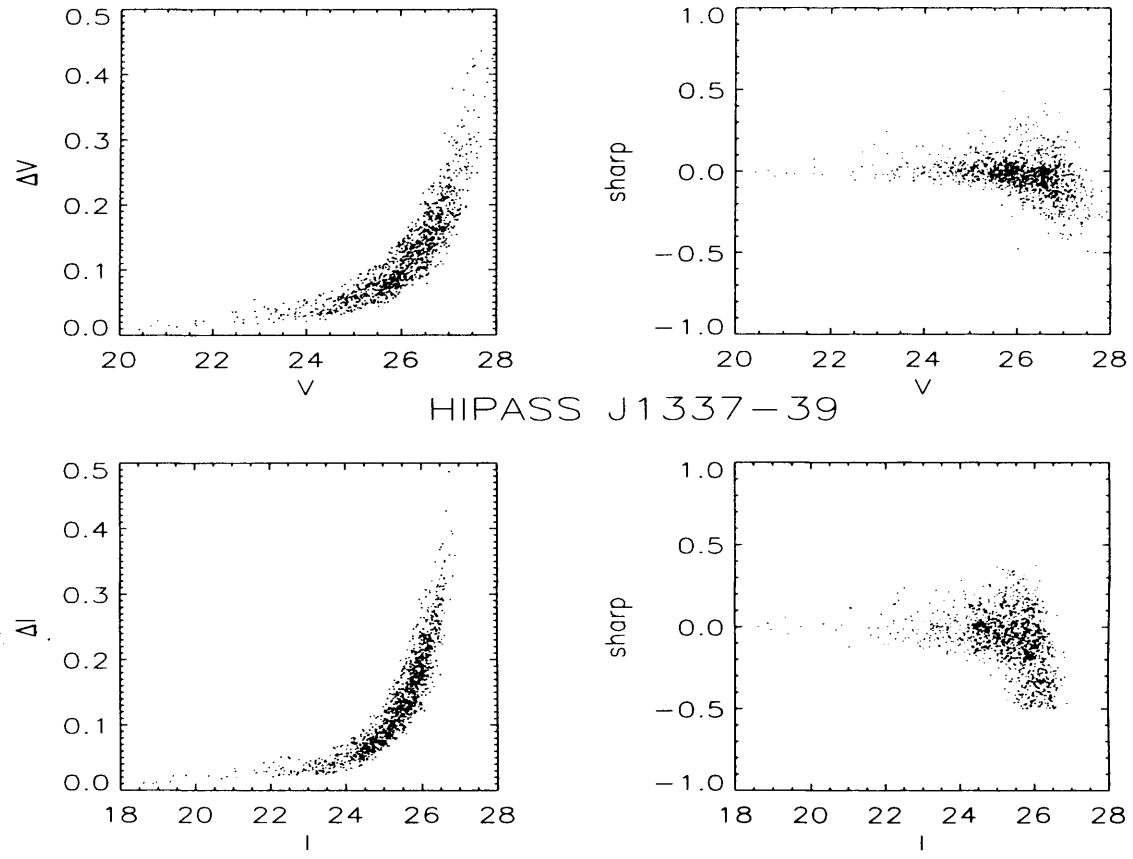

Figure 2.5: HIPASS J1337-39: Plot of photometric errors and *sharp* vs. apparent visual magnitudes in both V (*upper panel*) and I (*lower panel*) bands after applying the rejection criteria and transforming to the Johnson system.

removed from the list. The final list of stars were matched in both filters assuming a matching radius of 1 pixel (0.1″). The resulting colour magnitude diagrams (CMDs) for the three dwarfs are shown and discussed in the next chapters.

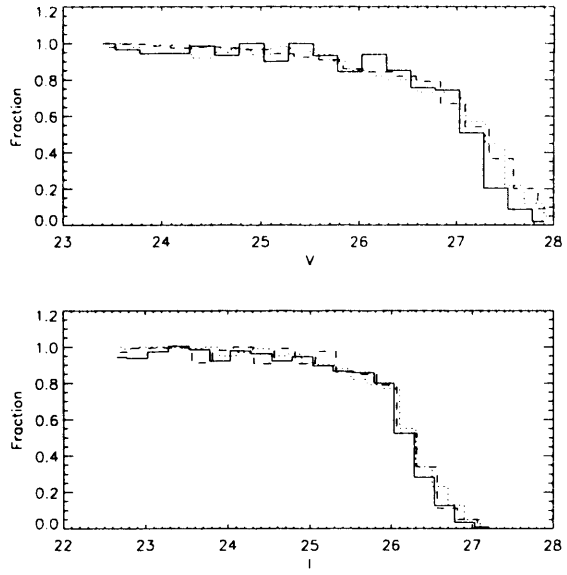

Figure 2.6: Completeness level of the photometry of the three galaxies based on artificial star test. The magnitude range has been divided in 0.2 mag bins. The solid line corresponds to HIPASS J1337-39, the dashed line to HIPASS J1321-31 and the dotted line to HIDEEP J1337-33. Our 50% completeness is at V = 27.3 and I =26.2.

2.4.2 Completeness

Artificial star tests have been performed to determine the completeness of our photometry. Since the galaxies fit into the WF3 chip I have performed tests only on this one. Using the ADDSTAR algorithm of DAOPHOT I have added stars of known I and V magnitudes to the original frames independently. For each 0.5 bin of magnitude I have added 400 stars. To avoid overcrowding effects I have created four images per each bin and included 100 uniformly distributed artificial stars in each of them. Each frame has then been processed in exactly the same way as the original images. The resulting photometry has been matched with the original list of stars and magnitudes created with ADDSTAR. Figure 2.6 shows the fraction of stars recovered in each filter for each of the galaxy. The percentage of recovered stars indicate that completeness is about 50%

at $V = 27.3$ and $I = 26.2$. However a limitation of the ADDSTAR task is that stars are created with the same PSF that is then used as a template to detect them. Thus, artificial stars are probably slightly easier to find than real stars and the completeness level may be a little optimistic.

2.5 Summary

The main aim of this first part of the thesis is to understand the peculiar properties of three gas-rich dwarf galaxies in Centaurus A found in the HIPASS survey. In this chapter I have briefly reviewed the main features of the group and compared the characteristics of the Local Group. Then I have presented the data set we have obtained, 21-cm imaging with ATCA and the WFPC2 photometry in two filter, and the procedure we have followed for the reduction.

In the following chapter I will discuss the main tools that will be used to discuss the properties of the three dwarfs and to reconstruct their star formation histories: a) the main features of the CMD that we expect to detect and what information on the age of the galaxies they may provide; b) the variation in the distribution of stars according to their age; c) the technique of the synthetic CMDs to simulate the evolution of a galaxy; d) finally, the use of HII regions, if any, to constrain the metallicity of a system.

Chapter 3

Analytical tools for decoding Star Formation Histories

There are two main techniques to derive SFHs of galaxies from optical photometry depending on the possibility of resolving individual stars within the system. If this is feasible one can directly identify different stellar populations within the galaxy corresponding to different stages of evolution. Deriving their spatial distribution gives an indication on how the SF process proceeded in each area of a galaxy. This kind of analysis can only be applied to objects within a few Mpc of the Milky Way and it is a very powerful technique which can trace back to the oldest stellar population in a system (> 10 Gyr). The technique requires the building of colour magnitude diagrams (CMDs) and the use of theoretical stellar evolutionary models which allow one to simulate the evolution of stellar populations in time at a certain abundance. The comparison between the empirical and the model diagrams enables deriving the best evolutionary scenario.

For more distant galaxies the use of optical and near infrared (IR) global colours as tracers of the star formation history is a well known and developed technique to discriminate between different evolutionary paths. Thanks to the recent improvements in galaxy evolution models (Bruzual & Charlot 2003, Fioc & Rocca-Volmerange 1997), this technique has been largely adopted in recent studies of spiral galaxies and also gas-rich LSB galaxies (Bell et al. 2000; van Zee 2001a).

Optical spectroscopy of HII regions is a well-known tool to determine the abundance of heavy elements such as O, C, N. Knowing the current abundance of the ISM can set further constrains on the past star

formation activity and the Hα luminosity provides the current star formation rate of a galaxy.

In this chapter I describe all the tools that will be used in the analysis of the dwarfs in the Centaurus A group and the sample of HI massive gasrich galaxies from the southern cap catalogue (SCC) extracted from HIPASS.

3.1 Colour Magnitude Diagrams: the age indicators

The analysis of the resolved stellar population of a galaxy provides the most effective tool to investigate both the variations in star formation and the evolution of its chemical composition. Using the photometry of the resolved stars in at least two filters it is possible to build a colour magnitude diagram (CMD) which gives the most accurate information on the different generations of stars formed.

The instrumental developments in the last decade have produced a great increase in the depth and accuracy of CMDs and nowadays this technique is widely used by the international community to determine the SFHs of nearby galaxies. From a CMD it is possible in principle to reconstruct the whole star formation history of a galaxy. With the combined use of ground-based telescopes and the Hubble Space Telescope the stellar content of the satellites of the Milky Way and the other Local Group dwarfs has been thoroughly investigated. However, only the HST is capable of performing this kind of analysis on objects outside the Local Group, even though it is limited to distances of about 10 Mpc (Ostlin 2000). For larger distances other techniques to obtain SFHs have to be adopted, such as the use of optical and near IR integrated colours.

The main sequence turn-off (MSTO) is usually adopted as the indicator of the oldest stellar population (t $\gtrsim$ 10 Gyr and $M_V \sim +4$) detectable in a galaxy. But CMDs allow one to investigate different stellar evolutionary phases such as the intermediate-age (from 1 to 10 Gyr old) asymptotic giant branch (AGB) and the core-helium burning stars in the red clump (RC), or, at younger ages (< 1 Gyr), the bright and massive blue loop (BL) stars (see Fig. 3.1). Such different evolutionary stages will be described in detail in the following section.

The WFPC2 observations of the three dwarfs in Centaurus A can only go as deep as $M_I \simeq -2$, about two magnitudes below the tip of the red giant branch ($M_I = -4.05$). Therefore with such data we can sample only the upper part of the red giant branch (RGB), the extended asymptotic giant branch (AGB) if present, the BL stars and the brightest edge of the main sequence as shown in Fig. 3.1.

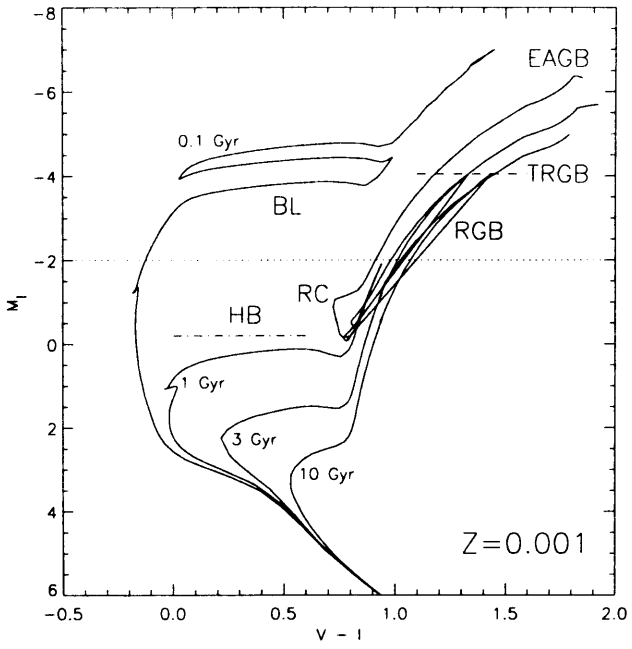

Figure 3.1: Colour magnitude diagram for a metallicity Z = 0.001 (1/20 of the solar value), with isochrones from Bertelli et al. (1994), ranging from 0.1 to 10 Gyr. The main features that are going to be used for the analysis of the SFH of the Centaurus A dwarfs are shown: the Blue Loop (BL) stars, the Red Giant Branch (RGB), the tip of the RGB (TRGB) and the extended Asymptotic Giant Branch (EAGB). Below the detection limit of our photometry - the dotted line at $M_I = -2$ - one can see the Red Clump (RC) and the Horizontal Branch (HB) indicated by the dash dotted line around $M_I \sim 0$. Isochrones related to this feature have not been included to avoid confusion on the diagram.

The main problem in analysing CM diagrams is the confusion between age and metallicity. The position of the RGB in the CMD moves to the red when a stellar population with a given metal content ages. However an increase in metallicity produces the same effect as aging (the "age-metallicity" degeneracy), making the RGB redder. For instance an age difference of about 4 Gyr is equivalent to a variation of 0.1 dex in metal abundance (Tolstoy 2003). Fig. 3.2 shows a clear example of this "conspiracy" in the LG dIrr Sextans A (Dohm-Palmer et al. 2003). The red part of the RGB has been overlaid with isochrones taken from Bertelli et al. (1994, 2002) at different ages and metallicity. It is clearly shown that different values of metal

abundances and ages can reproduce the same colour for the RGB. As a result, disentangling the effects of aging and metallicity in galaxies from their RGB alone is not possible; thus this feature on its own can not be used to uniquely derive the SFH of a galaxy. It is therefore necessary to measure directly, if possible, the abundances of stars or of the ISM.

Before discussing the morphologies of the CMDs obtained, I will briefly describe the characteristics of the main stellar age indicators. The old-age indicators such as the horizontal branch (HB) stars and the MSTO stars will be briefly discussed even though they can not be used in our analysis.

3.1.1 The young stellar population indicators

Core Helium Burning Stars: the Blue Loop (BL)

Stars of high and intermediate mass ($M \gtrsim 2.3\ M_{\odot}$), having exhausted the hydrogen-burning phase in their core, move away from the Main Sequence and evolve through loops across the CMD where helium has now become the main fuel for central nuclear reactions. They pass through a blue supergiant phase first and a red super giant one later on, but the blue edge of the loops is where stars spend most of the time during this stage. The luminosity at which the loop occurs depends on the mass of the stars, while the colour and the extent of the loop is related to the metallicity. The blue loop (BL) stars are about two magnitudes brighter than stars on the Main Sequence of the same age, forming a parallel line redward to it. They can probe the SFH back to almost 1 Gyr. Dohm-Palmer et al. (1997a,b) used the blue core-helium burning stars to infer the star formation history of Sextans A in the last 600 Myr, and used their spatial distribution to derive the variation of SFR throughout the galaxy.

At masses lower than 2.3 $M_{\odot}$, stars igniting the combustion of helium in their core move to the Red Clump (RC) at the bottom of the red giant branch (RGB) (Fig. 3.1), after having evolved through the red giant phase (see next section). This stage is the low-mass analogue of the BL stars. This feature though, is too faint to be detectable in our WFPC2 observations.

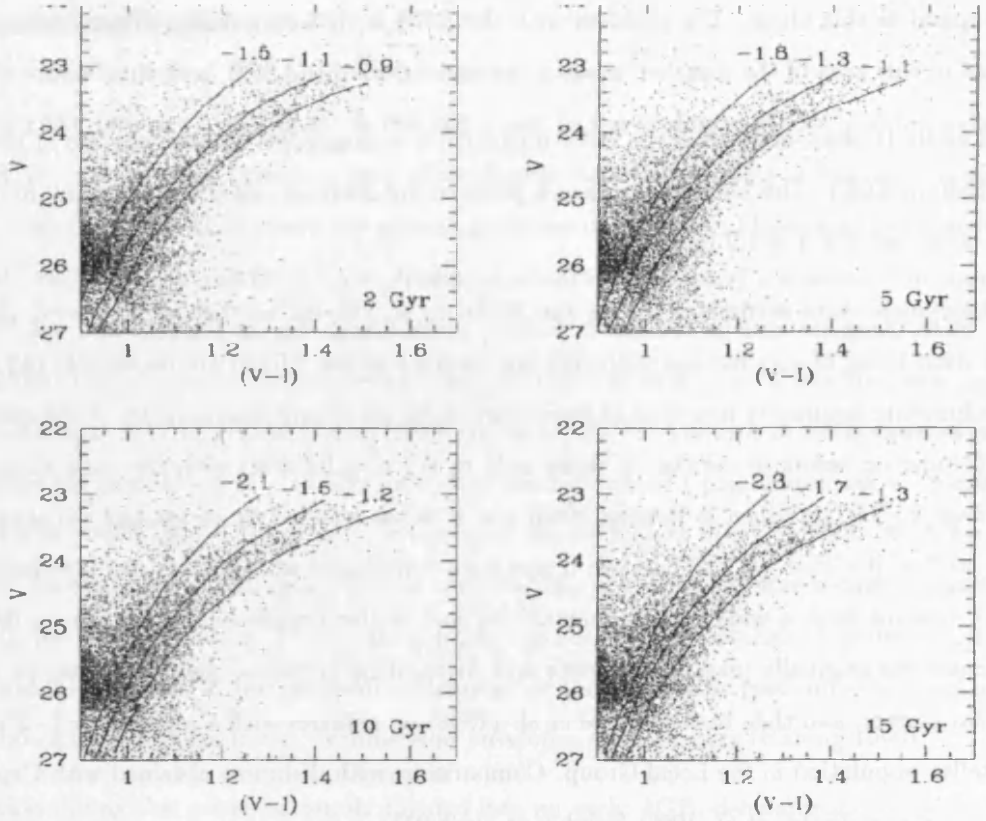

Figure 3.2: An example of age-metallicity degeneracy. The RGB of the LG dIrr Sextans A has been compared with stellar evolutionary tracks at different metallicities: a scenario with a relatively young RGBs (t = 2 Gyr) and high metallicity ([Fe/H]= −0.9) can fit the data as well as the presence of a very old population (t = 15 Gyr) with low metal abundance ([Fe/H]= −1.3). (Taken from Dohm-Palmer et al. 2003)

3.1.2 The intermediate age stellar population indicators

The Red Giant Branch

Stars with initial masses $\lesssim 2.3\ M_{\odot}$, after leaving the main sequence, enter the so-called RGB and start burning hydrogen in a shell around the helium core. The RGB can be used as a relatively coarse age indicator for populations older than 2 Gyr.

The lifetime of stars on the RGB is a function of the mass: the larger the mass, the shorter time the

stars spend in this phase. The problem with the RGB is that stars with different ages (1 Gyr to 10 Gyr) overlay in this area of the diagram, making the derivation of the SFH from this feature alone very difficult.

The RGB phase ends when the H-burning shell is extinguished and the ignition of He starts in the core (the Helium-flash). This usually occurs at a point of the diagram called the tip of the RGB (TRGB), where $I \simeq -4.05$ and $V - I \simeq 1.2$ to 1.7.

Low-mass stars accumulate along the RGB up to the tip as they evolve, with the most dominant population being of very old age, although not all stars at the TRGB are necessarily old stars. As a result, the bolometric luminosity functions of these stars shows an abrupt discontinuity at the magnitude of the tip. The bolometric luminosity of the tip varies only by 0.1 mag for stars with the same abundance and ages in the range 2 - 15 Gyr (Iben & Renzini 1983) and it is not affected by metallicity variations for populations with $-2.2 <$ [Fe/H]< -0.7. Therefore it has been introduced as a reliable distance indicator for resolved stellar systems with a wide range of metallicity and stellar populations older than a few gigayears. The technique was originally used by Da Costa and Armandroff (1990) on giant branches for standard Galactic globular cluster, and then tested by Lee et al. (1993) on galaxies with a metal poor ($-2.2 <$ [Fe/H]< -0.7) old stellar population in the Local Group. Comparisons with distances obtained with Cepheids show a very good agreement (Sakai et al. 1996; Dolphin et al. 2001).

The colour of the red giant branch at absolute magnitude $M_I = -3.5$ is usually adopted as the *indicator of the metallicity* of the galaxy under the assumption that the dominant stellar population is older than 7 Gyr. The mean metallicity is related to the colour of the RGB through the relation

$$[Fe/H] = -1.00 + 1.97q - 3.2q^2 \tag{3.1}$$

where the parameter $q = [(V - I)_{0,-3.5} - 1.6]$ is a function of the de-reddened giant branch colour index at absolute magnitude $M_I = -3.5$. The calibration of this method, introduced by Da Costa and Armandroff (1990), is based on the comparison of the RGBs with those of old Galactic globular clusters where the metallicity has been estimated from integrated spectroscopy or spectroscopy of individual giant stars. However, there are two basic assumptions behind this technique: first the bulk of the stars are more than a few Gyr old, and secondly, the metallicity is fixed and the ages are mixed. The second assumption implies that the mean metallicity of the galaxy is inevitably underestimated, because it does not take into account the increase in metal content due to the chemical enrichment.

The Asymptotic Giant Branch stars

The asymptotic giant branch (AGB) phase is the last stage in the evolution of low to intermediate mass stars ($\approx 0.8 - 8\ M_{\odot}$) before they transform into white dwarfs. After the burning of helium in the cores has stopped, these stars reach the AGB where the nuclear reactions of helium and hydrogen combustion occurs in a double shell, leading to the production and dredge-up of carbon and heavy elements. With luminosities up to a few $10^4\ L_{\odot}$ and spectral energy distributions peaked in the red or near infrared, AGB stars are among the brightest evolved stars. For this reason they are the best indicators of intermediate-age stars in galaxies inside and outside of the Local Group (Nowotny et al. 2003). The role of AGB stars as indicators of an intermediate age population (1 - 10 Gyr) was first pointed out by Cook, Aaronson, & Norris (1986). Gallart et al. (1994, 1996) used AGB stars to investigate the SF history of NGC 6822. AGB evolution is characterized by thermal pulses (also called helium shell flashes), and stars can lose a large amount of their mass ($\sim 0.4\ M_{\odot}$ for a 1 $M_{\odot}$ star, or 4.8 $M_{\odot}$ for a 6 $M_{\odot}$ assuming solar metallicity) by developing strong stellar winds, which contribute to the chemical enrichment of the interstellar medium. Complex molecules and dust are also claimed to form in the circumstellar envelopes of these stars (Habing 1996).

The evolution during this phase is usually divided into an early AGB, defined from the central helium exhaustion to the first major helium shell flash, and a thermally pulsating AGB (TPAGB), from the helium flash until the star evolves into a white dwarf. AGB stages are short-lived compared to the lifetime of a star and the length of this phase depends both on the metallicity and mass. More massive stars spend less time in this branch. Vassiliadis & Wood(1993) modelled the lifetime of AGB stars with initial masses 0.89 $\leq M/M_{\odot} \leq$ 5.0 and metallicities 0.001 $\leq$ Z $\leq$ 0.016. For a 1 $M_{\odot}$ star with Z = 0.001 the AGB phase lasts around 10 Myr (Vassiliadis & Wood 1993) and can be slightly longer for higher metallicities. At the low end of the range of masses investigated, Vassiliadis & Wood's model predicts that the ratio of the duration of the AGB phase compared to the core helium burning one is $\tau_{AGB}/\tau_{HeB} \sim 0.08$ (Vassiliadis & Wood 1993).

In particular, AGB stars with low masses ($\approx 0.8 - 2.0\ M_{\odot}$) ascend the RGB for the second time after evolving away from the red clump, and end up occupying the area above the TRGB and at redder colours. Since they appear in a CMD after the RGB phase, the presence of these stars has been mostly adopted as the evidence of a few Gyr old population. An example of their evolution is shown in Fig. 3.1 for the isochrones at 3 and 10 Gyr. According to Aparicio & Gallart (1995) the extent of this feature towards red colours increases with the metallicity. Thus, even AGB stars can give an indication of the abundance of a system. A straight, almost vertical AGB appears when the abundance is less than 1/20 solar (Cole et al.

1999). The extent of the AGB to the redder part of the diagram requires higher metallicities as it can be seen in LG dwarf galaxies such as Pegasus (Aparicio, Gallart, & Bertelli 1997) or NGC 6822 (Gallart et al. 1996).

AGBs are divided into two classes according to their chemical abundances: C-type, if their carbon abundance is greater than the oxygen one (C/O > 1), with spectra dominated by carbon species, or M-type if C/O < 1, characterized by oxides spectra such as TiO. Narrow band optical filters (TiO-filter and CN-filter) around 800 nm are usually adopted for the detection of the two types of stars (Nowotny et al. 2001, 2003) and the distinction between C and M AGB stars is based on the location of the stars in colour-colour diagrams (i.e. $V - I$, $TiO - CN$). According to Groenewegen and de Jong (1993) C stars may be used as standard candles as well as RGB, since their mean bolometric magnitude in the Galaxy and in the LMC is identical and independent of the abundance. A similar result has been found by Bettinelli and Demers (2000, 2002) in LG dwarfs with different metallicities such as Pegasus, DDO210 and Tucana, SagDIG and Leo I, concluding that the median absolute I magnitudes of C stars is almost constant and equal to $M_I \simeq -4.7$.

We will not be able to distinguish between C-type or M-type AGB stars within this data set because we have only one colour available from the WFPC2 photometry. However the detection of AGB stars in our case is extremely important. The presence of low mass AGB stars is usually taken as evidence for an intermediate-age population. Unambiguous identification of these stars would confirm that SF activity has taken place at ages that correspond to look-back times of several Gyr. This is the best indicator of an intermediate-age (1 - 10 Gyr) population we can use with our data set. As previously mentioned AGB stars are brighter and as red as or redder than the tip of the RGB, therefore they are much brighter than our photometric limit and should be easily observable. In addition, the slope of the AGB branch may give an additional indication of the metallicity of the galaxy: at metallicities greater than 1/20 solar (Z = 0.001) this feature extends towards colours redder than the RGB (as is shown in Fig. 3.3 for the dwarf spheroidal Fornax, with [Fe/H]= −1.3, i.e. Z = 0.001 (Mateo 1998)), while at lower metallicity the asymptotic giant branch extends almost vertically above the RGB, with very similar colours.

3.1.3 The old stellar population indicators

The horizontal Branch and RR Lyrae variables

Horizontal branch (HB) stars are burning helium in their cores and they form in stellar populations older than $\sim$ 10 Gyr. They have magnitudes around $M_I \sim 0$ and masses $M \lesssim 1.8 - 2.0\ M_\odot$. They represent the continuation of the RC towards bluer colours, with the difference that the HB is formed by lower mass and older stars, while the RC contains those with ages between 1 and 10 Gyr. The HB crosses the instability strips, and RR Lyrae variables belong to this class of stars. Metal-rich stars tend to form a red HB while metal-poor ones are characterised by bluer colours. At a given metallicity, variations of a few Gyrs in the age of the stars can change the morphology of the branch from a completely red (if dominated by stars with ages around 11 Gyr) to an entirely blue (if ages $\sim$ 15 Gyr).

The main sequence turn-off

The maximum luminosity of the main sequence (MS) (or the main sequence turn-off) becomes fainter with increasing age. With CMDs reaching the oldest MS turn-off one can obtain unambiguous information back to the oldest ages of a galaxy. The advantage of using the MS is that the relation between the mass-luminosity and lifetime of a star is well understood, and there is less intrinsic age-metallicity degeneracy.

3.1.4 Sculptor and Fornax: two examples of observed CMDs

As an example Fig. 3.3 shows the CMD of two nearby dwarfs: Fornax ($\sim$ 140 kpc, $(m - M)_0 = 20.70$) and Sculptor ($\sim$ 80 kpc, $(m - M)_0 = 19.54$). Their close distances allow us to look in detail at their SFHs.

Fornax appears to have been actively forming stars between 2 and 7 Gyr ago as indicated by the numerous AGB stars above the RGB with a wide range in luminosities (Aaronson & Mould, 1980, 1985; Azzopardi 1999). The well populated RC requires a population of 2 - 4 Gyr old stars (Tolstoy 2001). The detection of RR Lyrae (Stetson et al. 1998) and red and blue HB stars (Buonanno et al. 1999) demonstrates that Fornax contains a very old, metal poor component. HST observations of Fornax (Buonanno et al. 1999) revealed the MSTO of the old population, confirming the presence of stars older than 10 Gyr. The main sequence turn-off at brighter luminosities indicates an extended SF activity which has only recently ceased, with young main sequence stars not younger than 100 Myr (Stetson et al. 1998).

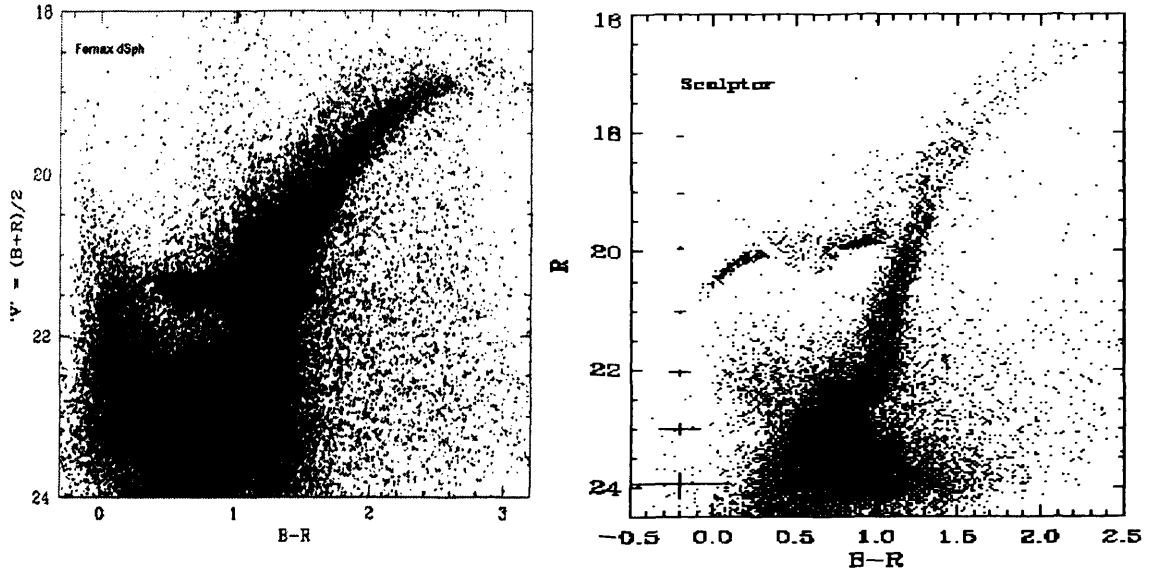

Figure 3.3: Colour magnitude diagrams of Fornax **(left)**, taken from Stetson et al. (1998) and Sculptor **(right)** from Smecker-Hane & Mc William (1999).

Sculptor is instead dominated by old stellar populations, as indicated by the well defined HB both on its blue and red edges, as well as the detection of RR Lyrae and an old ($\sim$ 15 Gyr) MSTO. Nevertheless there are sign that it has been forming stars until at least 7 - 8 Gyr from the detection of carbon stars (Azzopardi et al. 1986). There are no bright MS stars which exclude any recent SF event over the last 2 Gyrs (Monkiewicz et al. 1999).

3.2 Radial gradients and clustering in the stellar population

It is often found that young and old stellar populations are located in different regions of a galaxy, therefore investigating how population gradients occur in galaxies may help in understanding how a system has evolved. In spiral galaxies young stellar populations are generally found in the disc in correspondence with the spiral arms, while the older populations are more centrally concentrated within the bulge. Dwarf galaxies observations instead show that the young blue stars are more centrally concentrated, while the red and older ones are spread over a larger area and form an extended stellar halo.

Such radial gradients in the stellar distributions have long been observed in dSphs galaxies. Fornax probably represents the most interesting example among dSphs. Asymmetries in the spatial distribution were already noticed by Hodge (1961), but a most detailed investigation of the stellar population is provided by Stetson et al. (1998). The most distinctive feature of Fornax, as it has already been mentioned, is the presence of a conspicuous young main sequence indicating a recent star formation event lasting until 200 Myr ago. Such young populations as well as the reddest AGB stars are concentrated in a bar-like structure, while the oldest population detected, the HB stars, defines an extended halo with a spatial scale length larger than that of the intermediate-age red clump stars (4 - 6 Gyr; Stetson et al. 1998). Saviane et al. (2000) adopts the analysis of the stellar distribution as a way to break the age-metallicity degeneracy. The wide RGB of Fornax shows on its blue side a distinct sequence of stars which in principle could be made of a young, metal-rich population (see Fig. 3.3). Yet their distribution is very close to that of the old HB stars. Thus, according to the authors, the bluer RGB stars represent a rather old and metal-poor population.

There are several dSph/dE showing radial gradients in the stellar population, such as NGC 185 where recent star formation is detected in a central area 0.2×0.1 kpc^2 wide (Martinez-Delgado et al. 1999), or NGC 147 (Han et al. 1997) and ESO 410-G005 (Karachentsev et al. 2000). Red and blue HB stars are often distributed in different ways and provide another constraint on different star formation events: red HB are more centrally concentrated and they appear to be 3 - 4 Gyr younger than their blue counterpart in And I, Leo II and Sculptor (Da Costa et al. 1996).

There are also dSphs with no evidence of asymmetries in the distribution of stars such as Leo I (Held et al. 2000), Carina (Da Costa et al. 1996), Tucana (Saviane et al. 1996) and And II (Da Costa et al. 2000).

The transition type galaxy Phoenix shows a substructure of blue stars (between 100 and 250 Myr old) clumped in the center of the galaxy (Held et al. 1999). They are elongated in a direction perpendicular to the main optical axis and slightly offset towards the HI cloud found by Young & Lo (1997). Again old and intermediate age stars are diffused over a much wider area.

Stellar population gradients are also detected in dIrrs and BCDs galaxies both from optical and infrared observations. Nuclear star forming regions are superposed over a more extended halo of red stars as has been found by Loose & Thuan (1986), Kunth et al. (1988), Papaderos et al. (1996), van Zee (2001a). Nevertheless for more active dIrr galaxies the spatial distribution of younger populations becomes more and more irregular (Saviane 2001).

It is rather difficult to establish how old the red stars found in the halos of both BCDs and dIrrs are, because these objects are generally found so far from the Milky Way or outside the LG. Their HB stars are beyond the detection limit of current instruments and it is not possible to derive the unambiguous signature of metalpoor population more than 10 Gyr old.

The detections of a truly old population, as it has been previously pointed out, is extremely important as a proof that galaxies have started to experience star formation more or less at the same time throughout the Universe and that dwarf galaxies are primordial objects. Moreover, for star forming galaxies the detection of a HB is even more complicated than in dSphs, since it can be masked by an intermediateage subgiant branch of $\sim$ 1 Gyr old age, or by the blue main sequence of the youngest population (Saviane et al. 2001). Horizontal Branch RR Lyrae have so far been detected in the field of LG dIrrs IC 1613 (Saha et al. 1992) and in WLM (Rejkuba et al. 2000) in a region between the disc and the halo.

To conclude, the evolution in most dwarf galaxies leads to a central concentration of the younger population. different scenarios may explain the presence of radial gradients. The outer stars may have formed in the first evolutionary stage of the galaxy in a single short initial burst, or star formation may have occurred for an extended time throughout the galaxy, but then ceased several Gyr ago in the outer regions. Miller et al. (2001) suggest that radial gradients in the transition-type dwarfs LGS 3 may be connected to the progressive reduction of the gas supply in the outer part of a galaxy either by consumption or by stripping. The SF activity though continues in the centre where the gas density remains higher.

3.3 Modelling the Star Formation History of galaxies

The modelling of the star formation history (SFH) of a galaxy from its resolved stellar population is a field of research that has evolved rapidly in the last decade and it has been widely used to investigate the evolution of the Local Group members. A synthetic CMD is the expected photometric distribution of stars given a particular SFH. Two factors have contributed to the improvement of the predictive power of synthetic CMD: on the one hand the evolution of stellar evolution libraries, which are now covering a wide range of metallicity and evolutionary phases (including the AGB and the horizontal branch (HB)): on the other the development of codes for the computation of synthetic CMDs. An example is described in Fig. 3.4 (Aparicio 1998) where it shows the stellar population of a simulated galaxy at different ages. In the simulation it has been assumed that the galaxy star formation rate has been constant from 15 Gyr ago to date, and the

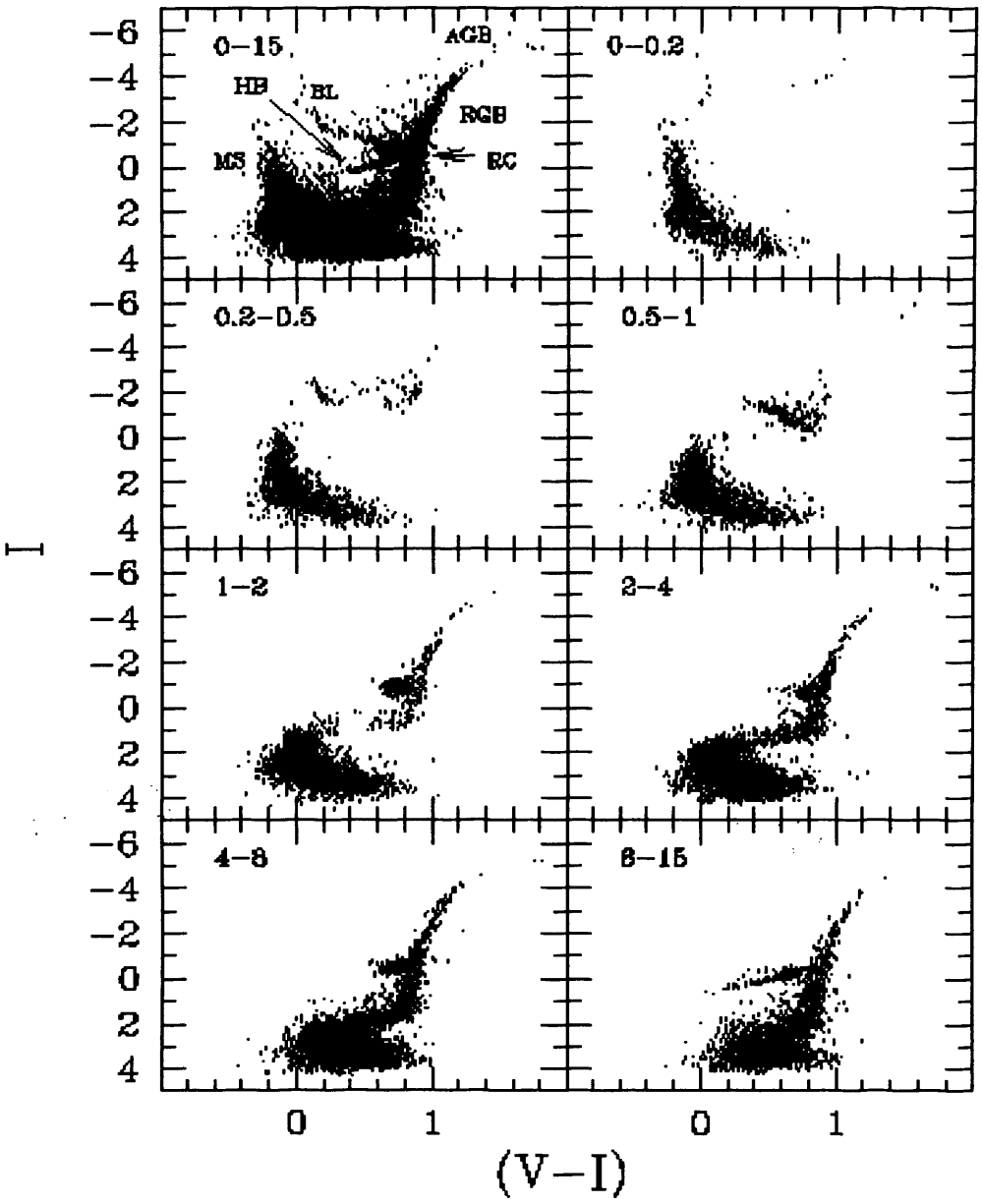

Figure 3.4: Synthetic CMD for a constant star formation rate and a linear chemical enrichment law, with an initial and final metallicity of $Z_0 = 0.0001$ and $Z_f = 0.004$ respectively. Each panel contains stars in a certain age range indicated in Gyr (from Aparicio 1998). Extended AGB stars may be seen at $M_I < -4$ in the panels at ages older than 1 Gyr, especially between 4 and 8 Gyr.

metallicity has linearly increased from Z = 0.0001 (1/200 solar) to Z = 0.004 (1/5 solar). From the analysis of the different regions and the distribution of stars across the diagram one can derive the SFH of the galaxy. It is interesting to note that the RGB begins to be populated only after 1 Gyr and that only between 2 and 4 Gyr the branch is well defined and populated up to the tip.

The method of deriving SFHs from synthetic CMDs consists of three main steps:

- the computation of the synthetic CMDs using stellar evolutionary models. Theoretical isochrones describe the evolution of stellar populations at a given metallicity and age for different initial masses. An initial mass function (IMF) $\phi(m)$ and a fraction of binary stars formed have to be assumed and implemented to transform evolutionary tracks in CMDs. A calculation of shorter evolutionary phases such as the Red Clump (RC), the Blue Loop (BL) and the AGB has now been included in stellar libraries, although many steps of the stellar evolution at these stages are not well understood yet. For instance, the colours and life-times of AGB stars depend on the mass-loss parameter, which is very difficult to calculate for these stars (Aparicio 1998). Although AGB stars provide a useful constraint on the intermediate-age SFH, uncertainties in predicting their evolution and the way they are distributed in the CMD prevent us deriving very accurate information from this feature yet (Aparicio 1998).

- the simulation of the observational effects affecting the photometry. This mainly implies the determination of the fraction of stars lost as a function of magnitude, especially at those magnitudes where the photometric detection limit is approached. This effect is parameterised by the completeness function (see Chapter 2) that is constructed with the help of artificial star tests. When a number of artificial stars with known photometry are added to the observed frames and processed in the same way as the data, this function corresponds to the fraction of detected stars in a certain range of magnitude.

- the comparison of the synthetic and observed CMDs to derive the best model. Many degeneracies intrinsic to the CMDs themselves (i.e. the age metallicity degeneracy of the RGB) and uncertainties in the stellar evolution models prevents a unique solution. The age-metallicity degeneracy of the RGB represents the most difficult obstacle to overcome, because it can be solved only if accurate photometry down to the main sequence turn-off point is available. Several techniques have been introduced for this kind of analysis, which generally make use of minimization algorithms. Gallart et al. (1996, 1999), for instance, define several regions in both the model and synthetic CMDs and compare the number of stars in each area through a χ^2 or a least squares method. The size and the location of each area is

determined considering the evolutionary path of stars in different phases with the help of evolutionary models.

Given the difficulty of the many degrees of freedom intrinsic to the problem, the approach adopted so far by several studies is to build different CMDs with varied SFHs and chemical enrichment scenarios and to search for the solution that best matches the observed photometry (Tolstoy 1996, Gallart et al. 1996, Aloisi et al. 1999). Aparicio (1998) suggests checking many models describing several SF scenarios, and to select all those that give an acceptable match. The average is then taken as the ultimate solution.

To model the SFHs of the HIPASS dwarfs I have used the StarFISH code (Harris & Zaritsky 2001) which is available to the astronomical community. In the following section I briefly describe the main characteristics of the code and the main steps it performs to compute the SFH of galaxy.

3.3.1 StarFISH: a public code to compute SFHs

StarFISH is a code written by Harris & Zaritsky (2001) which enables one to determine the star formation history of a mixed stellar population from its photometry. The code was originally written to be applied to the LMC, but it is designed with flexibility and generality in mind, thus it can be adapted to different objects (Makarova et al. 2003). StarFISH performs a χ^2 minimization between the observed photometric distribution and a model one which is built using theoretical isochrones from the Padua group (Bertelli et al. 1994, Girardi et al. 2002), each isochrone describing the photometric properties of a stellar population with a particular age and metallicity.

By adding the effects of distance, galactic extinction, the initial mass function, the binary fraction and photometric errors, the code constructs a library of synthetic CMDs from the theoretical isochrones.

Adjacent isochrones, as they are provided by the Padua group, differ in age by only $\Delta\log(t) = 0.05$, thus there is a significant photometric degeneracy between them. To avoid this degeneracy and to reduce the number of independent model parameters each synthetic CMD is built by groups of combined adjacent isochrones covering an age range $\Delta\log(t) = 0.2$. These CMDs are then linearly combined. The coefficients generating the final global CMD form an N-dimensional parameter space of possible SFHs. A fitting statistic (χ^2) is then applied to determine the sets of amplitudes that matches best the observed CMD. Such a best-fitting SFH is defined by the set of coefficients that have the lowest χ^2 value. The χ^2 index is defined in the following way. First the CMD is divided into subregions (by default it adopts a uniform gridding into boxes

of 0.25 mag × 0.25 mag width - Harris & Zaritsky 2001), if N_{D_i} is the number of stars distributed within the ith subregion of the observed CMD and N_{M_i} indicates the stars in the same subregion in the model CMD, χ^2 is given by the sum

$$\chi^2 = \sum_i \frac{(N_{D_i} - N_{M_i})^2}{N_{D_i}}. \tag{3.2}$$

Subregions where $N_{D_i} = N_{M_i} = 0$ are not included in the sum, while if $N_{D_i} = 0$ and $N_{M_i} > 0$, N_{D_i} is replaced with 1.0 in the denominator.

The error bars on the SFH amplitudes are determined by identifying the 68% (1σ) confidence level on each amplitude by investigating the χ^2 topology around the minimum. In each case the code iteratively steps away from the minimum and determines the χ^2 value until it increases to the 68% confidence limit. From the collection of tested points, the largest and smallest values for each amplitude are taken as upper an lower limit for the error bars. One has to bear in mind that these errors, rather than having a statistical significance, give an indication of how flexible the star formation rate can be before significantly affecting the good fit of a model to the data.

One advantage of this algorithm is that, contrary to other methods, it does not need to set an initial constraint on the SFH such as an a priori chemical enrichment law. The structure of the code allows one to build a library of CMDs with a wide range of metallicities, and the output produced by the algorithm provides a SFH for each set of isochrones at a given Z. This enables one to trace the number of stars formed for each metallicity assumed. By averaging the metallicity of the stars being formed in each age bin, it is possible to derive the chemical evolution of the system studied (Harris & Zaritsky 2001). However the method is unable to resolve metallicity differences of $\lesssim 0.3$ dex, because synthetic CMDs becomes photometrically too similar to be distinguished.

3.4 The metallicity of HII regions to break the age-metallicity degeneracy

The spectra of star forming regions ionised by young hot O, B stars provide a powerful tool to derive the current metal abundances of the ISM of galaxies. Narrow emission lines in the optical domain are in general observed superimposed on the stellar continuum. Oxygen, Nitrogen, Sulphur, Neon, Argon, Helium and the

Balmer series of Hydrogen (Hα, Hβ, Hγ, etc.) may be identified, and several methods have been applied to determine the corresponding abundances.

Oxygen is the element whose abundance can be best determined, since the most important ionisation stages fall in the optical domain. The first ionisation potential of oxygen is similar to that of hydrogen (around 13.5 eV), while the O^{++} ion requires an energy of 35.1 eV to be created, energy that is provided by the hottest stars in the HII region. The main transition observed are [OII]λ3727, [OIII]$\lambda\lambda$4959,5007. The lines originate from energy states just above the ground state, and are metastable with long lifetimes.

The basic mechanism of emission is given by the collision between an electron and an ion in the ground state. The ion is excited at the expense of the kinetic energy of the electron, therefore the process cools the gas. The collisional excitation is then followed by the emission of a photon. The rate of energy lost via a collisionally excited line is proportional to the factor $exp(-\Delta E/kT_e)$, where ΔE is the energy of the level of the transition, and T_e is the electron temperature, or the temperature of the ionised gas. Therefore the measurement of this parameter is necessary to convert the emission-line strengths into the metal abundances. In metal poor HII regions this is performed by measuring the [OIII]$\lambda\lambda$4959,5007 / [OIII]λ4363 ratio (Osterbrock 1989), a relation that will be discussed in the following chapter. The [OIII]λ4363 line is relatively strong in very low metallicity systems (Searle 1971), but it is too weak to be measured in objects with moderately low metallicity (12 log(O/H) $>$ 8.3). This is the consequence of the oxygen being the main coolant for the nebula. A higher oxygen abundance implies a more effective cooling: as the gas cools down, the electron temperature is lowered and the [OIII] lines are weaker. In this case, the electron temperature can not be directly derived and the oxygen abundance is estimated using an empirical method based on the intensity ratios of strongest lines. In general the ratio of the [OII]λ3727 and the [OIII]$\lambda\lambda$4959,5007 intensity to Hβ, R_{23} = [OII] + [OIII]/Hβ is used. This line ratio was calibrated and employed as an abundance indicator for extragalactic HII regions by Pagel et al. (1979), and since then it has been recalibrated several times (e.g. Edmunds and Pagel 1984; Dopita and Evans 1986, Mc Gaugh 1991). The high metallicity end of this relation is difficult to calibrate, and relies heavily on theoretical models. This calibration is one of the main sources of disagreement in the abundance values derived by different authors. Therefore other metallicity estimators using different elements such as Sulphur or Nitrogen, have also been introduced. Among them are the S_{23} parameter, introduced by Vilchez & Esteban (1996) defined as S_{23} = [SII]$\lambda\lambda$6717,6731 + [SIII]$\lambda\lambda$9069,9532/Hβ and the $N2$ calibrator, $N2$ = log([NII]λ6564/Hα) (Storchi-Bergmann, Calzetti & Kinney 1994) recently recalibrated by Denicoló et al. (2002), confirming the good correlation between $N2$

and the oxygen abundance.

As regards the other elements, the determination of the abundances is more difficult because all the ionisation stages do not give rise to observable emission lines. In general an ionisation correction factor has to be applied to derive the total abundance. The magnitude of this correction varies from element to element (Osterbrock 1974).

Ionisation correction factors to convert ionic into elemental abundance ratios rely on the assumption that the fractional ionic populations are similar for elements with similar ionisation potentials (IP). For example the IP of N^+ is 29.6 eV, while that of O^+ is 35.1 eV, so it is generally assumed that (N/O) = (N^+/O^+) (Osterbrock 1974).

Nebular abundances may be used to infer a first estimate of the metallicity of the galaxy to break the age-metallicity degeneracy. HII regions are associated with young populations, therefore they provide an upper limit to the metallicity for the stars born earlier than the region itself, such as the RGB stars. Obviously this method requires the presence of star forming regions, otherwise alternative techniques to derive the metallicity are needed, such as the use of the Ca ii triplet to trace abundances directly from RGB stars (Tolstoy et al. 2001).

3.5 Summary

I have presented a number of tools that can be used to analyse and interpret the resolved stellar population of galaxies. A two filter photometry of the individual stars of a galaxy enables one to build a CMD and to obtain a picture of its evolution by tracing the different generations of stars formed. I have described the indicators which provide information on star formation events at different times, generally grouped in young, intermediate and old populations, which, according to their age, tend to have different spatial distribution within a galaxy. The use of simulated CMDs has become an essential technique in the interpretation of observed diagrams, although the method is not free from uncertainties and intrinsic difficulties, for example the age-metallicity degeneracy. Independent methods to determine the metal content of a galaxy are therefore required. The spectra of HII regions, as described in the last section, provide the abundance of the ISM and can help to set some constraints on the chemical composition of a galaxy in order to break the age-metallicity degeneracy. All these tools presented in this chapter will be applied in the following chapters to the three dwarfs discovered by HIPASS in the Centaurus A group.

Chapter 4

HIPASS J1337-39

We will start our analysis of the properties of a sample of gas-rich galaxies extracted by the HIPASS survey with the three dwarfs of the Centaurus A group. Given their varied characteristics each galaxy will be described in a separate chapter. HIPASS J1337-39 is the first object to be discussed. Among the three dwarfs, 1337-39 is the only object with ongoing star formation activity. With an HI mass of 3.7 $\times 10^7$ $M_\odot$ and a total apparent magnitude m_B = 16.5 (Banks et al. 1999), it has a gas-mass-to-stellar ratio $M_{HI}/L_B = 3.1$ in solar units.

4.1 The neutral gas content

The aim of the ATCA observations was to confirm the HIPASS detections and to inspect the gaseous distribution of these objects. The neutral hydrogen plays a crucial role in the evolution of galaxies being the main fuel for the SF process. Therefore the ATCA observations were sought to determine the main properties of the HI discs of such gas-rich galaxies as their gas column densities, their extension compared to the optical disc, and a map of the velocity field to investigate their dynamics. These properties will then be compared to the picture obtained by the optical data to get an overview of the evolutionary state of these galaxies.

The map of the 21-cm emission of HIPASS J1337-39 is displayed in the right panel of Fig. 4.1 superposed on the B image of the field taken by the Digitized Sky Survey. The neutral gas shows a smooth distribution

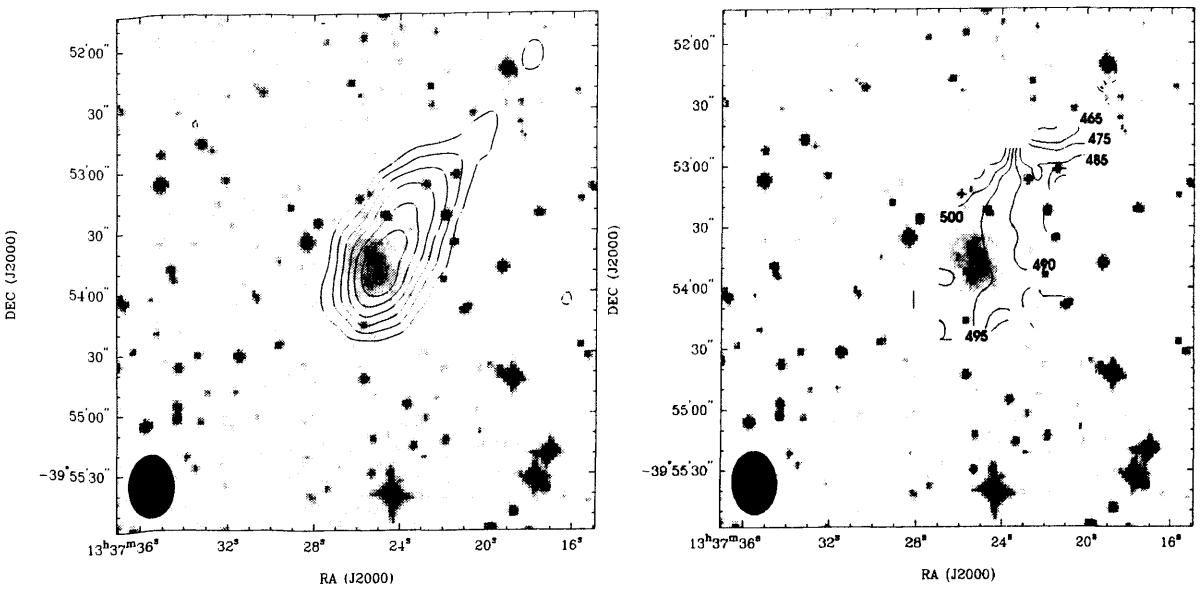

Figure 4.1: HIPASS J1337-39. **Left:** HI density contour maps overlaid on the Digital Sky survey field including the galaxy. The contour levels are: 2.5, 5.0, 7.5, 10, 12.5, 15, 17.5 $\times 10^{20}$ cm^{-2}. **Right:** The HI velocity field: contours are in the range between 475 km s^{-1}and 500 km s^{-1}.

with a one-sided extension along the north west direction which goes up to a projected radius of 1′30″($\sim$ 2 kpc at the assumed distance of 4.8 Mpc that we have derived from the I magnitude of the tip of the RGB - see section §4.5). 1337-39 has the highest average HI column density among the three dwarfs, and we traced the neutral gas out to an HI column density $N_{HI} = 2.5 \times 10^{20}$ cm^{-2} . The overall high column density may explain why this is the only galaxy with ongoing star formation. The density peak is at $\sim 2 \times 10^{21}$ cm^{-2} in correspondence with the Star Forming regions and slightly offset from the optical center of the galaxy (see Fig. 4.1).

The velocity field is shown in the right panel of Fig. 4.1. There is evidence of a small velocity gradient throughout the galaxy. The velocity contours become rather irregular in the outer edge of the galaxy, in correspondence with the edge of the HI "tail", while around the main optical body the velocity field looks fairly regular.

Fig. 4.2 shows the HI channel maps in the velocity range 471 km s^{-1}- 516 km s^{-1}. The disc appears to be slowly rotating although the rotation is not very sharply defined.

The narrow HI profile is shown in Fig. 4.3. It has a 20% velocity width $\Delta v_{20} \sim 50$ km s^{-1}and as we

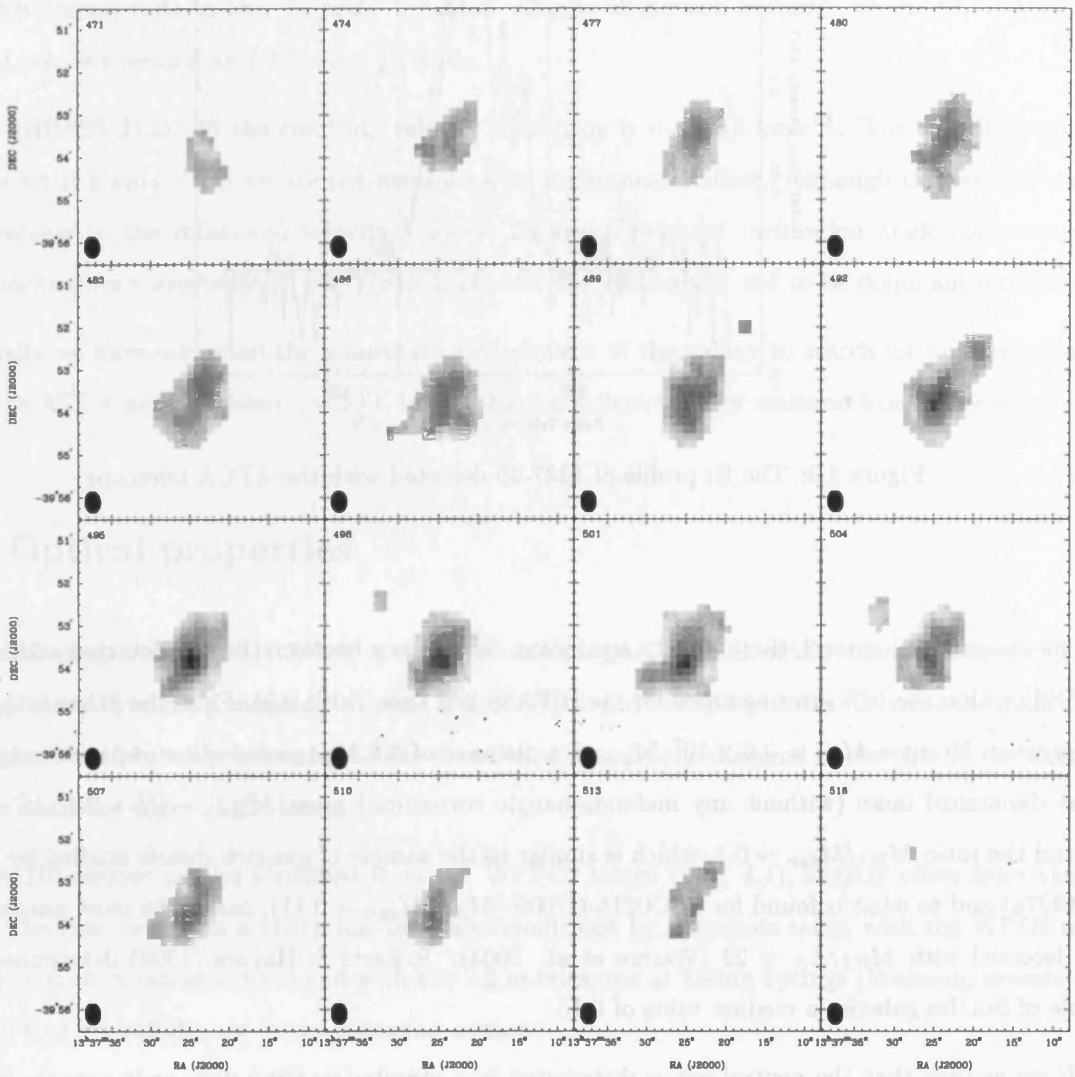

Figure 4.2: The HI channel map of 1337-39, where each panel is the average of three contiguous channels. The beam size is shown at the bottom-left corner of each image, and the radial velocity of each channel in $\mathrm{km\,s^{-1}}$ is indicated in the upper-left corner.

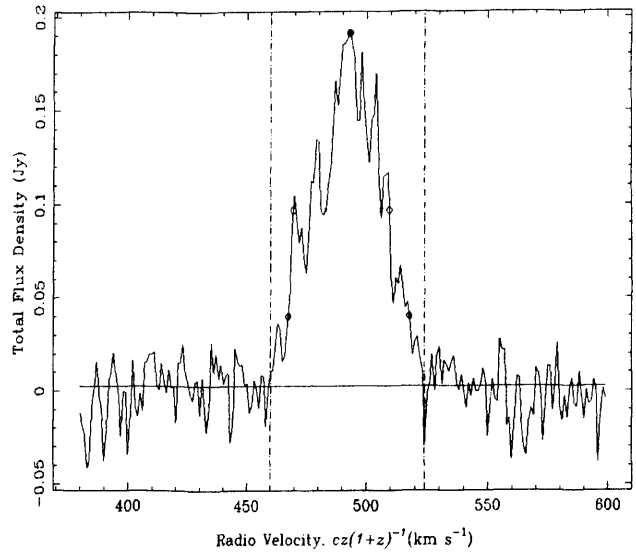

Figure 4.3: The HI profile of 1337-39 detected with the ATCA telescope.

have mentioned in chapter 2, there is not a significant discrepancy between the flux detected with ATCA and HIPASS (within the 10% error assumed for the HIPASS flux - see Table 2.3). From the 21-cm integrated flux we derive an HI mass $M_{HI} = 3.9 \times 10^7\ M_\odot$, at a distance of 4.8 Mpc (see section §4.5). A rough estimate of the dynamical mass (without any inclinationangle correction) gives $M_{dyn} = V_R^2 \times R_{HI}/G \sim 4 \times 10^8\ M_\odot$ and the ratio $M_{HI}/M_{dyn} \sim 0.1$, which is similar to the sample of gas-rich dwarfs studied by van Zee et al. (1997a) and to what is found for ESO0215-G?009 ($M_{HI}/M_{dyn} = 0.11$), one of the most gas-rich galaxies ever detected with $M_{HI}/L_B = 22$ (Warren et al. 2004). Roberts & Haynes (1994) determined for their sample of Sm/Im galaxies a median value of 0.15.

If we assume that the neutral gas is distributed in a circular rotating disc, as it appears to be, from the HI distribution we can measure the size of the gaseous distribution. The axial ratio of the contours at $N_{HI} = 5.0 \times 10^{20}$ cm^{-2} correspond to an inclination of $i \simeq 42°$.

The role of chaotic motions is in general more important in low mass galaxies (Lo & Sargent 1993; Young & Lo, 1996). As an estimate of the dispersion of the gas, in order to calculate the balance between rotation and chaotic motions, we have calculated the second moment with MIRIAD, defined as

$$\sigma = M_2 = \sqrt{\frac{\int I(v)(v - M_1)^2 dv}{\int I(v) dv}}$$

which corresponds to the intensity weighted velocity dispersion squared, where M_1 is the intensity weighted velocity defined as $\int I(v)vdv / \int I(v)dv$.

For HIPASS J1337-39 the resulting velocity dispersion is $\sigma_v \simeq 10$ km s^{-1}. The velocity resolution of our data set is 1 km s^{-1}, so we are not measuring an instrumental effect. Although the velocity dispersion is comparable to the rotational velocity - $V_R = 25$ km s^{-1}(without inclination angle corrections) or 37 km s^{-1}(inclination corrected) - $V \sin(i)/\sigma > 1$, chaotic motions appear not to be dominant for this dwarf.

Finally we have inspected the immediate environment of the galaxy to search for possible companions within the ATCA primary beam ($\sim 30'$), but we have not detected any emission from other sources.

4.2 Optical properties

The optical image of HIPASS J1337-39 is displayed in Fig. 4.4. The bulk of the stellar distribution shows an overall spherical symmetry, similarly to what is generally found in dSph galaxies. Outside the main spherical distribution stars probably belonging to the dwarf extend along the diagonal of the chip in the north-south direction until the edges of the frame.

Two HII regions can be identified from the WFPC2 image (Fig. 4.4), slightly offset from the optical centre. The star formation activity has been also confirmed by snapshots taken with the WIYN telescope (Knezek, *private communication*) and with the 2.3 m telescope at Siding Springs (Freeman, *private communication*) that we will discuss in the following section.

In Fig.4.5 we display the V surface brightness profile of the galaxy that we have derived from the WFPC2 image, after having convolved the image with a gaussian function with the task GAUSS in IRAF. The profile is well described by an exponential law, despite the presence of two bumps which are due to the HII regions. We have obtained a dereddened central surface brightness $\mu_0^V = 22.90 \pm 0.03$ mag arcsec^{-2}, which is about one magnitude below the sky brightness in the V band ($\mu_s^V ky = 21.8$ mag arcsec^{-2}), giving a total magnitude $m_V = 16.00 \pm 0.03$ mag.

Yet from its optical morphology this galaxy appears to be rather peculiar since on the one hand it

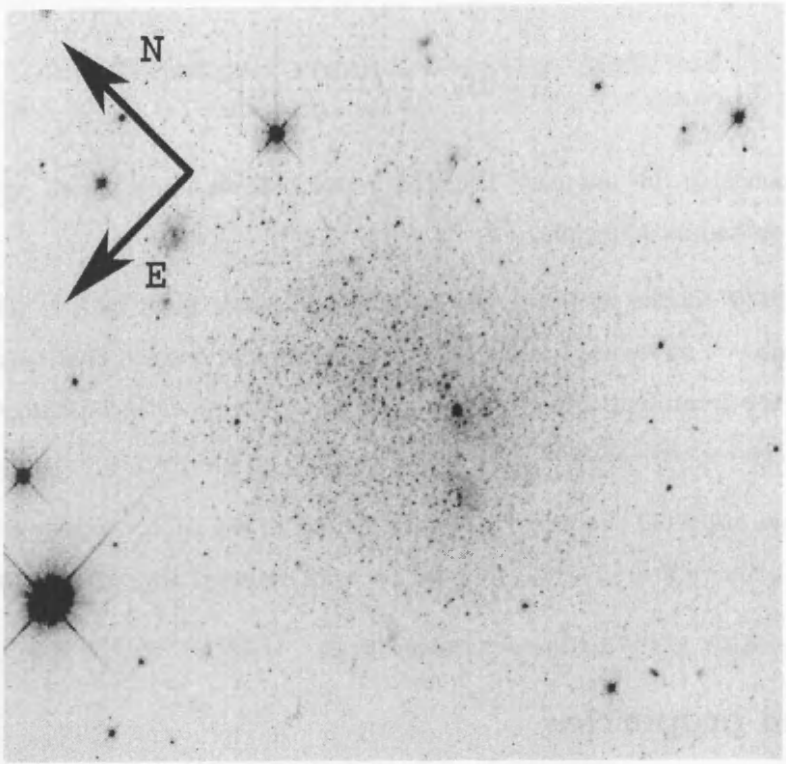

Figure 4.4: HIPASS J1337-39: The WFPC2 image of the galaxy taken with the filter F555W. The size of the frame is roughly 80″. North is on the upper-left corner, and East on the lower-left one. Two HII regions are clearly visible in the southern area of the galaxy.

shows a smooth and symmetric stellar distribution, which in general is found in dSphs, on the other it has SF regions and a large gas fraction which is more typical of dIrr galaxies. The sample of gas-rich dwarfs from van Zee et al. (1997a, 1997b) for example show irregular optical morphologies, while the optical appearance of 1337-39 is more similar to that of the so-called transition-type galaxies of the Local Group such as Phoenix or LGS 3. These galaxies though do not seem to have been forming stars in the last few hundred million years and even if neutral hydrogen has been detected, their gas fractions are low with $M_{HI}/L_B < 1$.

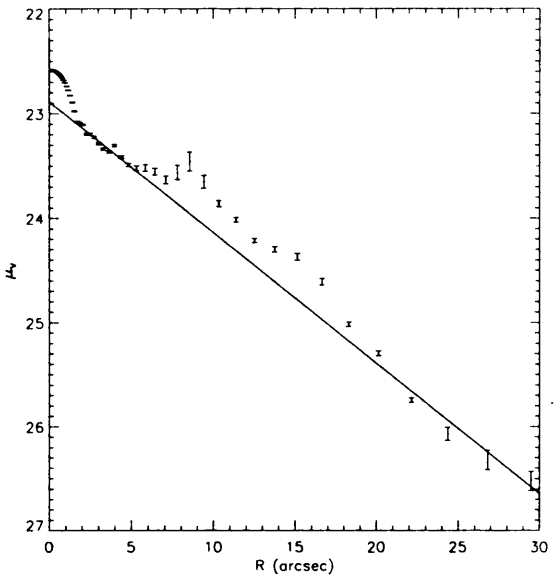

Figure 4.5: The V surface brightness profile of HIPASS J1337-39. We have obtained a central surface brightness $\mu_0^V = 22.90 \pm 0.03$ mag arcsec^{-2}, which is about one and a half magnitude below the sky brightness in the V band.

4.3 The spectral analysis of the HII regions: an independent constraint on metallicity from the oxygen abundance

We have observed 1337-39 with the Double Beam Spectrograph (DBS) on the 2.3 m telescope at the Siding Spring Observatory to study the chemical abundance of the HII region and to obtain an independent measure of the metallicity. This will help us to set a constraint on the current metal abundance of the ISM and possibly break the agemetallicity degeneracy that represents the main difficulty in the study of the stellar population.

The star forming region has been clearly detected with the DBS, which provides a spectral coverage of 3600 - 7000 Å. In this section we present the results of the analysis of the nebular emission lines.

Two exposures of 1337-39, each 2000 s long, were taken with both the blue and red grism. We performed the wavelength calibration using Neon - Argon lamps with exposures taken before and after the object observations. After the flux calibration, one-dimensional spectra were extracted from the two-dimensional

images by summing up all the pixels enclosed in the profiles of the Hα line. The background and sky lines were subtracted by averaging a region on either side of the extraction window. We have then identified the main emission lines and measured their fluxes. The data were reduced with the FIGARO package. The observed line intensities were corrected for interstellar extinction by comparing the observed and the expected hydrogen line ratios. Assuming the theoretical Balmer line value for case B recombination (Brocklehurst 1971), we have determined the reddening constant $C(H\beta) = (\log R_0/R)/\phi(\lambda)$ where $R_0 = I_{\lambda,0}/I_{H\beta,0}$ is the theoretical H line ratios relative to Hβ, R is the observed ratio, $\phi(\lambda) = (f(\lambda) - f(H\beta)$ is the extinction function relative to the Hβ line, where $f(\lambda) =< A(\lambda)/A(V) >$. For $A(\lambda)$ we have assumed the reddening law of Seaton (1979), with $R_V = 3.1$. The fluxes of the dereddened emission lines relative to Hβ, and the corresponding errors are displayed in Table 4.1. The Hα, Hβ fluxes are also listed at the bottom of the table with the extinction coefficient used.

The red and blue spectra are shown in Fig. 4.6, 4.7. Together with the usual hydrogen Balmer lines (Hα, Hβ, Hγ, Hδ), we find the oxygen lines [OII] λ3727, [OIII] $\lambda\lambda$4959, 5007. The [OIII]λ4363 and the Nitrogen [NII]$\lambda\lambda$6548,6584 lines are not detected, while very weak sulphur lines, [SII], are found at $\lambda\lambda$6717, 6731 (see Fig. 4.7).

The features of the spectra are typical of a low metallicity galaxy. Indeed there are many similarities with the spectra of the sample of gas-rich dwarf galaxies by van Zee et al. (1997b, 1997c) and of SagDIG (Saviane et al. 2002), such as the strong [O III]λ5007 line, the weak sulphur lines, and the undetectable or weak [NII] lines. The systems in the sample of van Zee have abundances ranging between 1/3rd and 1/24th of the solar value, while the oxygen abundance of SagDIG is about 2% of the solar value (Saviane et al. 2002).

Accurate oxygen abundances can be derived from the measurement of temperature-sensitive line ratios, such as [OIII]$\lambda\lambda$4959,5007/[OIII]λ4363. This method is usually addressed as the T_e - method. However, the absence of the temperaturesensitive line [OIII]λ4363 prevents the derivation of the electron temperature of the ionised gas and forbids the use of this method. Other metallicity estimators, such as the [NII] λ6548 and λ6584 Hα ratio, recently recalibrated by Denicoló et al. (2002) could not be used either because the [NII] line is missing.

Therefore, to determine the oxygen abundance, we had to use the R_{23} indicator, defined as R_{23} = ([OII]$\lambda\lambda$3727,3729 + [OIII]$\lambda\lambda$4959,5007)/Hβ. It is related to the strongest lines of the ionic species [OII] and [OIII], and it was introduced by Pagel et al. (1979). This indicator has been adopted for both low

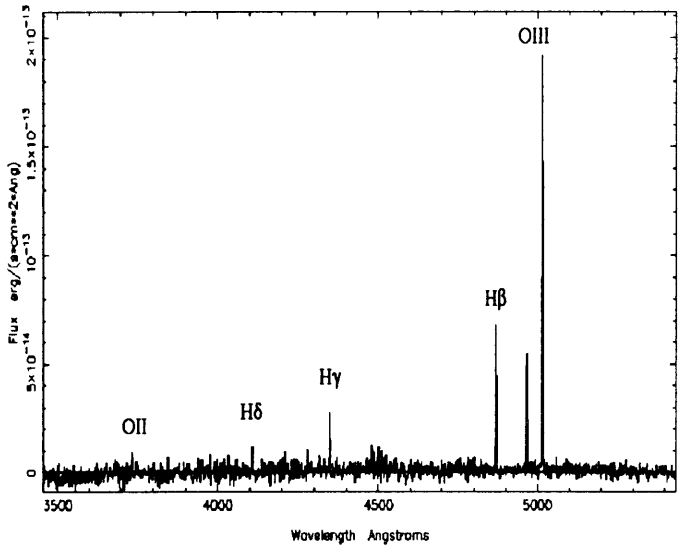

Figure 4.6: The blue part of the spectrum of the HII region of 1337-39 with the main nebular lines identified. The [OIII]λ4363 line is not visible, while we have detected the [OIII]λλ4959, 5007, the faint [OII]λ3727, and the usual lines of the hydrogen Balmer series.

and high metallicity HII regions as a valid alternative when the [OIII]λ4363 is not detected and the electron temperature can not be calculated directly (Skillman 1989, Mc Gaugh 1991, Pilyugin 2000).

Following Skillman (1989) we adopted his empirical relation between the oxygen abundance and the R_{23} parameter generally applied to low abundance HII regions (lower than 10% of the solar values).

$$12 + \log(O/H) = 1.21 \log(R_{23}) + 6.64 \tag{4.1}$$

We obtain 12 + log(O/H) = 7.35 ± 0.2 . As a comparison, the abundance of I Zw 18 is 12 + log(O/H) = 7.2 (Izotov & Thuan 1999). Therefore this galaxy appears to have a very low metal abundance.

More recently, Pilyugin (2000, 2001a, 2001b) has implemented the method of Mc Gaugh (1991) providing

Ionic species	$F(\lambda)/F(H\beta)$
[OII]	0.26 ± 0.06
Hβ	1. ± 0.05
[OIII](5007+4959)	3.61 ± 0.28
Hα	2.87 ± 0.20
[SII] 6717	0.07 ± 0.05
[SII] 6731	0.05 ± 0.03
$C(H\beta)$	0.053
$F(H\beta)^a$	$1.93 \cdot 10^{-13}$
$F(H\alpha)^a$	$5.53 \cdot 10^{-13}$

[a] In units ergs s^{-1} cm^{-2}

Table 4.1: Line flux ratios relative to Hβ. We also show the value of the reddening constant, $C(H\beta)$, that we have obtained and the Hα, Hβ fluxes.

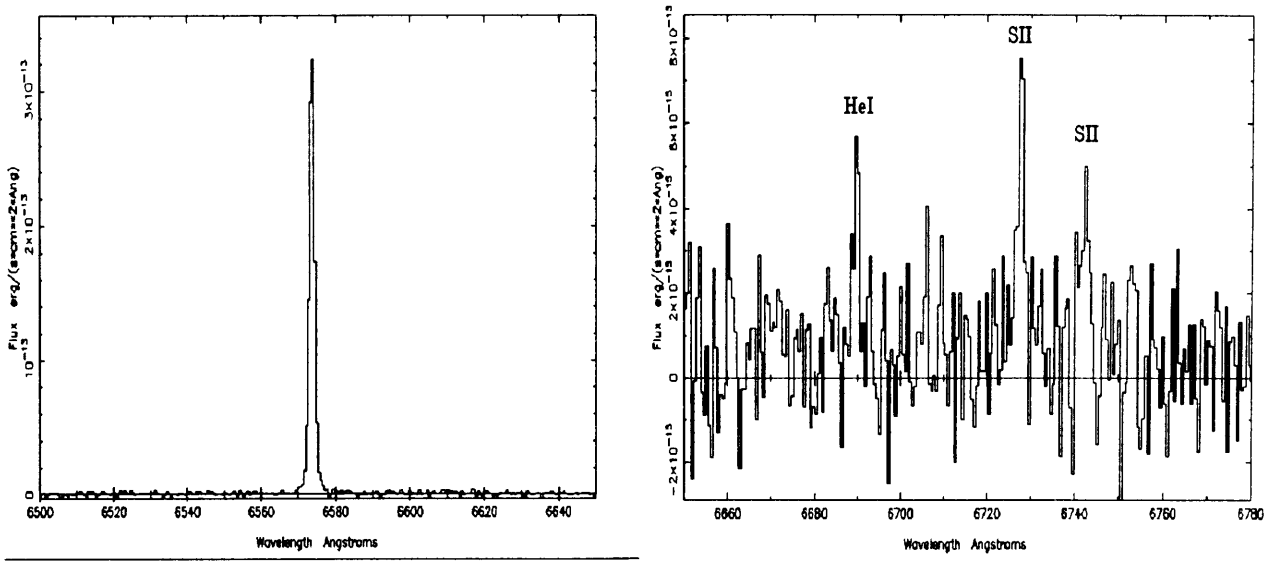

Figure 4.7: The emission line identification for the red part of the spectrum. The left panel shows the Hα line with no evidence of the [NII] lines at $\lambda\lambda$6548,6584, while in the right panel it is displayed the [SII] doublet and the [HeI] λ6678 LINE.

useful formulae to calibrate the R_{23} index both at high and low metallicity. Pilyugin transformed the relation between log(O/H) and R_{23} introducing the parameter R_3 =([OIII]$\lambda\lambda$4959,5007)/Hβ. In this case the equation for the oxygen abundance becomes

$$12 + \log(O/H) = 6.35 + 3.19 \times \log(R_{23}) - 1.74 \times \log(R_3) \tag{4.2}$$

which gives 12 + log(O/H) = 7.25, still compatible with the value we find using the relation by Skillman.

Given the solar oxygen metallicity $\log(O/H)_\odot + 12 = 8.83$ (Grevesse & Sauval 1998), and using the relation between the Iron and oxygen abundances given by Mateo (1998), we obtain [O/H] = log(O/H) $- \log(O/H)_\odot \approx 1/30$ solar and [Fe/H]= -1.95 ± 0.2.

It is important to stress though that the metallicity here determined using the indirect methods, such as the R_{23} index, may not be as reliable as the T_e method. Hidalgo-Gamez et al. (2002) in fact find that comparing the values obtained between the electron temperature method and the indirect ones by Olofsson

(1997), Pagel (1979) and Mc Gaugh (1994), large deviations are evident especially at low and high metallicity. Unfortunately we do not have any other chance of measuring the oxygen abundance given the spectrum we have obtained for the HII region. High S/N spectra taken at larger telescopes would be needed to place better constraints on the abundance of 1337-39, by allowing the measurement of the [OIII]λ4363 line and/or the [NII] lines.

To summarise, we have derived the oxygen abundance of HIPASS J1337-39 from the spectrum of its HII region. Since the metallicity is a measure of the degree of evolution of a system, the low abundance that we have derived suggests that 1337-39 is a poorly evolved system. To finally establish whether this is the consequence of an overall young age or not, we need to analyse the results of the resolved stellar photometry to constrain the age of the galaxy.

4.4 The morphology of the Colour magnitude Diagram

Once we have constrained the metallicity from the HII region we can proceed to the study of the stellar population from the colour magnitude diagram (CMD) of the galaxy. An initial estimate of the metallicity is essential to discuss the SFH of a galaxy. The stellar content of 1337-39 is displayed in the left panel of Fig. 4.8 where we show the (I; $V-I$) CMD built from our two filter photometry as described in Chapter 2. Photometric errors, obtained from the point spread function (PSF) fitting (see Chapter 2), are plotted on the right of the figure. The CMD clearly shows a population of blue young stars with colours $V-I<0.7$, the blue plume, and a larger number of red stars which mainly populates the upper part of the red giant branch (RGB) at colours $0.7<V-I<1.5$. The right panel of Fig. 4.8 shows instead the CMD of the two remaining chips of the WFPC2 (WF2, WF4) which do not contain the galaxy, and they have been used to estimate the contamination of the field by foreground stars.

One of our main objectives is to constrain the age of the stellar populations to infer if such gas-rich galaxies represent a class of recently formed systems, or if their evolution is "slowed down" or "retarded" because the conversion of gas into stars is not efficient. Several age indicators in the CMD have been discussed in Chapter 3 and they can be used to set constraints on the age of the galaxy. The RGB, for instance, is expected to host the oldest stellar population one can detect in this data set. As mentioned before, this feature contains also information on the distance and metallicity of a galaxy. Therefore we start our analysis of 1337-39 by describing the oldest discernible stellar population of the RGB. Then we continue

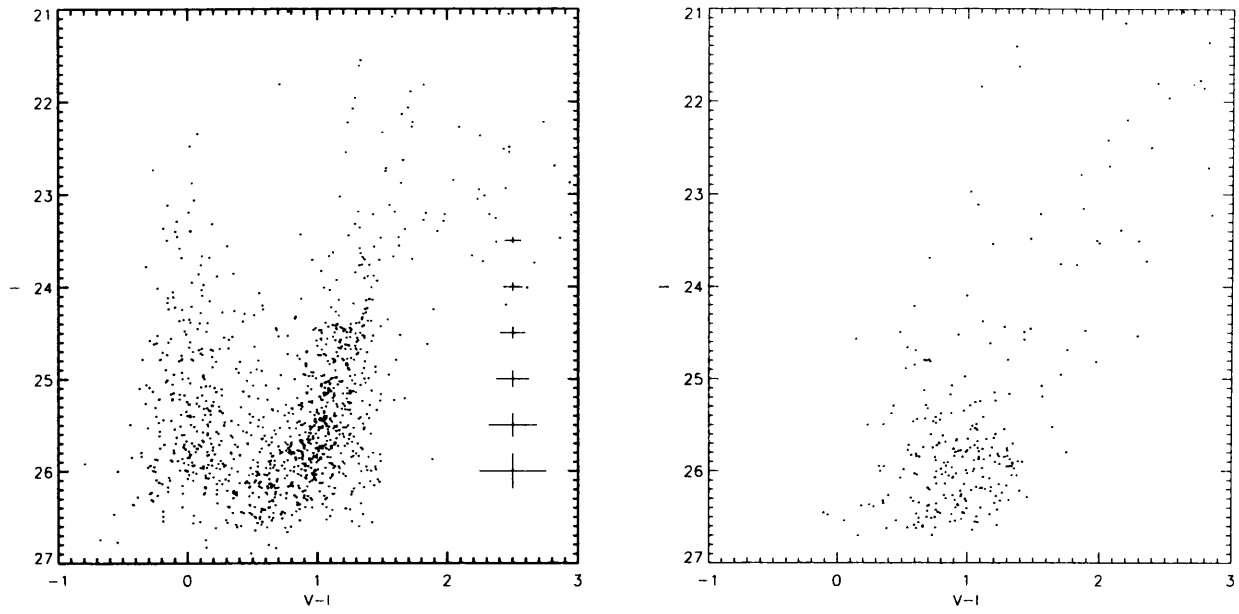

Figure 4.8: **Left**: The $(V - I)$, I color magnitude diagram of HIPASS J133739. **Right**: The CMD of the field region. This diagram has been constructed by using only the halves of the chips (WF2, WF4) not adjacent to the WF3 where the galaxy was positioned. This choice reduces the possible contamination of the field by stars belonging to the dwarf.

with the other age indicators until finally reaching the youngest and bluest stars.

4.5 The red giant branch (RGB): deriving the distance of the galaxy

The high concentration of stars at $I > 24.5$ and $0.8 < V - I < 1.5$ is the RGB, which is generally populated by old and intermediate age populations. As explained in chapter 3, the absolute magnitude of the tip of the RGB is considered a robust distance indicator. To determine this parameter we have selected stars with colours $0.8 < (V - I)_0 < 1.7$ and we have built the I luminosity function of these stars grouped in magnitude bins of $\pm$ 0.05 mag. An edge detection Sobel filter of kernel [−1, −2, 0, 1, 2] (Madore & Freeman 1995) has been applied to the function. The filter produces a sharp peak when a sudden drop in the original function

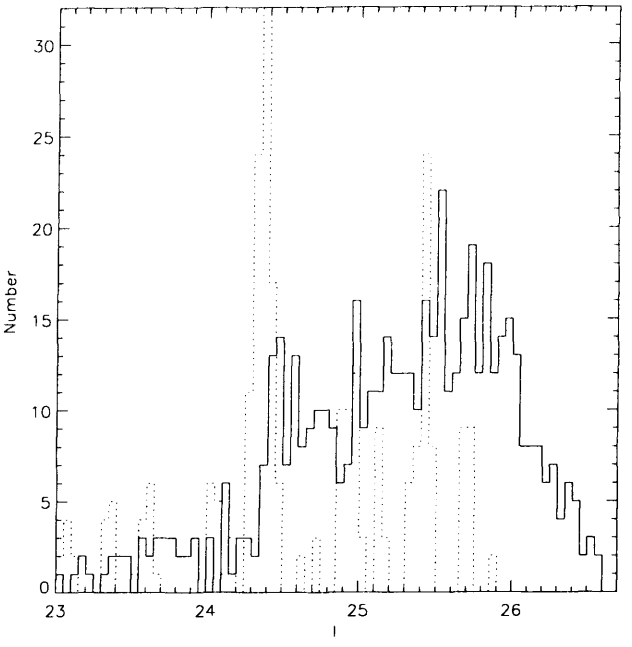

Figure 4.9: The luminosity function of the RGB of HIPASS J1337-39. The output of the edge detection Sobel filter is overlayed (dotted line). After having applied the filter we found the tip of the RGB at $I_0 = 24.37 \pm 0.11$.

occurs. The I luminosity function (*solid line*) and the output of the Sobel filter (*dotted line*) are both shown in Fig. 4.9. A cut-off in the RGB luminosity is found at $I = 24.37 \pm 0.11$, where the magnitudes have been already corrected for the galactic extinction using $E_{B-V} = 0.07 \pm 0.01$ and $A_I = 1.85 \times E_{B-V} = 0.14 \pm 0.02$ (Schlegel, Finkbeiner, & Davis 1998). The error on the magnitude of the tip results from the combination of: a) the uncertainty in the TRGB position defined as 1 bin width of the luminosity function (± 0.05 mag) - b) the uncertainty in the photometry at that magnitude (± 0.06 mag), c) the error in the photometric zero-point of the WFPC2 (± 0.05 mag) (Holtzmann et al. 1995a) d) the error in the aperture correction (± 0.05 mag) and e) reddening (± 0.02 mag). Assuming the I absolute magnitude of the tip at $M_I = -4.05$, the distance modulus is $(m - M)_0 = 28.42 \pm 0.11$, giving a distance $D = 4.8 \pm 0.2$ Mpc. This value places 1337-39 in the region of M 83 (4.5 Mpc) although it is at a projected distance of 10°($\sim$ 800 kpc) from the spiral (see Fig. 2.1).

4.6 A young or old galaxy?

4.6.1 A constraint on metallicity and age from the RGB

We can use the RGB to inspect the abundance of the red giant stars which are, potentially, the oldest population of stars hosted by the galaxy that we could detect. The simplest method to follow would be to compare the colour of the RGB of this dwarf with that of well-known metal-poor galactic globular clusters (GGCs) (Da Costa & Armandroff 1990). In Fig. 4.10a the fiducial RGB of M 15, one of the most metal-poor GCC with [Fe/H]= -2.17, is overlaid on the CMD of 1337-39.

Most of the RGB stars of the dwarf extends blueward of the fiducial line representing the globular cluster, which suggests an even lower metallicity. If we take as a reference the mean of the distribution of the stars in the RGB, the resulting de-reddened colour $(V-I)_{-3.5} = 1.14 \pm 0.13$ would give an abundance [Fe/H]= -2.6 ± 0.6, placing it among the lowest metallicity nearby dwarf galaxies. However, the error on the photometry at that magnitude ($M_{I,0} = -3.5$) is rather large, and secondly Lee et al.'s relation (Lee et al. 1993) is used in extrapolation, since the least metallic globular cluster is M 15 at [Fe/H]= -2.17. In any case, we can set an upper limit on the metallicity by saying that the 1337-39 lies at the extreme metal poor end of dwarf galaxies and its abundance has to be lower than [Fe/H]< -2.17.

However, this technique to derive the metallicity relies upon the hypothesis that the dominant population of the RGB is several Gyrs old (Population II stars). This assumption cannot be taken for granted for these galaxies because their high M_{HI}/L_B ratios are possibly indicative of systems with an overall young age. What we can say is that if the galaxy has population II stars, then its metallicity has to be lower than [Fe/H]< -2.17. It may also be that the observed colour of the RGB is due to a younger population of red giant stars with a higher metal abundance. The independent measure of the metallicity from the spectroscopical analysis of the HII region sets an upper limit to the metal content of the red stars of about 1/30 solar. The rather low oxygen abundance seems fairly consistent with the value of the metallicity obtained from the RGB.

As a final step, we compare the CMD features with isochrones at different metallicities to definitely constrain the possible range of abundances and ages which can produce the observed colour of the RGB, being at the same time coherent with the measured ISM abundance.

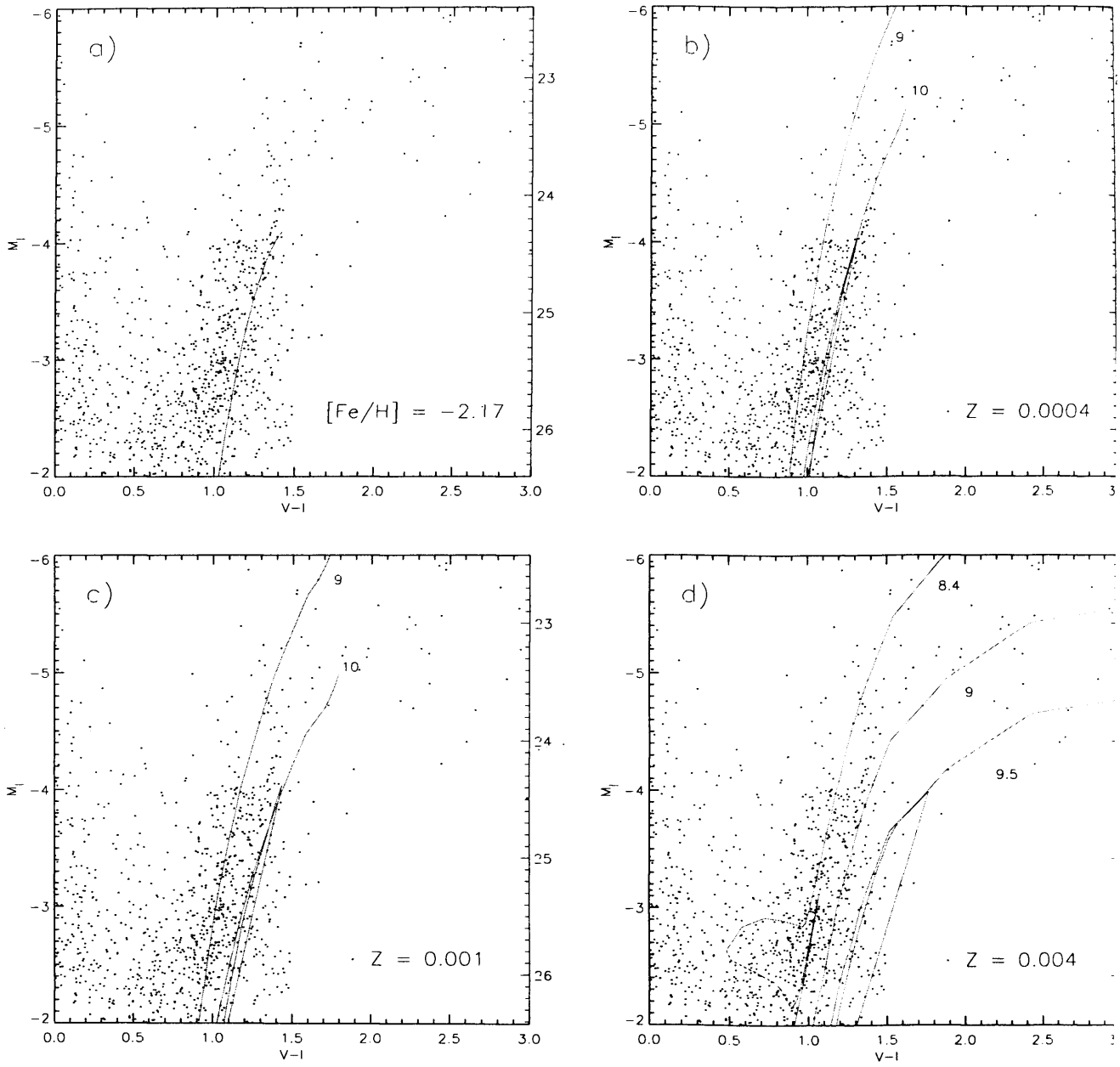

Figure 4.10: The RGB of HIPASS J1337-39 overlaid with the RGB of the galactic globular cluster M15 (panel a), and with Padua evolutionary tracks at Z= 0.0004 (panel b), Z = 0.001 (panel c) and Z = 0.004 (panel d). Different values of log(*Age*) have been chosen for each set of isochrones. For the two lowest abundances the age of the RGB stars would be between 1 and 10 Gyr, while for Z = 0.004 the red stars would be predominantly young, with an age less than 3 Gyr.

4.6.2 Comparison with stellar isochrones

Fig. 4.10b,c,d display the stellar tracks from the Padua group (Be94, Gi02) for three sets of metallicities which best fit the observed colour of the RGB: Z = 0.0004 (1/50 solar), Z = 0.001 (1/20 solar), Z = 0.004 (1/5 solar). The two lowest abundances describe a poor-metal scenario with an intermediate-age (1 - 10 Gyr) dominant stellar population. On the other hand, if the metallicity of the RGB is Z = 0.004, the bulk of the RGB stars would be younger than 1 Gyr, corresponding to a complete opposite scenario. This is the maximum metallicity allowed at which isochrones can match the position of the RGB in the diagram.

However the possibility of a $\sim$ 1 Gyr old RGB (Z = 0.004, i.e. 1/5 solar) seems highly unlikely, since it would be difficult to explain a population of old stars with a metallicity higher than the current abundance of the ISM.

Therefore, by comparing the colour and the shape of the RGB with the stellar evolutionary tracks we infer that the bulk of the red stars observed is a metal-poor population which is $\lesssim$ 10 Gyr old. Thus, the age of this dwarf galaxy may be consistent with the Hubble time, rather than being a recently formed system. Further evidence, supporting the low metallicity/intermediate-age population scenario will be discussed in the following sections, such as the presence of a low metallicity extended AGB branch. Moreover, simulated CMDs at different metallicity will be described to show how the change in the abundances affects the morphology of the diagram and eventually discriminate between different SFHs.

4.7 AGB stars: tracing the intermediate-age population

The presence of low mass AGB stars is usually taken as evidence for an intermediate-age population. Unambiguous identification of these stars would confirm that SF activity has taken place at ages that correspond to look-back times of several Gyr. For this reason the search for AGB in these gas-rich dwarfs is extremely important in order to set another constraint on their age. The distribution of intermediate-age AGB stars on the CMD depends very strongly on the metallicity: the higher the metallicity, the more extended this feature is towards colours redder than the RGB. At metallicities Z $\lesssim$ 0.001 the AGB extends almost vertically above the RGB instead of bending towards redder colours.

In the CMD (Fig. 4.8 and 4.10) there is evidence of a very narrow "red tail" elongated for roughly one magnitude above the tip with colours similar to the RGB ($1.2 < V - I < 1.6$). This would suggest the

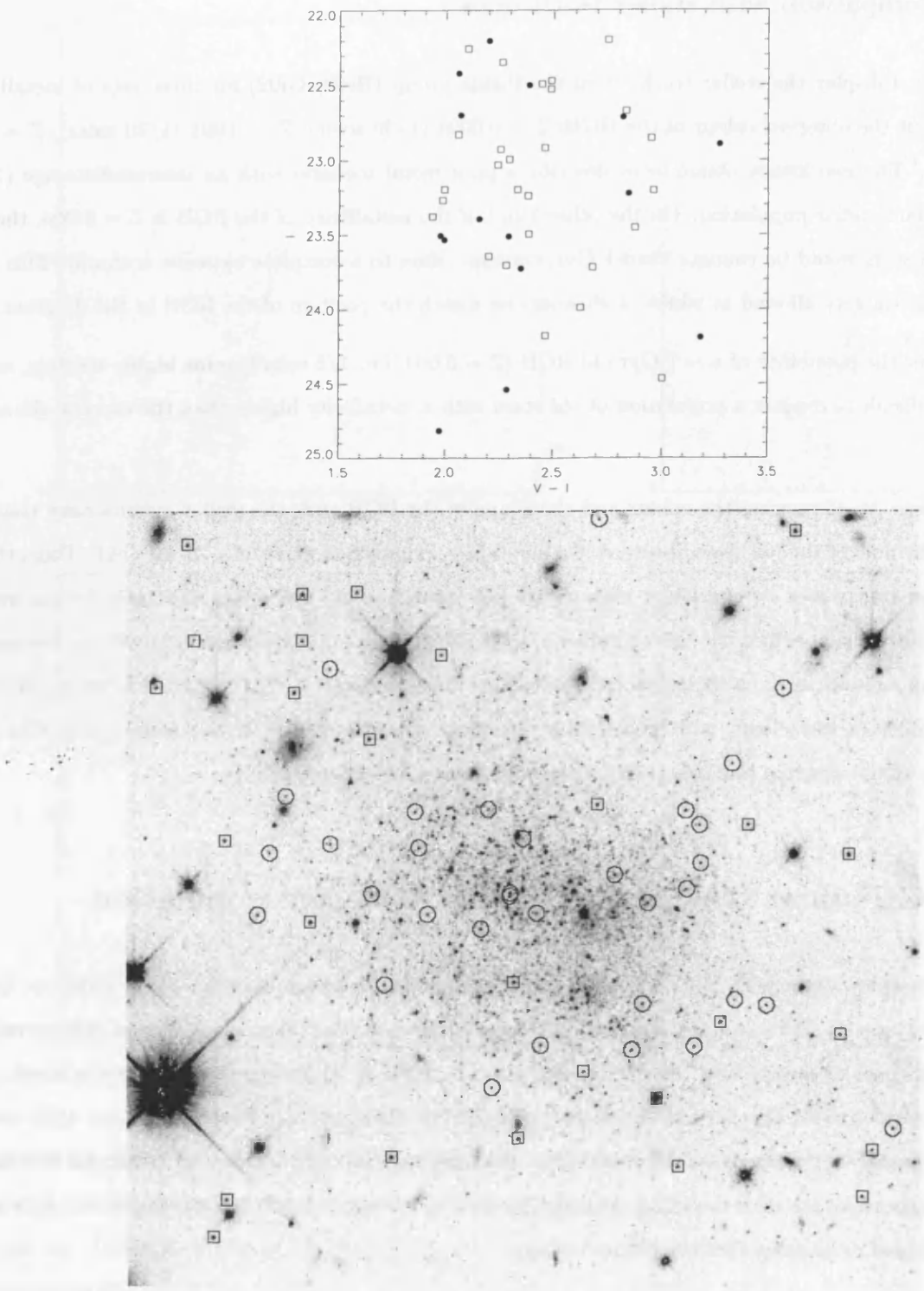

Figure 4.11: **Up:** An enlarged view of the CMD of the very red stars ($V-I \gtrsim 2$, $22 < I < 25$) found around 1337-39 (WF3) (*squares*), compared to the foreground contamination in the adjacent fields (*filled circles*). As one can see there is a probable contamination in this area. However, given the higher number of red stars detected in the WF3 chip ($\sim 3\sigma$), we cannot exclude that most of these stars belong to 1337-39. **Down:** The position of such very red stars on the WF3 frame (*squares*) compared to that of the AGB candidates (*circles*) with colours similar to the RGB ($1.2 < V-I < 1.7$).

presence of such a metal-poor intermediate-age AGB population. The isochrones at 10 Gyr ($\log(Age) = 10$) and Z = 0.0004 in Fig. 4.10b match the thin red tail of AGB stars and define an approximate lower limit on the age of the galaxy. If we use Z = 0.001 isochrones, the age of the AGB stars decreases to about 7 Gyr. Therefore the AGB can be taken as a further argument in favour of the low-metallicity and intermediate-age scenario, previously inferred from the RGB analysis.

We have also detected a number of very red stars at colours $V - I \gtrsim 2.0$ and brighter than the TRGB ($22 < I < 24.5$) whose nature is not very clear. We have looked at the CMD of the adjacent fields to check if there are stars with similar photometric properties ($V - I > 1.9$, $22 < I < 24.5$). We find 15 such stars in the field, compared to 27 stars detected around 1337-39. We plot the CMD of these two sets of stars in the upper panel of Fig. 4.11.

The probable contamination by foreground stars in the area is lower than the number of stars observed ($N_{obs} - N_{foreground} = 12 \pm 4$), thus we can not exclude that they may belong to the dwarf.

However, after having verified that they are point-source like in appearance, we have marked with squares their positions on the WF3 frame (displayed in the lower panel of Fig. 4.11), and we have compared their distribution to the less red ($1.2 < V - I < 1.7$) AGB stars candidate with magnitudes $-5 < M_I < -4$ (marked with *circles*). As one can see from the figure, they are mostly found at the border of the main body of the galaxy, with a wider distribution than the bluer AGB candidates.

The presence of these stars in HIPASS J1337-39 is a puzzle, because their red colours would not be easy to explain, and they would imply the presence of a higher metallicity population. Only isochrones at Z = 0.004 (1/5 solar), in fact, can match their location on the CMD, but this would be in sharp contrast with the lower abundance of the ISM that we have measured. If they belong to HIPASS J1337-39, their age is between 1 and 3 Gyr (as indicated in Fig. 4.10) and they must be younger than the bluer (and with a lower metallicity) AGB candidate stars. Moreover, if they are younger than the other AGB stars, how can they be so widely spread throughout the frame while the allegedly older AGB stars are more centrally concentrated and mostly detected within or around the optical body of the galaxy?

It is interesting to compare 1337-39 with other galaxies to see if similar features have been observed in other dwarfs. In SagDIG for example, one of the lowest metallicity dIrr galaxies in the Local Group, several stars at red colours have been detected in its CMD and they have been interpreted as an extended tail of intermediate-age AGB stars (see Fig. 4.12, Momany et al. 2002). Some of the red and bright stars

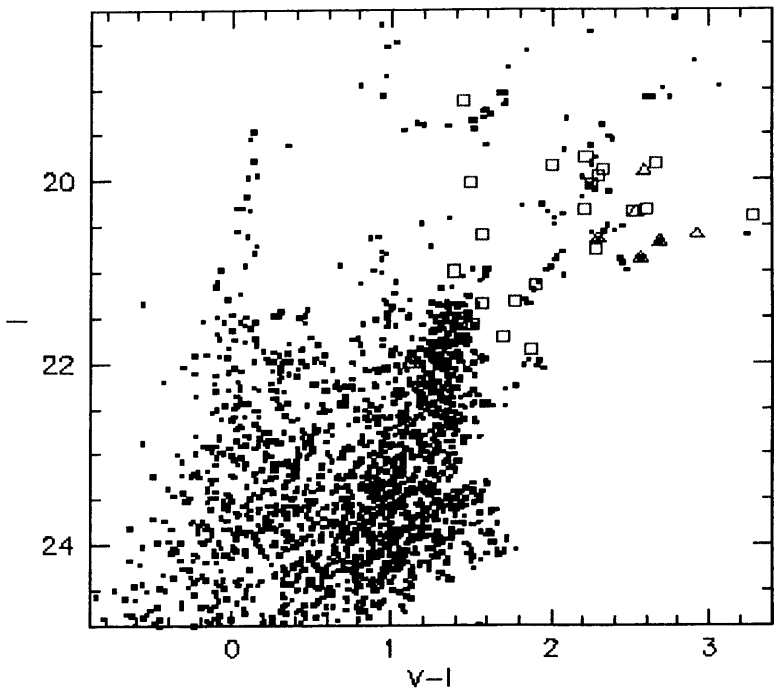

Figure 4.12: Colour magnitude diagram of Sag DIG from Momany et al. (2002). The RGB morphology and colour is typical of a low metallicity galaxy. At redder colours ($V - I \gtrsim 2$) several stars have been detected. The candidate carbon stars identified in previous surveys are indicated with *squares* (Cook 1987) and *triangles* (Demers & Battinelli 2001). The C stars do show similar photometric properties as those found with the WFPC2 observation of 1337-39.

observed by Momany and collaborators had been in fact previously catalogued by Cook (1987) and Demers & Battinelli (2002) as Carbon stars. Cook (1987) divided these stars into two classes, a luminous 1 Gyr population reaching up to two magnitudes above the TRGB, and a bluer and fainter population about 10 Gyr old. A classification which could fit with the kind of objects we are finding in this galaxy. However neither Cook, nor Momany et al. mention that these two population of AGB stars may have a different metal abundance. SagDIG is a metal poor galaxy and even the composition of the warm gas in the HII regions does not appear to be significantly metal enriched with respect to the red giant stars. Without further observations, either spectroscopy or narrow band photometry using the $Ti - O$, or CN filters it is not possible to discriminate the nature of these red stars in 1337-39 and to understand if they belong to the

dwarf galaxy rather than being foreground galactic stars.

It is also worth pointing out that stellar models are known to be uncertain in the AGB phase (Schulte-Ladbek et al. 1999) because their atmospheres contain difficult-to-model molecules, and mass loss is an important but ill-known parameter that determines their evolution. Nevertheless, even if uncertain, modelling is the only tool available to estimate the age of these stars and it will be used for the comparison with the data.

To summarise, it appears from the properties of the red features in the CMD of 1337-39, that the galaxy contains a dominant population which is at least several Gyr old, with a lower limit on the age set by the presence of candidate AGB stars. From the comparison with isochrones that fit the position of the AGB stars, one obtains at Z = 0.0004 an upper limit of $\sim$ 10 Gyr, or $\sim$ 7 Gyr if the metallicity of the isochrones is Z = 0.001. The presence of a possible population of very red stars in HIPASS J1337-39 remains a puzzle, and it does not fit very well with this scenario of a galaxy with an overall low metal abundance.

4.8 The recent star formation history

4.8.1 Looking for young stars in the CMD: the blue plume

The evidence of recent star formation activity in HIPASS J1337-39 is clearly inferred from the population of young and blue stars at colours $V - I \lesssim 0.5$ extending up to $I \simeq 22$ (Fig. 4.8). This "blue plume" is populated by intermediate mass stars in the main sequence (MS) phase and more evolved core helium burning stars that form the blue loop (BL). The BL stars generally form a parallel and redder track compared to the MS. The location of the different evolutionary stages on the diagram is shown by the isochrones at Z = 0.0004 in the left panel of Fig. 4.13.

We have chosen to use isochrones at Z =0.0004 to describe the young population because, although Z = 0.001 would represent a more appropriate choice given the measured ISM abundance, an updated set of isochrones with ages less than 100 Myr at that metallicity is not available yet. However there does not appear to be a large difference in the evolution of young stars between the Z = 0.0004 and Z = 0.001 sets of isochrones (Bertelli et al. 1994, Girardi et al. 2002).

Having set the metal abundance we can constrain the age of the young stellar population. The maximum

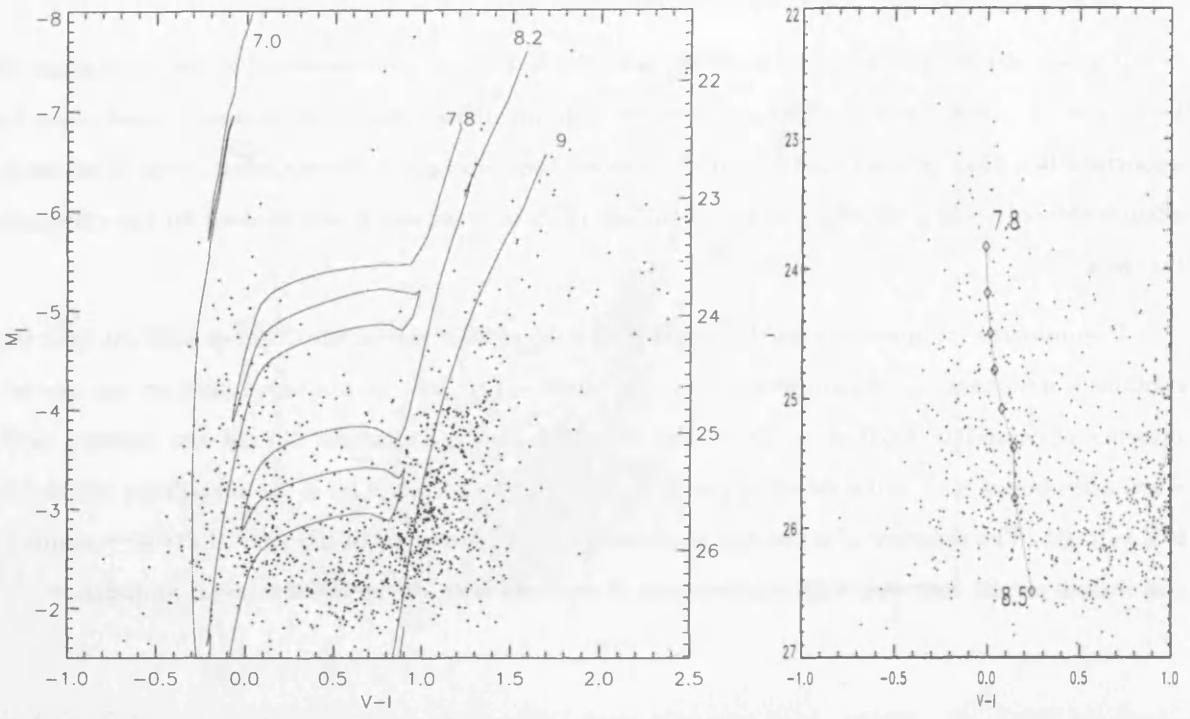

Figure 4.13: HIPASS J1337-39: (V-I, I) colour magnitude diagram overlaid with Padua evolutionary tracks at Z= 0.0004. The different isochrones correspond to $\log(Age) = 7$ (10 Myr), 7.8 ($\sim$ 60 Myr), 8.2 (150 Myr) and 9 (1 Gyr). (**right**) A close-up of the blue plume where it is indicated the location of the brightest and bluest point of the core helium burning evolution at different ages, to show the maximum age of the stars in the blue plume detectable with this data set.

luminosity of the main sequence is related to the age of the youngest population. At Z = 0.0004, the stars in the MS appear to be as young or younger than 10 Myr. To look further back in time in the recent SFH of the dwarf, one has to use the BL stars. The positions of the brightest blue supergiants in the diagram are consistent with isochrones around 35 and 60 Myr, showing that SF has been going on in a rather continuous way in the last 100 Myr. In the right panel of Fig. 4.13 the position of the bluest and brightest edge of the BL at different logarithmic ages (from 7.8 to 8.5) is overlaid on the blue plume of the CMD to emphasize the location of BL stars during their evolution along the diagram. This also shows the maximum age of the stellar population we can trace back by looking at BL stars in this galaxy. Given the 50% completeness limit

of our photometry at $I = 26.2$, one can see that BL stars older than log Age 8.4 ($\sim$ 250 Myr) are appreciably affected by incompleteness.

Finally, a few red bright stars with $22 < I < 24$ and $1 < V - I < 1.3$ are present, which are likely members of the galaxy and may be considered as red supergiant candidates. Their total number is small compared to the blue loop stars, but this is consistent with the fact that, at low metallicity, stars spend more time in the blue supergiant phase (Bertelli et al. 1994, Girardi et al. 2002).

4.9 Radial gradients in the stellar population

If we plot the spatial distribution of the stars roughly dividing them in blue ($V - I < 0.7$) and red ($0.7 < V - I < 1.5$) stars, as it is shown in Fig. 4.14, one can see that the two stellar population have a different spatial clumping in the galaxy.

The blue stars, shown in the upper panel, are more centrally concentrated with an almost spherical distribution. The peak density of the blue stars occur in the upper left corner of the distribution. They occupy a significant portion of the galaxy which suggests that 1337-39 may have experienced an extended epoch of SF activity throughout its central core.

The red stars (lower panel) occupy a larger area of the chip and their distribution is clearly more extended along the diagonal which goes from the upper left corner to the bottom right one (North - South direction), indicating a slightly more irregular morphology. There are two density peaks, one of which is related to the higher concentration of blue stars. The other is in the lower right area of the galaxy, on the opposite side compared to the blue ones. It is worth stressing that we have divided the red stars only according to their colours ($V - I > 0.8$) therefore the plot of the density contours include also the bright red stars above the tip of the RGB which are not necessarily all old stars and are related to the peak in the blue star distribution. Therefore even though red stars are widespread throughout the galaxy there seems to be two areas where the concentration of red stars is higher. One is related to the density peak of the blue stellar distribution, probably indicating a younger population of red stars, while the other is not. This may indicate that the SF process had moved from one edge to the other of the galaxy with time.

Radial gradients in the stellar population are quite common in dwarf irregular galaxies in the LG with ongoing star formation (Mateo 1998); e.g. in Sextans A (Aparicio et al. 1987), Leo A (Tolstoy 1996), WLM,

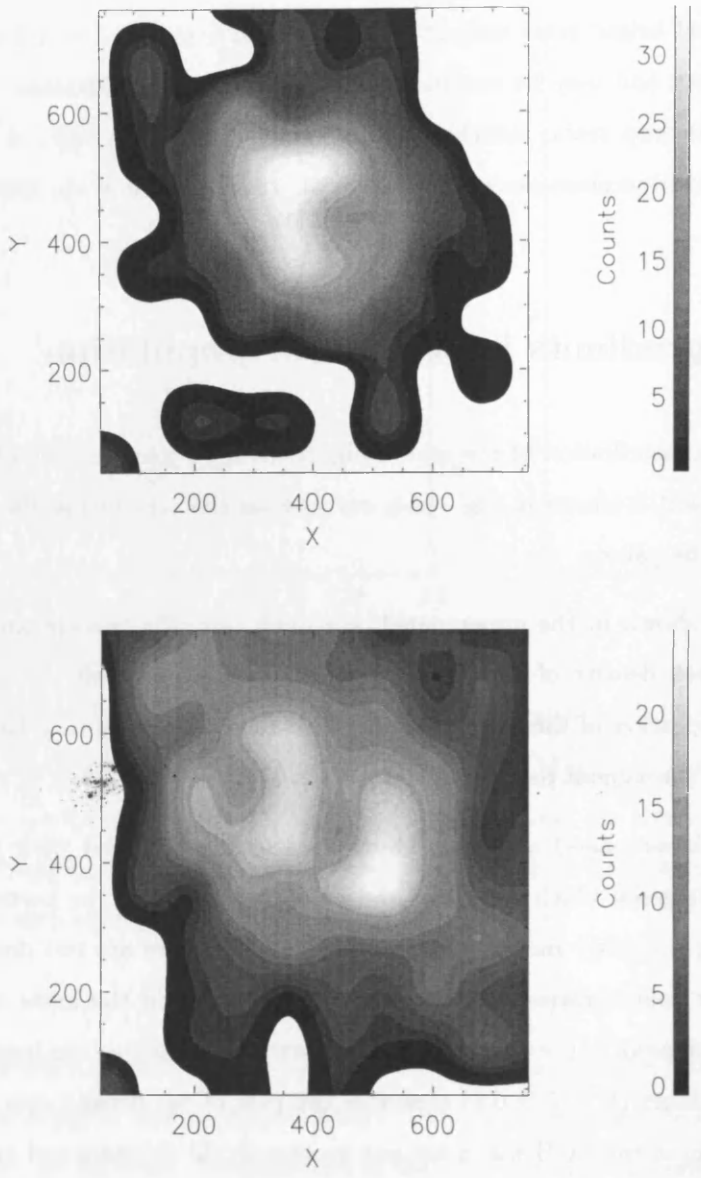

Figure 4.14: Density contours of the distribution of blue, $V - I < 0.7$ **(up)**, and red, $0.7 < V - I < 1.5$ **(down)**, stars in HIPASS J1337-39. The younger stars appear more centrally concentrated and are superposed to a more extended population of red stars.

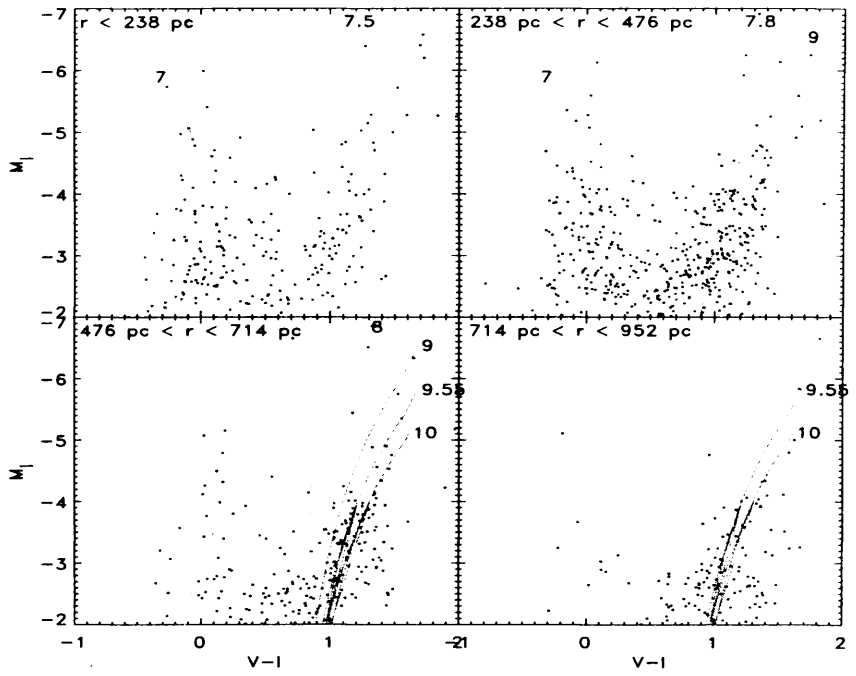

Figure 4.15: HIPASS J1337-39: CMDs for four concentric circular areas where the radii have been transformed from the angular (10″- 40″) to the physical scale. Padua tracks (Z= 0.0004) have been overlaid to underline the change in the age of the stellar population from the centre to the outer regions. Moving out from the inner to the outer circle, the blue stars progressively disappear, leaving only a population of red giant stars which according to the stellar isochrones may have an age between 4 and 10 Gyr.

IC 1613 and Sag DIG (Momany et al. 2002), but also transition-type dIrr/dSph like LGS 3 (Miller et al. 2001), Phoenix (Martinez-Delgado et al. 1999), and the dSPh Fornax (Stetson et al. 1998) all show centrally concentrated younger populations, indicating a varying SFH across the galaxy. HIPASS J1337-39 follows this same trend and shows a gradient in the distribution of the stars according to their ages, which is better clarified in Fig. 4.15.

If we assume that the young stars retain the velocity dispersion of the HI clumps from which they originated (which is found to be in general around $\sim 10\ \mathrm{km\,s^{-1}}$) the mixing times of stars within the discs of

galaxies are typically $\ll$ 1 Gyr. For instance the crossing time of a 500 pc region at that velocity is roughly 50 Myr. However the region of a galaxy that is accessible to stars born in a disc may be constrained by the energy and angular momentum of the interstellar gas clouds where they formed. Stars formed from interstellar clouds near the centre of a galaxy are unlikely to have sufficient energy or angular momentum to travel very far out in the stellar disc (Gallagher et al. 1998).

We have selected four regions in the WF3 chip containing the dwarf, by drawing four concentric circles around the center of the object. The radii of each circle go from 10" to 40" with the outer one including approximately the whole chip. Then we have plotted the CMD within each ring to study how the radial distribution of the stars varies.

Again, the young blue stars in HIPASS J1337-39 are concentrated in the centre of the galaxy but, as it is shown in Fig. 4.15, the main bulk of the recently formed stars is in the second ring at 237 pc < r < 474 pc, and indicates the correlation of the recent star formation episode with the peak of the HI distribution which appears to be slightly offset from the centre (see §4.4.1). Main sequence and blue supergiants stars with ages from 10 Myr to 100 Myr are mainly found in these two regions. In the second circle the RGB begins progressively to dominate and it becomes much more populated. By the fourth circle most of the young stellar population has disappeared. The narrowing of the red plume at larger radii could be interpreted as the presence of a much older population of RGB stars in the outer part of the galaxy which may be the signature of an extended old disk or "halo" as it is found in other dwarf galaxies such as Antlia (Aparicio et al. 1997), WLM (Minniti & Zijlstra 1996), Izw 403 (Schulte-Ladbeck et al. 1999).

4.10 Modelling the SFH of HIPASS J1337-39

We have used the StarFISH code of Harris & Zaritsky (2001) to investigate the SFH of the galaxy. We have combined the set of isochrones provided by the Padua group with different values of the metallicity and we have built synthetic CMDs of 1337-39. The code compares the observed CMD and a linear combination of synthetic CMDs built by a set of stellar isochrones which is provided by the user. It performs χ^2 minimization of the differences in the number of stars between the model and the data in the different regions of the CMD, having taken into account the scatter in the stars' photometry as follows from artificial star tests (see Chapter 3 for details). We have used the entire range of available ages (from 10^7 yr to $10^{10.2}$ yr) with a step of $\log(Age) = 0.2$. We have adopted a Salpeter initial mass function(IMF), a binary fraction of 0.5,

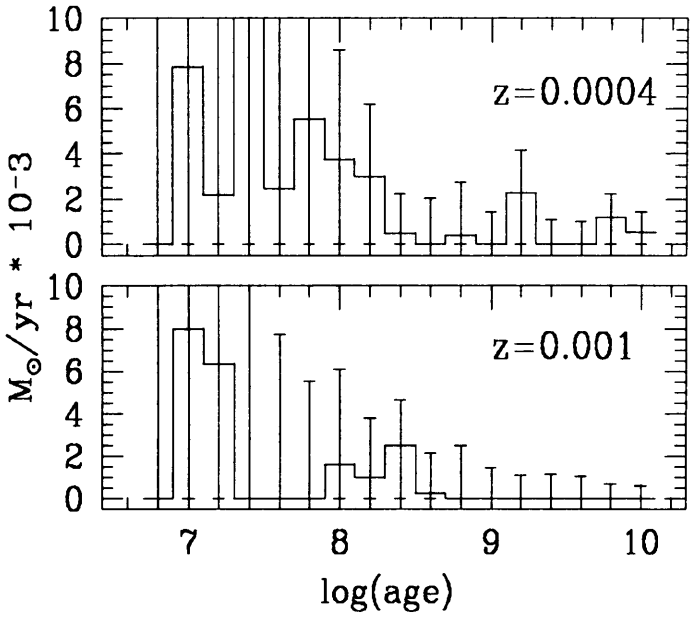

Figure 4.16: The SFH of 1337-39 obtained with a combination of stellar isochrones with metallicities Z = 0.0004 and Z = 0.001. We find two main episodes of star formation: one between 6 and 10 Gyr (log(Age) =9.8 - 10), and the other around 1.5 Gyr (log(Age) =9.2). An increase in the SFR seems to occur in the last 200 Myr.

and we have included the Galactic foreground extinction factor (neglecting to take into account the internal extinction of the galaxy). The distance modulus has been set to $(m - M)_0 = 28.42$.

The metallicity is constrained between 1/50th and 1/30th solar from the analysis of the CMD and the oxygen abundance respectively, corresponding to Z = 0.0004 and Z= 0.001. Therefore we have created a synthetic CMD with a combination of the two sets of isochrones at that abundance. The resulting SFH, for which we have determined a χ^2 value of 1.17, is shown in Fig. 4.16. For the lowest metallicity component (Z = 0.0004) there is evidence of an extended period of SF around 6 - 10 Gyr (log(Age) = 9.8, 10). The galaxy then appears to go through a rather quiescent period, until the following event occurring at $\sim$ 1.5 Gyr (log(Age) = 9.2). For ages around or less than 1 Gyr the SFR seems to be rather low with a remarkable enhancement in the last 200 - 250 Myr. The oldest stars have metallicities Z = 0.0004, while populations with higher metal abundance appear only in the last Gyr.

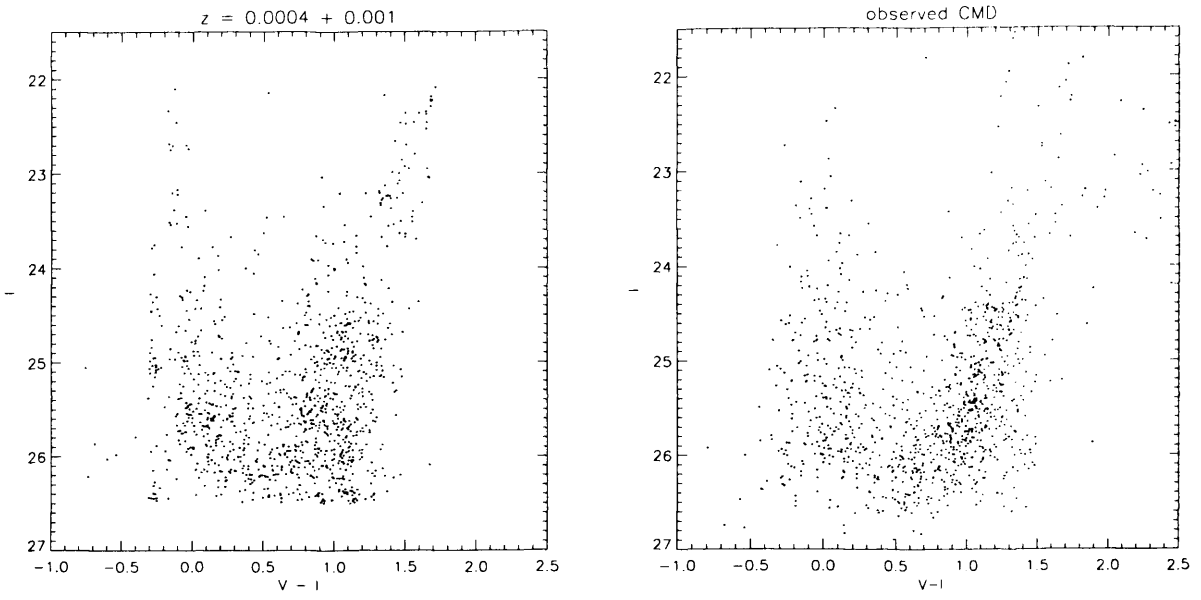

Figure 4.17: The comparison between the model **(left)** and the observed CMD of HIPASS J1337-39 **(right)**.

The error bars are determined by the code identifying the 68% (1σ) confidence interval on each amplitude. The number of stars in the diagram is low, especially the young blue ones, which makes the statistical analysis and modelling extremely difficult especially in this part of the diagram. For this reason the uncertainties in the SFR estimation are rather large at recent epochs.

The corresponding model CMD is displayed in Fig. 4.17 and compared to the observed data. The two diagrams look fairly similar. The RGB is well modelled and its average colour is consistent with the observed one. The main differences may be found in the modelling of the red stars above the tip of the RGB. Few intermediate-age AGB stars may be found in the two oldest age bins ($\log(Age) = 9.8, 10$) as one can see from Fig. 4.18 (showing how the stellar population of the model CMD varies in each age bin), even though they do not appear in the model CMD as a narrow plume just above the TRGB as it is found in the data. Moreover too many red bright stars with $22 < I < 24$ appear at $\log(Age) = 9.2$ (Fig. 4.18), indicating that the SFR in that age bin has been overestimated.

We have also built a synthetic CMD using only the highest allowed metallicity, Z = 0.004, to check how the CMD would look like in this scenario (Fig. 4.19). As expected, the first SF event occurs around 2.5

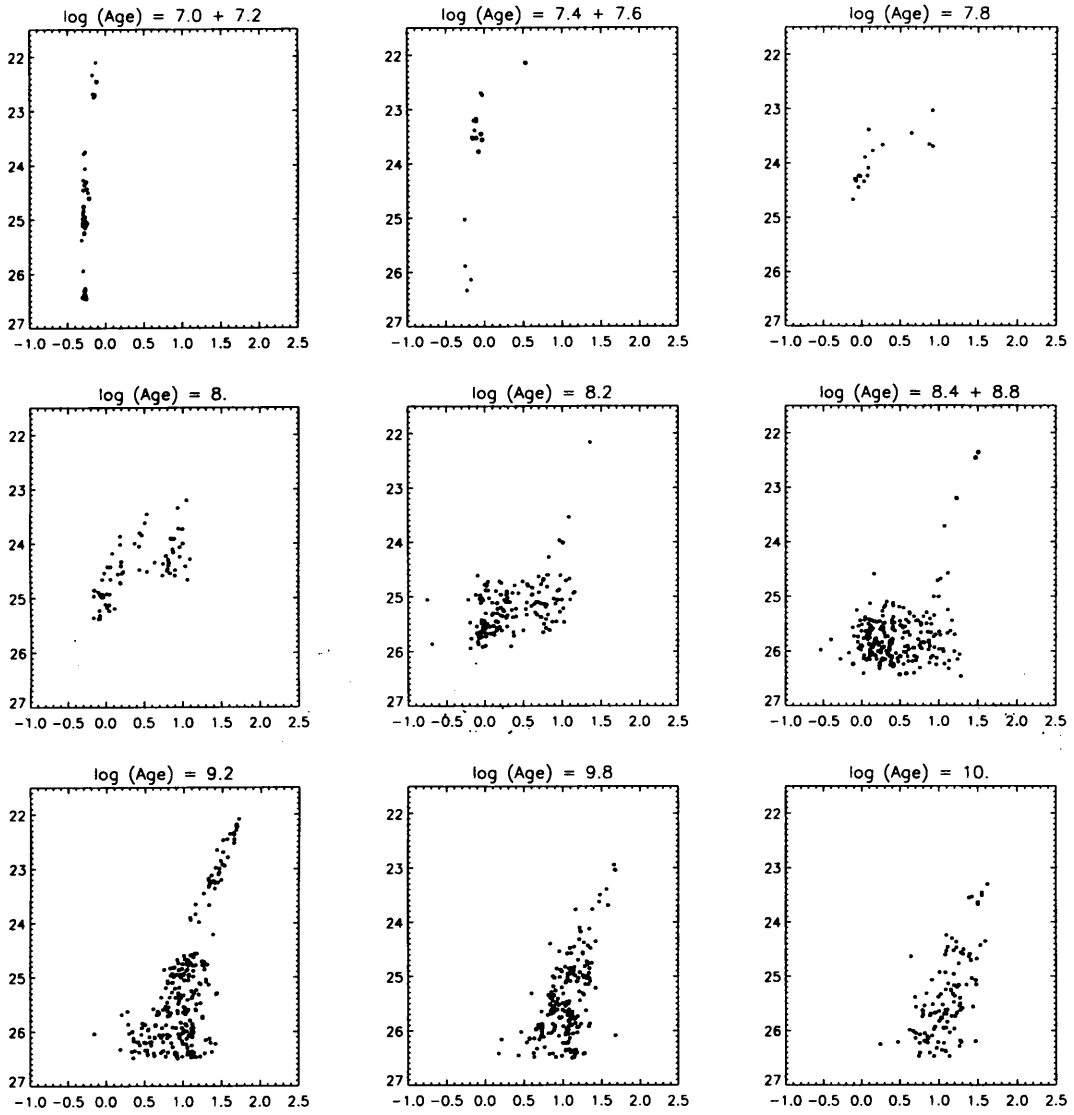

Figure 4.18: The synthetic CMD split in each age bin to show the age of the different feature of the diagram.

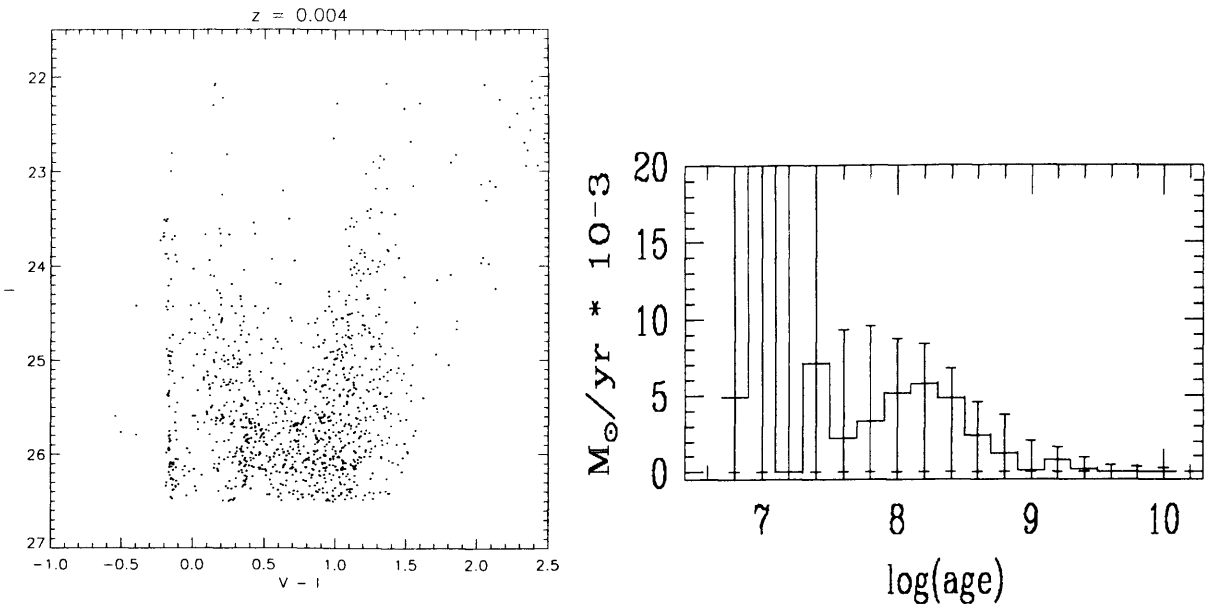

Figure 4.19: **Left:** The synthetic CMD obtained by using only isochrones at Z = 0.004. The model CMD is not very consistent with the observed data: the RGB has a larger dispersion in colour and the tip is not sharply defined. Neither at blue colours the model fits the observed features. The too narrow distribution of young blue stars is the result of a 10 Myr old SF episode with a largely overestimated SFR. **Right:** The corresponding SFH for Z = 0.004.

Gyr, but the SF activity starts to increase only in the last Gyr. The model CMD though fails to reproduce the observed diagram and the corresponding fit has a higher value of $\chi^2 = 1.62$. In particular, the RGB has a large dispersion in colour and the tip is not sharply defined. A large number of bright red stars at $(V-I) \sim 1$ is also generated by the code. Even at bluer colours the stellar distribution of the model diagram is not at all comparable with the observed blue plume, which shows a very narrow distribution of young blue stars originated by a SF episode at 10 Myr with a too high SFR.

To conclude, a scenario describing a low metallicity population with an age as old as 10 Gyr appears to be favoured by the analysis of the model CMDs.

4.11 Summary and discussion

Our results seem able to answer the question about whether HIPASS J1337-39 is a young galaxy or not.

As we showed in this chapter, to explain the colour of the RGB with a population of fairly young stars (age less than 1 - 2 Gyr), the metallicity of this population should be around 1/5 solar (Z = 0.004 $\rightarrow$ [Fe/H]$\simeq -0.7$). However this would be in sharp contrast with the metal abundance of the ISM which is at least 6 times lower. Therefore this seems to rule out the possibility of a young galaxy scenario with subsolar metallicity.

On the other hand, the comparison of the stellar photometry with theoretical isochrones at low metallicity (i.e. Z = 0.0004, in agreement with the HII region abundance) indicates that the RGB may contain stars as old as 10 Gyr. The detection of AGB stars gives further evidence that the galaxy may harbour an intermediate-age stellar population.

We have also built a synthetic CMD with isochrones at Z = 0.0004 and Z = 0.001, which is in reasonable agreement with the observed diagram (with $\chi^2 = 1.17$) and we have been able to reproduce the main observed features of the CMD. Again, it implies that within the time range that we have considered (10 Myr - 10 Gyr), the first episode of SF occurred $10^{+2.5}_{-2.0}$ Gyr ago (or $\log(Age) = 10 \pm 0.1$) . We find an average SFR over 10 Gyr of $\sim 2 \times 10^{-3}$ $M_{\odot}$ yr^{-1}, and the SFH of 1337-39 appears to be characterised by three main episodes of SF (between 6 and 10 Gyr, around 2.5 Gyr and in the last 250 Myr).

Nevertheless, to firmly prove the existence of an old stellar component one should unearth a population of horizontal branch (HB) stars, but this galaxy is probably too far away to resolve such faint stars even with very deep observations with the HST.

If our interpretation is correct and this galaxy harbours a stellar population older than a few Gyr, the low oxygen abundance that we have measured is rather remarkable, because it indicates that the galaxy has undergone little chemical enrichment during its evolution.

According to Lo & Sargent (1993) an abundance of 12 + log(O/H) $\approx$ 7.7 ($\sim$ 1/15 solar) can be reached in a few million years as the result of the explosion of the first stars born as supernovae. Therefore, as soon as star formation starts, the primordial gas should be rapidly enriched to this level. One possible explanation is that for small galaxies with relatively small potential fields, supernova explosions may be energetic enough to eject their heavy elements straight into the intergalactic medium. We will discuss more thoroughly this

possibility in the concluding chapter.

The case of SagDIG also supports a scenario where very low abundances can be maintained throughout the evolution of a dwarf galaxy, especially if it is an isolated system. In fact the metallicity estimated from the colour of the RGB ([Fe/H]= -2.1) is very close to the value derived for the warm gas in the HII region ([Fe/H]= -2.07 ± 0.2) (Saviane et al. 2002). According to the authors, the observed lower O abundance in SagDIG may be explained if part of the enriched gas is lost into the intergalactic medium, assuming that most of the gas outflows occurred in the last 200 Myr when the SFR was 10 times higher than in the past.

Finally, we have analysed the gaseous content of 1337-39 to investigate its distribution and its relation with the SF activity. The galaxy has an overall HI column density which is above 10^{20} cm^{-2} until 2 kpc from the center. The HI peak density (few times 10^{21} cm^{-2}) coincides with the area where the HII regions are found. The HI distribution around 1337-39 appears regular overall, however the presence of a "tail" in the gaseous disc is not completely clear.

There do not seem to be any objects within the 30′ field of view of the ATCA telescope to explain the slightly disturbed HI morphology as the effect of a tidal interaction with a close companion. Moreover, at the distance of 4.8 Mpc that we derived from the tip of the RGB, 1337-39 seems to be located on the margins of the Centaurus A group. The galaxy is about 10°($\sim$ 850 kpc) from M83, apparently the closest main member of the Centaurus A group. Among the other massive galaxies of the group NGC 5102 is at a radial distance d = 3.4 Mpc, while NGC 5253 is at d = 3.9 Mpc (Karachentsev et al. 2002) at an angular separation of about 8 degrees (see Fig. 2.1).

The shape of the HI distribution could be due the interaction with a hot intracluster medium. As described in Chapter 1, a galaxy moving with a velocity v_G through a hot diffused gas is subjected to a ram pressure given by $p_{ram} = \rho_{ICM} v_G^2$, where ρ_{ICM} is the density of the medium. However the efficiency of ram pressure stripping decreases in inverse proportion to the galaxy's distance from the center of the cluster. The hot gas density should be lower at the edge of the group and 1337-39 is one of the most distant dwarfs from M83. If the ICM is responsible of the HI tail in 1337-39, we should expect the gas from the other dwarfs closer to the galaxy to be completely removed. Nevertheless dwarfs with neutral hydrogen can be found in the neighborhood of M 83 (Karachentsev et al. 2002). Therefore this option does not seem to explain the HI morphology.

Finally, the HI distribution may be the result of a recent accretion of gas which would be consistent with

the irregularities in the velocity field in the HI tail. The possible accretion of an HI cloud may be related to the apparent increase in the SF activity around 100 - 200 Myr ago that we inferred from the analysis of the model and observed CMD. Higher resolution HI data are needed to investigate in more detail the structure of the gas distribution in 1337-39.

Chapter 5

HIDEEP J1337-33

Having been found in a deeper HI survey with a different mass threshold and column density sensitivity, the HI distribution of HIDEEP J1337-33 has slightly different properties than the other two HIPASS dwarfs. It has the lowest HI mass (see Table 2.2) and gas column density. The neutral gas mass is only 5×10^6 $M_\odot$ and its gas fraction is not as high as the others ($M_{HI}/L_B \simeq 1$ in solar units). As regards the optical appearance, we find a LSB optical counterpart ($\mu_0^B = 23.70 \pm 0.04$ mag arcsec^{-2}) and the dwarf does not seem to be currently forming stars. Therefore we are not able to independently constrain the metallicity by measuring the oxygen abundance. This will lead to some difficulties in the analysis of the CMD due to the age-metallicity degeneracy.

5.1 The neutral gas content

HIDEEP J1337-33 has a very smooth HI distribution that is centered on the stellar component of the galaxy, although the presence of local clumps and perturbations could be smeared out by the large beam size. In fact, as it has been described in Chapter 2, to improve the signal to noise in the ATCA observations we had to adopt a different reduction strategy for this galaxy, at the cost of resolution. This resulted in a larger beam size ($59'' \times 32''$) compared to the other dwarfs, therefore the resolution in the HI data of 1337-33 is poor. The beam size is in fact only slightly smaller than the gaseous extension (see Fig. 5.1). Fig. 5.1 shows the gas contour density overlaid on the WFPC2 mosaic in the F555W filter. The neutral gas extends beyond

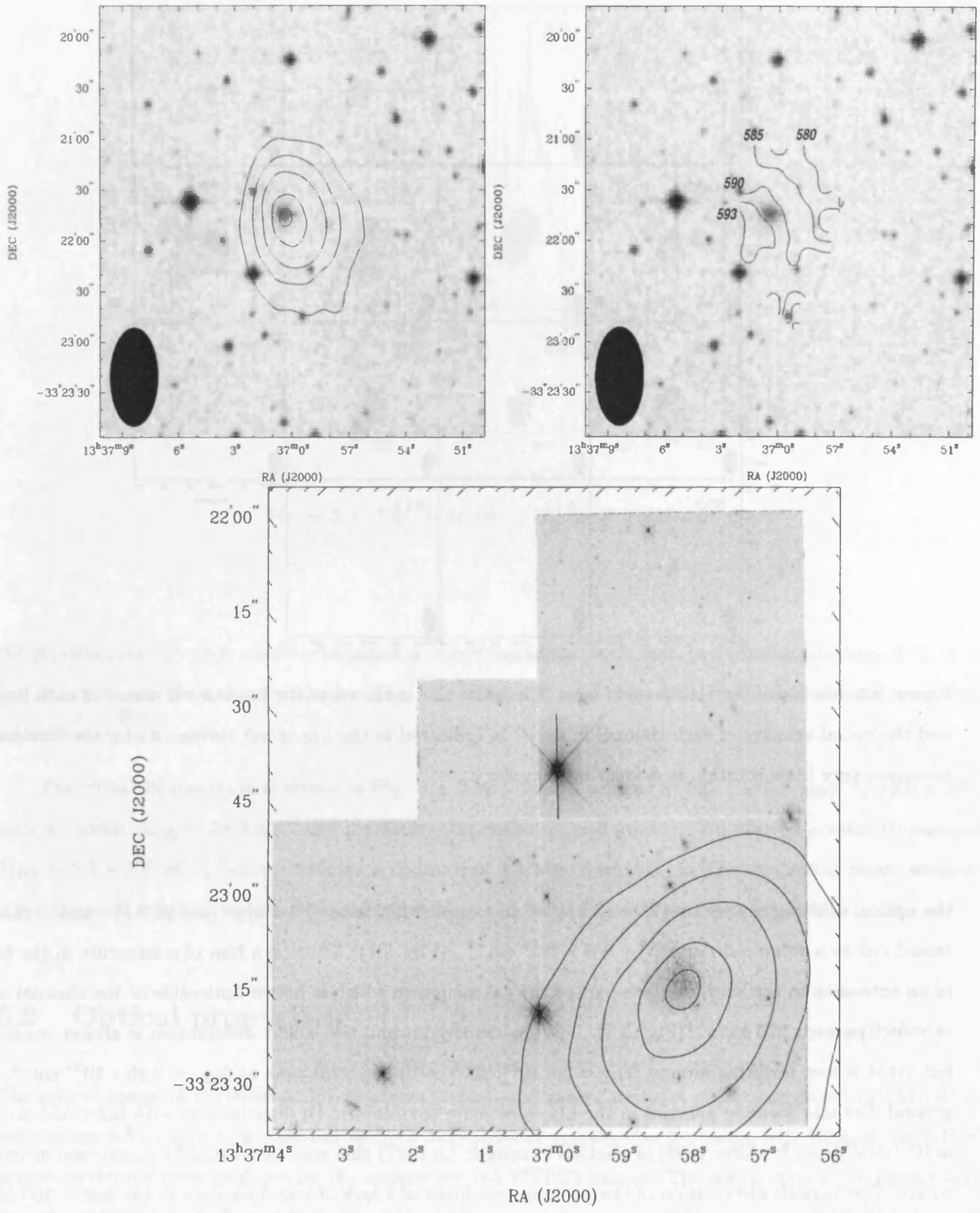

Figure 5.1: **Top-left:** HI density contours overlaid on the DSS field including the galaxy. The contour levels are: 0.5, 1.0, 1.5, 2.0, 2.25 $\times 10^{20}$ cm^{-2} . **Top-right:** The velocity field displayed in the range v = 575 km s^{-1}and v = 593 km s^{-1}. The beamsize is shown at the bottom left corner of the image. **Bottom:** The HI distribution overlaid on the WFPC2 field (F555W filter). The optical counterpart of the galaxy is all included within the $N_{HI} > 2 \times 10^{20}$ cm^{-2} contours.

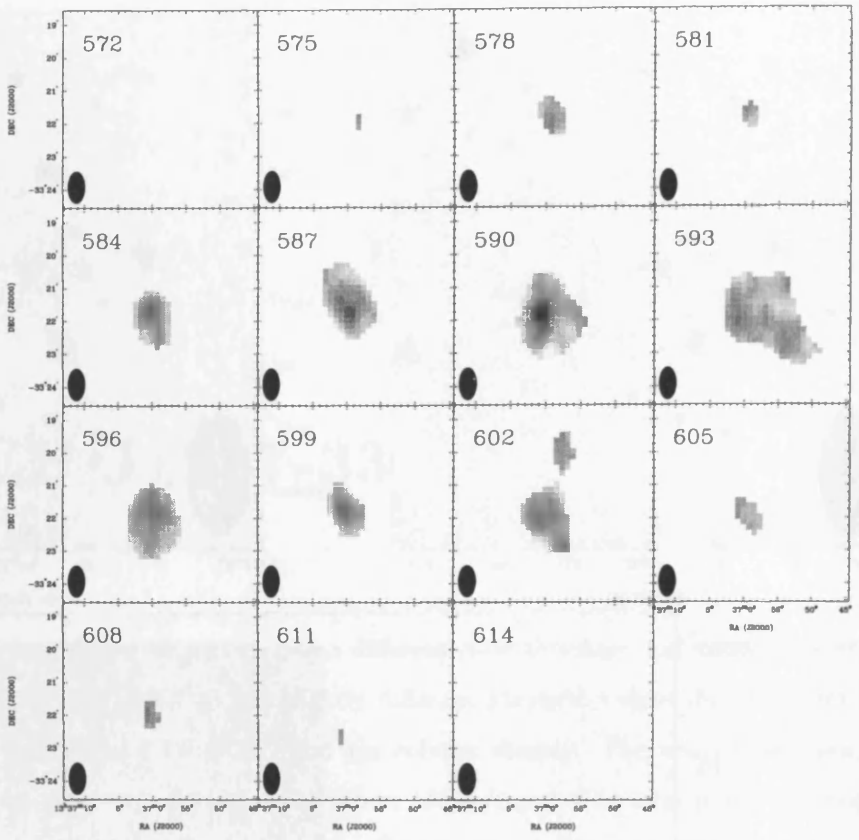

Figure 5.2: Mosaic of the HI channel maps. The beam size is shown at the bottom left corner of each image, and the radial velocity of each channel in km s^{-1}is indicated in the upper left corner. As for the isovelocity contours, very little rotation is evident in the galaxy.

the optical counterpart up to 45″- $\sim$ 1 kpc at an assumed distance of 4.4 Mpc (see §5.3.1) - and it can be traced out to a column density $N_{HI} = 5 \times 10^{19}$ cm^{-2} , (Fig. 5.1). There is a hint of a structure in the form of an extension in the south eastern part of the gas structure which is better noticeable in the channel map at velocities near 593 km s^{-1}(Fig. 5.2). The gas density around the stellar distribution is almost constant, but yet it is low, hovering around $N_{HI} = 2 \times 10^{20}$ cm^{-2} with a central peak at $N_{HI} = 2.35 \times 10^{20}$ cm^{-2} . In general dIrr star forming galaxies in the LG show more asymmetric HI distributions with holes and arcs as in IC 10 (Wilcots & Miller 1998) or SagDIG (Young & Lo 1997) that may be created by supernovae or stellar winds. The smooth distribution of the gas may give hints of a lack of star formation in the last $\sim$ 100 Myr, although one has to keep in mind that the low resolution of the observations may smear out irregularities in

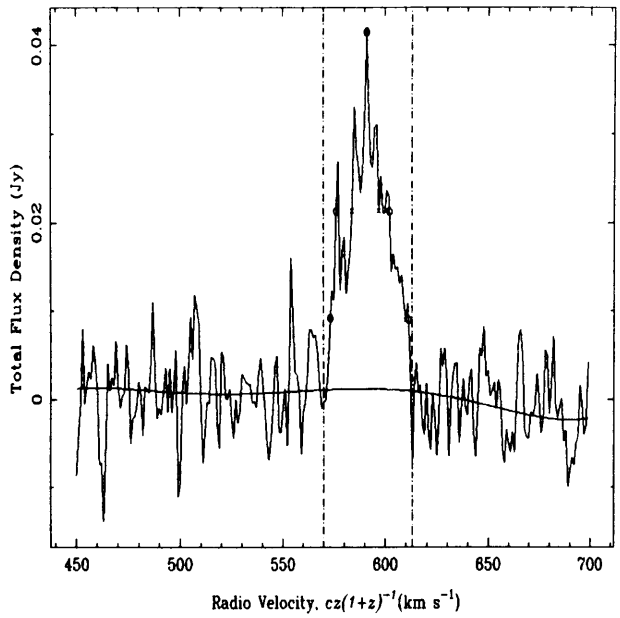

Figure 5.3: The HI profile of HIDEEP J1337-33.

the HI structure. There is small evidence of a velocity gradient both from the velocity contours (Fig. 5.1) and from the individual channel images (Fig. 5.2). From the axial ratio of the outermost contour we derive an inclination of $i \simeq 34°$.

The global HI spectrum is shown in Fig. 5.3. The profile is centred at 592.1 $\pm$ 0.8 km s^{-1}, with a 20% velocity width Δv_{20} = 38 km s^{-1}and a velocity dispersion $\sigma_v \simeq 8$ km s^{-1}. We derived a total HI mass of $M_{HI} = 5.1 \times 10^6\ M_\odot$, having assumed a distance of 4.4 Mpc (see §5.3.1). The dynamical mass, without any inclination angle correction, is found to be $M_{dyn} \simeq 8 \times 10^7\ M_\odot$ and the ratio $M_{dyn}/M_{HI} \simeq 15$.

5.2 Optical properties

The optical image of HIDEEP J1337-33 shows a small and rather compact object compared to 1337-39 as one can see from Fig. 5.4. It does not seem to have signs of ongoing star formation activity and the WIYN snapshots did not show evidence for HII regions nor the WFPC2 images. The stellar distribution looks very smooth and regular. In Fig. 5.5 is shown the surface brightness profile of the galaxy in the B band and the exponential law that fits it. B band exposures have been taken with the ESO MPI 2.2 m telescope

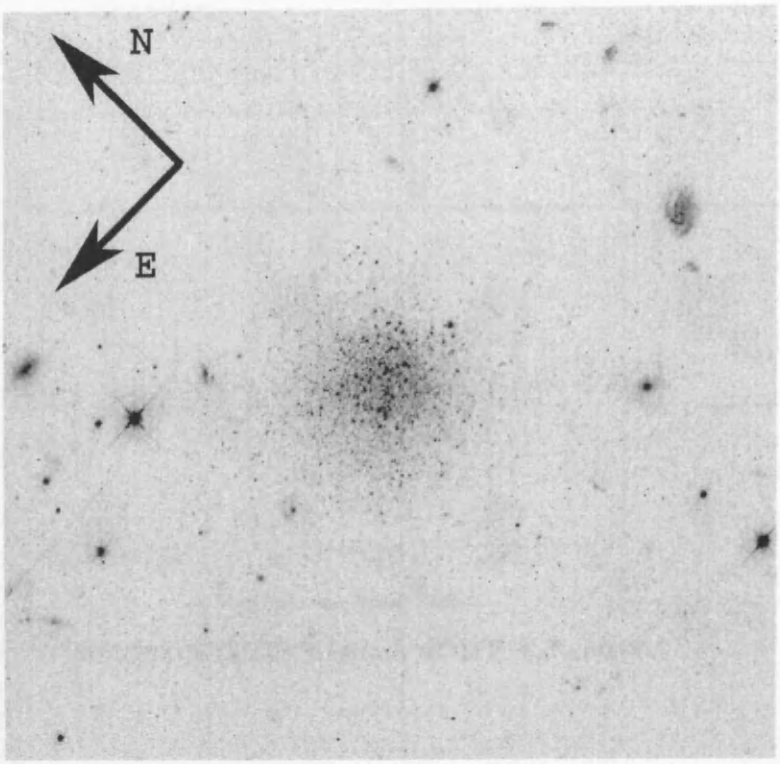

Figure 5.4: The WFPC2 image of HIDEEP J1337-33 taken with the filter F555W. The size of the frame is roughly 80″.

at La Silla in July 2003 as part of an observing run related to a different project, since a measure of its photometry in the B band was not available yet. We derive a dereddened central surface brightness equal to $\mu_0^B = 23.70 \pm 0.04$ mag arcsec^{-2}.

Its optical morphology and the presence of gas ($M_{HI}/L_B = 1.4$) makes this galaxy resemble the transition type dwarfs of the Local Group such as LGS 3, Phoenix, DDO 210 (although they have much lower M_{HI}/L_B ratios) and the more gas-rich dwarfs with intermediate properties between dSphs and dIrrs found by Skillmann, Côté & Miller (2003) in the Sculptor group. We will discuss later in more detail the common properties between such galaxies and HIDEEP 1337-33. In the following section we start describing the main features of the CMD and the observed stellar populations.

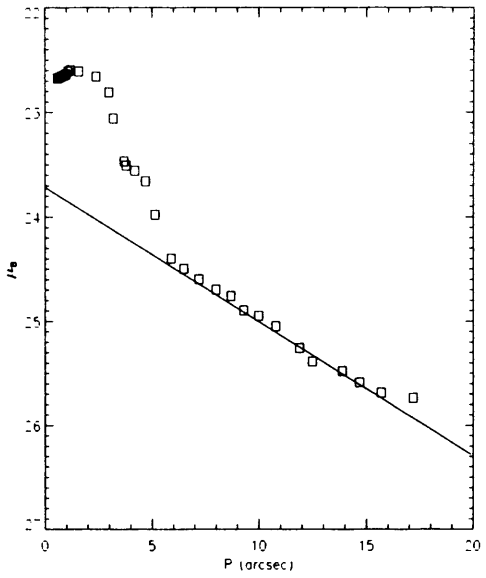

Figure 5.5: The B surface brightness of HIDEEP J1337-33. We find a dereddened central surface brightness $\mu_0^B = 23.70 \pm 0.04$ mag arcsec^{-2}.

5.3 The analysis of the Colour Magnitude Diagram

In the left panel of Fig. 5.6 the (I, $V - I$) morphology of the CMD is shown. The main features at red colours are a narrow RGB, a few candidate AGB stars, some of them with colour $(V - I) > 2$. The blue part of the diagram, on the other hand, is less populated, especially if compared to 1337-39, and seems to contain mostly blue loop stars, suggesting no current SF activity.

In the right panel we display the CMD of the fields (WF2, WF4 chips) adjacent to the galaxy which can be used as a comparison to check the galactic foreground contamination. As one can see from the figure, there does not appear to be a relevant presence of stars in the Galaxy which can affect our photometry.

5.3.1 The RGB, and the distance to HIDEEP J1337-33

The most prominent feature of the diagram is the RGB (Fig. 5.6). It is slightly redder than that of 1337-39 and it is located between $V - I = 1$ and $V - I = 1.6$.

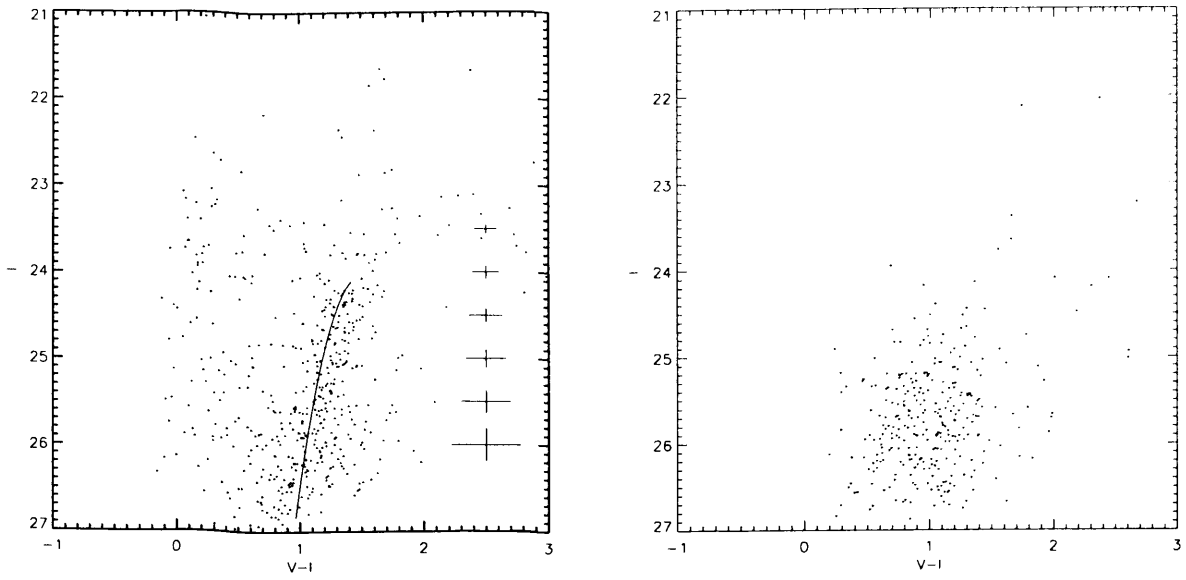

Figure 5.6: **Left:** $(V-I)$, I color magnitude diagram. The solid line correspond to the RGB of the galactic globular cluster M 15 and its location shows that the metallicity of 1337-33 is on average slightly higher than M 15 ([Fe/H]$= -2.1$). **Right:** The CMD of the fields in the WF2 and WF4 chips where the galaxy was not included. The diagram has been constructed by selecting the halves of the chips which were not attached to the WF3.

The distance can be determined from the I magnitude of the tip of the RGB as it has been done for 1337-39. The RGB cutoff occurs at $I_0 = 24.15 \pm 0.10$ (Fig. 5.7) assuming a galactic reddening $E_{B-V} = 0.049 \pm 0.008$ and $A_I = 0.09 \pm 0.01$. The error takes into account different factors of uncertainties due to the detection of the tip (the bin size in the luminosity function), the error in the photometry at that magnitude, and the errors in the zero point, reddening and aperture correction. The dereddened distance modulus is $(m-M)_0 = 28.20 \pm 0.10$ and the resulting distance to HIDEEP J1337-33 is $D = 4.4 \pm 0.2$ Mpc.

At an angular separation of about 3.5° from M 83 ($\lesssim$ 300 kpc at 4.5 Mpc) and a comparable radial distance ($d_{M83} = 4.5$ Mpc) HIDEEP J1337-33 seems to be located in a position within the group that is much closer to the massive spiral than 1337-39.

In Fig. 5.6 we have overlayed on the CMD of 1337-33 the RGB of the galactic globular cluster M 15,

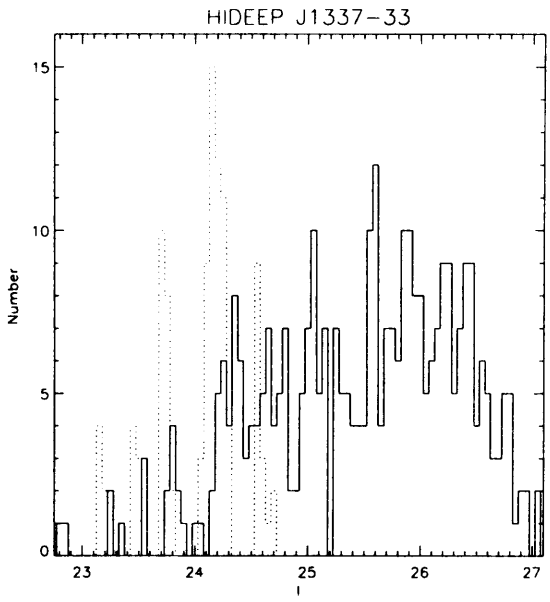

Figure 5.7: The I luminosity functions of HIDEEP J1337-33. The dotted line represents the output of the edge detection filter used to detect the tip. The peak indicates the position of the tip which has been found at $I = 24.15 \pm 0.1$

suitably scaled to the distance of 4.4 Mpc. The colour of the RGB of M 15, with a metallicity [Fe/H]= -2.17, is slightly bluer than the mean distribution of the observed RGB. Therefore, keeping in mind that such a comparison makes sense only if we assume that the galaxy has a population of stars which is at least 7 Gyr old (see Chapter 3), we obtain a lower limit on the average abundance of 1337-33. If we use the method by Lee et al. (1993) to estimate the metallicity from the colour of the RGB we find [Fe/H]= -1.9 ± 0.6, which is slightly higher than HIPASS J1337-39.

We have then compared the features of the diagram with Padua stellar evolutionary tracks. The Z = 0.001 set provides a better fit to the RGB. In this scenario, the population of the RGB appears to be as old as 10 Gyr. However, a different choice of the metallicity changes the upper limit on the age one can derive from the RGB. If we use the Z = 0.004 (1/5 solar) isochrones, as it is shown in Fig. 5.8, the oldest track which aligns the RGB is at about 4 Gyr. Tracks with ages around and older than 1 Gyr can also fit the position of the very red stars at $V - I > 2$, possibly AGB candidates that we will discuss in the next section. In this scenario, the blue part of what we define as RGB (i.e. stars with colours between 1 and 1.6

and luminosity fainter than $I = 24.2$) would be very young, with an age between 250 Myr and 1 Gyr, as one can see from the right panel of Fig. 5.8.

The age of the onset of the helium flash is between 0.9 and 1.5 Gyr, therefore, as pointed out in the previous sections, the stars with Z = 0.004 and ages $\lesssim$ 1 Gyr would be in the phase when they are ascending the AGB for the first time, rather than in the red giant phase. However AGB stars do not show a clear-cut cutoff in the luminosity as RGB stars do, thus, in this scenario a sharp decrease in the number of stars at $I \sim 24.2$, i.e. the tip of the RGB, would probably not be detectable in the diagram - as it clearly is.

Therefore, the shape of the red branch and the presence of a clear cut-off in the luminosity function around $I \sim 24.2$ can be taken (as we have already done for the previous object) as evidence of the existence of an intermediate-age population of red giants. A similar argument has been used in other systems (such as Leo A) when any other more reliable age indicator had not been detected in the CMD (Tolstoy et al. 1998). The presence of Population II stars with low metallicity doesn't exclude that a younger and more metal-rich population of stars may exist above the TRGB. We will analyse this possibility in the next section.

5.3.2 The Asymptotic Giant Branch

A small number of detections has been found above the TRGB (see Fig. 5.6) which can be possible AGB stars candidates, some of them with the very red colours ($V - I > 1.7$) we found in 1337-39. It is of interest to understand if they are stars belonging to the galaxy, since they might reveal the presence of a more metal-rich component. If so, they should have a metallicity greater then $Z = Z_{\odot}/20 = 0.001$, at which, according to synthetic models, the AGB branch starts bending horizontally towards the reddest part of the diagram (Fig. 5.8). The local contamination around $V - I > 1.7$, appears to be low according to Fig. 5.6. We have detected 11 ± 3 stars in the adjacent fields with $V - I > 1.7$ and $22 < I < 25$. We have marked the distribution of the stars found above the TRGB in Fig. 5.9. The squares correspond to the 24 stars detected with the reddest colours ($V - I > 1.7$) which are compared to the distribution of the fainter and bluer AGB star candidates just above the TRGB ($V - I < 1.7$ and $23.2 < I < 24.2$). The majority of these stars (both circles and rectangles) are very well localised within or around the main optical body of the dwarf. Some of the reddest stars though are clearly outside the dwarf and are likely to belong to the Milky Way, although there are examples in the LG galaxies such as IC 1613 (Albert, Demers, & Kunkel 2000) where Carbon stars extend even further out than the observed HI content.

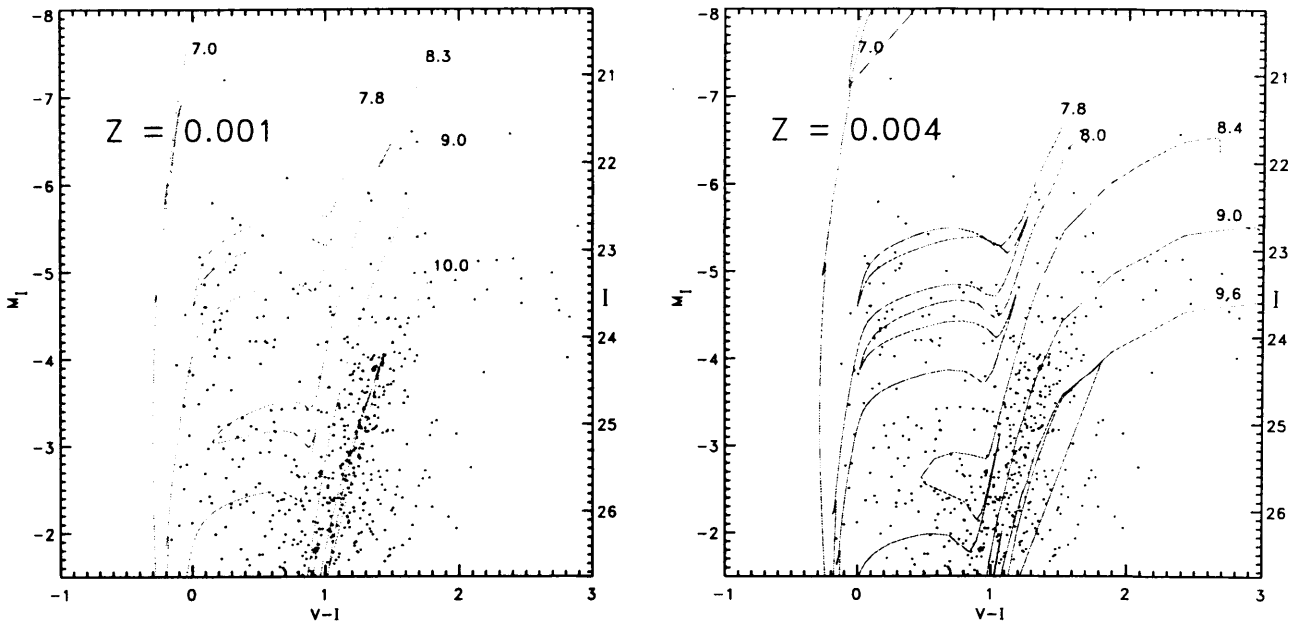

Figure 5.8: HIDEEP J1337-33: $(V - I)$, I color magnitude diagrams overlaid with isochrones at Z = 0.001 **(left)** and Z = 0.004 **(right)**. According to the metallicity used, the limit one can set on the age of the red giant population changes from 10 to 4 Gyr. At Z = 0.004, the blue part of the feature that we define as the RGB (i.e. stars with colours between 1 and 1.6 and luminosity fainter than I = 24.2) would be younger, with an age between 250 Myr and 1 Gyr, therefore it would be mostly populated by AGB stars rather than red giants. The age of the younger blue stellar population, which are mainly core helium burning stars is also shown for both metallicities. Blue and very young main sequence stars (age less than 10 Myr) seems to be lacking.

Thus, on the one hand it seems that there exists a population of old AGB stars with colours similar to that of the TRGB whose position on the CMD is fitted by low metallicity isochrones (Z = 0.001) as the RGB. On the other it is possible that we have also found a population of very red and bright AGB stars that formed at a later epoch with a higher metallicity. In fact, only isochrones at Z = 0.004 (1/5 solar) match their position on the diagram. The very red AGB population may give a hint of the chemical evolution of the galaxy through its different episodes of star formation. Unfortunately isochrones at Z = 0.004 also match the position of the fainter and bluer AGB stars, therefore we cannot entirely exclude that there is only one

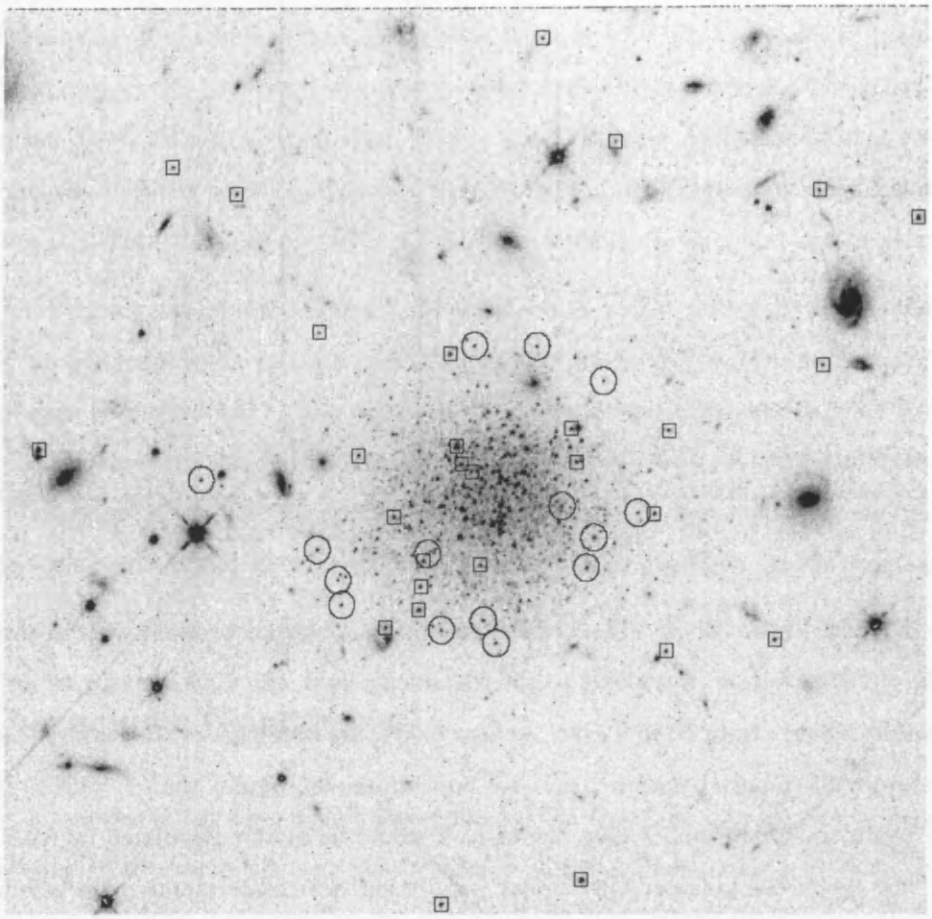

Figure 5.9: WFPC2 image in the filter F814W of HIDEEP J1337-33, marked with the positions of all the possible AGB candidates. The *circles* indicate the position of the stars with $V-I < 1.7$, while the *rectangles* correspond to the stars with the reddest colours ($V - I > 1.7$). The bluer and less luminous AGB stars appear to be concentrated in the outer part of the galaxy, while the very red ones are distributed both inside and around the main body of the galaxy. Some of the stars marked with rectangles found at the edge of the chips are clearly due to the Galactic contamination. From the analysis of the adjacent fields we would expect a local contamination along the chip of 11 ± 3 stars with $V - I > 1.7$ and $22 < I < 25$. The number of stars detected in the WF3 with those photometric characteristics are 24.

population of relatively young and more metal rich AGB stars.

With no detected HII regions we can not measure the metallicity of the gas. Spectroscopic follow-up observations or narrow band filters photometry are needed to classify unambiguously the reddest stars in 1337-33.

5.3.3 The faint blue plume: a suppressed recent star formation.

The blue plume of HIDEEP J1337-3320 (Fig. 5.6) is much less populated than 1337-39. There are few bright stars up to $I \sim 22.5$, which are likely the bluest extent of the helium burning phase as it appears from the comparison with the theoretical isochrones (Fig. 5.8). A well defined main sequence though is lacking. The "fading" blue plume implies a drop of the recent SF activity.

Isochrones at Z = 0.001 fitting the magnitudes and colour of the brightest blue loop stars indicate that the age of the most recent stars in this galaxy is around 60 - 100 Myr, when the last episode of significant SF activity probably occurred (see Fig. 5.8). A decreasing recent SFR is the most likely scenario one can infer from the "fading" blue plume of this galaxy.

5.4 Radial gradients in the stellar population

If one looks at the distribution of the stars in the galaxy as shown in Fig. 5.10, one can see that all stars bluer than $(V-I) = 0.8$ appear strongly concentrated in the centre of the galaxy with their number rapidly declining at larger radii. Red stars ($(V-I) > 0.8$) instead appear to have a slightly wider distribution throughout the frame. The peak of the distribution is also around the centre of the galaxy, but they show a less steep gradient with the radius.

Thus, 1337-33 follows the usual trend in the stellar spatial distribution observed in dwarf systems, indicating that SF may be longer sustained in the center where the gas reaches in general the highest density.

The CMDs for four zones of the galaxy are shown in Fig. 5.11. We have selected four circular regions around the centre of the galaxy with radii from 10″(218 pc at 4.4 Mpc) to 40″(872 pc). Isochrones from the Padua group at Z = 0.001 are overplotted to constrain the age of the stellar population. Again, one

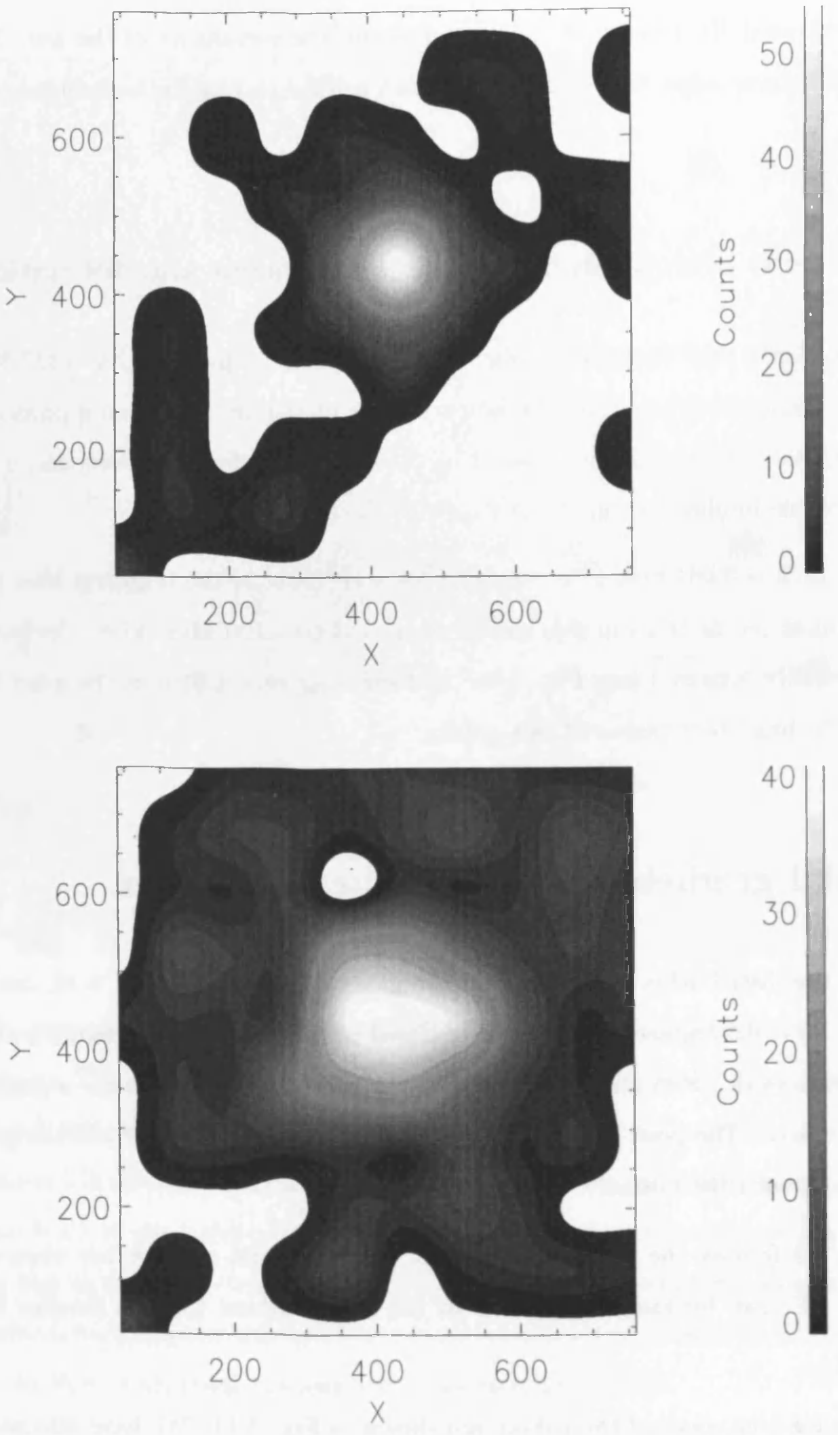

Figure 5.10: The distribution of blue stars (*upper panel*) and red stars (*lower panel*) in the WFPC2 frame. The stars have been selected only on the basis of their colour. In this plot blue and red stars mean that they have colours smaller or greater than $(V - I) = 0.8$.

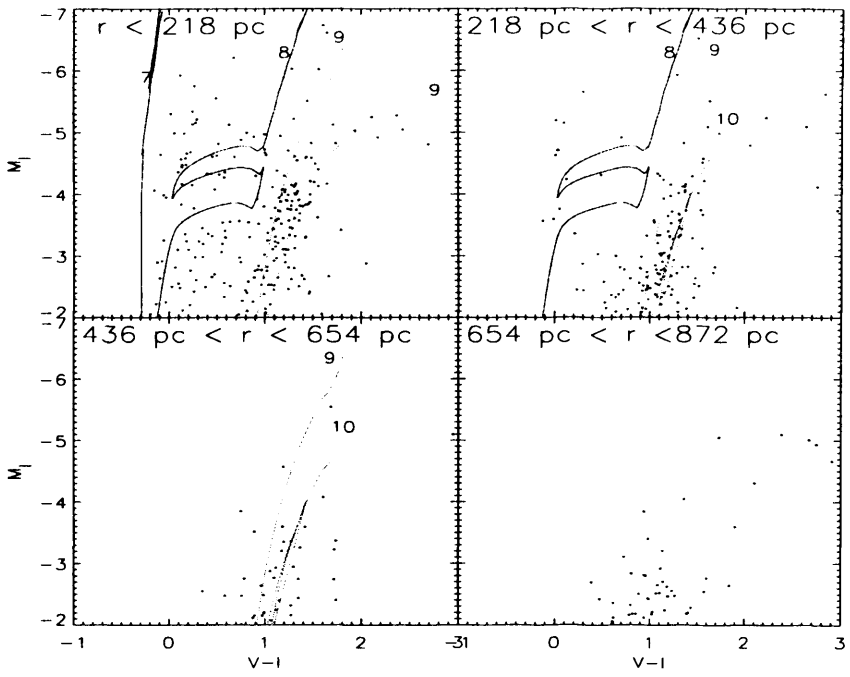

Figure 5.11: CMDs of stars in four different radial bins with Padua isochrones at Z = 0.001 overplotted. In the upper left panel we have also overlaid the 9 Gyr track at Z = 0.004 to fit the position of the very red AGB candidates which are mainly found in the first radial bin.

can see that most of the stars with ages less than 100 Myr are within 10″ from the centre of the galaxy. Nevertheless there is a remarkable number of red stars in this area. Even the majority of the very red AGB candidates is included in the first zone within 10″from the centre. If these stars belong to the galaxy and if they originate from gas which had been metal enriched by the previous episodes of SF, their age is around 1 - 2 Gyr, as one can see from the first panel of the Figure 5.11, where the 1 Gyr isochrone at Z = 0.004 is also displayed. Their number decreases in the intermediate circle, as well as the blue stars, compared to a more pronounced RGB population. In the third region young stars have completely disappeared while only a few RGB stars with ages greater than 1 Gyr can be found. Finally the fourth circle does not contain any more stars belonging to the galaxy. A few red stars with colours $V - I > 2$ which are probably foreground stars can be noticed in this final CMD. Their total number is 6 and it is comparable to the amount of foreground

stars expected in that fraction of the frame ($\propto (1 - R^2_{30''}/R^2_{40''}) \cdot N_{TOT} \simeq 5$, where $N_{TOT} = 11$ is the total number of foreground stars found in the adjacent fields).

The spatial distribution of the red giant stars is expected to be related to the general structure of a galaxy at the time when the dominant old stellar population formed. The extended population of red stars is generally interpreted as the presence of a halo of possibly old stars. All nearby low-metallicity dwarfs seem to contain an older stellar population. This has already been established for dIrr (Patterson & Thuan 1996) and BCD galaxies (Loose & Thuan 1986, Kunth et al. 1988) and in all galaxies near enough to resolve their stellar populations. Determining the age of these halos would give a proof that dwarf irregular galaxies contain a population of truly old stars, and therefore that dwarfs are primordial objects independent of their current morphology. However as we have mentioned before, the only unambiguous evidence of a truly old stellar population is given by the detection of an extended Horizontal Branch since stellar evolution models become degenerate in age and colour on the RGB after 1 Gyr. Given the distance of these galaxies, our data are not deep enough to reach such faint magnitudes, therefore we can not definitely constrain the age of HIDEEP J1337-33 with the current analysis. However, in analogy with other galaxies, the presence of a fairly extended population of red stars argues for a period of active star formation in the distant past of the galaxy, an hypothesis which is also indicated by the model of the SFH we have produced with the StarFISH code, that we will discuss in the following section.

5.5 The Star Formation History of HIDEEP J1337-33

We have used StarFISH to model the SFH of 1337-33. The best-fit SFH and the corresponding CMD are displayed in Fig. 5.12 where it is compared to the model CMD. The best fit is the result of the combination of three sets of isochrones, Z = 0.0004, Z = 0.001, Z = 0.004. For this model the χ^2 value is 0.61. The evolution of 1337-33 seems to be dominated by an early SF event at $10^{+2.5}_{-2.0}$ Gyr where the majority of the red giant stars have been formed (see also Fig. 5.13). After this episode the galaxy appears to have experienced few episodes of SF occurring around 4 Gyr ($\log(Age) = 9.6 \pm 0.1$) and 1 - 1.5 Gyr ($\log(Age) = 9.0 \pm 0.1$ and 9.2 ± 0.1) followed by periods of apparent inactivity. The SF seems to be triggered again around 250 Myr until about 100 Myr ago with an increasing SFR, then it starts decreasing until it drops off at $\log(Age) = 7.4 \pm 0.1$. At ages younger than 100 Myr the errors in the SFR become very large, affecting the results of the model for the youngest stars. Given the large uncertainty the events predicted around $\log(Age) = 7.4$

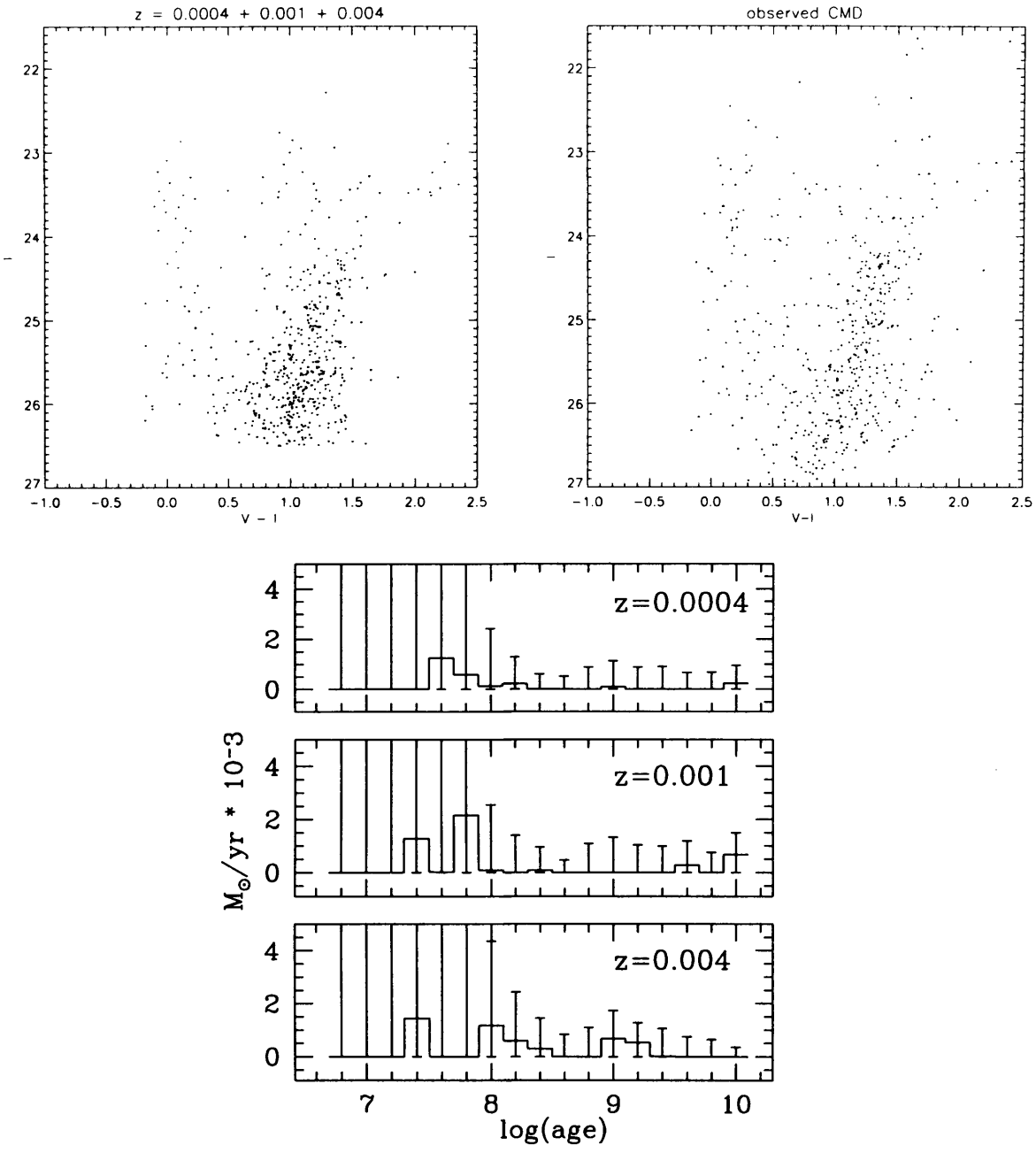

Figure 5.12: The best fit SFH of 1337-33 and the corresponding model CMD. AS a comparison we also show the observed CMD. We find a good agreement between the two diagrams although there is an overestimate of the old SFR which produces a more populated RGB at faint magnitudes.

($\sim$ 25 Myr) may not be very reliable.

The overall SFR appears to be very low, and it never exceeds 2×10^{-3} $M_{\odot}$ yr^{-1}. There is a degeneracy at 10 Gyr between the isochrones at Z = 0.0004 and Z = 0.001. Synthetic CMDs with Z = 0.0004 and Z = 0.001 are photometrically too similar for the method to be able to distinguish between them with the current data. We observe a consistent age-metallicity relation in the SFH. The oldest stars have Z = 0.0004/0.001 while there is no significant population with Z = 0.004 before log (Age) = 9.2 which suggests a gradual metal enrichment due to the previous SF episodes.

The model CMD reasonably matches the main features of the observed one. The main difference found is in the width of the RGB, too large in the model at faint magnitudes, which is probably due to an overestimate of the SFR in the 10 Gyr age bin. As one can see in the Fig. 5.13 where we have plotted the stars produced in the model CMD per each age bin, the majority of the red giant stars appear in the 10 Gyr interval. On the other hand, the recent SFR seems to be slightly underestimated, with a small difference in the number of young stars between the model and the data. The synthetic CMD also show a red tail of stars above the TRGB extending at colours $(V - I) > 1.5$), which appear at $\log(Age) = 9, 9.2$ with a higher metallicity (Z = 0.004).

To conclude, the evolution of 1337-33 seems to be characterised by a sequence of periods of low SF activity followed by quiescence (the so called "gasping" evolution). The average SFR is always below 2×10^{-3} $M_{\odot}$ yr^{-1}. At more recent epochs, we find an increase in the SF activity within the last 200 Myr, with a peak around 60 - 100 Myr, but there is no evidence of young stars with ages less than 10 Myr.

5.6 Summary and discussion

Despite the significant amount of neutral hydrogen compared to its stellar mass, there is no evidence of ionised gas in HIDEEP J1337-33 to constrain the current abundance of the ISM as in HIPASS J1337-39. Therefore deriving the age and the metallicity evolution of this galaxy from its CMD only is a very difficult task.

We have investigated its stellar content and we have found a dominant population of red giants. From the shape of the RGB, the comparison with stellar tracks, and the distribution of the red giant stars, we argue that such a population is at least of intermediate age, and that the galaxy has been experiencing star

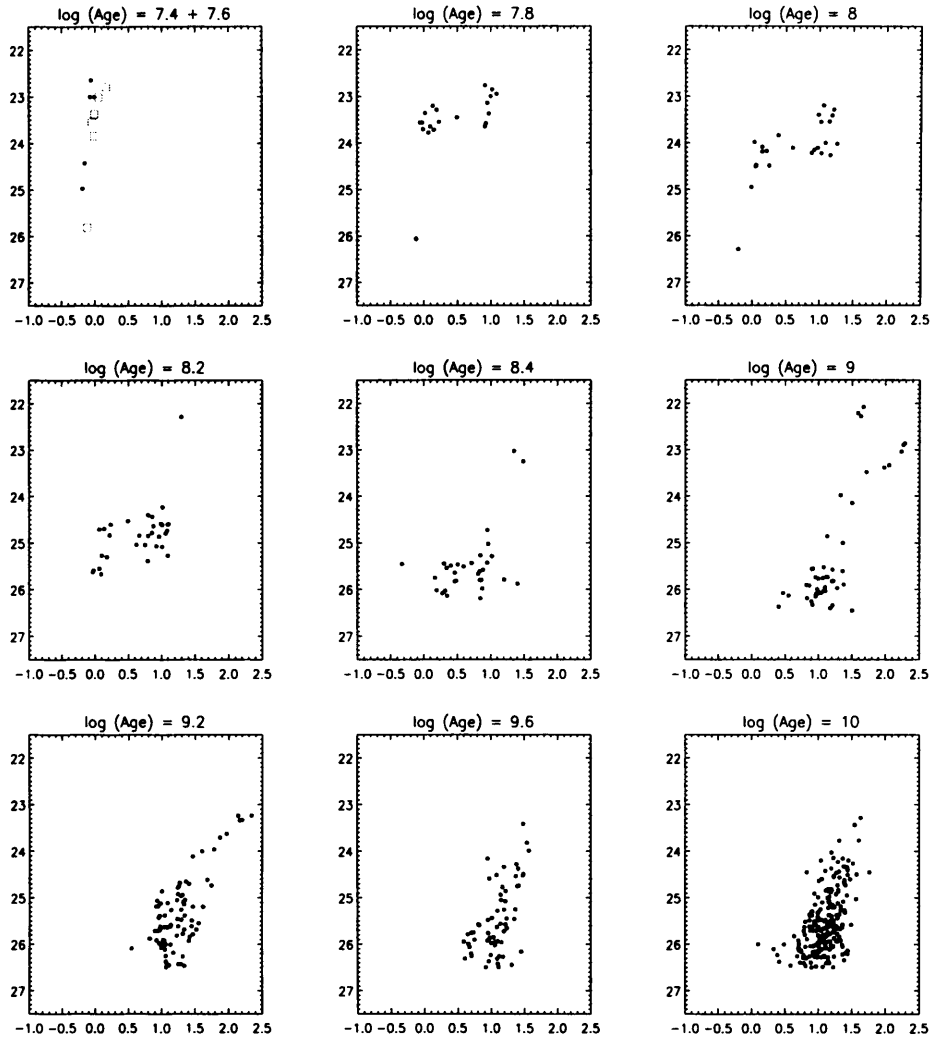

Figure 5.13: The synthetic CMD per each age bin to show the different SF events and the corresponding stellar populations formed. In the first panel we have shown stars belonging to two different age bins. Black dots refer to $\log(Age) = 7.4$, while squares correspond to $\log(Age) = 7.6$.

formation activity within the last 10 Gyr. We are not able to move such an analysis further back in time since most precise age indicators are fainter than the photometric limit we reach with the HST observations. The scenario we suggest is reasonably confirmed by the modelling of the CMD we have performed with the StarFISH code. 1337-33 seems not to be a young galaxy. The observed large gas fraction looks rather the result of a very low SFR which never seems to exceed 2×10^{-3} $M_{\odot}$ yr^{-1}. After the main event at $10^{+2.5}_{-2.0}$ Gyr when most of the red giant stars in the galaxy are formed (according to our model CMD), the subsequent evolution seems to be characterised by smooth episodes of SF activity and periods of quiescence.

We also find evidence for a shallow chemical enrichment. The CMD shows a population of candidate AGB stars whose very red colours are explained if we assume that their metallicity is about 4 times higher than that of the bulk of the red giant stars. Given their location within and around the dwarf, and having taken into account the foreground contamination, we argue that a dozen of such stars (4σ) are in 1337-33. Assuming Z = 0.004, we find that they could be between 1 and 4 Gyr old.

The shallow metal evolution may be a consequence of the low average SFR. Low mass dwarf galaxies undergoing a significant episode of SF are expected to be extremely metal poor, since the metal-rich debris are likely to escape the galaxy via strong SN-driven winds (De Young & Heckman 1994). On the other hand, the absence of intense bursts may reduce the outflow of the more metal-rich debris, leading to stellar populations with varied abundances. For instance, among the dwarf galaxies of the LG, the chemical evolution in LGS 3 is characterised by a slow increase with time, and it appears to have formed most of its stars very early (13 - 15 Gyr) and to have had a slowly decreasing SFR since then (below 10^{-4} $M_{\odot}$ yr^{-1}).

The gas density of 1337-33 is overall low ($N_{HI} < 2.5 \times 10^{20}$ cm^{-2}), and below the threshold found by Skillman (1987) for star forming dwarf galaxies ($N_{HI} = 5 \times 10^{20}$ cm^{-2}). This is probably the main reason why the galaxy is not currently forming stars.

As regards the local environment, this galaxy seems to be in a different position within the group compared to 1337-39, since we estimated a distance of less than 300 kpc from the massive spiral M 83. To conclude, the general properties of 1337-33, such as the low luminosity, the spherical symmetry of the optical appearance, the absence of current SF activity despite the large gas reservoir, make this dwarf similar to the so called "transition objects" of the LG, as DDO 210, LGS 3 and Phoenix, which show intermediate properties between dIrrs and dSphs. These systems are preferentially found nearer than dIrr (but not as close as dSph) to the most massive members of a group and they are generally interpreted as dIrr galaxies going through a period of temporary interruption of their star formation activity. In the conclusive chapter

we will discuss in more detail the differences and the common properties between these objects and the HIPASS dwarfs.

Chapter 6

HIPASS J1321-31

HIPASS J1321-31 is the most puzzling object among the three. With a mass of $M_{HI} \simeq 4 \times 10^7\ M_\odot$ and an apparent magnitude $m_B = 17.1$, it has the highest gas-mass-to-stellar light ratio ($M_{HI}/L_B \simeq 5$), yet Hα snapshots taken with the WIYN telescope do not reveal any HII regions. It is also the galaxy with the lowest SB among the three dwarfs. Banks et al. (1999) found a central SB $\mu_0^B = 24.2$ mag arcsec^{-2}. From the sky-projected map of the group it seems to be located in the region surrounding M 83. Its CMD shows that it has experienced a different SFH compared to the other dwarfs, and the first analysis of the main characteristics of its stellar population has been already published in Pritzl et al. (2003).

6.1 The neutral gas content

The HI distribution of HIPASS1321-31 (Fig. 6.1) extends up to a radius of 1′30″ (2.3 kpc at the distance of 5.2 Mpc that we have derived from the tip of the RGB in §6.5) and is clearly offset from the optical center. There are two peaks in the HI density but they fall at the border of the chip where the galaxy is located (WF3), showing poor correlation with the main optical counterpart. A density "depression" occurs in the center of the distribution. The column density is overall low and peaks at only 2.5×10^{20} cm^{-2}.

A small gradient in the velocity map can be seen in Fig. 6.1 and the velocity field seems rather disturbed. It is difficult to infer evidence of rotation from the contours: the isovelocity contours in the western side of the galaxy are more closed than those in the eastern, suggesting a variation in the kinematics between the

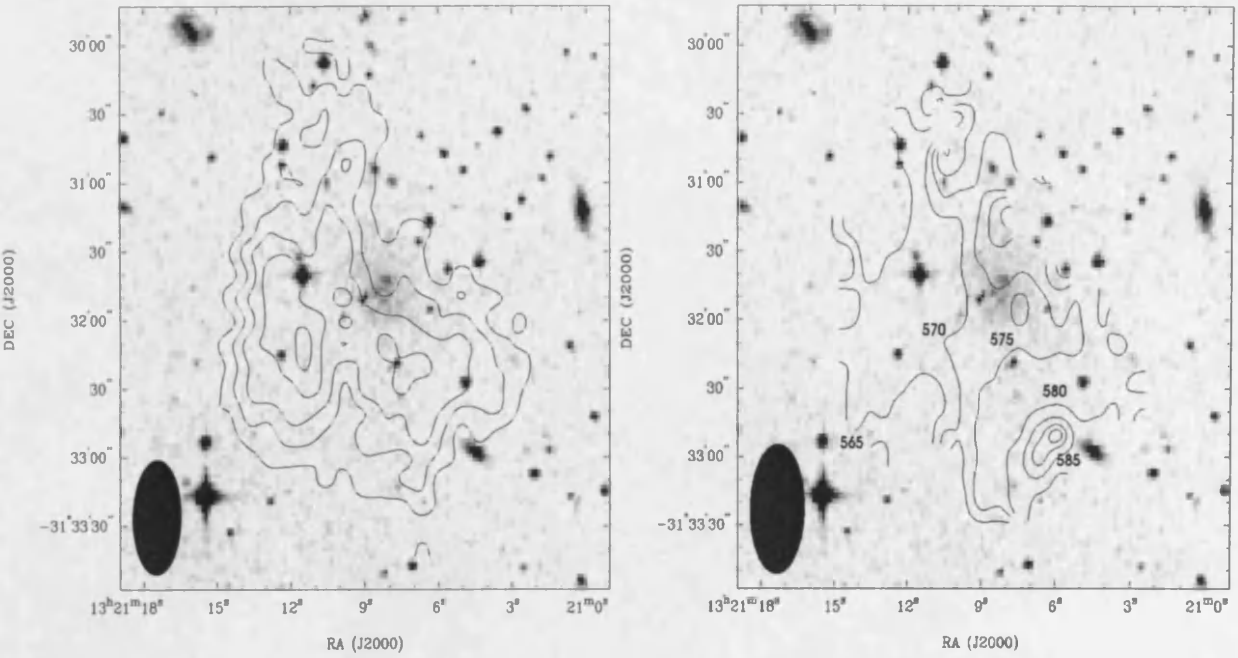

Figure 6.1: HIPASS J1321-31: **Left:** HI contour density maps overlaid on the DSS image of the galaxy. The contour levels are: 0.5, 1.0, 1.5, 2.0, 2.25, 2.35 $\times 10^{20}$ cm^{-2} . **Right:** The HI velocity field. There is evidence of a gradient in the velocity field, but it is difficult to infer from this map clear evidence of organized rotation.

two parts of the galaxy. Even from the HI channel maps (Fig. 6.2) there is no clear evidence for organized rotation. It is possible to identify a clump of gas in the south-western area of the galaxy which seem to be in expansion.

The HI profile (Fig. 6.3) is centred at 578.6 $\pm$ 0.8 km s^{-1}, with a 20% velocity width Δv_{20} = 59 km s^{-1}and a velocity dispersion $\sigma_v \simeq 8$ km s^{-1}. We derive a total HI mass of $M_{HI} = 3.7 \times 10^7$ $M_\odot$ (having assumed a radial distance d = 5.2 Mpc - see section §5.5).

Given the morphology of the gas it is not possible to estimate the inclination of the HI distribution. The dynamical mass, without any inclination angle correction, is found to be $M_{dyn} = 7 \times 10^8$ $M_\odot$. We have looked through the ATCA cube to inspect the local environment of the dwarf. There is no sign of HI clouds or other low mass gas-rich objects in the 30′× 30′field of view up to our column density limit of $N_{HI} = 5 \times 10^{19}$ cm^{-2} .

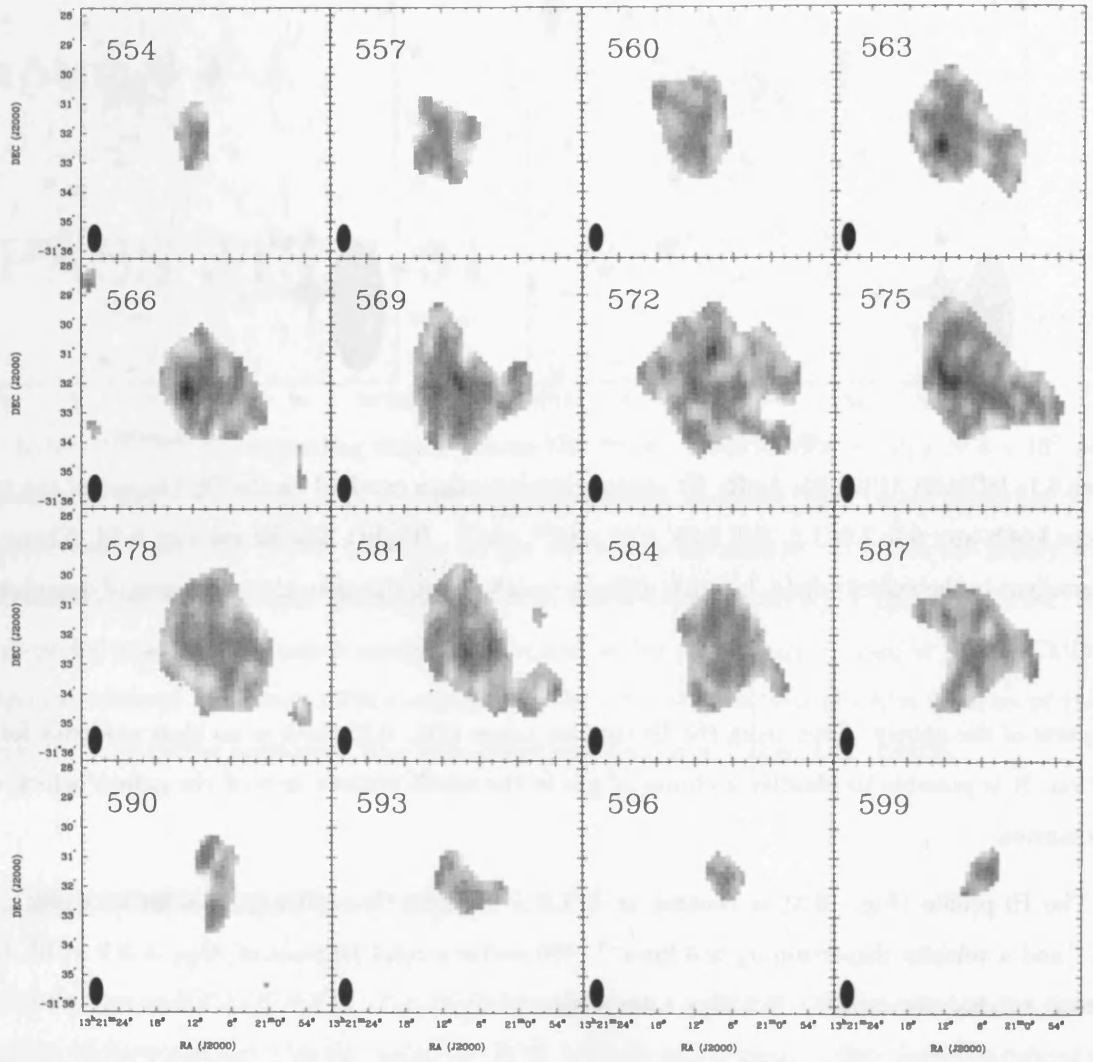

Figure 6.2: HIPASS J1321-31: HI channel map. The beam size is shown in the bottom-left corner on each plane. The heliocentric velocity in $\mathrm{km\,s^{-1}}$of each plane is marked on its upper-left corner.

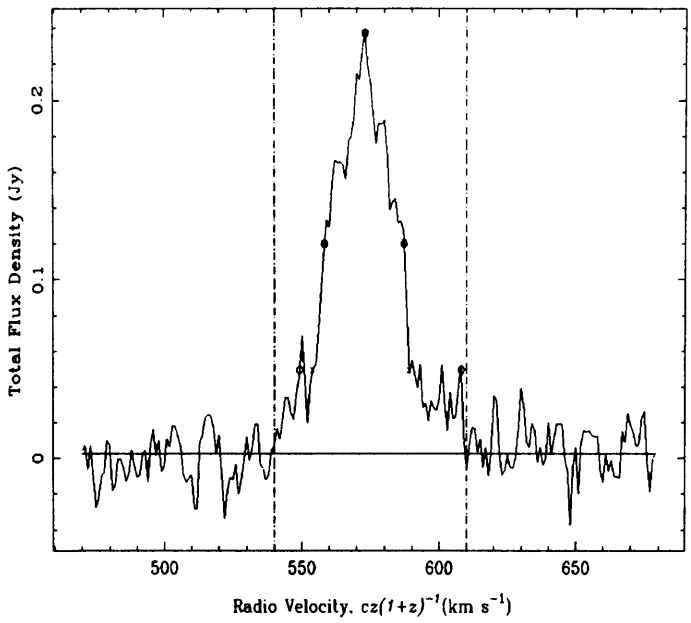

Figure 6.3: The HI profile of HIPASS J1321-31 obtained with ATCA.

6.2 The optical properties

HIPASS J1321-31 was first observed in the optical by Banks et al. (1999) after its discovery in the HIPASS survey. The optical follow-up of the 21-cm detection showed a faint ($m_B = 17.1 \pm 0.2$) and low SB optical counterpart ($\mu_0^B = 24.2$ mag arcsec^{-2}), whose profile was fitted by an exponential law.

A much more detailed view of the dwarf is given by our WFPC2 image (Fig. 6.4), which shows a very diffuse stellar distribution. There are hardly any lumps or substructures, but one can notice two bright small regions about 2″ across at an angular separation of 7″ one from the other. It is difficult to tell from the image whether they are HII regions or star clusters, but they are not foreground stars. If they are HII regions they were too faint to be detected in the Hα snapshots we have taken with the WIYN telescope. Given the low column density around the optical counterpart (1 - 2 $\times 10^{20}$ cm^{-2}), the presence of HII regions in this galaxy would be very unusual.

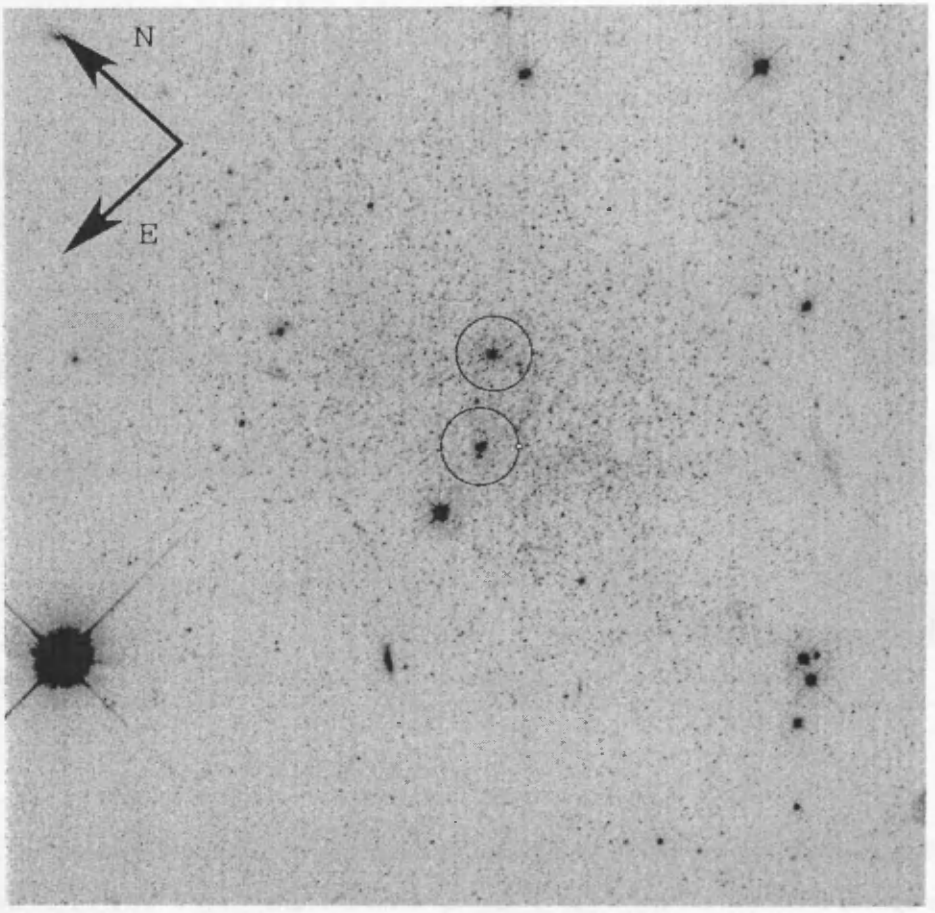

Figure 6.4: WFPC2 image in the F555W filter of HIPASS J1321-31. The two circles show the candidate HII regions in the galaxy. The size of the field is approximately 80″.

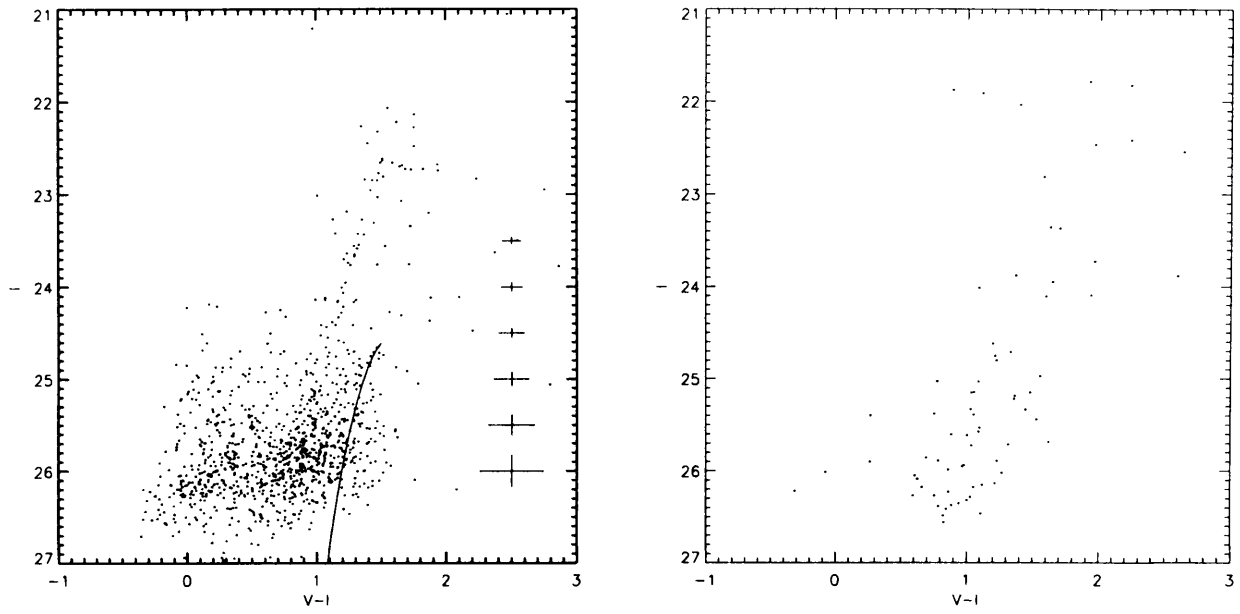

Figure 6.5: **Left:** $(V-I, I)$ colour magnitude diagram, once again compared with the RGB of the GCC M 15, showing a clear red plume of luminous stars extending up to $I = 22.6$. Note that the magnitudes have not been corrected for the galactic extinction in this diagram. **Right:** CMD of the two fields around the galaxy. As it appears from the diagrams there is not a remarkable large population of stars at magnitudes and colours corresponding to the red plume.

6.3 The Color Magnitude Diagram

HIPASS J1321-31 contains a population of blue but not very bright stars, reaching at most $I = 24$ mag (Fig. 6.5). There seems to be a well populated RGB, at magnitudes fainter than $I \sim 24.5$. Unlike 1337-33 and 1337-39 we did not detect any bright very red stars above the tip of the RGB at colours $(V-I) > 2$. But the most striking feature of the CMD is the very unusual red plume which extends at bright magnitudes up to $I \sim 22.6$ with colours $1 < (V-I) < 2$ (Fig. 6.5). A similar feature has no analogues in the galaxies of the LG with resolved stellar photometry. The position of these stars has been checked against any defects in the WF3 chip and we ruled out the possibility that the photometry was affected by such effects. Comparison with the other fields surrounding the galaxy (Fig. 6.5), indicates that there are not foreground stars with similar photometric properties which could explain such a feature. Moreover, these stars are scattered across

the optical extent of the galaxy both inside and at the border of the main stellar distribution as one can see from Fig. 6.6, which seems to indicate that they belong to 1321-31.

Three possible scenarios which may explain the nature of these unusual red plume stars have been already discussed in Pritzl et al. (2003) and we will summarise them in the next section, showing what we think is the most likely explanation. Then we will show how the comparison with theoretical isochrones and the simulation of CMDs may be used to further constrain our interpretation suggested in Pritzl et al. (2003).

6.4 A RGB or a population of red supergiant stars?

At first glance the most obvious option would be that the red plume is the upper extension of the RGB. If so, the tip would be at $I \simeq 22.6$, a much brighter value than the one expected at the distance of the Centaurus A group ($I \sim 24$). This would place 1321-31 at about 2 Mpc, half-way between the Local Group and Cen A. However, this distance would conflict with the radial velocity of the HI distribution related to the galaxy. The HI detection of 1321-31 from HIPASS has given a heliocentric velocity of ~ 570 km s^{-1}which is consistent with its membership of the Centaurus group. Unless the 21-cm emission detected corresponds to a local velocity cloud not associated with 1321-31, a possibility which seems highly unlikely, this is an important constraint in understanding the nature of this plume. A stronger case against this nearby hypothesis is given by the shape of the I luminosity function at magnitudes fainter than 22.6 (Fig. 6.7), which appears to be relatively flat. If $I = 22.6$ mag were the assumed tip, the flatness of the luminosity function would indicate a very peculiar RGB, where the number of stars is always found to increase going from the tip to fainter magnitudes. The combination of distance difficulties and a flat luminosity function argue that the red plume is not a RGB.

As a comparison, the only galaxy in the LG with a narrow and sparsely populated RGB is Leo A, whose stellar population has been studied by Tolstoy et al. (1998). The evolutionary history of Leo A has been a puzzle for a few years until the recent discovery of RR Lyrae stars (Dolphin et al. 2002) which definitely confirmed the existence of an ancient ($\gtrsim 11$ Gyr) population. In fact its narrow RGB, compared to the well defined Red Clump had been previously considered as evidence that the galaxy was predominantly young, with an age of around or less than 2 Gyr. Even if its RGB is narrow compared to other dIrr galaxies, because the SF activity has been probably very low between 2 and 10 Gyr, the number of stars in this

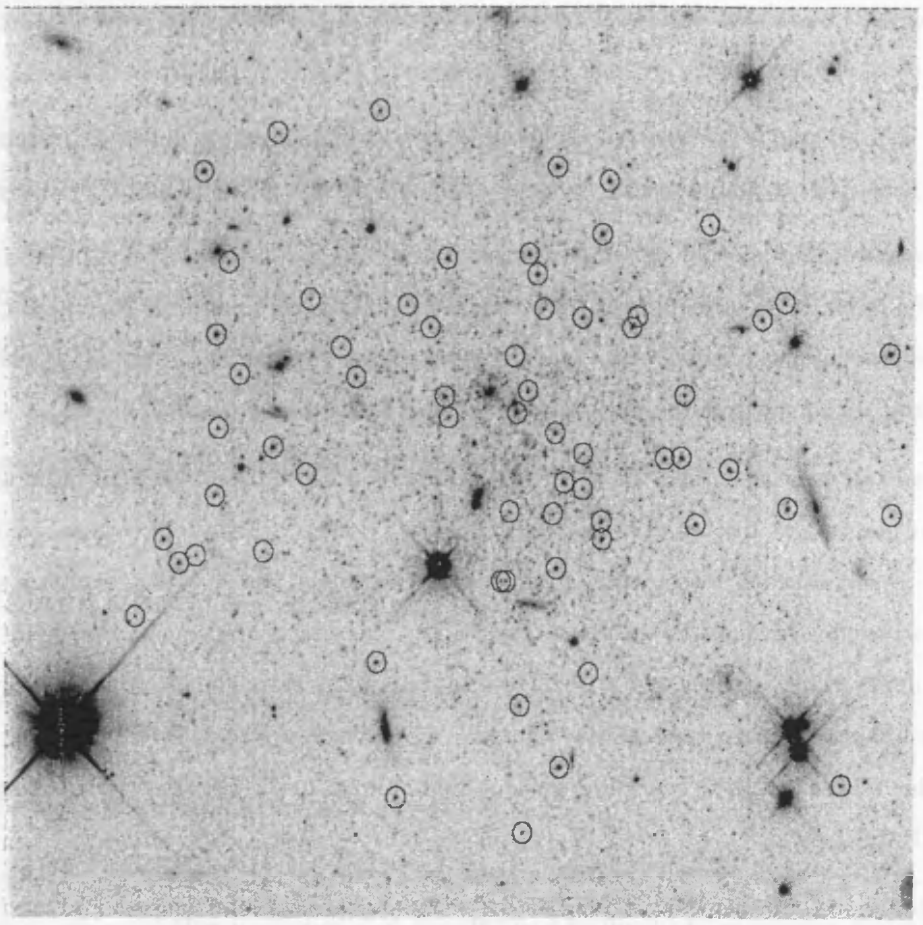

Figure 6.6: WFPC2 image in the F814W filter of HIPASS J1321-31. The circles show the distribution of the stars that constitute the bright red plume seen in Fig. 6.5.

feature gradually increases until the RGB ends up in the Red Clump, i.e. the luminosity function of the red giant stars is never flat, even when the RGB is fainter and less populated than usual. As mentioned before, the red plume in 1321-31 does not show this gradual enhancement at decreasing magnitudes which one should expect if that was the RGB. Its shape is uniform for about two magnitudes and then abruptly widens at $I \sim 24.5$. Moreover, the plume ends its descent at the bluer edge of the group of red stars found below $I \sim 24.5$. If such a feature was the natural extension of the RGB, this sudden change in colour would not have a clear explanation.

Could the red plume be made of luminous AGB stars? This option has also been ruled out. Low metallicity ($Z \lesssim 1/20$ solar), low mass AGBs do extend vertically above the TRGB, after the RGB phase.

Theoretical evolutionary models indicate that these stars can not reach such bright magnitudes above the tip of the RGB. More metal-rich bright AGBs seen in LG galaxies such as Sextans A or IC 1613 extend towards brighter luminosities but they tend to bend redward of the tip of the RGB, while the plume of 1321-31 begins its ascent from the bluer edge of what is thought to be its RGB.

A more likely scenario for the red plume is that it is populated by core-helium burning stars in the Red Super Giant phase as we discussed in Pritzl et al. (2003). However the lack of corresponding blue HeB stars is puzzling. Dwarf galaxies in the Local Group such as Sextans A, and IC 1613, exhibit a strong population of blue stars reaching luminosities as high as the RSGB. These stars are generally made up of a combination of massive upper main sequence and evolved intermediate-mass stars younger than 200 Myr. Moreover the comparable luminosity of the red and blue plumes is an indication of high levels of ongoing SF. The absence of bright blue stars in 1321-31 cannot be due to observational problems, since we have detected such stars in other HIPASS dwarfs.

Blue stars have been detected in 1321-31, but they appear as a faint blue "hump" in the diagram. The absence of bright blue stars would suggest that there is not very recent SF[1] (less than 10 Myr), and that SF activity took place for a few hundred million years, but then dropped at a very recent time. The comparison with stellar isochrones in the following section will enable constraining the age of the blue stellar population.

One way to explain why bright blue stars are missing is to assume that the galaxy went through a phase of enhanced SF activity less than 1Gyr ago, when the stars now populating the red plume were formed.

[1] As regards the very recent SF, one needs to keep in mind that the spatial resolution of the WF chip would have difficulty in resolving the crowded stars in the possible candidate HII regions that we have pointed out in section §5.2. Therefore, those stars would not appear in the CMD.

After this episode, the SFR gradually decreased and it dropped off around a 100 Myr ago. The red plume stars represent the low mass component of the stars produced in that episode (with initial masses around or slightly less than 3 $M_{\odot}$). The more massive stars which in general occupy the bright blue spike of the diagram (the blue supergiants) would have already vacated that area of the diagram. The same thing occurred for the brightest RSGB stars, leaving the RSG branch currently inhabited by such lower mass (and fainter) stars. The corresponding blue HeB stars with the same mass would be at too faint magnitudes ($I \gtrsim 26$) to be clearly detected in the CMD - as one can see in Fig. 6.8.

Therefore an interesting question is not only why the SF increased in the past, but also why it appears to have stopped a few hundred million years after the event. Starbursts can last tens of millions of years and significant amounts of energy will be released into the interstellar medium. If there has been intense SF activity less than 1 Gyr ago, the heating up of the cold component of the ISM may have been responsible for the interruption of the SF activity.

To further discuss this scenario one needs to compare theoretical isochrones with the data, thus it is necessary to define the RGB and determine the distance modulus of this galaxy.

6.5 Locating the Red Giant Branch

With these assumptions in mind, we have defined as the RGB the feature located at $1< V-I < 1.7$, extending up to $I \sim 24.5$. Filtering the I luminosity function of these stars with a Sobel filter we have obtained the tip of what we think is the RGB of 1321-31.

The luminosity function and the output of the edge detection filter are shown in Fig. 6.7. The tip has been found at $m_I = 24.55 \pm 0.11$ (Pritzl et al. 2003). The maps of the galactic extinction (Schlegel, Finkbeiner, & Davis 1998), give for the local reddening the value $E_{B-V} = 0.062 \pm 0.01$, and applying the extinction coefficients one obtains $A_I = 0.12 \pm 0.02$. The dereddened distance modulus is $(m-M)_0 = 28.60 \pm 0.13$ yielding a distance $D = 5.2 \pm 0.3$ Mpc, that places the galaxy at the edge of the group beyond M 83. We do not use the formula of Lee et al. (1993) to estimate the metallicity of the RGB because the error on the colour at the I magnitude $M_{I,-3.5}$ (value used in the relation calibrated by Lee and collaborators) is 0.15. There is a too large scatter in the RGB of 1321-31. Therefore as an estimate of the metallicity we use only the comparison with the CMD of the GCC M15 that we have overlaid on the CMD of 1321-31 in Fig. 6.5. The majority of the red stars of 1321-31 are bluer than the fiducial RGB, therefore, provided that they

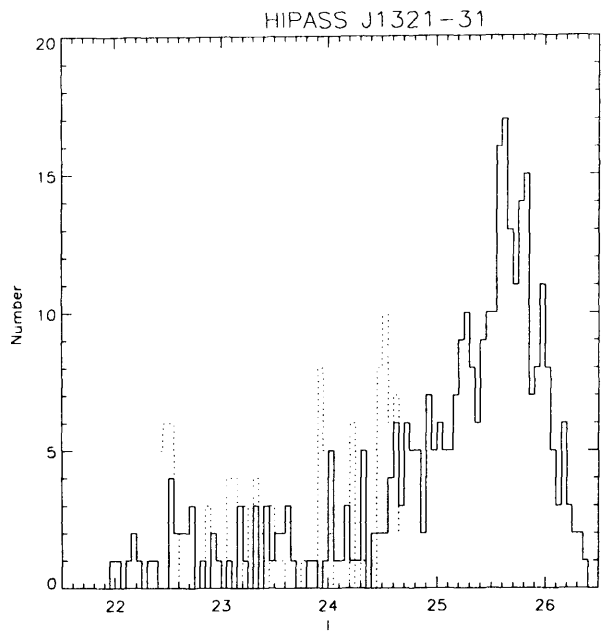

Figure 6.7: The I luminosity function of HIPASS J1321-31 (*solid line*). The *dotted line* represents the output of the the edge detection Sobel filter used to detect the tip of the RGB. Its highest peak indicates the position of the tip which has been found at $m_I = 24.55 \pm 0.11$.

are several Gyr old, they have a metallicity lower than [Fe/H]= -2.1.

6.6 Looking for Asymptotic Giant Branch stars

Although a very small number of stars appear above and redward of the TRGB in the diagram, there is no clear evidence of AGB stars in 1321-31. The number of detections is comparable to the foreground contamination in the adjacent fields (right panel of Fig. 6.5). The lack of AGB stars is puzzling, since the detection of an RGB would suggest that a population of intermediate-age stars should exist. We are not able to firmly constrain the age of this galaxy at this stage of the analysis. The comparison with stellar tracks and the simulation of the SFH will be discussed in the following sections to present the different evolutionary scenarios for 1321-31.

6.7 Constraining the age of the red plume and the RGB

Having derived the distance modulus, Padua isochrones can then be adjusted to the observed magnitudes of 1321-31 to set age constraints on the different features. We have chosen Z = 0.0004 as the lowest metallicity set after comparing the RGB to that of M 15 (Fig. 6.5). As it appears from Fig. 6.8, the lifetime of these stars at such metallicity is around 500 Myr ($\log(Age) = 8.7$) and their mass is in the range 2 - 3 $M_{\odot}$. The synthetic tracks indicate that the red core helium burning phase would be much brighter while the corresponding blue loop stars would be too faint to be detected in our observations. The presence of the faint blue stars at $-0.1 < V - I < 0.4$ implies that the SF process must have continued after this event, probably at a decreasing rate, and dropped off at an age that can be set around 100 Myr ago (see top panel of Fig. 6.8).

Adopting a slightly higher metallicity, Z = 0.001 (Fig. 6.8 bottom-left), results in a variation in the age of the red plume, but the overall star formation scenario would be the same. The RSGB stars and those in the blue "hump" would have different ages and correspond to different events of SF. The age of the RSGB stars would be around 300 Myr ($\log(Age) = 8.5$) in this case.

With an even higher metallicity (Z = 0.004, Fig. 6.8) a 100 Myr old isochrone can fit both the brightest stars of the "blue hump" (with $I < 25.5$) and the red plume. In this scenario, blue and red stars formed at the same time, at a more recent epoch, and the enhancement in the SF dates back to only 100 Myr. However this interpretation seems very unlikely because blue and red plume stars show different spatial distributions: the first are more centrally concentrated (see right panel of Fig. 6.9) while the latter appear randomly distributed throughout the optical body of the galaxy (Fig. 6.9, left panel). If both type of stars were coeval it would be difficult to explain their different location within the galaxy. Thus red plume stars have to be older than the blue ones to explain their scatter and we can rule out the higher metallicity (Z = 0.004) scenario.

To strengthen the case for the red plume being an evolved RSGB, one can notice also that the tip of this feature is around $I \sim 22.6$ mag or $M_I = -6.1$ mag. Other dwarf galaxies found in Karachentsev et al (2003a, b, c) with well populated "ordinary" RSGBs have tips in the range $-7.0 < M_I < -8.7$. Thus, even the faintest tip of the RSGB in these galaxies is still 1 mag higher than 1321-31. This suggests that the stellar population of its RSGB is in comparison older and populated by lower mass stars, while the more massive and brighter stars have already evolved to a different phase, leaving the area of the diagram where

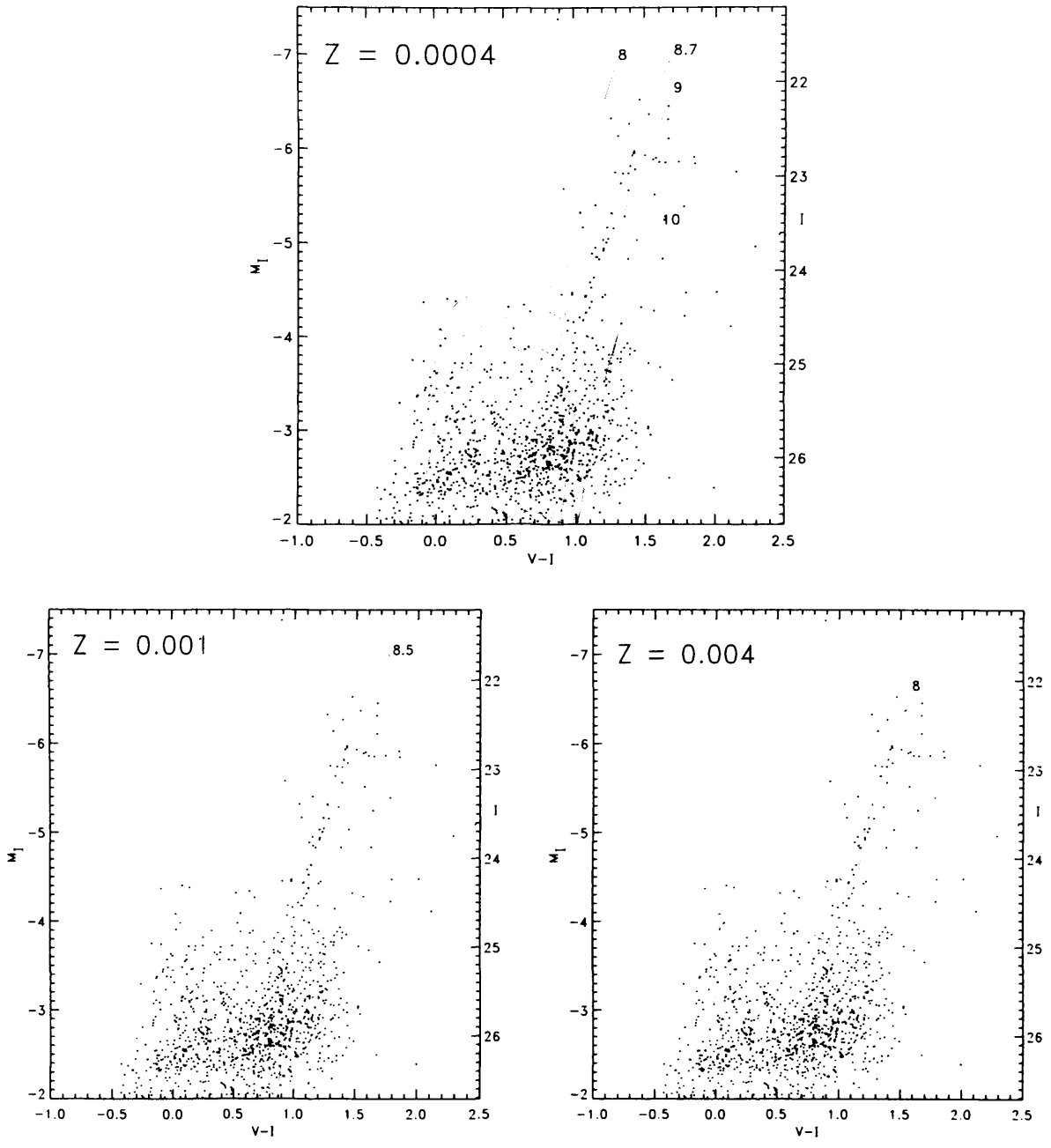

Figure 6.8: HIPASS J1321-31: $(V-I, I)$ colour magnitude diagrams overlaid on Padua stellar evolutionary tracks at metallicities of Z = 0.0004, 0.001 and 0.004. For the highest metallicity we show both the isochrone that fits the location of the red plume (to show how the age of the feature may change with the metal abundance) and the oldest isochrone that would set an upper limit to the age of the RGB at that metallicity.

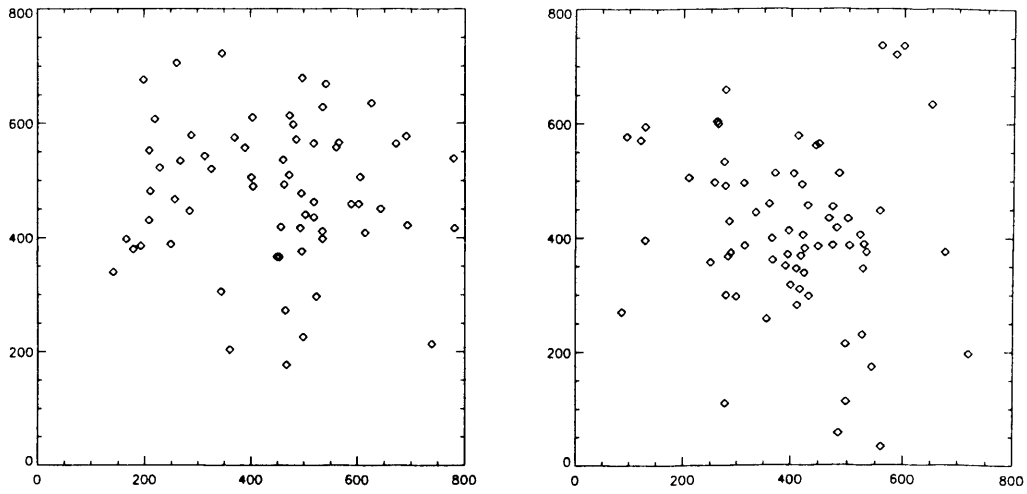

Figure 6.9: The spatial distribution of the stars in the red plume (**left**) and of the brightest blue ones with $I < 25.5$ (**right**). There is a difference in the distribution of the two populations which suggests that they have been formed at different epochs. Such a difference in location rules out the hypothesis that the red plume has a higher metallicity, Z = 0.004, and that these stars are the redder counterpart of the ones in the blue hump.

the brightest stars are generally found.

The constraint on the metallicity of the red plume and the comparison with stellar tracks is the only tool we have at this stage of the analysis to estimate the age of the RGB.

If we assume that the metallicity of the plume is Z = 0.0004 - 0.001, we derive the usual scenario of a very low metallicity galaxy with an RGB which is fitted by isochrones as old as 10 Gyr as one can see from Fig. 6.8.

A higher metallicity scenario at a younger age is displayed in the bottom right corner of Fig. 6.8. In that case, the maximum age of the RGB would be set at around 3 Gyr. The modelling of the SFH will give us further hints to discriminating between these two scenarios.

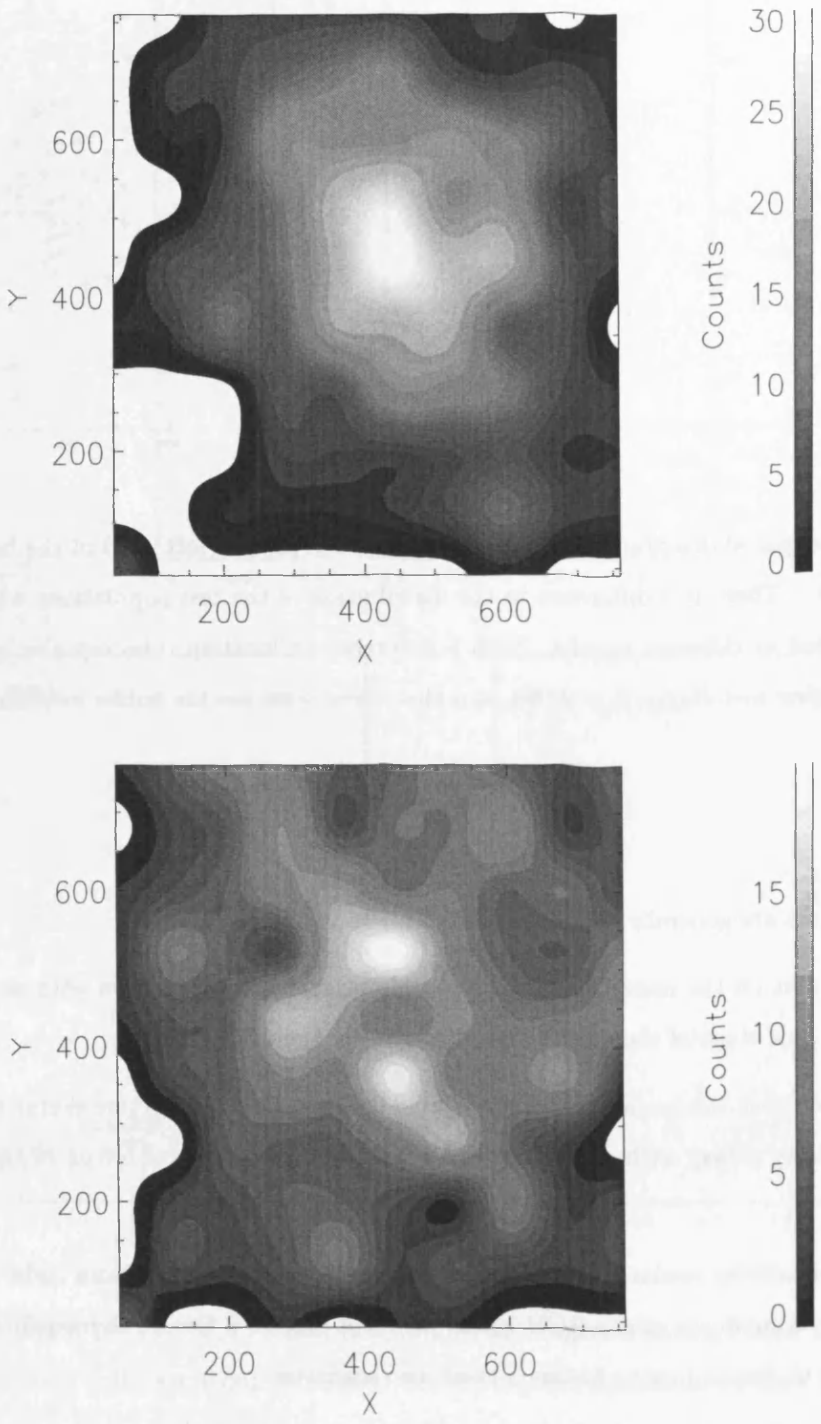

Figure 6.10: The distribution of blue stars (*upper panel*) and red stars (*lower panel*) in the WFPC2 frame. The stars have been selected only on the basis of their colour. In this plot blue and red stars mean that they have colours smaller or greater than $(V - I) = 0.6$.

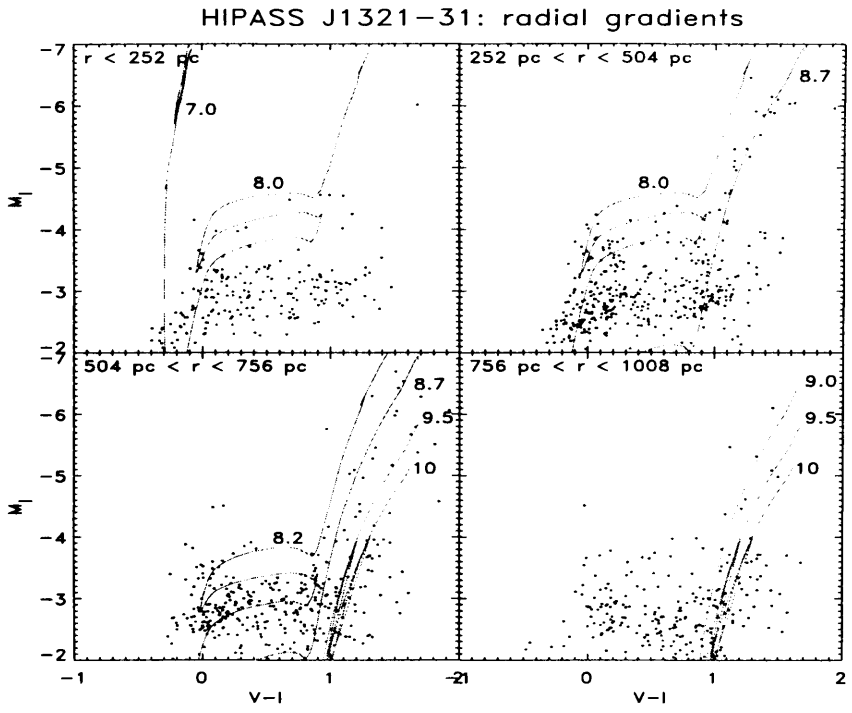

Figure 6.11: HIPASS1321-31: gradient in stellar population in four circular bins centered in the middle of the WF3 chip. The stellar tracks overlaid correspond to Z = 0.0004.

6.8 Radial gradients in the stellar population

As we have already done for the other two galaxies, in order to study the radial distribution of the stars of 1321-31 we have plotted both their position on the chip according to their $(V - I)$ colour - i.e. higher or lower than 0.6 - as shown in Fig. 6.10, and the CMD for four concentric circles centered in the WF3 (Fig. 6.11) with radii going from 10″to 40″.

The red stars are uniformly spread throughout the whole chip with two peaks, while the density of blue stars is higher in the centre - as seen in the other galaxies . What appears from Fig. 6.10, which differs from the other two dwarfs, is that the blue stars are detected even at larger radii and the gradient of their distribution is shallower. Given the large amount of gas available ($M_{HI}/L_B = 5.0$) and its extension well

beyond the stellar distribution (see Fig. 6.1) it is likely that conditions for small local events of SF may have been occurred even in the outer optical regions in the recent past.

From (Fig. 6.11) it is possible to see blue stars up to the third ring (504 pc $< r <$ 756 pc). The stars in the red plume are mainly found in the second and the third bins but they are fairly spread throughout the galaxy rather than being clustered in specific regions. If the estimated age of the red plume stars is around or greater 500 Myr, they had the time to spread out around the galaxy losing their initial spatial coherence. If we assume that the young stars retain the velocity dispersion of the HI clumps from which they originated (which is found to be in general around $\lesssim$ 10 $\mathrm{km\,s^{-1}}$) the crossing time of a 500 pc region is roughly 50 Myr. Therefore, once the HII region is disrupted stars can diffuse away and "lose memory " of their original location in a fairly short time.

6.9 The Star Formation History: a poststarburst galaxy?

We have modelled the SFH and CMD of 1321-31 with StarFISH (Fig. 6.12) trying different combinations of three sets of isochrones (Z = 0.0004, 0.001, 0.004). Using tracks with Z = 0.0004 and Z = 0.001 yields the best-fit SFH (see top-right) and the model CMD (top-left) for comparison with the observed CMD (bottom-left). We find that a model CMD with metallicity as high as Z = 0.004 (bottom-right) cannot reproduce the observed data.

The best-fit SFH suggests that 1321-31 formed its red giant branch at $\log(Age) = 9.8 \pm 0.1$, i.e. the first detectable SF event occurred at $6^{+1.6}_{-1.3}$ Gyr ago. The RGB appears to be relatively "young". This does not exclude though the existence of an older than 10 Gyr (and fainter) population of stars that we are not able to detect, such as HB stars. Nevertheless it seems that the algorithm has underestimated the older SFR of the galaxy, because the model RGB is less populated than the observed one. There may be some problems in modelling this feature because the stars below the tip of the RGB are closer to the photometric limit (the galaxy is more distant than the other two dwarfs) and the majority of them are affected by larger photometric errors.

As regards the more recent SFH, the code fails to reproduce a narrow red plume. The feature appears already at $\log(Age) = 8.8$ (see Fig. 6.13), but the majority of these stars formed at $\log(Age) = 8.4$ where a stronger episode of star formation occurs. We would expect the narrow red plume to be the result of a single burst of SF at a single metallicity. However the small number of stars in it made it difficult for the

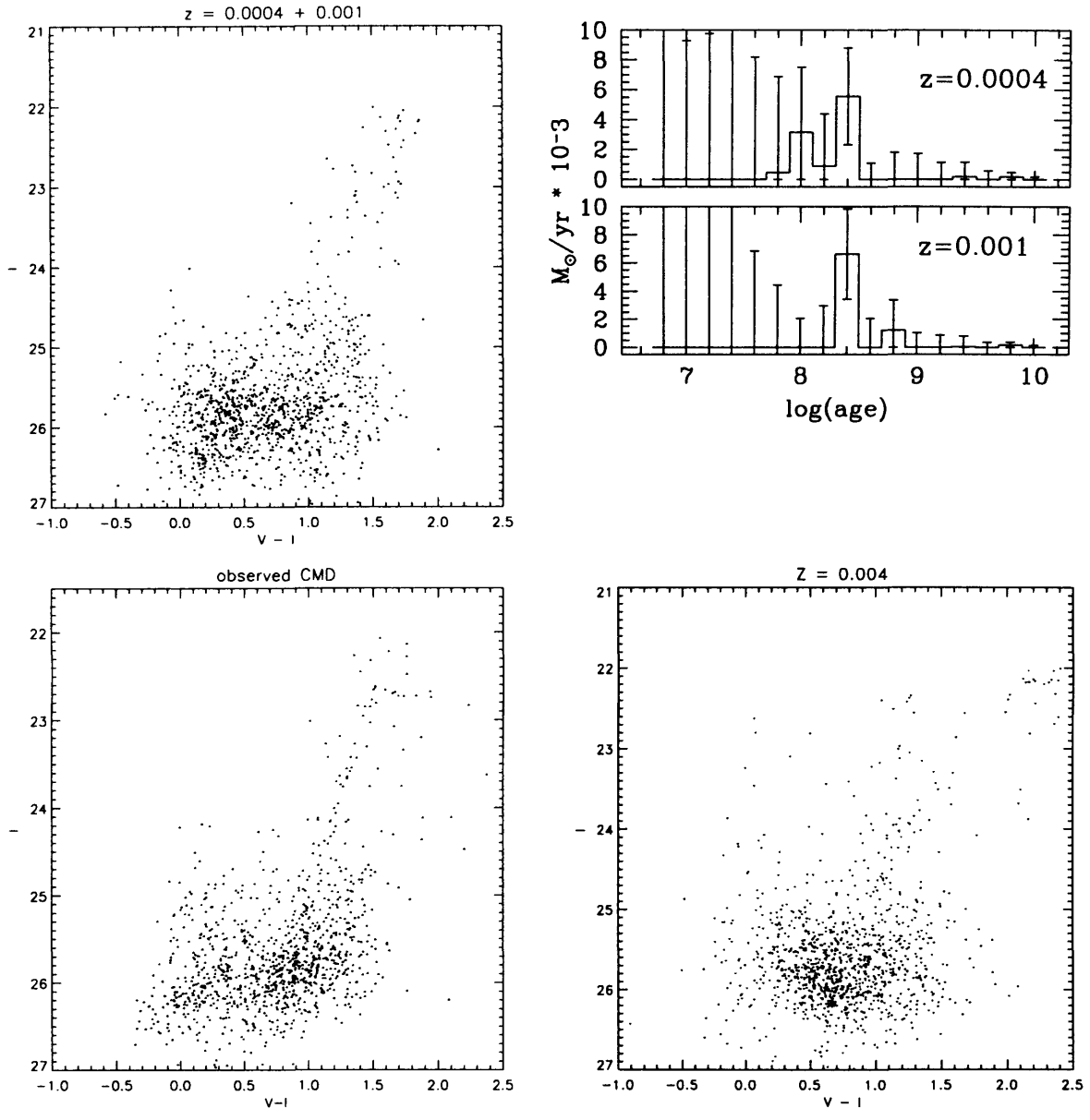

Figure 6.12: The best-fit model CMD (**top-left**) and the corresponding SFH of HIPASS J1321-31 (**top-right**) is compared to the observed one (**bottom-left**) and the model CMD obtained using only the Z = 0.004 set of isochrones (**bottom-right**).

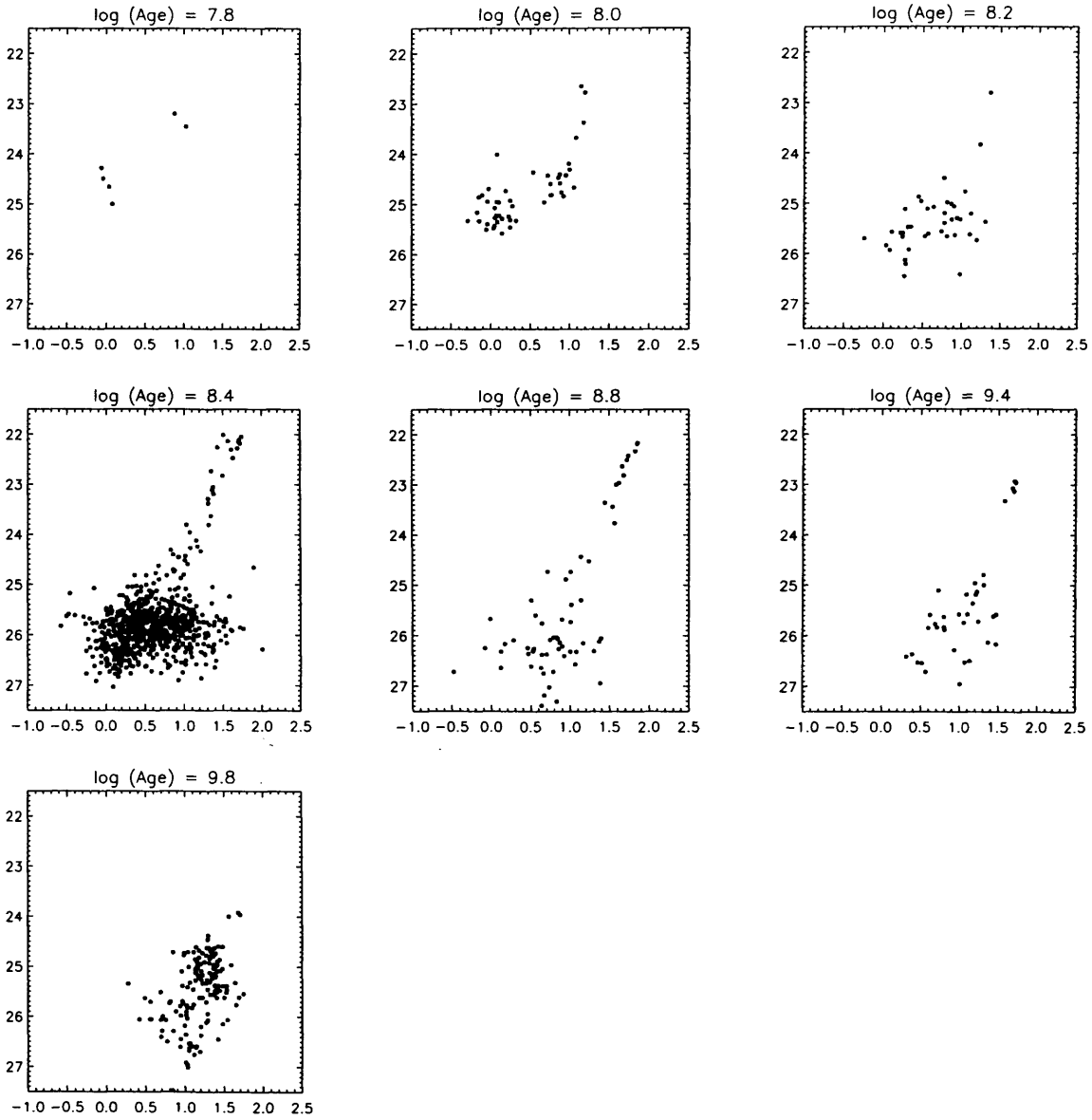

Figure 6.13: The best-fit model CMD split by age bins. The red plume begins to appear at $\log(Age) = 8.8$, but the majority of the stars formed at $\log(Age) = 8.4$.

code to model such a sharp burst with the statistics available.

At $\log(Age) = 8.4$ the SFR is about $6 \times 10^{-3} M_{\odot}$ yr^{-1}, six - ten times higher than the past SF episodes (taking into account the uncertainties on the SFRs). If we use the predicted SFR to estimate the mass in stars born in the age bin at $\log(Age) = 8.4$, we obtain $M_{\star} \simeq 7 \times 10^5$ $M_{\odot}$, which is rather high compared to a luminosity of 7.4×10^6 $L_{\odot}$. It is possible that the recent SFR is slightly overestimated because the number of predicted blue stars is higher than those observed, nevertheless StarFISH finds that a large fraction the stellar population was formed in the recent past, and that the galaxy probably went through a starburst phase.

On the other hand the "burst" that occurred in 1321-31 is not as high as is found in BCDs. In VII Zw 403 for example, the SFR at its peak was $\sim$ 30 times higher than the typical one, and the starburst phase lasted for a few hundred million years (Schulte-Ladbeck 1999).

In summary, the simulations of the SFH of 1321-31 have given us the following insights into the SFH of 1321-31.

- The choice of low metallicity isochrones provide a better fit, supporting the hypothesis that the galaxy has an intermediate-age stellar population. As we go back to ages older than 1 Gyr we find that the RGB stars are only about $6^{+1.6}_{-1.3}$ Gyr old.

- The SFR seems to have been significantly higher in the last 500 Myr than it was between 1 and 10 Gyr ago. The red plume originated around 500 Myr ago although the theoretical feature is not as narrow as the one observed.

6.10 Summary and discussion

HIPASS J1321-31 appears to be a very uncommon galaxy both from its gaseous distribution and optical morphology. It has a large amount of HI (with the highest M_{HI}/L_B ratio among the three objects), with a very irregular distribution and low column density ($\lesssim 2.5 \times 10^{20}$ cm^{-2}) which is clearly offset from the optical counterpart.

The stellar distribution is very diffuse and it is characterised by bright red stars which are scattered throughout the whole optical diameter of the galaxy forming a peculiar red plume when plotted on the

CMD. The lack of a corresponding population of bright blue stars indicates that the galaxy has experienced a peculiar star formation history. Three scenarios for the origin of this anomalous red plume were discussed - RGB, AGB, or RSGB stars - and we have concluded that it is composed of core helium burning post main sequence stars with ages less than 1 Gyr which are likely to be related to an epoch when the galaxy experienced an increase in the SFR (Pritzl et al. 2003).

Having excluded that the red plume is made of red giant stars, we have identified what we think is the RGB and we inferred that the formation of the red plume was not associated with the birth of the galaxy since an older RGB is present (Pritzl et al. 2003).

Constraining the age and metallicity from the CMD alone has been difficult, as we have already discussed for HIDEEP J1337-33, and in this case it has been even more problematic because there is a lack of AGB stars.

We built models of the SFH of the galaxy with different metallicities and found that the best fit was given by assuming a very low abundance for the stellar population implying, as in the other dwarfs, that the red giant branch is made of intermediate-age stars.

The SFH between 1 and 10 Gyr is characterised by very few events and an overall low SFR (below $2 \times 10^{-3}\ M_{\odot}\ yr^{-1}$). We find that the RGB stars are only $6^{+1.6}_{-1.3}$ Gyr old, a few Gyr younger than what we have estimated for the other two dwarfs.

Such a low rate is consistent with the scenario of a gas-rich object evolving "slowly", compared to the large amount of gas present (van Zee et al. 1997a).

At more recent ages ($<$ 1 Gyr) the model SFH confirms that the red plume is related to an epoch of increased SFR as we suggested in Pritzl et al. (2003). We have discussed whether such an event may be considered as a starburst. The predicted SFR implies that a large fraction of the stellar population of 1321-31 was produced during this event. The offset of the gas distribution and the interruption of the star formation activity may provide further evidence that the galaxy went through a starbursting phase, which heated and pushed away the gas from the optical center of the galaxy. We will discuss in the next chapter what are the consequences of intense SF events on the ISM and on the fate of a galaxy. After this main episode the SFR started to decrease and the SF activity stopped around 100 Myr ago.

HIPASS J1321-31 is different from the other HIPASS dwarfs. It does not seem to be a galaxy that formed less than 1 Gyr ago, since we have detected the RGB and we have established an upper limit of

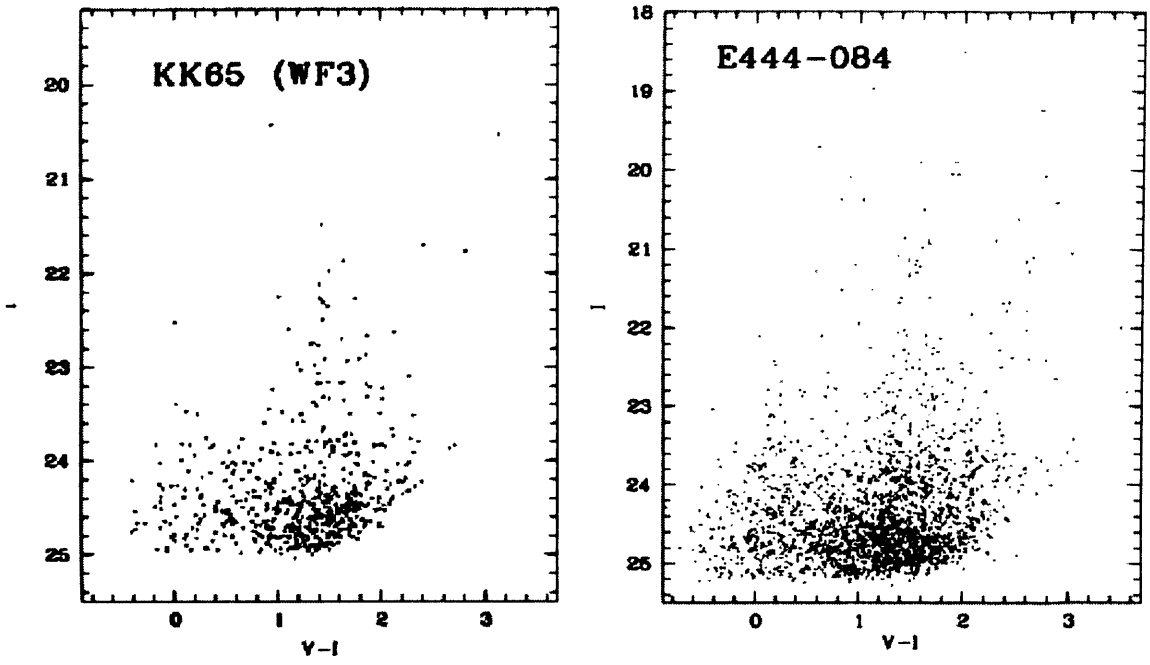

Figure 6.14: CMD of two dwarf galaxies observed with the HST as part of the SNAP survey. The objects show similar pronounced red plumes as HIPASS J1321-31. Note that the exposure times in this case are only 600 seconds, against the 5200 seconds total integration time of our data (from Karachentsev et al. 2002, 2003a).

6 Gyr for the age of its oldest red giant stars. However it does appear to have a predominantly young population with an age which is less than 500 Myr.

Looking at nearby dwarf galaxies outside the LG such as those imaged with the HST in the SNAP survey (Karachentsev et al 2003) we have found that the peculiar red plume of 1321-31 is not unique. Similar features are found in KK 65 and ESO 444-084, another galaxy in the Centaurus A group (Karachentsev et al. 2003, a, b, c). KK 65 shows a dispersed RSGB with a faint population of blue stars, but the difference in magnitude between the tip of the RSGB and the blue plume is smaller compared to HIPASS J1321-31 (Fig. 6.14). We have compared their properties in Table 6.10 remarking that both dwarfs are gas-rich but have higher luminosity than 1321-31 and consequently low M_{HI}/L_B ratios.

Finally, we want to point out that the optical image in the F555W filter displays two compact bright

	$v_\odot$	r	m_B	M_B	M_{HI}	M_{HI}/L_B
	$\mathrm{km\,s^{-1}}$	arcmin			$10^7 \cdot M_\odot$	$M_\odot / L_\odot$
HIPASS J1321-31	572	0.7	17.1	-11.7	3.7	5.0
ESO 444-G084	591	2.3	15.1	-13.5	5.6	1.4
KK 65	554	2.2	15.6	-12.7	1.6	0.9

Table 6.1: The comparison of the physical properties of HIPASS J1321-31 and the dwarf galaxies with similar CMD found in the SNAP survey.

regions which may be interpreted as areas where SF is currently taking place, although the search for Hα emission has failed to reveal such regions with exposures taken with the WIYN telescope. The galaxy has also been one of the targets of the Survey for Ionization in Neutral-Gas Galaxies (SINGG), yet no obvious evidence of ionised gas has been detected (Knezek private communication). We have not even detected blue and bright blue stars in the CMD to give evidence of ongoing SF activity, but if SF is localised to these small regions only, we would not be able to resolve the single stars in those areas, and they would not appear in the diagram. The presence of SF regions would be surprising given the low column density that we have measured throughout the optical disc.

Chapter 7

Conclusions

There are several issues that we have tried to answer with this study of three gas-rich dwarf galaxies found in the Centaurus A group.

These galaxies have been originally selected because of their high M_{HI}/L_B ratios and low optical luminosity which make them unique objects in the very nearby universe: in fact they do not seem to have used the majority of their gas content, compared to their mass in stars, and they do not show obvious signs of massive SF despite their large fractional HI mass.

We will use this final chapter to address these issues and try to answer them now that the analysis has been carried out. Here we list the main questions that led us to start this study and a brief summary of the steps we have followed during our analysis of these puzzling gas-rich dwarf galaxies.

- The first issue is to determine if we have found a class of young galaxies, since this would be a natural explanation for their high gas-mass-to-stellar-light ratios.
- As soon as we showed that these galaxies were not formed recently (i.e. less than 1 Gyr ago), we have estimated their age as far back in time as the data set allowed us to.
- If they host an intermediate-age population (possibly as old as 10 Gyr in HIPASS J1337-39 and HIDEEP J1337-33, and 6 Gyr in HIPASS J1321-31) as the observations we have presented seem to show, the next question which we have to ask is why they still have such a large amount of gas. Is it because of a recent infall, or because they have experienced a low SFR throughout their evolution?

- There is little we can say about gas infall given our data set. A higher resolution HI analysis would allow a better view of the HI distribution in these galaxies. However we investigated their star formation histories by looking at their stellar populations. We have found that the evolutionary history of these galaxies is characterised by low average star formation rates and that periods of star formation activity alternate with periods of quiescence.

- The next issue is to understand what determines such low SFRs. Is it a consequence of their internal properties i.e. a too diffuse ISM with low HI column densities, the absence of a cold ISM component, the low metallicity and dust or is it due to their local environment. Or a possible combination of these effects?

- Another question to address is the role of SN in affecting the SFR of such galaxies and what is the impact on their gas content of repeated SN explosions? Given our estimate of the SFR would the consequent rate of SN be able to blow away their discs and make the gas gravitationally unbound? In the galaxy where HII regions have been detected, we find poor chemical enrichment. Therefore what are the implications of our results compared to these current models predicting mass and metal loss due to SN explosions in dwarf galaxies?

- Then we compare the HIPASS dwarfs with the nearby dwarf galaxies of the LG for which deep data samples have been obtained allowing a detailed study of their SFH's. The evolution of dwarf galaxies in the LG is varied and in general not well understood. Yet, there do not seem to be in our neighbourhood objects with such extreme properties and high M_{HI}/L_B ratios. Is it because our group is dynamically more evolved than the Centaurus A group, or more precisely than the Cen A and M 83 subgroups (see also section 2.2)? There do seem to be LG objects which have properties in common with the three HIPASS dwarfs, but they all have lower gas fractions. We compare their common characteristics and/or differences.

- To conclude, there is an open debate about the evolutionary link between dSph and dIrr galaxies. The HIPASS dwarfs show properties intermediate between the two classes of galaxies, therefore they offer a unique opportunity to investigate this issue. We discuss what these galaxies can tell about dwarf galaxy evolution, whether they perhaps represent the missing evolutionary link in the transformation from one morphological type to the other, or alternatively they represent a separate class of dwarf galaxies.

7.1 How old are the Centaurus A dwarfs

The first fundamental issue in the study of these objects is to determine or at least constrain the ages of these objects. Whether they are "young" galaxies just experiencing their first star formation episodes, or "old" galaxies that formed their first generation of star (at least) several Gyr ago, can be decided only by looking at their resolved stellar populations.

There is little work of such a kind in these galaxies. So far, SFHs of some dwarf gas-rich galaxies have been obtained from their integrated colours. For the first time we have presented a study of the resolved stellar population of gas-rich dwarfs building their CMDs in two filters (V and I).

In all the HIPASS dwarfs examined, a clear RGB has been detected. This sets a lower limit on their age of at least 1 - 2 Gyr, the minimum time for RGB stars to appear after a first starburst. In principle, the RGB can be populated by stars much older than this minimum age (10 - 12 Gyr) and the presence of a well defined tip of the RGB, as we find for the three dwarfs, is generally considered as a reliable proof for the existence of an old population of stars (older than 1 - 2 Gyr) (Tolstoy et al. 1998). This is the first evidence of the presence of a several Gyr population in these dwarfs.

Secondly, we have looked for AGB stars. The detection of AGB stars above the TRGB is considered as an unambiguous evidence of the presence of an intermediate-age (1 - 10 Gyr) population (Caldwell et al. 1998). Two out of three galaxies (HIPASS J1337-39 and HIDEPP J1337-33) do show AGB candidate stars. The lack of AGB stars in 1321-31 is puzzling since we would expect the presence of intermediate-age stars given that the RGB has been well detected.

Then, as a first stage of the analysis, we have constrained the age and the metallicity of the stellar population by comparison with theoretical isochrones from the Padua group (Bertelli et al. 1994, Girardi et al. 2002). This gave a first hint on the metallicity and age of the different stellar populations when it was not possible to infer their abundance without a direct measurement. As regards HIPASS J1337-39, we have been able to measure the oxygen abundance from the analysis of its HII region and we have derived a current low ISM metallicity ($Z \sim 1/30$ solar). Constraining the age and metallicity of the other two galaxies has been more difficult due to the age-metallicity degeneracy. We have used different arguments mostly based on the morphology and the colour of the RGB which are more uncertain than a direct measure of the abundance. Yet we think that our conclusions are both consistent and reliable.

Hence we have adopted two sets of low metallicity isochrones (Z = 0.0004 - 0.001) and inferred that the

red giant stars in the diagram may be as old as 10 Gyr. As mentioned before, in two out of three dwarfs (1337-39 and 1337-33) this result is strengthened by the detection of AGB stars.

The red stars in dwarf galaxies constitute an underlying sheet on which is superposed, with a more centrally concentrated distribution, the bluer and younger stellar population.There is still a debate on whether the "red halos" found in dwarfs contain an old stellar population as it is found for example in spiral galaxies. The dwarf galaxies in the LG where the age of the oldest population has been constrained by the detection of HB stars, do show such red halos. Therefore we can argue that the presence of an extended distribution of red stars in the HIPASS dwarfs may hint as well at the existence of an old stellar population which is at least 10 Gyr old.

Modelling has offered another point of view on the issue. Using the StarFISH code we have found that SF activity between 8 and $\sim$ 12 Gyr ago (log (Age) = 10 $\pm$ 0.1) would explain the appearance of the RGBs in both HIPASS J1337-39 and HIDEEP J1337-33 strengthening the hypothesis of a first population of stars which is around 10 Gyr old. This result does not exclude the possibility that the dwarfs may contain older populations of stars which are beyond our detection limits.

The situation appears more controversial for HIPASS J1321-31. Its first episode of SF (in the $\sim$ 10 Gyr time range we have considered) seems to have occurred at $6.3^{+1.6}_{-1.3}$ Gyr ago (log (Age) = 9.8 $\pm$ 0.1). The SFH of this galaxy appears to be characterised by a very weak activity until about 1 Gyr ago and only in the last 300 Myr we find a significant increase in the SF activity, which then drops again in the last 100 Myr. Therefore it appears that 1321-31 has a dominant population with an age between 100 Myr and 300 Myr but it seems that the stars in its RGB formed around 6 Gyr ago.

Therefore study of the stellar population of these dwarfs seems to rule out the possibility that they are recently formed systems (with ages less than 1 Gyr) since we have detected an intermediate-age population which is at least 6 Gyr old in 1321-31, and probably older (up to 10 Gyr) in the other two dwarfs. The presence of an ancient component (> 10 Gyr) would definitely show that these galaxies are primordial objects despite their large gas reservoirs. Unfortunately observations reaching the horizontal branch magnitude or the main sequence turn-off are not currently feasible.

7.2 A recent gas infall or a low SFR?

Since we have derived the presence of intermediate-age stellar populations, the question that naturally follows is why have they been able to keep such large amounts of gas? Have they recently accreted intergalactic gas? Or have they evolved for some reason at a low SFR?

An example of gas accretion in the LG is given by IC 10, in which infall has also caused recent star formation. The HI outer envelope of IC 10 has a very extended, clumpy and counter-rotating structure that has been interpreted as a possible infalling cloud of 10^7 $M_\odot$ (Wilcots 2003). With the current resolution of our HI data we can not distinguish such features in the HIPASS dwarfs. However one galaxy (1337-39) shows a peculiar HI tail with an irregular velocity field that may give hint of a possible accretion of gas.

On the other hand, having modelled the SFHs of these galaxies with StarFISH we are able to give an estimate of their average SFR, and we obtain over a 10 Gyr time range the following values: 2×10^{-3} , 0.6 $\times 10^{-3}$ and 0.2 $\times 10^{-3}$ $M_\odot$ yr^{-1} for HIPASS J1337-39, HIPASS J1321-31 and HIDEEP J1337-33 respectively. The gas depletion time scale $\tau_g \equiv M_{HI}/\mathrm{SFR}$ gives an indication of the time needed to consume the present amount of gas at the average rate. We thus obtain timescales which are much longer than the Hubble time ($\sim$ 20, 60, 25 Gyr respectively). Even without infall these galaxies will continue to retain much neutral hydrogen for several more gigayears.

The resulting gas depletion timescales are comparable to those of the sample of gas-rich dIrr galaxies studied by van Zee (2001b), with a median value around 20 Gyr. We can conclude that the arguments presented so far (the constraint on the age of the oldest detectable stellar population, the estimated SFRs, the gas depletion timescales), are all evidence of an evolution characterised by an overall low SFR. We think this is the main reason of the presence of such a large amount of neutral hydrogen in these systems.

7.3 The interplay between SFRs, gas density and metallicity: why gas-rich galaxies are "retarded"?

A low SFR may be the consequence of either their intrinsic physical properties (i.e. a low gas density, and/or a low metallicity which makes the cooling process less efficient) or of their location in the group (if they are far away from massive members they experience less interactions to trigger SF events). Likewise the

processes which are responsible for gas stripping such as ram-pressure or tidal interactions may be inefficient.

Let us discuss the internal processes first. Recent work on the gas distribution in normal and low surface brightness dwarf galaxies indicates that the global gas densities in these galaxies are well below the threshold for star formation (Toomre 1964) across the entire stellar disc, suggesting that it is difficult to initiate a global burst of star formation (Hunter & Plummer 1996; van Zee et al. 1997a,b; Hunter, Elmegreen, & Baker 1998). Van Zee (1997a, 1997b; 2001a, 2001b) concludes, after the analysis of several gas-rich dIrr galaxies, that the star formation process in such objects is more likely to occur as a random percolation of the star formation activity across the stellar disc, rather than episodic global starburst events followed by periods of quiescence. According to van Zee star formation is a localized phenomenon, occurring only in those regions where the gas density is sufficiently high to allow molecular cloud formation and subsequent star formation. The onset of the star formation activity across the galaxy is expected to be a quiescent phenomenon since it is unlikely that the entire disc will have sufficient gas density to permit a global starburst. van Zee has also compared the gaseous distribution of gas-rich LSB dIrrs and BCDs and found a fundamental difference between the two types of galaxy. While the neutral gas in the BCDs sample is centrally concentrated, with the density peaks all above 10^{21} cm^{-2} , coinciding with the region of star formation, in the LSB sample the gaseous distribution is much shallower, roughly constant throughout the disc and below 10^{21} cm^{-2}.

Gas density seems to play a fundamental role in the efficiency of SF in galaxies. In our small sample we find a similar trend. Current SF occurs only in 1337-39, the galaxy where the HI density is highest and above 10^{21} cm^{-2}. This is also the galaxy with the highest average SFR. The other two systems, where the peak column density is about one order of magnitude lower, and the gaseous distribution is almost constant throughout the optical disc, show no signature of current SF.

We can have an idea of the SF threshold for these objects by calculating the critical density using the Toomre criterion, although the validity of such a relation for low mass and irregular galaxies is still under debate (see Introduction).

Assuming a thin, isothermal disc, the critical gas density given by the Toomre criterion (1964) (see also Chapter 1, §1.3.1) is

$$\Sigma_c = \frac{\alpha c}{3.36G}\left[1.4\frac{V}{R}\left(1+\frac{R}{V}\frac{dV}{dR}\right)^{\frac{1}{2}}\right] \tag{7.1}$$

where c is the velocity dispersion which ranges between 6 - 9 km s^{-1}, α is a dimensionless geometrical

parameter with a value of 0.7 for spiral galaxies (Kennicutt 1989), R is the radius of the galaxy, V the rotational velocity at the radius R. To get an estimate of this threshold density we will assume (for a simplified approach) a solid body rotation curve (V $\propto$ R). We obtain, for HIPASS J1337-39, that the critical density is $N_{HI} \sim 1 \times 10^{21}$ cm^{-2}. The calculation for the other galaxies give roughly similar values. Only 1337-39 has a column density that exceeds such critical density, since 1321-31 and 1337-33 have almost constant HI column density around 2 $\times 10^{20}$ cm^{-2}. In fact 1337-39 is the only object with clear evidence of ongoing SF.

An example of how different initial mass densities (including both stellar and gas) may lead to different evolutionary paths is given by Carraro et al. (2001). Although this study concentrates mainly on the evolution of dwarf elliptical galaxies their simulations of the SFH in four galaxy models with different initial mass density (shown in Fig. 7.1) gives an idea on how this parameter may affect the evolution of a galaxy. In particular one can see how the SFR changes from a single very old starburst for the highest density object to many short episodes lasting less than 100 - 200 Myr superimposed on a shallower nearly periodic SFR with a typical timescale of about 1 Gyr. Their simulations show how the optimal conditions for SF are more difficult to attain in a low density medium and as a consequence, the SF activity becomes irregular and discontinuous (Carraro et al. 2001).

According to Hirashita (2000) such an irregular SF activity is also common in small size dIrr galaxies and is the consequence of the balance between the heating process of the ISM due to SN, stellar winds and the emission of UV radiation (i.e. stellar feedback) and the cooling rate. For a characteristic radius of 1 kpc the heating from the stellar feedback is very efficient with a characteristic propagation time scale of 10^8 yr where a propagation speed of the "feedback wave" of $\sim$ 36 km s^{-1}has been assumed following Dopita et al. (1985). The radiative cooling-time of the heated gas defines the timescale in which the gas heated by supernovae falls back into the galaxy. One has to keep in mind that the radiative cooling rate in a galaxy depends also on its metal content. For a dIrr Hirashita estimates that

$$t_{cool} \sim 7 \times 10^8 \left(\frac{\zeta}{0.1}\right)^{-1} yr \tag{7.2}$$

where ζ is the metallicity of the galaxy normalized by the solar abundance.

Thus the combination of a small typical size (which makes the feedback more effective) and low abundances (determining an inefficient cooling rate) "conspire" to produce in dIrr galaxies an irregular and

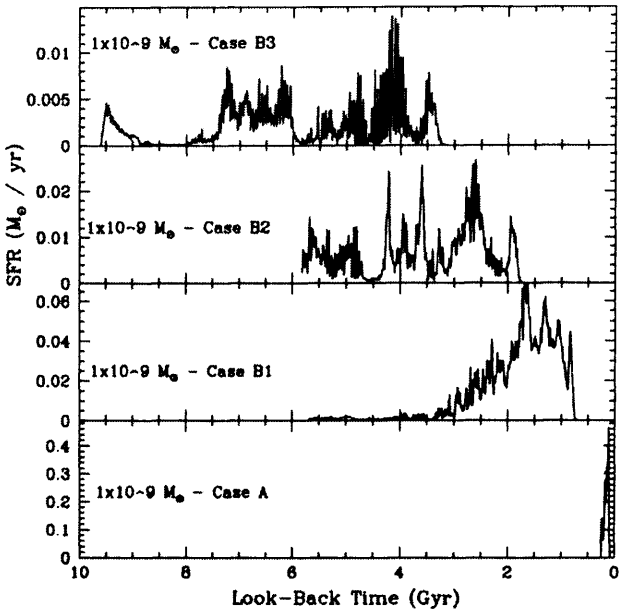

Figure 7.1: A simulation of the variation of the SFR in four galaxy models with the same value of the total mass but different initial density (Carraro et al. 2001). The density decreases from the bottom to the top panel. For the single burst episode at the bottom of the figure (case A), the initial density is 3.9 $\times 10^6$ $M_\odot$ /kpc^3 ($\sim$ 0.2 cm^{-3}). For the other simulations the density has been fixed at about 1/70 (B1), 1/300 (B2), and 1/700 (B3) of model A. Many short episodes superimposed on a shallower SFR with a timescale of about 1 Gyr characterise the evolution of low density systems. At the highest density the model produces only a single very old starburst. The zero time has been chosen as the moment in which a lump of dark matter and baryonic dark matter detaches from the Hubble flow and begins to collapse.

"intermittent" SFR (Hirashita 2000).

According to Ferrara and Tolstoy (2000) the evolution of dIrrs may be understood as the result of fluctuations of the SF activity around a mean level which is constant or slightly decreasing. Bursts of SF may occur easily in these galaxies but they do not last long enough to significantly alter the long-term effects of a low and constant SFR.

For our sample of galaxies the metallicity is around 1/20 - 1/50 solar, and so the cooling time may be between 1.5 and 3.5 Gyr, as follows from Eq. 1.2. Therefore low gas density and low metal abundance may

explain the low SFRs and the "gasping" SFH characterised by periods of activity and quiescence.

7.4 The efficiency of SN-driven mass and metal ejection

Having established that the SF in HIPASS dwarfs has occurred for several Gyr raises two more issues. First one must consider whether the star formation events experienced by these galaxies may have been strong enough to blow out their gas. Secondly, how can SF activity extended so long in time be consistent with the low abundances estimated?

The mass loss from dwarf galaxies is an extremely important process which may significantly affect their evolution. This mechanism has been often suggested as the main issue in understanding the possible evolutionary link between dSphs and dIrrs. However, determining the efficiency of mass loss implies the introduction of some assumptions on the nature of the dark matter halo.

Hydrodynamic models initially indicated that a starburst could have a totally disruptive effect on the ISM of low-mass galaxies (Dekel & Silk 1986). However, more recent models, including a large dark matter component, have shown that it is much more difficult to remove the ISM with a single starburst than previously thought (Mac Low & Ferrara 1999, hereafter McF99). According to McF99 mass ejection (with the disruption of the gaseous content) is very efficient only for galaxies with $M_{gas+stars} = M_{bar} \lesssim 10^6\ M_\odot$. Galaxies with $M_{bar} \gtrsim 10^7\ M_\odot$ are less affected by starburst events.

The fate of a galaxy after a starburst is predicted by McF99 for different gaseous and stellar masses, and for various mechanical luminosities of the starburst L, i.e. the fraction of the total energy released by a supernova into the ISM as mechanical energy, given a certain rate of SNe per year. This parameter is expressed as L_{38} (units of 10^{38} ergs s^{-1}). The dark-to-visible mass ratio used in the simulations is derived from Persic et al. (1996) and corresponds to $\phi = M_h/M_{bar} = 34.7(M_{bar}/10^7\ M_\odot)^{-0.29}$, where M_h stands for the mass of the dark matter halo. For the baryonic mass range of our dwarf galaxies, $10^7\ M_\odot \lesssim M_{bar} \lesssim 10^8\ M_\odot$, this gives a dark-to-visible mass ratio $35 \gtrsim \phi \gtrsim 20$ which is a factor 2 higher than the dynamical-baryonic-mass ratios that we have found from the velocity widths of the 21-cm emission lines ($20 \gtrsim M_{dyn}/M_{bar} \gtrsim 10$).

To have an idea of the effects on the dwarfs of the most intense SF episodes obtained with StarFISH, we have calculated the L_{38} parameter for each galaxy. We have assumed that the energy released by a SN

event is about $E_0 = 10^{51}$ ergs, a tenth of which is deposited into the ISM while the rest is radiated away (Thornton et al. 1998) We have estimated the amount of stellar mass produced in the SF episodes with the highest SFR for each dwarf in their recent past where the time resolution of the SFH is higher (for example for 1321-31 we have considered the event at log(Age) = 8.4, for 1337-39 the most recent event at 10 Myr, and for 1337-33 the one at log(Age) = 7.8). We have then calculated the number of SNe produced in each SF event (N) and derived L_{38} as $NE_0/10\Delta t$ where Δt is given by the width of the corresponding age bin. We have then plotted the results in the M_{bar} - L_{38} plane (Fig. 7.2). In the plane three main areas are defined: the *Blow-Away* region, where the ISM is completely ejected from the galaxy, the *Blow-Out/Mass Loss* region which defines the masses and mechanical luminosities at which only part of the ISM is ejected from the galaxy during a starburst, and finally the upper-left corner region defines where the mass losses are negligible (*No Mass Loss*).

As one can see from the figure, all the three dwarfs are included in the area of the plane where they undergo blow-out of the gas, but where the ISM will not be completely ejected.

On the other hand, the metal ejection by stellar winds and SN is much more dramatic. According to the simulations of McF99, about 60% of the metal-enriched material is expelled from a galaxy with $M_{bar} = 10^9$ $M_\odot$, a fraction that increases up to 100% for $M_{bar} = 10^8$ $M_\odot$, which is the order of magnitude of the total baryonic mass of our dwarfs. Metals easily escape from low mass dwarf galaxies because the chemical enriched material produced by the stars is entrained within the hot bubble of gas where it reaches the edge of the galaxy and the sound speed is higher than the escape velocity (Legrand 2000). When this bubble reaches the outer envelope of cold gas, the hot gas inside blows right away leaving the cold material behind. In the more massive objects ($M_{bar} > 10^9$ $M_\odot$) a significant fraction of the metal-enriched gas is retained by the gravitational potential of the dark matter halo and will eventually falls back onto the galaxy after it cools down (McF 99). On the other hand, one way for low mass dwarf galaxies to retain their metal-enriched material is to experience low luminosity SF events. A lower rate of SN may reduce the outflow of the metal-enriched gas into the intergalactic medium (McF99; Ferrara & Tolstoy 2000) leading to a gradual increase in the metal abundance of the ISM.

An example of a low mass dwarf galaxy showing a smooth chemical enrichment is LGS 3 in the LG, which has a total luminosity of 7 $\times 10^5$ $L_\odot$ and a total gas mass $M_{HI} = 3 \times 10^5$ $M_\odot$ (Miller et al. 2001). Miller and collaborators determined the star formation history of LGS 3. After an early episode of SF (13 - 15 Gyr) the galaxy appears to have experienced slowly decreasing SFR since then (below 10^{-4} $M_\odot$ yr^{-1}).

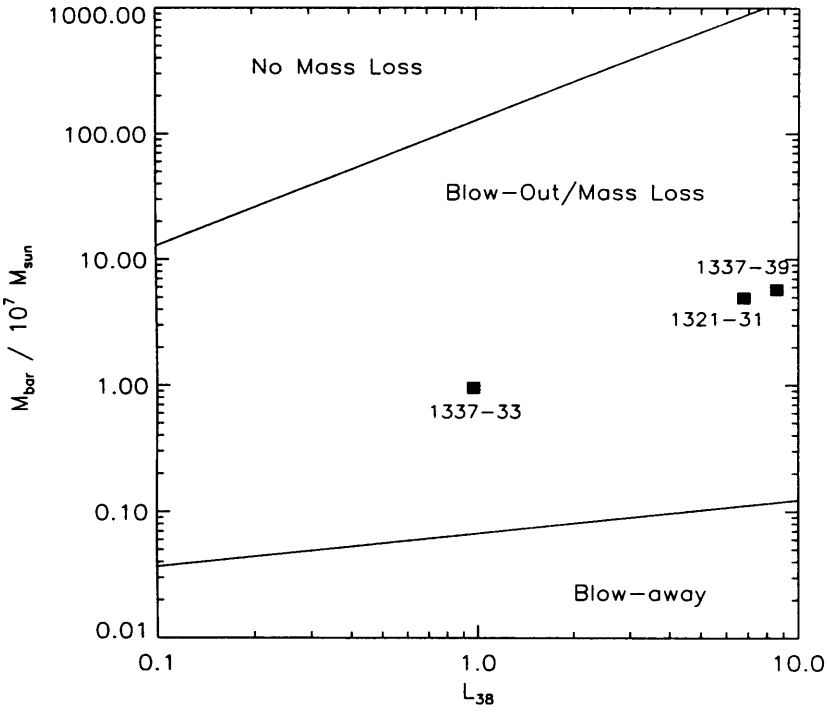

Figure 7.2: Values of the baryonic mass of a dwarf galaxy and the starburst luminosity showing the regions where blow-away, blow-out or no gas loss may occur (see McF99 for details). The filled squares represent the location on the plane of the HIPASS dwarfs, having considered the most intense SF events in their recent history. As one can see from the picture, all the dwarfs galaxies are in the area of the diagram where only blow-out may occur, i.e. only the hot enriched gas is ejected. The episodes of SF are not able to eject the whole ISM and the galaxies according to the McF99 model are able to retain the bulk of their gas content.

Stars older than 8 Gyr have [Fe/H]= −1.5, while those younger than 1 Gyr have [Fe/H]= −0.8 (Miller et al. 2001). As regards the recent SFH, they found that only 600 $M_{\odot}$ of stars have formed in the last period of measurable star formation between 100 and 200 Myr ago. Even if all these stars formed simultaneously, they estimate that the energy output transferred from the SN to the ISM is much less than the amount needed to blow any of the gas out of the galaxy. Thus the observed chemical evolution of the stellar population of LGS 3 suggests that much of the enriched gas from stellar evolution has remained in the galaxy (Miller et al. 2001).

This is what may also have happened in HIDEEP J1337-33, which is the galaxy with the higher metallicity among our three dwarfs and seems to show two stellar populations with different chemical abundance. From analysis of the CMD and the comparison of its main features with theoretical isochrones we showed that the dominant population of the RGB and the very red AGB stars cannot be fitted by the same set of evolutionary tracks, suggesting that an ISM chemically enriched by the first generation of stars may have been reprocessed into stars in the later SF events.

7.5 The effects of the environment

The number of massive satellites (like the Small Magellanic Cloud) around the main members of small and loose groups like the LG or Centaurus A is very small compared to the number of Milky Way-like galaxies in rich clusters (Mayer et al. 2001). Satellite-satellite interaction may be neglected as a mechanism able to affect the evolution of galaxies, since the rate of effective "harassment" between satellite galaxies is less than one in every 10 Gyr (Mayer et al. 2001). Thus, the giant galaxies are the main evolutionary drivers in these environments. M 83 is the closest massive spiral to the HIPASS dwarfs, so we have calculated their location and dynamical status in relation to this bright spiral galaxy to check if there is a possible connection between the environment of the dwarfs and their observed properties. The distance from M83 is given by

$$R^2 = D^2 + D_{M83}^2 - 2D \cdot D_{M83} \cdot cos\theta \tag{7.3}$$

where θ is the angular separation from M 83, D the distance of the dwarf we have measured and D_{M83}.

We have also calculated the radial velocity relative to M83 according to

SOURCE	D_{M83}	V_{LG}	$(V - V_{M83})$	M_{HI}/L_B
	kpc	$km\,s^{-1}$	$km\,s^{-1}$	$M_\odot L_\odot$
HIPASS J1337-39	910	257	23	3.1
HIPASS J1321-31	780	345	47	5.
HIDEEP J1337-33	315	370	24	1.4

Table 7.1: Cen A dwarfs: the distance from M83, the radial velocities respect to the Local Group and M83 the distance of M83.

$$(V - V_{M83}) = V \cdot cos\lambda - V_{M83} \cdot cos(\theta + \lambda) \tag{7.4}$$

where $\tan\lambda = D_{M83} \cdot \sin\theta/[D - D_{M83} \cdot cos(\theta)]$ (Karachentsev et al. 2002). In Tab. 7.1 we display the results for the three objects.

The three dwarfs, as shown in Table 3, all present positive radial velocities relative to M83. Excluding HIDEEP J1337-33, the location of the other two dwarfs in the group seems more similar to those of the dIrr in the LG like WLM, SAGDIG or Gr 8, at about or less than 1 Mpc away from the more massive galaxies of the group.

Being in the outskirts of the group the lack of close massive galaxies or gas clouds may have prevented the triggering of frequent star formation events via collisions or tides in the discs of the most distant dwarfs from M 83 like 1337-39 and 1321-31. This could be advanced as an additional explanation for their "retarded" evolution so that they have been able to preserve most of their primordial gas content.

Because of its relative closeness of M 83, the case of HIDEEP J1337-33, which indeed has the lowest M_{HI}/L_B of the three (see Table 2.2), is slightly different.

Gas-rich dIrr galaxies are found in the LG, but the main difference from the HIPASS dwarfs is that they are not as gas-rich. Their M_{HI}/L_B ratios in fact are in general around or below 1. We may wonder

if one of the reasons why we do not find this type of dwarf galaxy in the LG is because of the differences between the two environments.

The LG includes 36 members (van den Bergh 2000b) and it appears to be constituted of 4 subgroups (Mateo 1998) of which the MilkyWay and Andromeda ones are the most prominent. The third group consists of an extended cloud of dIrr galaxies such as SAG DIG, WLM, DDO 210 and the dSph Tucana. The fourth is a rather small subgroup where NGC 3109 is the most luminous member and includes Sextans A, Sextans B and Antlia. According to van den Bergh their distance (1.72 Mpc) and velocity to the centroid of the LG (114 ± 12 km s^{-1}) suggest that these objects form a distinct grouping (van den Bergh 1999). There is only one galaxy GR 8 which cannot be clearly assigned to any of these subgroups (Mateo 1998).

Half of all the members are located within 450 kpc of the barycenter of the LG, with only three objects, Sag DIG, DDO 210, and Tucana, being more than 1 Mpc away (Courteau & van den Bergh 1999), showing that the (binary) core of the LG is relatively compact. According to Karachentsev (1996) the properties of the LG (such as the group radius, the velocity dispersion, the crossing time, the zero-velocity radius) are quite common in the nearby Universe and it is a quite ordinary representative of loose groups.

As we have pointed out in Chapter 2, Centaurus A is the richest environment among nearby groups (including about 50 objects) and shows a different structure compared to our local grouping of galaxies. Its main members span a wider morphological range including both early-type (the S0 peculiar galaxy Cen A) and late-type systems (e.g. the irregular NGC 5253). They appear distributed along an extended "loose chain" which, according to Côté et al. (1997) gives evidence of the fact that the group is not virialised.

The structure of Centaurus A has been analysed in detail by Karachentsev et al. (2002), although one has to keep in mind that distances and radial velocities have been obtained so far only for 1/3 of the members. Karachentsev and collaborators also come to the conclusion that the group seems not to be in virial equilibrium, and that it may be formed by two subgroups centred on Cen A and on M 83, where M 83 and its satellites, at an average distance of 940 ± 90 kpc from the Cen A subgroup (Karachentsev et al. 2002), are moving away from it at a velocity $v_{M83-CenA} \simeq 55$ km s^{-1}.

Côté et al. (1997) estimated the crossing time of the group as a whole and found a long timescale, 4.5 Gyr, which is a considerable fraction of the Hubble time. If one considers the two subgroups separately the characteristic crossing times become 3 Gyr and 2.3 Gyr for the Cen A and the M 83 group respectively (Karachentsev et al. 2002), assuming average velocity dispersions of 89 and 62 km s^{-1}and mean projected

separations of the companions of 263 and 142 kpc respectively. A similar calculation for the LG using a linear dimension of 140 kpc and a radial velocity dispersion of 68 $\mathrm{km\,s^{-1}}$(Karachentsev 1996) leads to a crossing time of 2 Gyr, which is very similar to M 83.

If a loose group is not yet in equilibrium, it is likely that interactions and/or mergers have been less frequent, therefore one would expect that the HI content of its members should be higher compared to a more compact group of galaxies.

Thus, to check if there are differences between the HI content of the LG and Centaurus A as a whole group[1], we compare the gas fractions of their smaller members, without including their primary galaxies. We have plotted in Fig. 7.3, the M_{HI}/L_B ratios of the catalogued galaxies which have been detected at 21-cm both in the LG and in Centaurus A. The HI sources in Centaurus A have been taken from Côté (1997), Banks (1999), and Karachentsev et al. (2002), and the updated fluxes have been extracted by the HIPASS brightest galaxy catalogue (Koribalski et al. 2004). The reddening corrected optical magnitudes have been taken from the Nasa Extragalactic Database (NED). The M_{HI}/L_B ratios for the dwarfs of the LG come from Mateo (1998).

As one can see in the Figure, 95% of the satellite of the LG have M_{HI}/L_B ratios below 1.5 in solar units, against $\sim$ 60% of the objects in Cen A. The remaining 40% has much higher M_{HI}/L_B ratios up to $\sim$ 6. Therefore this suggest that the Centaurs A groups is on average a more gas-rich environment than the LG.

7.6 Comparison with similar objects in the LG

As a final step of this analysis we think it is interesting to look for those objects in the LG which most resemble our HIPASS dwarfs and compare their general properties and SFHs. For most of the dwarfs in our neighborhood the stellar population has been studied in detail to derive information on their SFHs and evolution. Therefore such a comparison may give further hints on the understanding of our gas-rich dwarfs. Some of these objects have been already discussed in Chapters 4, 5 and 6.

[1] For those members for which distances are not known, it is not possible to distinguish whether they belong to the Cen A or M 83 subgroup. Therefore for this comparison we consider Centaurus A as a single group

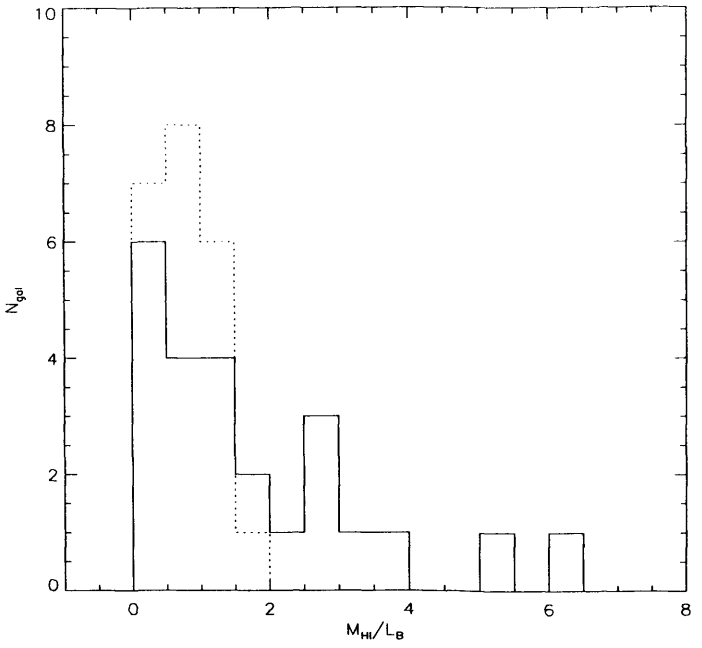

Figure 7.3: The comparison between the M_{HI}/L_B ratios of 24 galaxies in the Centaurus A group (solid line) and 22 galaxies in the LG (dotted line). As one can see the majority of the galaxies in the LG have gastostellarmass ratios less than 1.5, while the sample of the Centaurus A galaxies extend to higher M_{HI}/L_B ratios. The updated HI fluxes for the galaxies of Centaurus A have been derived from the HIPASS brightest galaxy catalogue (Koribalski et al. 2004), while the B magnitudes have been taken from the Nasa Extragalactic Database (NED). The values of M_{HI}/L_B for the LG galaxies come from Mateo (1998).

7.6.1 1337-39

SAG DIG is the galaxy of the LG that is most like 1337-39. It is considered the most remote object belonging to the LG, since it is located at a distance of 1.29 ± 0.09 Mpc from the LG barycenter (van den Bergh 2000b). From the red giant branch SAG DIG appears as the most metal poor dIrr of the LG ([Fe/H]= −2.1 ± 0.2). The youngest stars are located near the major peaks of emission in the HI distribution (which appears as a complete asymmetric ring with a central depression), whereas the red giants and intermediate-age AGB stars define an extended halo or disc with scale length comparable to the size of the hydrogen cloud.

	M_{HI}	M_{HI}/L_B	$SFR_{t>200\,Myr}$	12 + log(O/H)
	$10^7\ M_\odot$	$M_\odot/L_\odot$	$M_\odot\ yr^{-1}\ kpc^{-2}$	
1337-39	3.9	3.1	1×10^{-4}	7.35
SAGDIG	1.2	1.6	3×10^{-4}	7.23

Table 7.2: The observed properties of 1337-39 compared to those of Sag DIG (Saviane et al. 2001; Momany et al. 2002). The past SFR corresponds to the age interval 200 Myr - 15 Gyr for Sag DIG (Karachentsev et al. 1999), and 200 Myr - 10 Gyr for 1337-39. To calculate the normalized SFR of 1337-39 we have considered a characteristic radius of 700 pc.

The CMD of this galaxy has many features in common with that of 1337-39: the well populated blue plume tracing an increased recent SF activity between 30 and 100 Myr (Momany et al. 2002), the blue RGB typical of a low metallicity population and the evidence for AGB stars above the TRGB. The data available for SAG DIG are not deep enough to resolve the older stellar population.

Another interesting dIrr of the LG to compare with 1337-39 is WLM, located at 900 kpc from the Milky Way in an isolated region of the LG. There is strong evidence for an ancient population of stars in WLM. It is the only low mass dIrr system that contains a globular cluster, for which Hodge et al. (1999) determined an age of $\sim$ 15 Gyr. It is one of the few dIrrs of the LG for which it has been possible to detect HB stars. The SFH of this galaxy has been simulated by Dolphin (2000b) and shows a constant low star formation rate with an average value of $\sim$ 1 - 2 $\times 10^{-4}\ M_\odot\ yr^{-1}$ with periods of enhanced SF activity. The time of initial SF has been set at about 12 Gyr ago with a SF episode ($7 \times 10^{-4}\ M_\odot\ yr^{-1}$) which produced about half (by mass) of the total SF that WLM has had over its lifetime (Dolphin 2000b). After that event the SFR declined considerably even though the uncertainties in the simulations of the SFH between 2.5 and 9 Gyr are large. Within the past 1 Gyr the SF activity raised again and it is still ongoing, as shown by the presence of HII regions (Hodge & Miller 1995) WLM shows how isolated and fairly gas-rich dIrr galaxies ($M_{HI}/L_B = 1.2$) have experienced SF even at ancient epochs and contain an old population of stars.

	M_{HI}	M_{HI}/L_B	<SFR>	[Fe/H]
	$10^6\ M_\odot$	$M_\odot/L_\odot$	$M_\odot\ \mathrm{yr}^{-1}$	
1337-33	5	1.4	2×10^{-4}	$-1.7 \div -1.3$
LGS 3	0.34	0.33	4×10^{-5}	$-1.5 \div -1$

Table 7.3: The comparison between the properties of 1337-33 and LGS 3 taken from Miller et al. (2001). The SFR has been expressed in $M_\odot\ \mathrm{yr}^{-1}$ units for comparison with the values given by Miller et al. (2001). As regards the metallicity of 1337-33 we have indicated the range derived from the analysis of the CMD.

7.6.2 1337-33

As mentioned in Chapter 5, the general properties of 1337-33, such as the low luminosity, the spherical symmetry of the optical appearance, the absence of current SF activity despite the large gas reservoir, make this dwarf similar to the so called "transition objects" such as LGS 3, Pegasus, Antlia. All these galaxies have low luminosities ($M_B = -9.9$; -12.3; -10.2) and M_{HI}/L_B less than 1 in solar units (0.33; 0.44; 0.58). They are among the lowest mass objects ($M_\star \sim 10^6\ M_\odot$) which have been able to retain gas and to experience SF until a few hundred million years ago. Therefore they are extremely important to study because they show how the process of gas consumption and quiescence takes place in dIrr.

Pegasus appears to be at a projected distance of 400 kpc from M 31 but it does not seem to be bound to the spiral galaxy (Gallagher et al. 1998). With a gas-to-stellar-mass ratio $M_{HI}/L_B = 0.2$ it shows a current low SFR $\approx 3 \times 10^{-4}\ M_\odot\ \mathrm{yr}^{-1}$. If its evolution continues to proceed at this rate, it will take about 13 Gyr to exhaust all its gas. According to Gallagher et al. (1998) SF in Pegasus is temporarily "down", but that does not mean that it could not possibly reestablish a normal level of SFR in future. The prominent RGB and the extended AGB indicate that the SF at intermediate-age has been more intense than during its more recent history. Pegasus would have been brighter about 2 Gyr ago (Gallagher 1998). This galaxy may be taken as an example of galaxies that undergo occasional intense episodes of SF that last for 0.5 - 1 Gyr and then enter in a more quiescent phase lasting one to few Gyr (Cole et al. 1999).

	M_{HI}	M_{HI}/L_B	$SFR_{t>1\,Gyr}$	[Fe/H]
	$10^6\ M_\odot$	$M_\odot/L_\odot$	$M_\odot\ yr^{-1}\ kpc^{-2}$	
1321-31	3.7	5.1	1.6×10^{-4}	−2.1 (?)
DDO 210	0.2	1.9	1.5×10^{-4}	−1.86

Table 7.4: The comparison between the properties of DDO 210 (Lee et al. 1999) and 1321-31. The normalized SFR has been calculated for lookback times t > 1 Gyr to compare it to the value given by Lee et al. (1999). To calculate the normalized SFR we have assumed a 1 kpc radius for 1321-31. As for 1337-33, we have put an estimate of the metallicity of 1321-31 derived from the colour of the RGB (see Chapter 6).

LGS 3 is localised in the M 31 subgroup but it is not yet certain whether it is one of its satellites. With both a smooth gaseous and stellar distribution is probably the galaxy that most resembles 1337-33 in the LG. Its SFH appears to have not been characterised by strong bursty events. After an early event around 13 - 15 Gyr it has been followed by a uniform and low SFR (around $10^{-4}\ M_\odot\ yr^{-1}$). The SFH has been constant in the centre of the galaxy while it has been decreasing in the outer region, indicating that as the gas is consumed or probably stripped, SF concentrates toward the center of a system (Miller et al. 2001). The smooth chemical enrichment of the stellar population suggests that there have not been sufficiently violent bursts of SF to expel a large fraction of the metals outside the galaxy. Metals have enriched the ISM and then they have been reprocessed into stars.

7.6.3 1321-31

Finding a galaxy in the LG with properties similar to HIPASS J1321-31 is difficult.

The relative isolation and the recent drop in the SF activity make it similar to objects like DDO210, but again the large amount of HI (with its peculiar distribution) and the puzzling red plume put this object in a category on its own. DDO 210 seems to have experienced a similar SFH. Its current SFR is negligible, but it shows an enhancement of the SF in the last few hundred million years compared to the average value

for its entire lifetime (Lee et al. 1999). The normalized SFR of DDO 210 for $1 < t < 15$ Gyr is compared in Table 7.4 with the SFR of 1321-31 for $1 < t < 10$ Gyr. At more recent epochs DDO 210 continued to form stars for a longer time than 1321-31, since there is evidence of SF until 30 Myr ago (Lee et al. 1999).

The CMD of Phoenix shows features that may be interesting to compare with the red plume and the recent SF of 1321-31 (less than 1 Gyr). There is a faint blue plume of stars at an estimated age of 100 - 125 Myr (Martinez-Delgado 1999) and a few intermediate-mass stars in the reddest extent of their corehelium burning phase whose age has been estimated around 800 Myr (see Fig. 13 in MartinezDelgado 1999). These stars are not as many and as luminous as those in 1321-31, but this could be an example of the evolution of less than 1 Gyr old populations in a nearby system where star formation stopped a few hundreds of Myr ago.

As a counterexample, one may consider the Tucana dwarf (Saviane et al. 1996), which at a distance of approximately 900 kpc from the Galaxy is a quite isolated and low luminosity galaxy ($M_V \sim -9.5$). It shows a completely different scenario on how isolated galaxies can evolve compared to 1321-31. It reveals a predominantly old metalpoor stellar population with no signs of intermediate-age populations or recent star formation. Apart from an HI cloud discovered in its proximity (whose connection to Tucana is not clear), this isolated dSph seems to be gas-deficient despite its large distance from the main members of the Local Group.

7.7 What can these galaxies tell about dwarf galaxy evolution?

Nearby dwarf galaxies are one of the best environments in which to study in detail how stellar evolution proceeds. Accurate analysis of their resolved stellar photometry (when feasible) and of their gas content (if present) is essential for a better understanding of the internal processes that influence the SF evolution of a galaxy, such as the metal abundance and the density of the ISM, or external effects, such tidal interaction or merging.

Dwarf galaxies in the LG all show varied and very complex SFHs. Dwarfs are all unique objects: it is difficult to find a common pattern in their evolution. It appears that SF has occurred either continuously over long period of time or in fewer objects such as Carina or Sculptor, in distinct episodes (Grebel 1997). All LG galaxies for which sufficiently deep photometry was available do seem to contain at least an intermediate-age population of stars, and for the majority of them old populations of stars have been uncovered. Therefore

SF started in the LG at an epoch comparable to the Hubble time.

But what do we know about other groups? Do dwarf galaxies outside the LG behave in the same way? Have they formed at the same time as in the LG? In order to get a complete overview of the evolution of dwarfs we need to extend the same analysis to nearby environments.

This was one of the aims of this study even though the observational limits are challenging. Study of dwarf galaxies outside the LG have been already carried out, but they have been mostly restricted to BCDs (SchulteLadbeck et al. 1999; 2001; Tosi et al. 2001; Cannon et al. 2003). Instead the HIPASS dwarfs with their gas large fractions, their low Sbs and faint luminosities, give an insight on a different evolutionary behaviour, where galaxies can evolve in a smooth and more quiescent way.

We do seem to find an intermediate-age population, showing that the timing of SF occurred several Gyr ago. However we need further analysis and deeper data to verify that the SF activity started in these galaxies at the same time as in the LG dwarfs.

The idea that very small galaxies should experience a single primary and possibly cataclysmic episode of SF during their lifetimes does not appear to occur in the HIPASS dwarfs we have studied, in analogy with what is found in the LG. We have pointed out that according to recent simulations (MCF99; Ferrara & Tolstoy 2000), their ISMs seem to be stable to SF events even if they happen to be fairly strong as we have found in 1321-31. The HIPASS dwarfs show that low mass galaxies can retain their ISM even if they have experienced SF activity for several Gyr. We have also shown that if their evolution were to proceed at the same average rate that they have experienced so far, it will take at least another Hubble time to consume all their gas.

Therefore it seems highly unlikely that these objects will become dSphs. Their evolutionary rate is too slow and their positions within the group too isolated to reach the SFR necessary to burn all the hydrogen. With a hydrogen mass of about 10^7 $M_\odot$, they would need to reach a SFR of 10^{-2} $M_\odot$ yr^{-1} and to maintain it for 1 Gyr in order to consume their gaseous fuel. This seems highly unlikely given their SFHs. It is likely that the low gaseous density, and the inefficiency of the cooling mechanism due to the low metallicity would prevent the possibility of a long SF period at a high rate. Shorter episodes of SF activity would require higher rates of 10^{-1} $M_\odot$ yr^{-1} for 100 Myr.

Is it possible for these galaxies to turn into BCDs? One of the key question of dwarf galaxy evolution is whether there is a link between starbursting systems and quiescent gas-rich galaxies. Do all gas-rich low mass

galaxies go through a starburst phase during their evolution? Are BCDs and quiescent gas-rich galaxies the same objects viewed at different stages of their evolution? The starburst phase is expected to be a transitory event, lasting only a few hundred million years. Gas-rich galaxies in principle have large reservoir of gas to ignite an intense SF activity. If there is a link between these two type of galaxies, is it plausible that dIrrs represent the quiescent phase of more active starburst galaxies? According to van Zee the majority of dIrr do not go through a starburst phase, and BCDs do not represent a common phase in the evolution of gas-rich dIrr. This is mainly due to different intrinsic properties between gas-rich dIrrs and BCDs (van Zee 2001b). BCDs have steeper rotation curves and lower angular momenta, which cause a centrally concentrated, high density gas distribution favouring the triggering of a starburst. From the simulation of the SFH we have found only in HIPASS J1321-31 a significant increase in its past SFR (between six an ten times the SFR experienced from 1 to 10 Gyr, taking into account the uncertainties on the SFR values) which could give hints of a starburst phase. It is difficult to say whether 1321-31 had experienced a BCD phase or not. The enhancement in the SF is probably not strong enough to argue that 1321-31 went through such a stage. Therefore it seems unlikely that the HIPASS dwarfs have experienced a BCD phase in their past, suggesting that factors other than richness in gas have to play role in the triggering of a BCD phase in dwarf galaxies.

We are still left with the intriguing issue of what prevents the conversion of the gas content of a galaxy into stars. We have suggested some possible mechanisms that may be responsible for the observed "slow" evolution of the HIPASS dwarfs. Understanding the characteristics of the ISM and the conditions of the local environment may be crucial in order to infer why SF is inefficient in our dwarfs. Our analysis of the resolved stellar populations and the gaseous distributions goes in this direction and allows us to examine the correlation between neutral gas and star forming regions, and to estimate the timescale of the main evolutionary episodes of the history of these galaxies, as well as their location within the group. However a complete understanding of what prevents stars from forming in these environments has not been reached yet, and the "big issue" at the very beginning of this thesis *The big question in star formation is not how to form stars, but how to prevent stars from forming* (MordecaiMark Mac Low) still needs a definite answer.

7.8 Future work

Our analysis has left some open issues that we can investigate in more detail in the near future.

The high M_{HI}/L_B ratios of these galaxies may be explained if they have recently accreted gas, but

the resolution of our 21-cm maps is not sufficient to distinguish substructures and irregularities in the HI distribution. Therefore higher resolution 21-cm maps would be needed in order to look for infall and to investigate in more detail the dynamics of the ISM.

WFPC2 snapshots (600 s) of the remaining two dwarfs discovered in the HIPASS survey (HIPASS J134837 and HIPASS J135147) are available, being observed as part of the SNAP survey. In the literature we have not found yet their CMD published. Therefore one of our next task is to get these images and build the corresponding diagrams to have a look at the common properties and/or differences between these gas-rich dwarf galaxies.

Our analysis of the age of the stellar population could not be extended to look-back times older than 10 Gyr due to the limits of our photometry. A definite proof that these galaxies contain a truly old population would be given by the detection of the HB stars and would definitely confirm that SF in such systems began at the same time as in our LG dwarfs. Such a study is not possible with the telescopes available to date. We may argue that with the launch of the James Webb Space Telescope (JWST), whose size will be three times larger than the HST, observations with similar exposure times to our HST run ($\sim$ 5000 s) would allow to lower the photometric limit of possibly two more magnitudes, from $I = 26$ mag to $I = 28$. This would enable to reach just the magnitude at which the HB branch is expected ($M_I \sim 0$ or $I \sim 28$ at the distance of 4.5 Mpc). However to firmly establish the presence of such stars one should be able to reach a photometric limit that should be 1 - 2 magnitudes lower.

The next stage of this analysis is to extend the study of the stellar populations and SFH of gas-rich galaxies to a much larger and more varied sample. The HIPASS catalogue has been now published counting many previously uncatalogued gas-rich objects. Among these new detections we think that an interesting subset are the gas-rich giant galaxies which have HI masses greater than 10^{10} $M_\odot$ and M_{HI}/L_B ratios greater than 1 - none of which have been studied before.

We have already selected and followed-up some of them in the optical and near IR to investigate their stellar populations. In the Appendix we describe the initial analysis of seven of such objects, extracted from a subset of the HIPASS survey, the South Celestial Cap (Kilborn et al. 2002). This is a project that is still ongoing.

7.9 Final conclusion

The development of multi-beam 21-cm receivers has finally allowed us to detect large numbers of galaxies in *blind* HI surveys, and thus to find new classes of objects whose evolution from gas into stars has been retarded for one reason or another. This analysis of extreme gas-rich dwarfs in a nearby group is but the beginning of a number of such studies which, in the long run, will hopefully tell us how galaxies of many different masses and kinds evolve by turning their gas into stars - surely one of the key processes in astrophysics.

Appendix A

Observations of HI giant galaxies

A.1 Introduction

Our studies of galaxies with high M_{HI}/L_B ratios have been focused entirely on gas-rich low surface brightness dwarf galaxies as we discussed in the previous chapters. Some of the galaxies with the highest M_{HI}/L_B ratios detected are in fact dwarf galaxies. Several examples are included in the sample of van Zee (1997a, 1997b, 1997c, 2001a) and, more recently, one of the highest gasmasstostellar ratios for a galaxy has been measured for the nearby LSB dwarf ESO215-G?009 (Warren et al. 2004) with $M_{HI}/L_B = 22 \pm 4\ M_\odot\ /L_\odot$. These systems appear to be fairly numerous: in the HIPASS Bright Galaxy Catalogue (BCG) for example (Koribalski 2004), which includes the 1000 sources with highest HI peak density, among the 150 low luminosity ($M_{B,0} > -16.5$) dwarf galaxies found, about 1/3 have $M_{HI}/L_B > 3$, although the optical data on which their ratios are based is not reliable. Gas-rich galaxies seem to be more often found among low surface brightness, low luminosity dwarf systems. On the other hand HI massive systems with high M_{HI}/L_B ratios do turn up in the HIPASS survey and need to be studied.

There are not many studies on such systems in the literature. For example among HI massive galaxies one can find objects such as the giant LSB galaxies. The most typical example of such systems is Malin 1 (Bothun et al. 1997). However, even if it has a large HI mass ($4 \times 10^{10}\ M_\odot$), this galaxy is not particularly gas-rich ($M_{HI}/L_B = 0.17$) as shown by recent HI measurements (Matthews et al. 2001). After the discovery of Malin 1 (Bothun et al. 1987), a handful of LSB giants have been revealed in catalogues such as the UGC,

NGC and ESO (Impey & Bothun 1989; Pickering et al. 1997; Schombert 1998), although LSB giants remain relatively rare (Minchin et al. 2003).

The HI content of a sample of thirteen LSB giants has been recently investigated by Matthews et al. (2001). Their study confirms the idea these galaxies have in general large HI masses (M_{HI} ranges between 2.5 $\times 10^9$ $M_\odot$ and 7.1 $\times 10^{10}$ $M_\odot$), but only five objects have $M_{HI}/L_B > 1$.

However, apart from the HI study by Matthews et al. (2001), similar analysis of HI massive galaxies are lacking, and the few studies performed consist of 21-cm followups of galaxies originally detected in the optical band.

To extend the analysis of the properties of gas-rich systems, we have selected a sample of HI massive galaxies which have been extracted from an HI catalogue and we discuss their properties.

The objects have been taken from a region of the HIPASS survey which has been comprehensively catalogued for galaxies, the South Celestial Cap (SCC) region (Kilborn et al. 2002). It covers all Right Ascension, and Declination $< -62°$. 536 galaxies have been found in the region, and we concentrated on those with the highest HI masses. Twentyseven galaxies have an HI mass greater than 2×10^{10} $M_\odot$, i.e. around ten times that of the Milky Way. Most of them were observed in high resolution at the Australia Telescope Compact Array in 2001 (Kilborn et al. 2002) to confirm their optical counterparts. We have selected fourteen galaxies for which the ATCA data were already available, while there are still a few more galaxies awaiting such observations. The optical observations of these galaxies were performed with the ESO telescopes in La Silla and they were divided into two observing runs because of the different position in the sky of the objects. In this final part of the thesis we concentrate on the first set of observations, which includes seven objects. The remaining galaxies will be discussed as part of another PhD thesis (Garcia 2004).

The HI detections correspond to an optical counterpart in every case. The optical morphologies are varied, in fact we find not only low surface brightness, but also very bright spiral galaxies. This is the most striking difference compared to low mass HI rich galaxies which in general appear as LSB systems. The M_{HI}/L_B ratios range between 1 and 4 in solar units (see Table A.1).

To fully determine the nature of these HI giants, we need information on their stellar populations, star formation histories and metallicities. With this aim we have obtained optical BVI imaging with the WFI at the 2.2 m telescope and we have J band data for three of the seven objects to complete the study of their stellar population. Near IR imaging is a better tracer of the underlying stellar structure than the optical as

the effects of extinction (which are particularly worrying in gas-rich giants) are largely reduced, and near IR bands are also good tracers of the older stellar populations. By investigating the old stellar population we can set constraints on the evolution of this peculiar class of galaxies. Near IR colours can also give hints on the metallicity of a galaxy (Galaz et al. 2002). These bands are also extremely important for our study, because the sample of galaxies chosen is at low Galactic latitude.

A.2 Observations and data reduction

The seven targets were observed in the optical BVI bands at the ESO/MPI 2.2m telescope in La Silla during two nights in July 2003 (period 71). The near IR observing run was scheduled at the NTT telescope in the same period, and it was planned to obtain both J and K photometry for the same galaxies. Unfortunately all the time was lost due to bad weather conditions. We applied for extra time with a DDT proposal and we could observe only three of them in the J band in October 2003. Therefore we do not have the complete data set that we had originally foreseen.

21-cm high resolution followup with the ATCA telescope have been provided by Virginia Kilborn (*private communication*). In the following sections we also show the 21-cm maps obtained by the combination of the Parkes and ATCA data. The main properties of these galaxies are summarised in Table A.1.

A.2.1 Optical photometry

Optical BVI observations consisted in sets of 600 s (B and I bands), and 500 s (V) exposures, reaching a total exposure time in the three bands of 40, 25 and 30 minutes respectively. We adopted a 2 $\times$ 2 binning to reach a fainter isophotal magnitude in the three bands. Data reduction was performed with the CCDPACK Starlink Software. The Wide Field Instrument at the 2.2 m telescope is a mosaic of 8 CCDs with a total field of view of $34' \times 33'$(each chip corresponds roughly $8' \times 16'$) and a pixel size of 0.238 pixel/arcsec. We placed our targets in the chip called 51. After bias subtraction and flat field correction the individual exposures were registered and combined. Photometric calibration has been achieved with standard stars from Landolt (1992) which were frequently imaged during the run. Foreground stars have been removed by replacing them with the surrounding sky. After sky subtraction, we performed the surface photometric analysis with the task ELLIPSE in IRAF.

A.2.2 The near IR photometry

J band observations were carried out at the NTT telescope using the SOFI instrument in October 2003 as part of the DDT programme. To obtain a SB limit comparable to the optical one, we have chosen an observation time of 1 h. Each image is the combination of several short exposures with a typical integration time of 60 s each. Between each readout the telescope was offset to a new position avoiding redundancy in the shifts between object and sky. Given the limited size of the field of view of the telescope (5.5 arcmin) compared to the extension of the objects, it was necessary to obtain separate sky exposure to remove the sky background.

Flat fields were obtained with a standard calibration procedure provided by the ESO staff (Vanzi 2002). Again the data reduction and analysis was carried out with both IRAF and CCDPACK. After flatfield correction we subtracted from each target frame the adjacent sky frame, given the high variability of the sky in the near IR.

We used the IRAF ellipse fitting task to fit radial profiles to the SB distribution in all images.

A.3 The sample: comparison of HI , optical and near IR data sets

We will now briefly discuss the properties of these galaxy and present the results from the surface photometry. The main characteristic coming out from this data set is that these are disc galaxies with different morphologies and surface brightnesses.

IC 4745

IC 4745 is an edgeon spiral classified as an Sab peculiar with a bright bulge and an extended dusty disc, characterised by dust absorption lanes (Fig. A.1). The disc is warped as it appears from both the HI distribution and the optical (top panel). At both edges the disc extends at very low SB reaching $\mu_B \sim 26$ mag arcsec^{-2} as one can see from the SB profile (centerright panel). There is a central depression in the distribution of neutral gas as expected in galaxies with big bright bulges, and the peak of the gas density is found in the southern edge of the disc. In the J band the bulge is bright and clearly detected (bottomleft panel), while the disc appears less extended than in the B band (centerleft panel). This pattern is very common in disc

galaxies and it is a clear indication of an older population of stars located in the centre of the galaxy.

IC 4745 has a radial velocity of $v = 4708$ km s^{-1}. The closest catalogued galaxy to IC 4745 is ESO 103-G049, at a heliocentric velocity $v = 4832$ km s^{-1}and at an angular separation of 9.8′which does not appear in the B image in Fig. A.1. However it is interesting to note that at a closer projected distance one can see from the B image (centerleft panel) two compact objects: a very diffuse, LSB one to the east of the galaxy and a brighter one in the bottom right corner of the image. Both may be possible satellites of the galaxy.

IC 4831

IC 4831 is a large spiral showing both a bright bulge and an extended disc with evidence of SF regions (Fig. A.2). It is classified as a SBb. Its radial velocity is $v = 4348$ km s^{-1}. The HI disc presents a density depression at the centre of the galaxy, while the highest density peaks occur in both edges of the disc (top panel). The nearest galaxy from NED is at 7.5′and is IC 4833, with a radial velocity $v = 3582$ km s^{-1}. This galaxy is not included in the B image we are showing in the center-left panel of Fig. A.2, however there is a possible low mass companion at about 2′, which may be linked to IC 4831. This object does not seem to have been identified in NED.

ESO 075-G006

ESO 075-G006 is a face-on barred spiral with an extended spiral structure which forms a double system (Fig. A.3). Its companion, AM 2119-695 (see center-left panel) is at a radial distance of about 1′. ESO 075-G006 has a radial velocity of 10605 km s^{-1}and it is the farthest galaxy in the sample. It is also the object with the highest HI mass detected with the Parkes telescope and M_{HI}/L_B ratio (see Table A.1). From the HI map it seems as if the gas forms a continuous distribution which embeds both objects (top panel). This may explain the high gas mass value measured. The morphology of the gas around ESO 075-G006 appears disturbed, probably as the consequence of tidal interactions with its companion. The distribution is offset from the center and the peak is found in the disc, at about 1′from the central bulge. As regards the optical/NIR images the central bulge and a bar are clearly detected as one can see also from both the B (center-left) and the J (bottom-left) exposures. The galaxy is classified as a SBb. There is a nearby bright star which affects the results of the photometry, especially in the I band.

ID	v (km s^{-1})	$\log M_{HI}$	M_{HI}/L_B	m_B^0	m_V^0	m_J^0	A_B	Type
IC 4745	4708	10.46	1.8	13.9	13.0	10.6	0.3	Sab
IC 4831	4348	10.44	1.2	13.3	12.5	10.1	0.2	SBb
ESO 075-G006	10605	10.90	4.2	15.6	14.6	12.1	0.2	SBa
ESO 099-G005	3258	10.31	0.8	12.6	11.8	-	1.2	SBab
ESO 100-G008	7777	10.38	0.7	14.2	14.4	-	0.8	Sb
ESO 136-G012	4381	10.40	1.2	13.4	13.2	-	1.2	SBc
IC 4696	4679	10.36	0.8	13.3	12.6	-	0.4	SBbc

Table A.1: Observed properties of the sample of HI massive giants selected from the SCC catalogue (Kilborn et al. 2002). The J band magnitudes are displayed for only three objects. The HI masses are taken from Kilborn et al. (2002), thus they correspond to the value measured with the Parkes telescope.

ESO 099-G005

ESO 099-G005 has a peculiar morphology both as regards the HI content and the optical appearance (Fig. A.4). The gaseous distribution, which extends for about 5′(∼ 5 times the optical radius) is highly irregular showing several lumps around the optical counterpart and a density depression in the centre (top). The optical image shows a bright bulge, with an extended LSB ring-shaped disc (bottom-left panel). The object has a low galactic latitude (∼ −6°) therefore it is in a region where the contamination by foreground Galactic stars is high. The galaxy is classified as a barred spiral, SBab. The galaxy seems to be fairly isolated. It has a heliocentric velocity $v = 3258$ km s^{-1}. We have not found any nearby obvious companions, but there is 1.2 magnitudes of foreground absorption. WK 4943 is at about 7.3′, but there is no velocity measurement for this galaxy.

ESO100-G008

ESO 100-G008 is a spiral galaxy in a double system with a smaller spiral and appears to be currently interacting with its companion (Fig. A.5). ESO 100-G008 has a radial velocity of 7777 km s^{-1}, and on NED the only identified galaxy with a velocity compatible with that is IRA 155866358 ($v = 7964$ km s^{-1}). The gaseous distribution detected with ATCA extends to the companion object, but it does not show a particularly disturbed morphology (top). In the optical the galaxy shows a small bulge and a more extended disc with tidal structures and HII regions both in the leading and in the trailing tails giving evidence of the interaction with the companion (bottom-left). The field is highly contaminated by Galactic Plane foreground stars. ESO 100-G008 is classified as a Sb galaxy.

A.3.1 ESO 136-G012

ESO 136-G012 is classified as an SBc type and it is at low galactic latitudes in a region of high foreground stellar contamination (Fig. A.6). It shows a very compact bulge and an extended LSB disc, hardly visible in the B exposure with two large spiral arms extending much farther out than the central region (bottom left panel). At the edge of the arm, at about 1.5′in the south east direction, there is a compact LSB object which is possibly interacting with the galaxy. This object has been identified as WKK 5727 and has a radial velocity of 4424 km s -1 compatible with that of ESO 136-G012 (4381 km s^{-1}). Its position roughly coincide with one of the two peaks in the HI distribution (top panel). The other is offset from the optical center of

the galaxy and is located towards the edge of the other arm.

IC 4696

IC 4696 is a spiral with a weak bar (SBbc) showing sparse HII regions mostly concentrated in the inner part of the disc (bottom-left panel of Fig. A.7). The HI disc extends for about three times the optical radius and shows a higher density region in the north-eastern side of the disc (top panel). There do not seem to be nearby companions to this system. The closer galaxy on the chip is 2MASX J18211488-6442028 at 6.4′, but there are no radial velocity measurements for this object.

A.4 Colour-Colour diagrams of the massive gas-rich galaxies

To investigate the past star formation history we intend to use colourcolour diagrams, whose comparison with a grid of stellar population models (Fioc & Rocca-Volmerange 1997) provides an estimate of the age of the dominant population, once a star formation scenario is assumed. We have generated a grid where the metallicity ranges from Z = 0.0004 (1/50 solar) to Z = 0.5 (2.5 solar). The SFH is parameterised by using an exponential decreasing SFH with timescale τ ranging from 1 Gyr to 32 Gyr (see Fig. A.8). We show the $B-V$, $J-V$ diagram for IC 4745, IC 4831, and ESO 075-G006.

From this preliminary diagram one can see that the galaxies have experienced different star formation histories. IC 4745, and IC 4831 have a solarlike metallicity, and a short timescale τ, which implies that their star formation activity was higher in the past. ESO 075-G006 is almost at the border of the grid, and also shows a SFH similar to the other two galaxies, with a slightly higher metallicity and even shorter SF timescale.

A.5 Summary

To summarise, our preliminary results:

- The near IR and optical images show both early and late type spirals whose morphology clearly shows a central bulge and a disc component. The presence of a bulge suggests that the galaxies have a

significant population of old stars which is centrally concentrated. Five out of seven galaxies show a barred morphology.

- The HI distribution is varied among the galaxies. The peak in the gas density is in general offset from the optical centre, especially if there is a bright bulge at the centre of the galaxy.
- Four out of seven objects appear as isolated systems. It is possible that for the others the gas-masses have been overestimated due to the inclusion of the companion in the large beamsize of the Parkes telescope. This would explain the high M_{HI}/L_B ratios for some but not all of them.
- Comparing optical and near IR colours with synthetic models of stellar evolution, we can derive a first constraint on the metallicity of the objects and an indication of their SFH.

A second list of galaxies with similar properties has been observed during period 73 at the ESO telescope in the same optical and near IR bands. We still have to finish the data reduction. When these data are available we will have a larger sample to compare and more information to derive the stellar populations and SFHs of the HI massive galaxies uncovered in HIPASS. For the moment we can say no more.

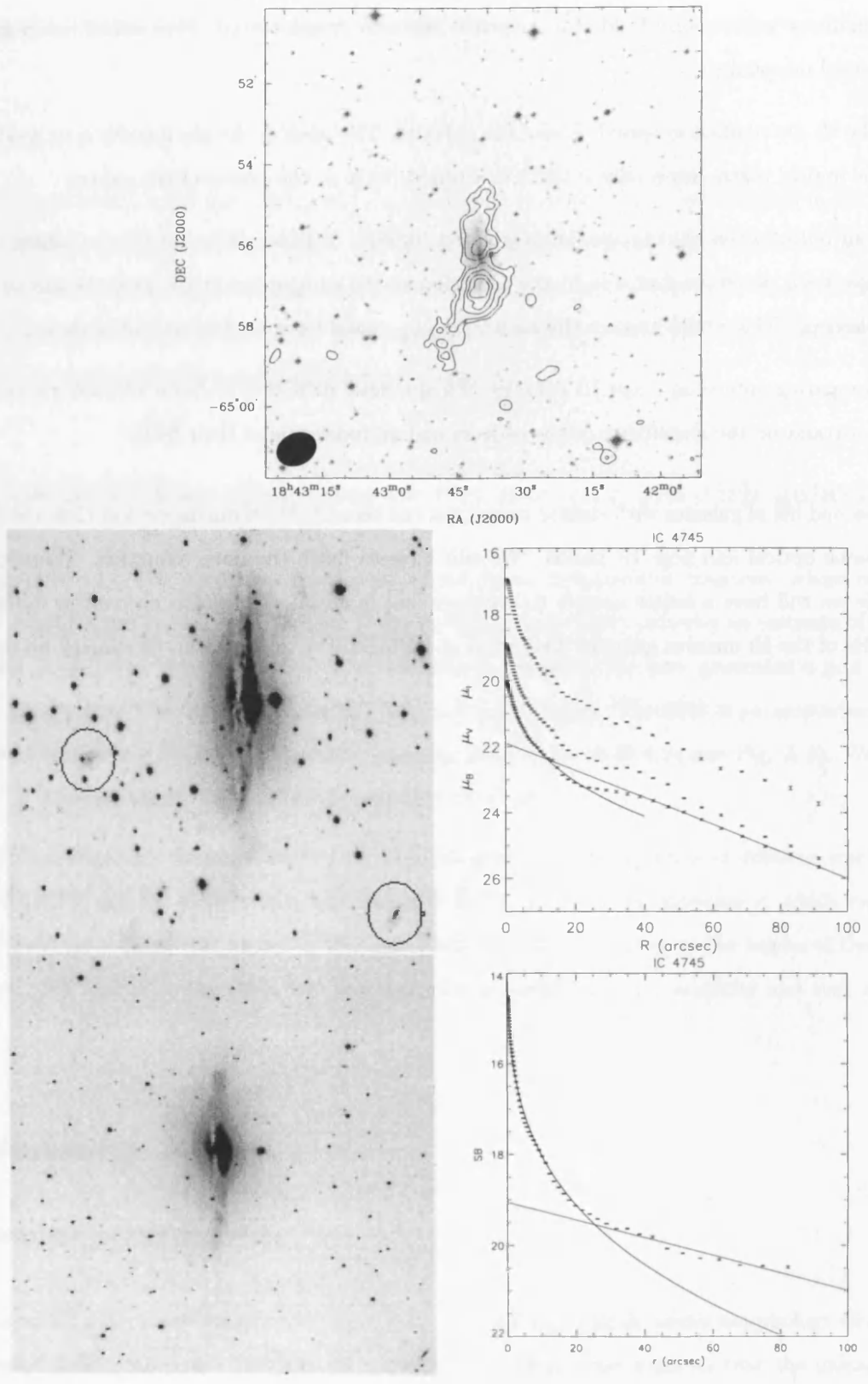

Figure A.1: IC 4745. *Top*: The 21-cm map obtained from the combination of the Parkes and ATCA observation. The HI contours are at 0.2, 0.3, 0.5, 0.7, 0.9 Jy beam^{-1} km s^{-1}. *Center – left*: B band image. The circles indicate two uncatalogued galaxies which may be possible satellites of the galaxy. *Center – right*: The B, V, I surface brightness profiles. *Bottom – left*: J band image and the J surface brightness profile (*Bottom – right*).

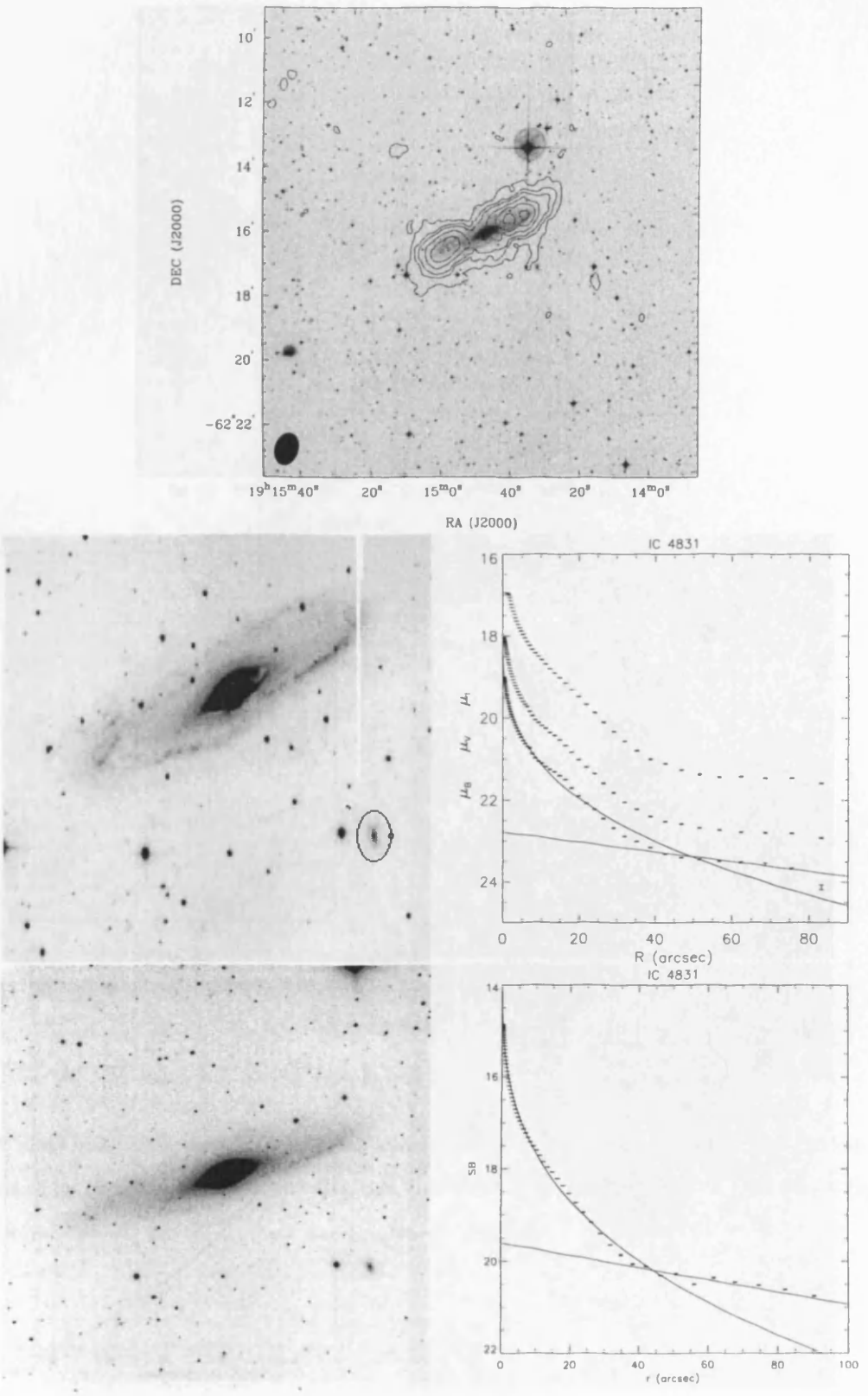

Figure A.2: IC 4831. *Top*: The 21-cm map obtained from the combination of the Parkes and ATCA observations. The HI contours are at 0.3, 0.7, 1.0, 1.5, 2.0, 2.5 Jy beam^{-1} km s^{-1}. *Centerleft*: B band image. The circle indicates an uncatalogued galaxy which may be a possible satellite of IC 4831. *Center – right*: The B, V, I surface brightness profiles. *Bottom – left*: J band image and the J surface brightness profile (*Bottom – right*).

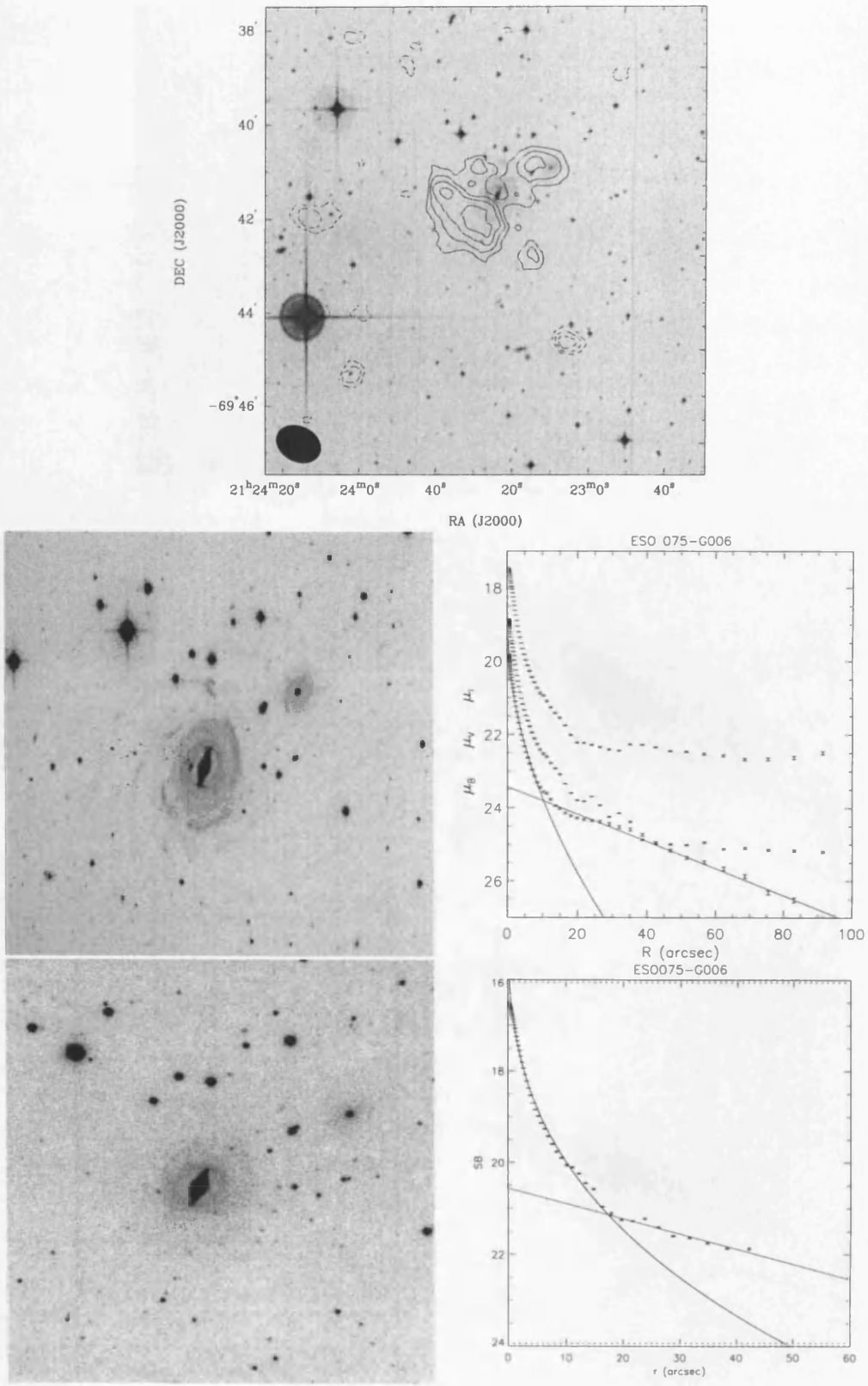

Figure A.3: ESO 075-G006. *Top*: The 21-cm map obtained from the combination of the Parkes and ATCA observations. The HI contours are at 0.2, 0.3, 0.4, 0.5, 0.6 Jy beam^{-1} km s^{-1}. *Center – left*: B band image. *Center – right*: the B, V, I surface brightness profiles. *Bottom – left*: J band image and the J surface brightness profile (*Bottom – right*).

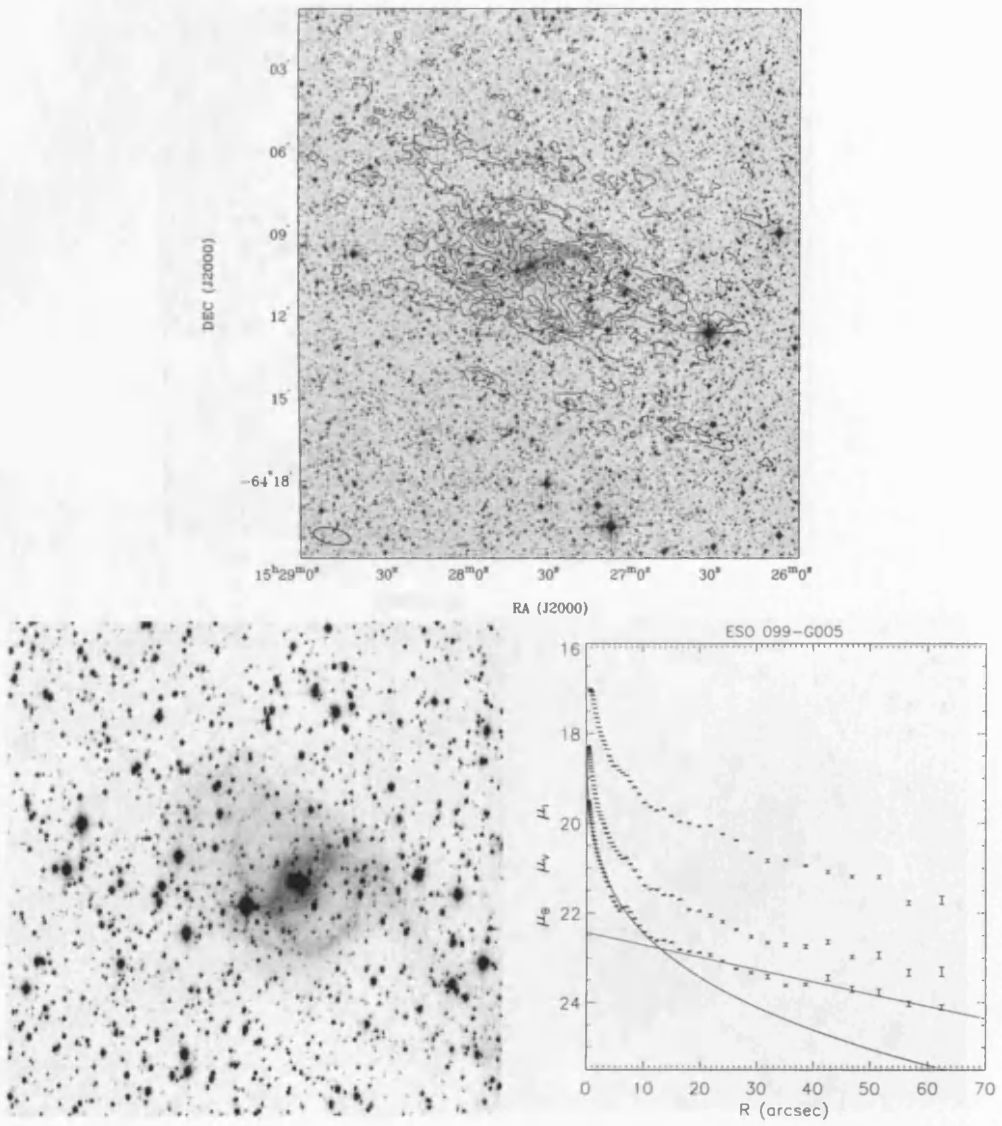

Figure A.4: ESO 099-G005. *Top*: The 21-cm map obtained from the combination of the Parkes and ATCA observations. The HI contours are at 0.2, 0.4, 0.6, 0.8, 1.0, 1.2 Jy beam^{-1} km s^{-1}. *Bottom – left*: B band image. *Bottom – right*: the B, V, I surface brightness profiles.

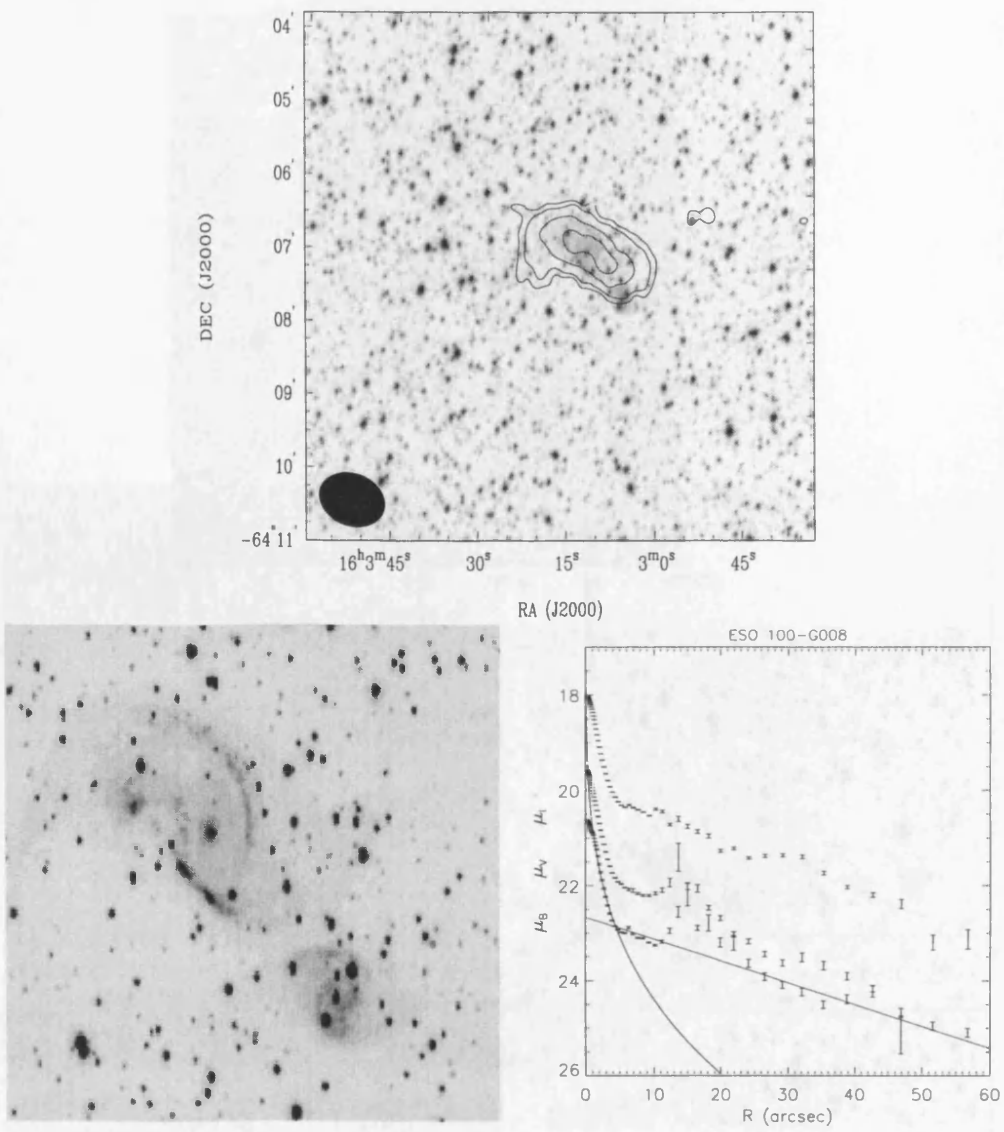

Figure A.5: ESO 100-G008. *Top*: The 21-cm map obtained from the combination of the Parkes and ATCA observations. The HI contours are at 0.3, 0.5, 1, 1.5, 2.0 Jy beam^{-1} km s^{-1}. *Bottom – left*: B band image. *Bottom – right*: the B, V, I surface brightness profiles.

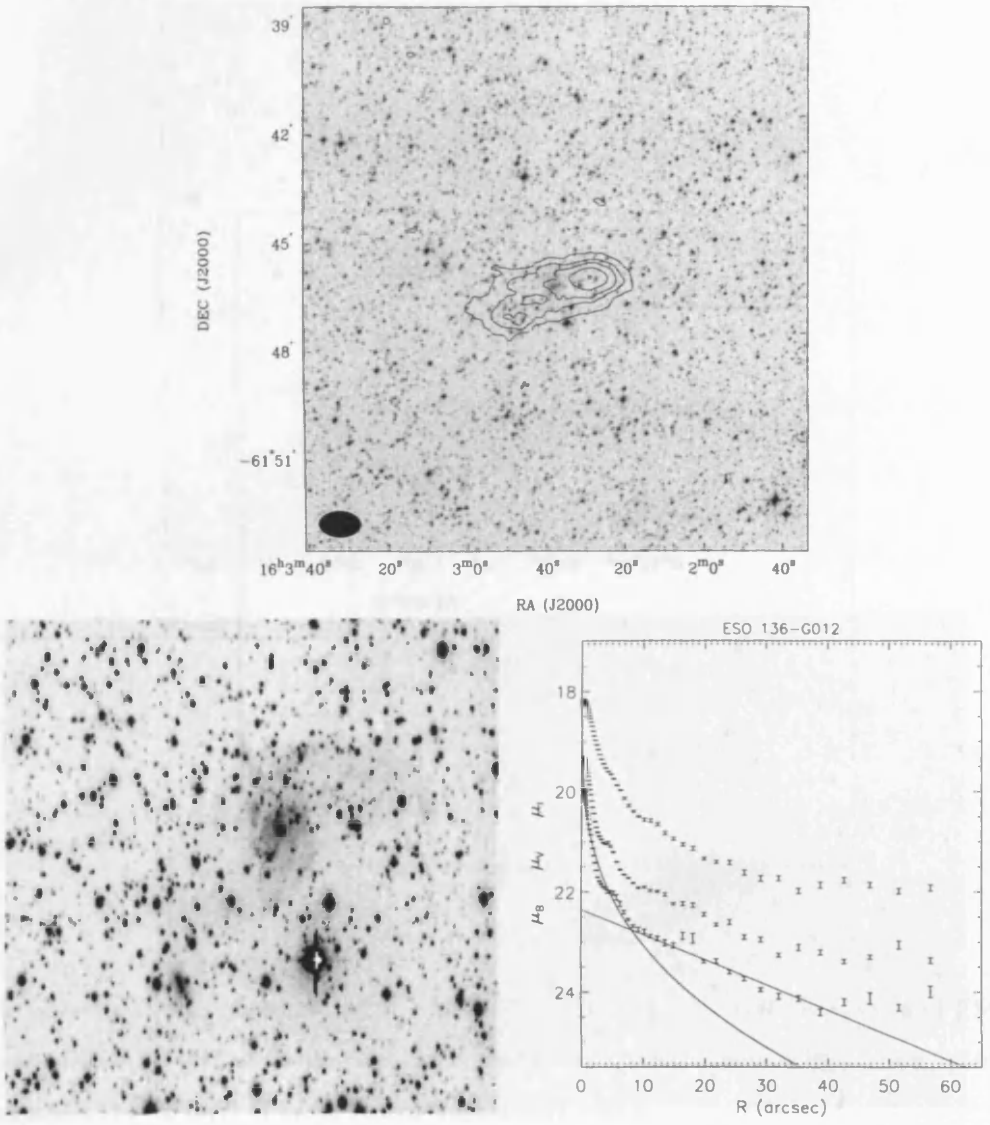

Figure A.6: ESO 136-G012. *Top*: The 21-cm map obtained from the combination of the Parkes and ATCA observations. The HI contours are at 0.3, 0.7, 1, 1.5, 2.0 Jy beam^{-1} km s^{-1}. *Bottom – left*: B band image. *Bottom – right*: the B, V, I surface brightness profiles.

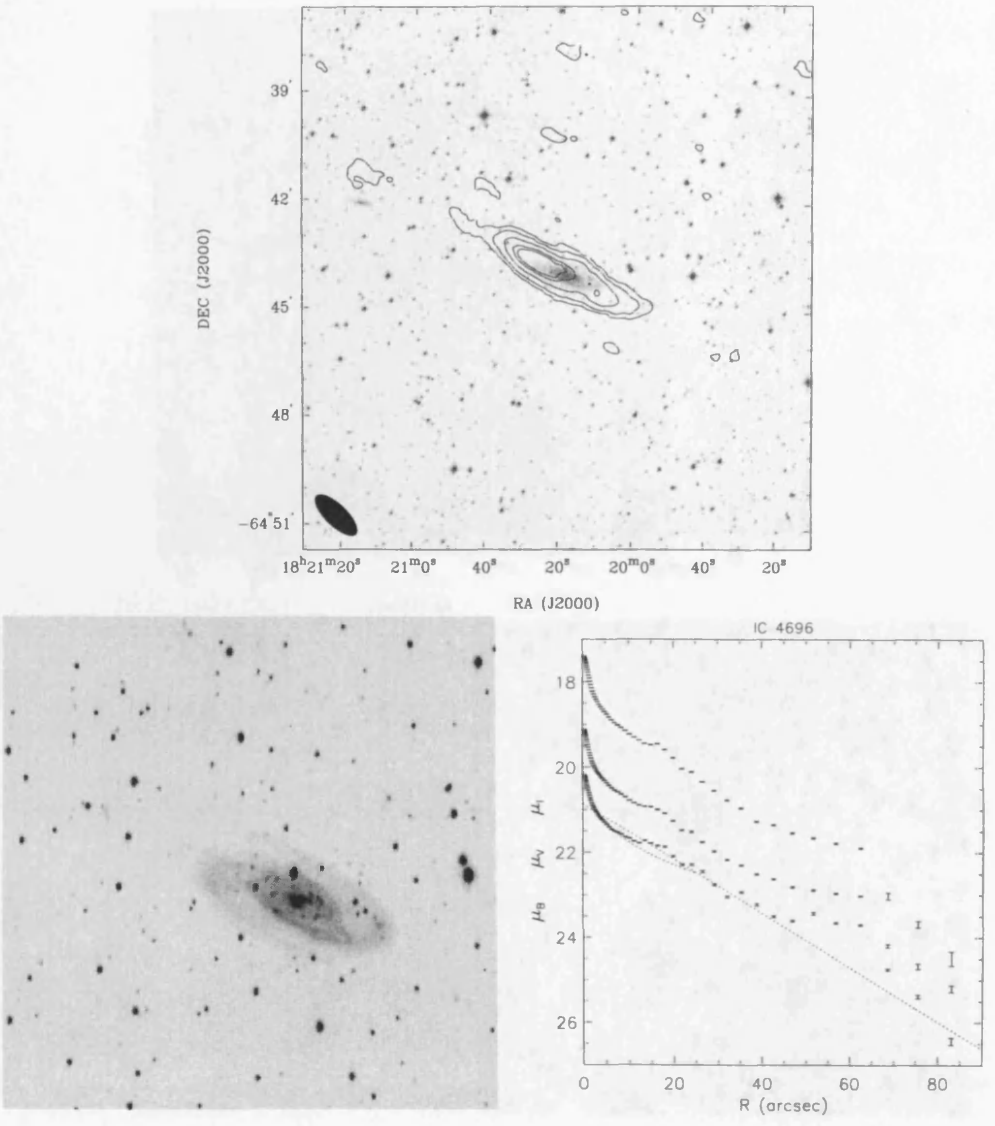

Figure A.7: IC 4696. *Top*: the 21cm map obtained from the combination of the Parkes and ATCA observations. The HI contours are at 0.5, 1, 1.5, 2, 3, 3.5 Jy beam^{-1} km s^{-1}. *Bottomleft*: B band image. *Bottom – right*: the B, V, I surface brightness profiles.

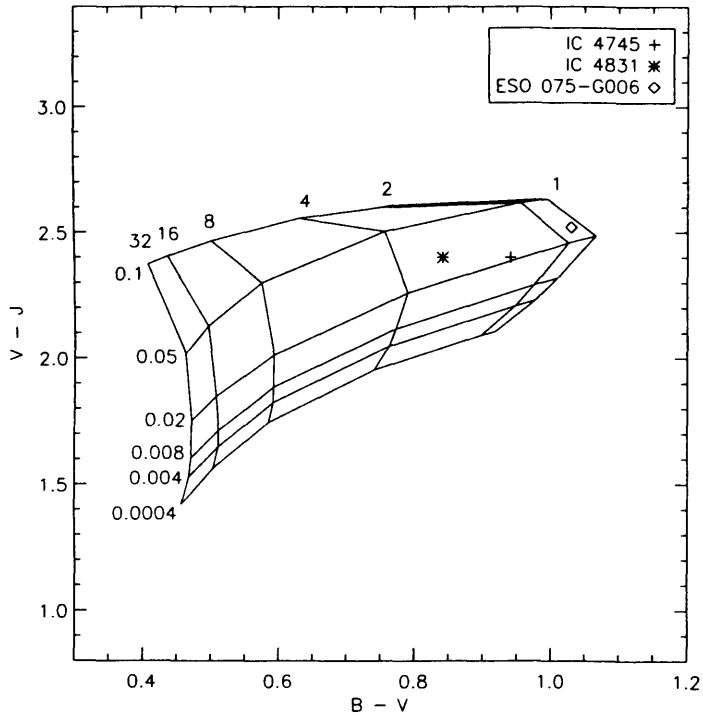

Figure A.8: Galactic extinction corrected $B - V$, $V - J$ colours for IC 4745, IC 4831 and ESO 075-G006, overlaid on the PEGASE grid of stellar population models for different metallicities (from 1/50 to 2.5 solar) and SF timescales (1 - 32 Gyr) (Fioc & Rocca-Volmerange 1997).

Bibliography

[1] Aaronson, M., Mould, J., 1980, ApJ, 240, 804

[2] Aaronson, M., Mould, J., 1985, ApJ, 290, 191

[3] Abadi, M.G., Moore, B., Bower, R.G., 1999, MNRAS, 308, 947

[4] Abraham, R.G., Merrfield, M.R., Ellis, R.S., Tanvir, N.R., & Brinchmann, J., 1999, MNRAS, 308, 569

[5] Albert, L., Demers, S., Kunkel, W.E., 2000, AJ, 119, 2780

[6] Allen, R.J., in Gas and Galaxy Evolution, PASP, vol. 240, eds., J.E. Hibbard, M.P. Rupen, and J.H. van Gorkom

[7] Aloisi, A., Tosi, M., Greggio, L., 1999, AJ, 118, 302

[8] Aparicio, A., & Gallart, C., 1995, AJ, 110, 2105

[9] Aparicio, A., Dalcanton, J.J., Gallart, C., Martinez-Delgado, D., 1997, AJ, 114, 1447

[10] Aparicio, A., Gallart, C., & Bertelli, G., 1997, AJ, 114, 669

[11] Aparicio, A., 1998, in The Magellanic Clouds and Other Dwarf Galaxies, Bonn (1998), eds., T. Richtler and J.M. Braun, p. 107

[12] Armandroff, T.E., Da Costa, G.S., 1993, AJ, 106, 986

[13] Arp, H., 1994, A&A, 288, 738

[14] Azzopardi, M., Lequeux, J., Westerlund, B. E., 1986, A&A, 161, 232

[15] Azzopardi, M., Ap&SS, 265, 291

[16] Banks et al., 1999, 1999, ApJ, 524, 612

[17] Barton, E.J., Geller, M.J., & Kenyon, S.J., 2000, ApJ, 530, 660

[18] Beijersbergen, M., de Blok, W.J.G., & van der Hulst, J.M., 1999, A&A, 351, 903919

[19] Bell., E.F., Barnaby, D., Bower, R.G., de Jong, R.S., et al., 2000, MNRAS, 312, 470

[20] Bertelli, G., et al., 1994, A&AS, 106, 275 (Be94)

[21] Bettinelli, P., & Demers, S., 2000, AJ, 120, 1801

[22] Binney, J., & Tremaine, S., 1987, Galactic Dynamics, Princeton University Press

[23] Bothun, G., Impey, C., Malin, D., & Mould, J., 1987, AJ, 94, 23

[24] Boyce et al., 2001, ApJ, 560, L127

[25] Brandner, W., 2002, in Modes of Star Formation and the Origin of Field Populations, ASP Conference Series, Vol. 285, eds. E.K. Grebel & W. Brandner

[26] Bruzual, G., & Charlot, S., 2003, MNRAS, 344, 1000

[27] Brocklehurst, M., 1971, MNRAS, 153, 471

[28] Buonanno, R., et al. 1999, AJ, 118, 1671

[29] Caldwell, N., Kennicutt, R.C., Schommer, R.A., 1994, AJ, 108, 1186

[30] Caldwell, N., Armandroff, T.E., Da Costa, G.S., & Seitzer, P., 1998, AJ, 115, 535

[31] Cannon, J.M., DohmPalmer, R.C., Skillman, E.D., et al., 2003, AJ, 126, 2806

[32] Carignan, C., et al., 1998, AJ, 116, 1690

[33] Carignan C. & Purton C., 1998, ApJ, 506, 125

[34] Carraro, G., Chiosi, C., Girardi, L., & Lia, C., 2001, MNRAS, 327, 69

[35] Carraro, G., 2002, in Modes of Star Formation and the Origin of Field Populations, ASP Conference Series, Vol. 285, eds. E.K. Grebel & W. Brandner

[36] Castellanos, M., Diaz, A.I., & Terlevich, E., 2002, MNRAS, 329, 315

[37] Cole, A.A., et al., 1999, AJ, 118, 1657

[38] Combes, F., 1986, in Star forming Dwarf Galaxies and Related Objects, eds. D. Kunth, T.X. Thuan, & J. Tran Thanh Van

[39] Combes., F., 2001, in The Central kpc of Starbursts and AGN, ASP Conference Series, eds. J.H. Knapen, J.E. Beckman, I. Shlosman, and T.J. Mahoney

[40] Combes, F., 2004, in Recycling intergalactic and interstellar matter, IAU Symposium 217, Sydney (2003), ASP Conference Series, p. 440, eds. P.-A. Duc, J. Braine, and E. Brinks

[41] Conselice, C.J., 2002, in Modes of Star Formation. ASP Conference Series, Vol. 285, eds. E.K. Grebel., & W. Brandner

[42] Cook, K.H., Aaranson, M., & Norris, J., 1986, ApJ, 305, 634

[43] Cook, 1987, PhD Thesis, Arizona Univeristy, Tucson

[44] Corteau, S., & van den Bergh, S., 1999, AJ, 118, 337

[45] Côté, S., Freeman, K.C., Carignan, C., & Quinn, P., 1997, AJ, 114, 1313

[46] Cuillandre, J.C., Lequeux, J., Allen, R.J. et al., 2001, ApJ, 554, 190

[47] Da Costa, G.S., & Armandroff, T.E., 1990, AJ, 100, 162

[48] Da Costa, G.S., Armandroff, T.E., Caldwewll, N., Seitzer, P., 1996, AJ, 112, 2576

[49] Da Costa, G.S., Armandroff, T.E., Caldwewll, N., Seitzer, P., 2000, AJ, 119, 705

[50] Davies, J.I., Phillips, S., Disney, M.J., 1990, MNRAS, 244, 385

[51] Demers, S., & Battinelli, P., 2002, AJ, 123, 238

[52] de Blok, W.J.G., van der Hulst, J.M., & Bothun, G.D., 1995, MNRAS, 274, 235

[53] de Blok, W.J.G., McGaugh, S.S., van der Hulst, J.M., 1996, MNRAS, 283, 18

[54] de Blok, W.J.G., van der Hulst, J.M., 1998, A&A, 336, 49

[55] de Boer, K.S., et al., 1998, A&A, 338, L5

[56] Deharveng, J.M., Sassen, T.P., Buat, V., Bowyer, S., Lampton, M., Wu, X., 1994, A&A, 289, 715

[57] Deharveng, J.M., et al. 1997, A&A, 326, 528

[58] Dekel, A., & Silk, J., 1986, ApJ, 303, 39

[59] Denicolo, G., Terlevich, R., Terlevich, E., MNRAS, 2002, 330, 69

[60] De Young, D.S., Heckman, T., M., 1994, ApJ, 431, 598

[61] de Vaucouleurs, G., 1975, in Galaxies and the Universe, eds. A. Sandage, M. Sandage, & J. Kristian Chicago Univeristy Press, 557

[62] de Vaucouleurs, G., 1979, AJ, 84, 1270

[63] Disney, M.J., 1976, Nature, 263, 573

[64] Disney, M.J., & Phillips, S., 1983, MNRAS, 205, 1253

[65] Disney, M.J., 1999, in The Low Surface Brightness Universe, IAU Col. 171, eds. J.I. Davies, C. Impey, & S. Phillips

[66] Disney, M.J., 2002, in Extragalactic Gas at Low Redshift, ASP Conference Proc., 254, eds. J.S. Mulchaey, & J.Stocke

[67] DohmPalmer, R.C., et al., 1997a, AJ, 114, 2514

[68] DohmPalmer, R.C., et al., 1997b, AJ, 114, 2527

[69] DohmPalmer, R.C., Skillman, E.D., Gallagher, J., Tolstoy, E., Mateo, M., et al., 1998, AJ, 116, 1227

[70] DohmPalmer, R.C., et al. 2003, AJ, 126, 187

[71] Dolphin, A., 2000a, PASP, 112, 1397

[72] Dolphin, A., 2000b, ApJ, 531, 804

[73] Dolphin, A.E., et al., 2001, ApJ, 550, 554

[74] Dolphin, A.E., Saha, A., Claver, J., et al., 2002, AJ, 123, 3154

[75] Donas, J., Deharveng, J.M., Laget, M., Milliard, B., Huguenin, D., 1987. A&A, 180, 12

[76] Done, C., Madejski, G.M., Smith, D.A., 1996, ApJ 463, L63

[77] Dopita, M.A., Mathewson, D.S., & Ford, V.L., 1985, ApJ, 297, 599

[78] Dopita, M.A., Evans, I.N., 1986, ApJ, 307, 431

[79] Dufour, R.J., 1979, AJ, 84, 284

[80] Dressel, L.L., 1988, ApJ, 329, L69

[81] Edmunds, M.G., Pagel, B.E.J., 1984, MNRAS, 211, 507

[82] Elmegreen, B.G., 1993, ApJ, 411, 170

[83] Ferguson, A.M.N., Wyse, R.F.G., Gallagher, J.S., & Hunter, D.A., 1998, ApJ, 506, L19

[84] Ferrara, A., Tolstoy, E., 2000, MNRAS, 313, 291

[85] Fioc, M. & RoccaVolmerange, B., 1997, A&A, 326, 590

[86] Freeman, K.C., 1970, ApJ, 160, 811

[87] Galaz, G., Dalcanton, J.J., Infante, L., & Treister, E., 2002, AJ, 124, 1360

[88] Gallagher, J. S., Faber, S. M., & Balick, B., 1975, ApJ, 202, 7

[89] Gallagher, J.S., Hunter, D.A., Tutukov, A., 1984, ApJ, 284, 544

[90] Gallagher, J.S., Tolstoy, E., DohmPalmer, R.C., 1998, AJ, 115, 1869

[91] Gallart, C., Aparicio, A., Chiosi, C., Bertelli, G., Vilchez, J.M., 1994, ApJ, 425, L9

[92] Gallart, C., Aparicio, A., Bertelli, G., & Chiosi, C., 1996, AJ, 112, 1950

[93] Gallart, C., Freedman, W.L., Aparicio, A., Bertelli, G., & Chiosi, C., 1999, AJ, 118, 2245

[94] Gallego et al, 1995, ApJ, 445, L1

[95] Giovannelli, R., & Haynes, M., 1986, ApJ,

[96] Girardi, M., et al. 2000, ApJ, 530, 62

[97] Girardi, L., et al., 2002, A&A, 391, 195 (Gi02)

[98] Gondhalekar, P.M., Johansson, L.E.B., Brosch, N., Glass, I.S., & Brinks, E., 1998, A&A, 335, 152

[99] Graham, J.A., 1979, ApJ, 232, 60

[100] Grebel, E.K., 1997, RVMA, 10, 29

[101] Grebel, E.K., & Stetson, P.B., 1999, in The Stellar Content of the Local Group, IAU Symp. 192, eds P.Whitelock & R. Cannon

[102] Grebel, E.K., 2002, in Modes of Star Formation and the Origin of Field Populations, ASP Conference Series, Vol. 285, eds. E.K. Grebel & W. Brandner

[103] Grevesse, N., & Sauval, A.J., 1998, Space Science Reviews, 85, 161

[104] Groenewegen, M.A.T, and de Jong, T., 1993, A&A 267, 410

[105] Habing, H.J, 1996, A&AR, 7, 97

[106] Han, M., et al., 1997, AJ, 113, 1001

[107] Hameed & Devereux, N.A., 1999, AJ, 118, 730

[108] Hawarden, T.G., Mountain, C.M., Legget, S.K., Puxley, P.J., 1986, MNRAS, 221, 41

[109] Harris, G.L.H., Poole, G.B., Harris, W.E., 1998, AJ, 116, 2866

[110] Harris J, & Zaritsky D., ApJS, 136, 25

[111] Heckman, T.M., Armus, L., Miley, G.K., 1990. ApJS, 74, 833

[112] Heckman, T.M. 1999, Ap&SS, 266, 3

[113] Held, E.V., Saviane, I., Momany, Y., 1999, A&A, 345, 747

[114] HidalgoGmez, A.M., & Olofsson, K., 2002, A&A, 389, 836

[115] Hirashita, H., 2000, PASJ, 52, 107

[116] Hodge, P.W., 1961, AJ, 66, 249

[117] Hodge, P.W., Miller, B.W., 1995, ApJ, 451, 176

[118] Holtzmann, J.A., Burrows, C.J., Casertano, S., Hester, J., et al. 1995a, PASP, 107, 1065

[119] Holtzmann, J.A., Hester, J.J, Casertano, S., Trauger, J.T., Watson, A.M., and the WFPC2 IDT, 1995b, PASP, 107, 156

[120] Huang, J.H., Gu, Q.S., 1996, in Barred Galaxies, eds. R. Buta et al., ASP Conf. Series Vol. 91

[121] Hutcheimer, W.K., Karachentsev, I.D., & Karachentseva, V.E., 1998, A&A, 322, 375

[122] Hutcheimer, W.K., & Skillman, E.D., 1998, A&ASS, 127, 397

[123] Hummel, E., van der Hulst, J. M., Keel, W. C., Kennicutt, R. C., Jr., 1987, A&ASS, 70, 517

[124] Hunter, & D.A., Plummer, J.D., 1996, ApJ, 462, 732

[125] Hunter, D.A., 1997, PASP, 109, 937

[126] Hunter, D.A., Elmegreen, B.G., Baker, A.L., 1998, ApJ, 493, 595

[127] Iben, I., Jr, & Renzini, A., 1983, ARA&A, 21, 271

[128] Impey, C., & Bothun, G., 1989, ApJ, 341, 89

[129] Impey, C., et al. , 1996, ApJS, 105, 2091

[130] Impey, C., & Bothun, G., 1997, ARA&A, 35, 267

[131] Isobe, T., Feigelson, E.D., 1992, ApJS, 79, 197

[132] Israel, F.P., Tacconi, L.J., & Baas, F., 1995, A&A, 295, 599

[133] Izotov, Y. I., & Thuan, T. X. 1999, ApJ, 511, 639

[134] Jerjen, H., Freeman, K.C., Bingelli, B., 1998, AJ, 116, 2873

[135] Jerjen, H., Binggeli, B., & Freeman, K.C., 2000a, AJ, 119, 593

[136] Jerjen, H., Freeman, K.C., & Binggeli, B., 2000b, AJ, 119, 166

[137] Jerjen, H., Binggeli, B., & Barazza, F.D., 2004, AJ, 127, 771

[138] Kamaya, H., & Hirashita, H., 2001, PASJ, 53, 483

[139] Karachentsev, I.D., 1996, A&A, 305, 33

[140] Karachentsev, I.D., Sharina, M.E., Grebel, E. K., et al. 2000, 542, 128

[141] Karachentsev, I.D., Sharina, M.E., Dolphin, A.E., Grebel, E.K., et al., 2002, A&A, 385, 21

[142] Karachentsev, I.D., et al. 2003a, A&A, 398, 479

[143] Karachentsev, I.D., et al. 2003b, A&A, 398, 467

[144] Karachentsev, I.D., et al. 2003c, A&A, 404, 93

[145] Kenney, J.P.D, & Young, J.S, 1986, ApJ, 301, L13

[146] Kenney, J.P.D, & Young, J.S., 1988, ApJSS, 66, 261

[147] Kenney, J.P.D, & Young, J.S., 1989, ApJ, 344, 171

[148] Kenney, J.P.D., Koopmann, R.A., 2001, PASP, vol. 240, eds J.E. Hibbard, M.P.Rupen, and J.H. van Gorkom.

[149] Kennicut, R.C., & Kent, S.M., 1983, AJ, 88, 1094

[150] Kennicutt, R.C., Roettiger, K.A.; Keel, W.C., van der Hulst, J. M., Hummel, E., 1983, AJ, 93, 1011

[151] Kennicutt, R.C., 1989, ApJ, 344, 685

[152] Kennicutt, R.C., 1998a, ARA&A, 36, 189

[153] Kennicutt, R.C., 1998b, ApJ, 498, 541

[154] Kilborn, V.A. et al., 2002, AJ, 124, 690

[155] Knezek, P.M., 1999, in The Low Surface Brightness Universe, PASP, Vol. 170, eds. J.I. Davies, C. Impey, and S. Phillips

[156] Koopmann, R.A., Kenney, J.P.D., 1998, ApJ, 497, L75

[157] Koopmann, R.A., Kenney, J.P.D., Young, J.S., 2001, ApJSS, 135, 125

[158] Koribalski, B., et al., 2004, AJ, 128, 16

[159] Kundic, T., Hernquist, L., & Gunn, J.E. 1992, Bulletin of the American Astronomical Society, Vol. 25, p.739

[160] Kunth, D., Maurogordato, S., Vigroux, L., 1988, A&A, 204, 10

[161] Lang, R.H., et al. 2003, MNRAS, 342, 738

[162] Larson, R.B., & Tinsley, B.M., 1978, ApJ, 219, 46

[163] Lebouteiller, V., Kunth, D., et al. 2004, A&A, 415, 55

[164] Legrand, F., A&A, 354, 504

[165] Lee, M.G., Freedman, W.L., & Madore, B.F., 1993, ApJ, 417, 553

[166] Lee et al., 1999, AJ, 118, 853

[167] Le Lilievre, M., & Roy, J.R., 2000, AJ, 120, 1306

[168] Lilly S.J, Le Fevre O., Hammer F. & Crampton D., 1996, ApJ, 460, L1

[169] Lo K.Y., Sargent W.L.W. & Young K., 1993, AJ, 106, 507

[170] Lonsdale, C.J., & Helou, G., 1987, ApJ, 314, 513

[171] Loose, H., & Thuan, T.X., 1986, ApJ, 309, 59

[172] Mac Low, M.M., & Ferrara, A., 1999, ApJ, 513, 142

[173] Madore, B.F., & Freedman, W.M., 1995, AJ, 109, 1645

[174] Maia, M.A.G., & Willmer, C.N.A., 1997, in IAU Symp. 186, Galaxy Interactions at Low and High redshift, Kyoto, Japan.

[175] Majewski, S.R., et al., 2002, in Modes of Star Formation and the Origin of Field Populations, ASP Conference Series, Vol. 285, eds. E.K. Grebel & W. Brandner

[176] Makarova, L., Grebel, E., Karachentsev, I.D., et al., 2003, Ap&SS, 285, 107

[177] Maloney, P., Black, J.H., 1988, ApJ, 325, 389

[178] Martin, & Kennicut, R.C., 2001, ApJ, 555, 301

[179] MartinezDelgado, D., Gallart, C., Aparicio, A., 1999, AJ, 118, 862

[180] Maschenko, S., Carignan, C., & Bouchard, A., 2004, MNRAS, 352, 168

[181] Massey, P., & Armandroff, T., 1995, AJ, 109, 2470

[182] Mateo, M.L., 1998, ARA&A, 36, 435

[183] Matthews, L.S., & Gao, Y., 2001, ApJ, 549, L191

[184] Matthews, L.S., van Driel, W., & MonnierRagaigne, D., 2001, A&A, 365, 1

[185] Mayer, L., et al., 2001, ApJ, 559, 754

[186] McGaugh, S.S., 1991, ApJ, 380, 140

[187] McGaugh, S.S., 1994, ApJ, 426, 135

[188] McGaugh, S.S., 1994, ApJ, 426, 135

[189] McGaugh, S.S., & Bothun, G.D., 1994, AJ, 107, 530

[190] Meyer, M.J., et al., 2004, MNRAS, 350, 1195

[191] Mihos J.C., & Hernquist, L., 1996, ApJ, 464, 641

[192] Miller, B.W., Dolphin, A.E., & Hodge, P., 2001, ApJ, 562, 713

[193] Minchin, R.F., et al., 2003, MNRAS, 346, 787

[194] Minchin, R.F., et al., 2004, MNRAS in press

[195] Minniti, D., & Zijlstra, A.A., 1996, ApJ, 467, L13

[196] Momany, Y., Held, E.V., Saviane, I., & Rizzi, I., 2002, A&A, 384, 393

[197] Moore, B., Katz, N., Lake, G., Dressler, A., Oemler, A., Jr., 1996, Nature, 379, 613

[198] Moore, B., Lake, G., Katz, N., 1998, ApJ, 495, 139

[199] Moos, H.W., Cash, W.C., Cowie, L.L., et al., ApJ, 538, L1

[200] Nilson, P.N., 1973, Uppsala General Catalog of Galaxies, Uppsala Astron. Obs. Ann., 6

[201] Noguchi, M., 1996, ApJ, 469, 605

[202] Nowotny, W., Kerschbaum, F., Schwarz, H. E., Olofsson, H., 2001, A&A, 367, 557

[203] Nowotny, W., Kerschbaum, F., Olofsson, H., Schwarz, H. E., 2003, A&A, 403, 93

[204] O'Neil, K., Bothun, G.D., & Cornell, M.E., 1997, AJ, 113, 1212

[205] O'Neil, K., Bothun, G.D., Schombert, J.M., Cornell, M.E., & Impey, C.D., 1997, AJ, 114, 2448

[206] O'Neil, K., Bothun, G.D., Schombert, J.M., 2000, AJ, 119, 136 (OBS2000)

[207] O'Neil, K., Hofner, P., Schinnerer, E., 2000, ApJ, 545, L99

[208] Osterbrock, D.E., 1974, Astrophysics of Gaseous Nebulae, W.H. Freeman, San Francisco, CA

[209] Pagel, B.E.J., Edmunds, M.G., Blackwell, D.E., Chun, M.S., Smith, G., 1979, MNRAS, 189, 95

[210] Papaderos, P., Loose, H.H., et al. 1996, A&AS, 120, 207

[211] Pickering, T.E., Impey, C.D., van Gorkom, J.H., Bothun, G.D., 1997, AJ, 114, 1858

[212] Pogge, R.W., & Eskridge, P.B., 1993, AJ, 106, 1405

[213] Poggianti, B.M., Smail, I. Dressler, A., Couch, W.J., et al. 1999, ApJ, 518, 576

[214] Pompea, S.M., Rieke, G.H., 1990, ApJ, 356, 416

[215] Pritchet, C., 1979, ApJ, 231, 354

[216] Pritzl, B.J., Knezek, P., Gallagher, J.S., Grossi, M., Disney, M.J., et al. 2003, ApJ, 596, L47

[217] Pustilnik, S.A., Brinks, E., Thuan, T.X., et al., 2001, AJ, 121, 1413

[218] Pilyugin, L.S., 2000, A&A, 362, 325

[219] Pilyugin, L.S., 2001a, A&A, 373, 56

[220] Pilyugin, L.S., 2001, A&A, 374, 412

[221] Quirk, W., 1972, ApJ, 176, L9

[222] Rejkuba, M., Minniti, D., Gregg, M.D., et al., , 2000, AJ, 120, 801

[223] Richter, P. et al., 1998, A&A, 338, L9

[224] Roberts, M.S., 1968, AJ, 73, 945

[225] Roberts, M.S., & Heynes, M.P., 1994, ARA&A, 32, 115

[226] Romanishin, W., 1990, AJ, 100, 373

[227] Rosenberg, J.L., & Schneider, S.E., 2000, ApJS, 130, 177

[228] Rosenberg, J.L., & Schneider, S.E., 2002, in Extragalactic Gas at Low Redshift, ASP Conference Series, Vol. 254, eds. J.S. Mulchaey & J.T. Stocke

[229] Rubio, M., Lequex, J., Boulanger, F., 1993, A&A, 271, 9

[230] RyanWeber, E., et al. 2002, AJ, 124, 1954

[231] Saha, A., Freedman, W.L., Hoessel, J.G., Mossman, A.E., 1992, AJ, 104, 1072

[232] Saha, A., et al., 1995, ApJ, 438, 8

[233] Sakai, S., Madore, B.F., & Freedman, W.L., 1996, ApJ, 461, 713

[234] Sanders, D.B., Solomon, P.M., Scoville, N.Z., 1984, ApJ, 276, 182

[235] Sanders, D.B., & Mirabel, I.F. 1996, ARA&A, 34, 749

[236] Saviane, I., Held, E.V., Bertelli, G., 2000, A&A, 355, 56

[237] Saviane, I., Held, E.V., Momany, Y., Rizzi, L., 2001, in Memorie della Societ Astronomica Italiana, Vol. 72, p. 773

[238] Saviane, I., Rizzi, L., Held, E.V., Bresolin, F., Momany, Y., 2002, A&A, 390, 59

[239] Sauvage, M., Thuan, T.X., 1992, ApJ, 396, L69

[240] Schlegel, D.J., Finkbeiner, M.D., & Davis, M., 1998, AJ, 500, 525

[241] Schmidt, M., 1959, ApJ, 129, 243

[242] Schombert, J., et al., 1992, AJ, 103, 1107

[243] Schombert, J., 1998, AJ, 116, 1650

[244] SchulteLadbeck, R.E., Hopp, U., Crone, M.M., & Greggio, L., 1999, ApJ, 525, 709

[245] Searle, L., 1971, ApJ, 168, 327

[246] Seaton, M.J., 1979, MNRAS, 187, 73

[247] Shlosman, I., Begelman, M.C., & Frank, J., 1990, Nature, 345, 679

[248] Skillman, E.D. et al. 1988, A&A, 198, 33

[249] Skillman, E.D., 1989, ApJ, 347, 883

[250] Skillman, E.D., Bothun, G.D., Murray, M.A., & Warmels, R.H., 1987, A&A, 185, 61

[251] Skillman, E.D., 2001, A&SS, 277, 383

[252] Skillman, E.D., Cote , S., Miller, B.W., 2003, AJ, 125, 610

[253] SmeckerHane, T., Mc William, A., 1999, in Spectrophotometric Dating of Stars and Galaxies, ASP Conf. Proc., Vol. 192, eds. Ivan Hubeny, Sally Heap, and Robert Cornett, p.150

[254] SmeckerHane, T., et al. 2002, ApJ, 566, 239

[255] Solanes, J.M., Manrique, A., GarcaGomez, C., GonzalezCasado, G., Giovanelli, R., Haynes, M.P., ApJ, 548, 97

[256] Solomon, P.M., et al. , 1987, ApJ, 319, 730

[257] Soria, R., Mould, J.R., Watson, A.M., et al., 1996, ApJ, 465, 79

[258] Spraybery et al., 1993, ApJ, 417, 114

[259] Sprayberry, D., Impey, C.D., Bothun, G.D., Irwin, M.J., 1995, AJ, 109, 558

[260] Stetson, P.B., 1987, PASP, 99, 191

[261] Stetson, P.B., 1994, PASP, 106, 250

[262] Stetson, P., et al. 1998, PASP, 110, 533

[263] Stetson, P.B., Bruntt, H., & Grundhal, F., 2003, PASP, 115, 413

[264] StorchiBergmann, T., Calzetti, D., Kinney, A.L., 1994, ApJ, 429, 572

[265] Telesco, C.M., & Harper, D.A., 1980, ApJ, 235, 392

[266] Telles, E. & Terlevich, R. 1995, MNRAS, 275, 1

[267] Thim, F., Tammann, G.A., Saha, A., Dolphin, A., et al., 2003, ApJ, 590, 256

[268] Tosi, M., Sabbi, E., Bellazzini, M., et al., 2001, AJ, 122, 1271

[269] Tolstoy, E., 1996, ApJ, 462,762

[270] Tolstoy, E., Gallagher, J.S., Cole, A.A., et al., 1998, AJ, 116, 1244

[271] Tolstoy, E., 2001, in The Magellanic Clouds and other dwarf galaxies, (Aachen 2001), eds. Klaas S. De Boer, RalfJuergen Dettmar, and Uli Klein, p.61

[272] Tolstoy, E., Irwin, M.J., Cole, A.A., et al., 2001, MNRAS, 327, 918

[273] Toomre, A, 1964, ApJ, 139, 1217

[274] Tully, R.B., 1987, ApJ, 321, 280

[275] Tumlinson et al., 2002, ApJ, 566, 857

[276] van den Bergh , 1959, , Pub. David Dunlap Obs., 2, 159

[277] van den Bergh, S., 1980, PASP, 92, 122

[278] van den Bergh, S., 1999, AJ, 117, 2211

[279] van den Bergh, S., 2000, AJ, 119, 609

[280] van den Bergh, S., 2000b, PASP, 112, 529

[281] van den Bergh, S., Cohen, J., Crabbe, C., 2001, AJ, 122, 611

[282] van der Hulst, J.M., Skillman, E.D., Smith, T.R., Bothun, G.D., McGaugh, S.S. & de Blok, W.J.G, 1993, AJ, 106, 548

[283] van Driel, W., KraanKorteweg, R.C., Binggeli, B., & Huchtmeier, W.K., 1998, A&A, 127, 397

[284] van Gorkom, J.H., van der Hulst, J., Haschick, A., & Tubbs, A., 1990, AJ, 99, 1781

[285] van Zee, L., Haynes, M.P., & Giovannelli, R., 1995,, AJ, 109, 990

[286] van Zee, L., et al., 1996, AJ, 112, 129

[287] van Zee, L., Haynes, M.P., Salzer, J.J., Broeils, A.H., 1997a, AJ, 113, 1618

[288] van Zee, L., Haynes, M.P., Salzer, J.J., 1997b, AJ, 114, 2479

[289] van Zee, L., Haynes, M.P., Salzer, J.J., 1997c, AJ, 114, 2497

[290] van Zee, L., et al., 1998, AJ, 116, 1186

[291] van Zee, L., 2001a, AJ, 121, 2003 van Zee, L., 2001b, AJ, 122, 121

[292] Vassiliadis, E., & Wood, P.R., 1993, ApJ, 413, 641

[293] VidalMajar, A., Kunthy, D., Lecavalier des Etangs A., et al. 2000, ApJ, 538m L77

[294] Vilchez, J.M., Esteban, C., 1996, MNRAS, 280, 720

[295] Vollmer, B., Cayatte, V., Balkowski, C., Duschl, W.J., 2001, ApJ, 561, 708

[296] Warren, B.E., Jerjen, H., Koribalski, B.S., 2004, AJ, 128, 1152

[297] Weedman D.A., Feldman, F.R., Balzano, V.A., Ramsey, L.W., Sramek, R.A., Wuu, C.C. et al., 1981, ApJ, 248, 105

[298] Wilcots, E.M.,& Miller, B.W., 1998, AJ, 116, 2363

[299] Wilson, C.D., 1995, ApJ, 448, L97

[300] Wolfire, M.G., et al., 1995, ApJ, 443, 152

[301] Wong, T., & Blitz, L., 2002, ApJ, 569, 157

[302] Young, J.S., & Scoville, N., 1982, ApJ, 260, L11

[303] Young, J.S., et al., 1986, ApJ, 311, L17

[304] Young, J.S., 1989, in The ISM in Galaxies, eds. H. Thronson & M. Shull

[305] Youn, J.S., Knezek, P.M., 1989, ApJ, 347, L55

[306] Young, L.M., & Lo, K.Y., 1996, ApJ, 462, 203

[307] Young, L.M., Lo, K.Y., 1997, ApJ, 490, 710

[308] Young, L.M., 1999, AJ, 117, 1758

[309] Young, L.M., 2000, AJ, 119, 188

[310] Zwaan, M.A., Briggs, F.H., Sprayberry, D., & Sorar, E., 1997, ApJ, 490, 173

[311] Zwaan, M.A., Briggs, F.H., & Sprayberry, D., 2001, MNRAS, 327, 1249

[312] Zwaan, M.A., et al. 2003, AJ, 125, 2842

[313] Zwaan, M.A., et al. 2004, MNRAS, 350, 1210

Acknowledgements

I would like to thank my supervisor Prof. Mike Disney for having introduced me to the "realm" of Astronomy after having spent a lot of time studying particle physics. Above all I would like to thank Mike because he always let me find by myself the direction I wanted follow during my PhD. Sometimes this has been difficult, but on the other hand it has been also very stimulating. I also would like to thank him for his patient and careful help in the writing of the thesis which has been more complicated during the last year after I went back to Rome.

Going along within the group, I really have to thank Robert Minchin, for the big help he has been always willing to give, let alone for sorting out in a few minutes all my problems with StarFISH, but also for having been always keen in discussing and clarifying all my doubts at any time.

Then I would like to thank Diego Garcia and Catherine Vlahakis, especially for the big support they gave me in the last hectic days before the submission.

I also want to thank Dr. Erwin de Blok, for his prompt reading of the thesis, for having taken some of the data we have used in this study, and for his valid suggestions; and I have to thank Dr. Jon Davies because he is always keen in sharing his big expertise on dwarf galaxies.

Another big thank you goes to Sabina Sabatini, who volunteered to teach me IDL without knowing that this would have been a difficult task even for an expert like her, and because she has always been ready to discuss my "astronomical" doubts during the PhD. I also want to thank her and Francesco because they have always been a bench mark during the three years I have spent in Cardiff.

I want to thank Dr. Patricia Knezek for having invited me at the NOAO in Tucson, Arizona, where I have had the opportunity of learning a lot of things that were very important for my thesis. And Dr. Bart Pritzl for the useful discussions on colour magnitude diagrams.

Then I have to thank Prof. Ken Freeman for his help during the observing run in Siding Springs, Australia, and for having taken some other data we have used in this thesis.

Finally I would like to thank Douglas Boyd and Dimitris Stamatellos for having let me know one of the best (if not the best) bar of Cardiff. The list continues, there are people that have left Cardiff some time ago, people that are still here, such as Sarah Roberts, the "Baes" - Marteen, Begga, and little Sterre - Ifijenia, Jing, Rodney, and all the kung-fu people.